nuclear fusion

fusion nucléaire

ядерный синтез

fusión nuclear

ATOMIC AND PLASMA–MATERIAL INTERACTION DATA FOR FUSION

(Supplement to the journal Nuclear Fusion)

VOLUME 3

INTERNATIONAL ATOMIC ENERGY AGENCY, VIENNA, 1992
AGENCE INTERNATIONALE DE L'ENERGIE ATOMIQUE, VIENNE, 1992
МЕЖДУНАРОДНОЕ АГЕНТСТВО ПО АТОМНОЙ ЭНЕРГИИ, ВЕНА, 1992
ORGANISMO INTERNACIONAL DE ENERGIA ATOMICA, VIENA, 1992

The following States are Members of the International Atomic Energy Agency:

AFGHANISTAN
ALBANIA
ALGERIA
ARGENTINA
AUSTRALIA
AUSTRIA
BANGLADESH
BELARUS
BELGIUM
BOLIVIA
BRAZIL
BULGARIA
CAMBODIA
CAMEROON
CANADA
CHILE
CHINA
COLOMBIA
COSTA RICA
COTE D'IVOIRE
CUBA
CYPRUS
CZECHOSLOVAKIA
DEMOCRATIC PEOPLE'S REPUBLIC OF KOREA
DENMARK
DOMINICAN REPUBLIC
ECUADOR
EGYPT
EL SALVADOR
ESTONIA
ETHIOPIA
FINLAND
FRANCE
GABON
GERMANY
GHANA
GREECE
GUATEMALA
HAITI
HOLY SEE
HUNGARY
ICELAND
INDIA
INDONESIA
IRAN, ISLAMIC REPUBLIC OF
IRAQ
IRELAND
ISRAEL
ITALY
JAMAICA
JAPAN
JORDAN
KENYA
KOREA, REPUBLIC OF
KUWAIT
LEBANON
LIBERIA
LIBYAN ARAB JAMAHIRIYA
LIECHTENSTEIN
LUXEMBOURG
MADAGASCAR
MALAYSIA
MALI
MAURITIUS
MEXICO
MONACO
MONGOLIA
MOROCCO
MYANMAR
NAMIBIA
NETHERLANDS
NEW ZEALAND
NICARAGUA
NIGER
NIGERIA
NORWAY
PAKISTAN
PANAMA
PARAGUAY
PERU
PHILIPPINES
POLAND
PORTUGAL
QATAR
ROMANIA
RUSSIAN FEDERATION
SAUDI ARABIA
SENEGAL
SIERRA LEONE
SINGAPORE
SLOVENIA
SOUTH AFRICA
SPAIN
SRI LANKA
SUDAN
SWEDEN
SWITZERLAND
SYRIAN ARAB REPUBLIC
THAILAND
TUNISIA
TURKEY
UGANDA
UKRAINE
UNITED ARAB EMIRATES
UNITED KINGDOM OF GREAT BRITAIN AND NORTHERN IRELAND
UNITED REPUBLIC OF TANZANIA
UNITED STATES OF AMERICA
URUGUAY
VENEZUELA
VIET NAM
YUGOSLAVIA
ZAIRE
ZAMBIA
ZIMBABWE

The Agency's Statute was approved on 23 October 1956 by the Conference on the Statute of the IAEA held at United Nations Headquarters, New York; it entered into force on 29 July 1957. The Headquarters of the Agency are situated in Vienna. Its principal objective is "to accelerate and enlarge the contribution of atomic energy to peace, health and prosperity throughout the world".

Printed by the IAEA in Austria
December 1992

ATOMIC AND PLASMA-MATERIAL INTERACTION DATA FOR FUSION

(Supplement to the journal Nuclear Fusion)

VOLUME 3

INTERNATIONAL ATOMIC ENERGY AGENCY, VIENNA, 1992

The volumes of ATOMIC AND PLASMA-MATERIAL INTERACTION DATA FOR FUSION are published by the International Atomic Energy Agency as supplements of the journal NUCLEAR FUSION.

For these supplements, papers, letters and reviews are accepted which deal with the following topics:

— Elementary collision processes in fusion plasmas involving photons, electrons, ions, atoms and molecules;
— Collision processes of plasma particles with surfaces of fusion relevant materials;
— Plasma-material interaction phenomena, including the thermophysical response of materials.

Each submitted contribution should contain fusion relevant data and information in either of the above areas. Original contributions should provide new data, using well established methods. Review articles should give a critical analysis or evaluation of a wider range of data. They are normally prepared on the invitation of the Scientific Editor or on prior mutual consent. Each submitted contribution is assessed by two independent referees.

Every manuscript submitted must be accompanied by a *disclaimer* stating that the paper has not been published and is not being considered for publication elsewhere. If no copyright is claimed by the authors, the IAEA automatically owns the copyright of the paper.

Guidelines for the preparation of manuscripts are given on the inside back cover. Manuscripts and correspondence should be addressed to: The Editor, NUCLEAR FUSION, International Atomic Energy Agency, Wagramerstrasse 5, P.O. Box 100, A-1400 Vienna, Austria.

Publisher: International Atomic Energy Agency, Wagramerstrasse 5, P.O. Box 100, A-1400 Vienna, Austria

Scientific Editor: R.K. Janev, Atomic and Molecular Data Unit, Division of Physical and Chemical Sciences

Editor: C. Bobeldijk, Division of Scientific and Technical Information

Manuscript Editors: J.W. Weil, Division of Publications
Maria Demir, Division of Publications

Annual subscription price (one issue): Austrian Schillings 300,—
Airmail delivery (optional): Austrian Schillings 40,— to any destination

---

ATOMIC AND PLASMA-MATERIAL INTERACTION DATA FOR FUSION, VOLUME 3
IAEA, VIENNA, 1992
STI/PUB/23/APID/3

EDITORIAL NOTE

The present volume of Atomic and Plasma-Material Interaction Data for Fusion is devoted to atomic collision processes of helium atoms and of beryllium and boron atoms and ions in fusion plasmas. Most of the articles included in this volume are extended versions of the contributions presented at the IAEA experts' meetings on Atomic Data for Helium Beam Fusion Alpha Particle Diagnostics and on the Atomic Database for Beryllium and Boron, held in June 1991 at the IAEA headquarters in Vienna, or have resulted from the cross-section data analyses and evaluations performed by the working groups of these meetings. The critically assessed cross-section data for various classes of collision processes and individual reactions are needed primarily for fusion research dealing with modelling the neutral helium beam interaction with reactor grade fusion plasmas (including various plasma diagnostic applications), and for studies of transport and radiation properties of beryllium and boron impurities in tokamak edge plasmas. However, the broad energy range of most of these data makes them useful also for other fusion studies, such as those on helium exhaust and impurity recycling problems.

The analyses of the data status and needs presented in several articles in this volume also identify those collision processes of helium, beryllium and boron atoms and ions in fusion plasmas for which the cross-section information is either inadequate or missing. Therefore, appropriate suggestions for further experimental and theoretical work on completing the required cross-section information are given, with an indication of the desirable accuracies.

Vienna, November 1992

R.K. Janev
Scientific Editor

CONTENTS

REQUIREMENTS FOR COLLISION DATA ON THE SPECIES HELIUM, BERYLLIUM AND BORON IN MAGNETIC CONFINEMENT FUSION

H.P. SUMMERS[1], M. von HELLERMANN, F.J. de HEER[2], R. HOEKSTRA[3]
JET Joint Undertaking,
Abingdon, Oxfordshire,
United Kingdom

ABSTRACT. Requirements for collision data on helium, beryllium and boron are reviewed in the light of the directions of present and planned tokamak fusion experiments. The occurrence of the atoms and ions of these species and their roles in plasma behaviour and diagnostic measurements are described. Special emphasis is placed on alpha particle detection in reacting plasmas and on beryllium and boron in divertor configuration machines. The atomic reactions required to exploit the species in models and diagnostic analysis are gathered together and their relative importance indicated. The paper is an introduction to the detailed studies of collision cross-sections presented in the other contributions to this volume.

1. INTRODUCTION

Although the usual primary species in present tokamak fusion experiments is deuterium and that in future ignited plasma experiments such as ITER will be a 50% mixture of deuterium and tritium isotopes, it is well known that other elemental species play a crucial and sometimes decisive role in plasma behaviour. Helium, beryllium and boron are of particular importance. Beryllium is the element of lowest Z with conductive and thermal properties which make it a possible plasma facing surface material for fusion reactors. As such, it has been under test in JET as a coating material of a few hundred monolayers from evaporators, as a solid limiter and as strike zone plates in X-point operation [1]. It will be used initially for the dump plates in the pumped divertor structure under assembly at JET. Boron, on the other hand, which is deposited on carbon facing surfaces by, for example, glow discharges in B_2H_6 mixtures [2], appears to confer benefits similar to those of solid beryllium, that is, in gettering oxygen and achieving low Z_{eff} and radiant losses in the plasma. 'Boronization' is a widely used strategy at this time in most fusion experiments based on a carbon first wall such as TEXTOR and JT-60. Helium is different. It is the product of the tritium/deuterium fusion reaction, that is, the internal kinetic energy source and the spent fuel of the self-sustaining reacting plasma. Retention and redistribution of the alpha particle birth energy amongst the plasma ions, and then transport, recycling and exhaust of the thermal alpha particles are evidently key issues for a reactor [3, 4]. Previous collections of atomic data for helium include those of Janev et al. [5]; atomic data for edge studies have been reviewed by Janev et al. in Ref. [6].

An objective of this volume is to assemble and improve the atomic collision data required for modelling helium, beryllium and boron in the reactor regime. It is essential, however, that such data are extended to and are consistent with those in studies of the present generation of subcritical fusion devices. It is in these devices that models and behaviours of the species are under experimental test. It must also be recognized that the species play a dual role in a plasma, namely as components in the overall plasma models on the one hand and as diagnostic probes of plasma parameters in their own right on the other. In seeking to provide a commonality of sound atomic collision data for helium, beryllium and boron, a working principle is that data for modelling should be dressed with a consistent set of atomic data which support associated experimental diagnosis.

Section 2 describes the occurrence and behaviour of helium, and Section 3 those of beryllium and boron in fusion plasmas. Methods for their measurement and their exploitation in a diagnostic sense, which use atomic collisions, are also examined. In Sections 4 and 5, detailed ranked lists of atomic reactions are

Permanent affiliations:
[1] University of Strathclyde, Glasgow, United Kingdom.
[2] FOM-Institute for Atomic and Molecular Physics, Amsterdam, The Netherlands.
[3] Kernfysisch Versneller Instituut, Groningen, The Netherlands.

assembled to support these aspects. Also an indication of the accuracy with which the associated cross-sections need to be known is given. The study is heavily weighted towards helium and alpha particle detection using helium beams. Deuterium beams, associated beam stopping and D/He^{+2} charge exchange have been described in detail before and are excluded. Likewise, broad ionization, recombination and radiated power under electron collisions of light species are already familiar and, therefore, detail in this area is reduced and mostly new aspects only are emphasized.

2. ASPECTS OF HELIUM AND ITS MEASUREMENT

The presence of helium in the plasma arises in four ways. (1) It can be introduced in the initial gas fill for the discharge, usually as a minor constituent ($\sim 5\%$ of either ^3He or ^4He) for coupling ion cyclotron radio-frequency (RF) power to the plasma. (2) It can be introduced by gas puffing at the periphery of the plasma during a discharge, principally as an edge probe (see, for example, results on TEXTOR [7]). (3) Fast ($E \gtrsim 30$ keV/u) neutral beams of ^3He and ^4He are used at JET for heating and deep helium deposition [8], and similar but less powerful beams are also used as diagnostic beams (for example, $E \sim 15$ keV/u at TFTR and $E \lesssim 50$ keV/u at JT-60 [9]). A diagnostic beam at $E \gtrsim 50$ keV/u has been suggested for ITER. (4) Deuterium/tritium fusion will provide a fast alpha particle source ($E \sim 880$ keV/u) in the core of a reacting plasma. These various sources result in a range of different distributions in space and velocity space.

The stationary radial thermal alpha particle distribution reflects the balance of ionization, recombination and transport, and then the sources and recycling parameters of helium in a plasma. The ionization state of thermal helium is maintained primarily by electron collisions, although, at the highest ion temperatures achieved ($T_i \gtrsim 30$ keV), ionization by ion impact becomes important. The first two ionization stages, He^0 and He^{+1}, are strongly edge localized, while He^{+2} extends over the whole plasma volume.

The fusion alpha particles, by contrast, are expected to display a 'slowing down' distribution function confined primarily to the hot central part of the plasma (see, however, Ref. [10] for more detail). This function is parametrized essentially by the source rate and the critical velocity at which slowing down by collisions with electrons gives way to ion scattering, and the slowing down distribution merges with the thermal alpha particle distribution.

In ion cyclotron resonance heating (ICRH) of the plasma, the minority alpha particles are accelerated to high energies ($\lesssim$ a few MeV) and diffuse and slow down away from the absorbing layer. Thus, they are expected to have a slowing down distribution function somewhat similar to that of fusion alpha particles, but with different spatial aspects, depending on the location of the layer. The details of the ICRH driven alpha particle distributions have been described in Ref. [11]. To a degree, therefore, ICRH accelerated alpha particle distributions provide a test area for fusion alpha particle detection methods.

The He^0 atoms in a neutral beam show an exponential attenuation in the plasma owing to ionizing and charge exchanging collisions with plasma ions. (The beam has in general significantly populated $2\,^1S$ and $2\,^3S$ metastable state populations as well as the ground state $1\,^1S$. Attenuation of the metastable populations is quite different from that of the ground population.) For fast penetrating beams with energies $\gtrsim 20$ keV/u, electron collisions are less effective than ion collisions in this respect. Also the beam atoms are themselves excited in such collisions and radiate. This gives the 'beam emission spectrum' [12]. The beam/plasma interaction creates a number of secondary populations, namely:

(a) Halo atoms: These are D^0_{plasma} atoms formed by the charge exchange (CX) reaction between D^+ and He^0 in the beam. They migrate in a random walk by further CX reactions until they are ionized. Typically, they are localized within ~ 30 cm of the beam itself for plasma temperatures of ~ 15 keV.

(b) Prompt and plume ions: These are X^{+z_0-1} ions such as He^{+1} formed by CX reactions between X^{+z_0} and He^0 in the beam. It is helpful to distinguish between the initially formed ions in excited states (prompt) which radiate rapidly and the ground state ions which travel significant distances along field lines (plume). The former give the 'CX spectrum'. The latter, re-excited by electron collisions, can again radiate before finally ionizing in positions away from their point of formation (in JET, ~ 40 m for C^{+5} and ~ 6 m for He^{+1} at 5 keV and 5×10^{13} cm^{-3}) [13].

(c) The slowing down ionized beam population: For example, for $^3He^0$ beams at 50 keV/u in JET, the slowing down time of the fast $^3He^{+2}$ after double ionization is ~ 0.3–0.6 s. This population behaves in a manner similar to that of fusion alpha particles in the late phase of their slow down. There is also the singly ionized He^{+1} population in this group which is essentially a plume and is distinguished from (b) only by its

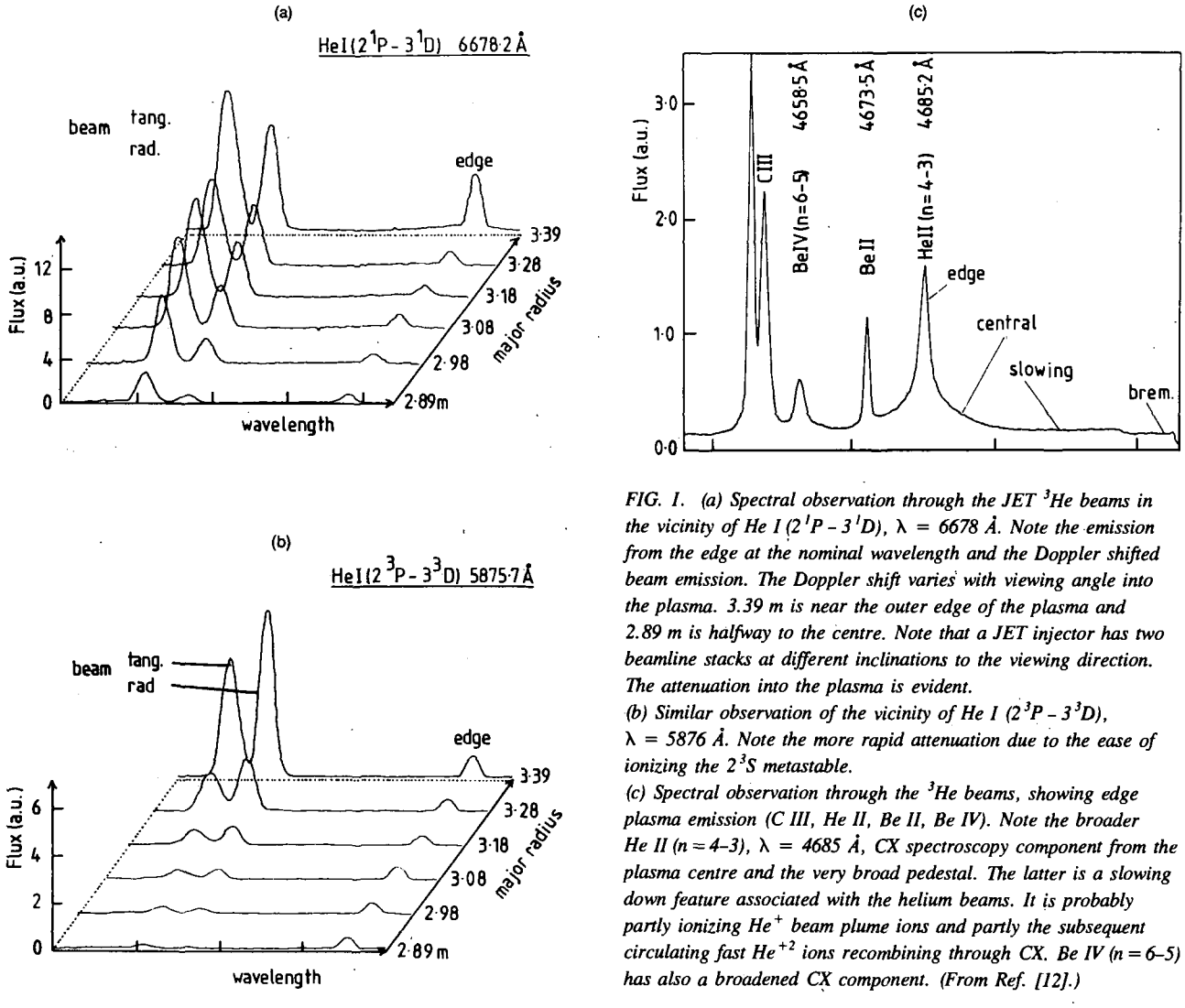

FIG. 1. (a) Spectral observation through the JET ^{3}He beams in the vicinity of He I ($2\,^1P - 3\,^1D$), λ = 6678 Å. Note the emission from the edge at the nominal wavelength and the Doppler shifted beam emission. The Doppler shift varies with viewing angle into the plasma. 3.39 m is near the outer edge of the plasma and 2.89 m is halfway to the centre. Note that a JET injector has two beamline stacks at different inclinations to the viewing direction. The attenuation into the plasma is evident.
(b) Similar observation of the vicinity of He I ($2\,^3P - 3\,^3D$), λ = 5876 Å. Note the more rapid attenuation due to the ease of ionizing the $2\,^3S$ metastable.
(c) Spectral observation through the ^{3}He beams, showing edge plasma emission (C III, He II, Be II, Be IV). Note the broader He II (n = 4–3), λ = 4685 Å, CX spectroscopy component from the plasma centre and the very broad pedestal. The latter is a slowing down feature associated with the helium beams. It is probably partly ionizing He^+ beam plume ions and partly the subsequent circulating fast He^{+2} ions recombining through CX. Be IV (n = 6–5) has also a broadened CX component. (From Ref. [12].)

fast velocity distribution [14]. Plasma ion and electron collisions are effective in destroying this population by reionization and CX.

(d) Neutralized fast alpha particles created by the double charge transfer reaction between He^{+2} and He^0: These particles can in principle escape from the plasma, but are attenuated by reionizing and charge exchanging collisions with plasma ions in a manner similar to that of neutral helium beams themselves. Neutralized thermal alpha particles will also be formed, but are of less interest.

Turning to measurement of these populations, since the alpha particles are non-radiating and confined in the plasma, such measurement must be enabled by electron capture. Two routes for such measurement are double charge transfer (neutralization) followed by external neutral particle detection and energy analysis, and single charge transfer followed by analysis of the cascade radiation of the He^{+1} particle. Projection of solid pellets of lithium into a plasma has been suggested as a means of providing a high concentration of suitable donors [15]. Penetrating neutral helium beams also provide suitable donors in the core of the plasma because of the efficiency of the resonant double charge transfer reaction. Neutral beam driven detection only is addressed here. It is noted that a 50 keV/u diagnostic neutral helium beam has been proposed to enable neutral particle detection on ITER and a 100 keV/u deuterium beam as a CX diagnostic, although modifications of ITER plans continue. Because of the size and densities of the expected ITER plasma, a 50 keV/u He^0 beam would

only penetrate one quarter of the way to the centre of the ITER plasma. Helium beams, of course, also allow a spectroscopic approach (see Ref. [12]). Detection of neutralized alpha particles using neutral helium beams depends on (i) penetration of the neutral helium beam to the point of collision with an alpha particle, (ii) neutralization of the alpha particle by double charge transfer, and (iii) escape of the He^0 from the plasma for measurement. Recent results at JT-60 and JET are given in Refs [9] and [16]. The CX spectroscopy measurement also depends on (i), but (ii) is replaced by single charge transfer, and the emitted photons escape without loss. Neutral particle detection and CX spectroscopy are complementary. Observed CX spectrum lines from slowing down alpha particles (for example He II, $n = 4$–3, $\lambda = 4685$ Å) are expected to be highly distorted owing to Doppler shifts in the line of sight and cross-section effects [17]. The spectrum lines are a measure of the alpha particles at energies of $\lesssim 200$ keV/u. This is because of the unavoidable thermal bremsstrahlung background and the decreasing CX cross-section at high energy. There is an important issue for both diagnostic approaches. The precise beam characteristics and attenuation are essential for quantitative measurements. They are usually evaluated theoretically from the stopping cross-sections and the input beam geometry. However, the helium beam emission spectrum allows a key in situ measurement. For these reasons, beam emission spectroscopy, CX spectroscopy and neutral particle detection are best viewed as mutually supporting diagnostics to be carried out simultaneously in alpha particle measurements.

Charge exchange spectroscopy and beam emission spectroscopy with helium beams are quite new and have some specific problems and opportunities qualitatively different from those of deuterium beams. This is in plasma impurity ion measurements and field measurements distinct from the specific use in fast alpha particle detection as described above. The CX cross-sections in the formation of excited states of hydrogen-like impurity ions allow CX spectroscopy measurements of the impurity ion concentrations. These concentrations must be consistent with the beam attenuation, which is a sensitive function of the impurity content. At the same time the excitation cross-sections of the helium beam atoms in collision with the impurity ions give rise to the beam emission spectrum. The beam emission spectrum of helium includes both singlet and triplet lines and characterizes the ground state and the metastable state beam content as well as the attenuation into the plasma. This is an important issue, since the metastable states $2\,^1S$ and $2\,^3S$ are efficient CX donors to quite highly excited states of impurity ions. A significant metastable content can introduce a large correction to impurity concentrations inferred on the assumption of ground state helium donors. The metastable content of helium beams on entry into the plasma has been the subject of some discussion [18–20]. For a beam formed by He^+ acceleration, neutralized in He^0, $\lesssim 7\%$ seems likely. The differential attenuation of the ground state and the metastable state populations in the plasma and the regeneration of the metastable populations in the plasma are important. The beam emission spectrum can clarify this. Since ion collisions cannot cause a spin change in He^0 by electron exchange, excitation of the triplet side from the singlet side in the plasma must result from electron collisions or from spin system breakdown in higher $n\ell$ shells. For stationary He^0, the spin system breakdown reaches $\sim 50\%$ for $4f\,^1F$ and $4f\,^3F$ (Van den Eynde et al. [21]), but it must be noted that the motional Stark effect perturbs and mixes ℓ-states significantly. This is particularly so for the $n = 4$ and possibly the $n = 3$ levels at beam energies of $\gtrsim 50$ keV/u. Collisional radiative redistribution (and ionization) effects are also pronounced for such levels. Sudden shifts of spectral emission from visible (for example $4\,^1D - 2\,^1P$) to VUV (for example $4\,^1P - 1\,^1S$) wavelengths can occur, depending on the mixing. Thus, the singlet and triplet side emission is diagnostic of magnetic fields, densities and beam energies within the plasma.

3. ASPECTS OF BERYLLIUM AND BORON AND THEIR MEASUREMENT

The sources of beryllium and boron are the surfaces with which the plasma interacts. These are the effective limiters, divertor throats and dump plates, and the vessel walls. The energy and particle fluxes to the surfaces lead to impurity sputtering and release as neutral atoms or molecules which ionize rapidly as they move into the plasma. Subsequently, they return to the surfaces, generally in highly ionized states. Of special interest at this time is the axisymmetric pumped divertor which seeks to entrap and retain impurities and minimize their release. High density, low temperature, strongly radiating conditions in the divertor are required, in the creation of which impurity radiation plays an important role. Species such as beryllium and boron are fully ionized over the bulk of the plasma, occurring as partially ionized atoms only in the edge plasma, i.e. in the peripheral confined plasma and in the unconfined scrape-off layer plasma (see Stangeby and McCracken [22] for a comprehensive review of the edge plasma).

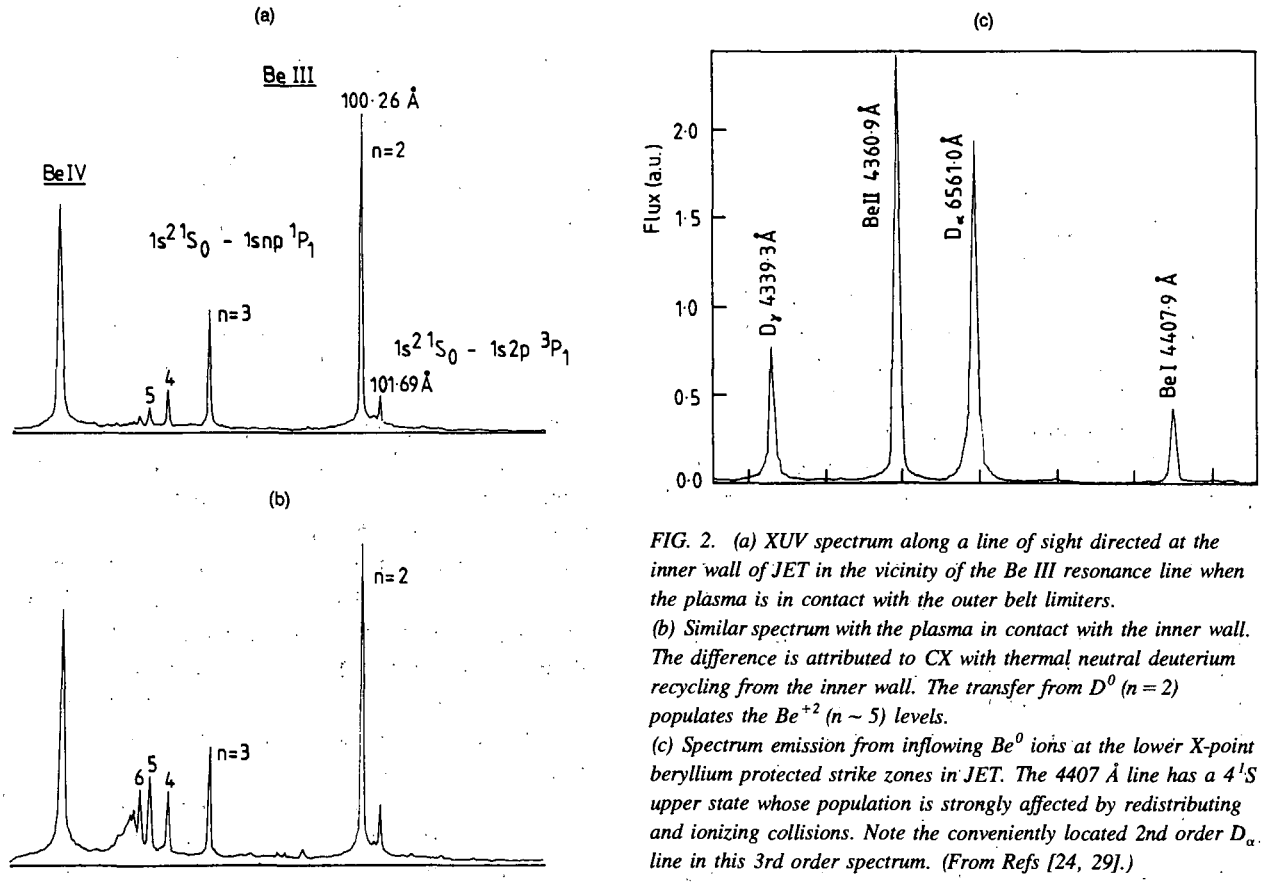

FIG. 2. (a) XUV spectrum along a line of sight directed at the inner wall of JET in the vicinity of the Be III resonance line when the plasma is in contact with the outer belt limiters.
(b) Similar spectrum with the plasma in contact with the inner wall. The difference is attributed to CX with thermal neutral deuterium recycling from the inner wall. The transfer from D^0 ($n = 2$) populates the Be^{+2} ($n \sim 5$) levels.
(c) Spectrum emission from inflowing Be^0 ions at the lower X-point beryllium protected strike zones in JET. The 4407 Å line has a $4\,{}^1S$ upper state whose population is strongly affected by redistributing and ionizing collisions. Note the conveniently located 2nd order D_α line in this 3rd order spectrum. (From Refs [24, 29].)

The neutral and ion population distributions are usually distinguished, since only the latter are tied to the magnetic field. Also the neutral distribution can be markedly non-thermal, reflecting its sputtering or molecular dissociation origin. We can make a further subdivision into populations of beryllium and boron ions in neutral deuterium rich environments and those with low neutral deuterium concentration. The deuterium itself has a number of populations of different velocity distributions and spatial extent, namely molecules, initially dissociated atoms and then the successive CX generations produced in D/D^+ collisions. The low temperature, high density divertor plasma is a region of high neutral deuterium concentration. The relative populations and fluxes of deuterium and impurities are important, and observations of impurities and deuterium are usually linked.

In addition to the edge related populations, there are of course the distinct population distributions of Be^{+3}, and B^{+4} located in the beam penetrated plasma core. Be^{+4} and B^{+5} recombine through CX with D^0 or He^0 in the beams. They are reionized in the beam free region where they form part of the plume populations. Except for these populations, the ionization state of the beryllium and boron ions depends principally on electron collisions (typical edge temperatures are $\lesssim 200$ eV and the divertor plasma near the target plates may be ~ 10 eV). Collisional ionization, radiative and dielectronic recombination are the main processes, although the low ionization stages are generally inflowing in an ionizing environment, so recombination is less important. The metastable state populations, such as $Be^0(2s2p\,{}^3P)$, as well as the ground state populations of the ionization stages must be viewed dynamically. The ionization and recombination of the neutral and singly ionized species are affected by stepwise collisional radiative processes. In the deuterium rich regions the ionization state is modified by CX collisions with neutral deuterium. Ground state deuterium is the principal donor affecting the ionization balance. The radiated power can be very sensitive to this change. For example, at 5 eV $\lesssim T_e \lesssim$ 10 eV, Be^{+2} and B^{+3} are dominant in abundance in an equilibrium plasma, but not radiating. The radiation is by the lithium-like ions Be^{+1} and B^{+2}. Charge exchange enhances the lithium-like stage and the radiated power without changing the dominant ionization stage [23]. Evidently, a generalized collisional-radiative treatment is required to include these points properly in models.

This implies a wide need of good fundamental cross-section data.

Turning to measurement, spectroscopy is the primary tool. Objectives are identification of species, observation of geometrical spread of ionization shells, deduction of fluxes, assessment of metastables and spectrum line based diagnostics of electron and ion temperatures and electron density. Primary measurements are of the resonance lines. At ~ 10 eV, the lithium-like lines Be II, λ = 3131 Å, and B III, λ = 2066 Å, dominate the radiated power, with the helium-like lines at λ ~ 100 Å and ~ 60 Å important at $\gtrsim$ 40 eV. Diagnostic spectroscopy selects additional spectrum lines to identify the contribution of metastable states and to aid deduction of electron temperature and density. There are considerable benefits in visible spectroscopy (principally simple absolute calibration) for studying emission near localized surfaces and this influences the range of atomic data required. Useful visible radiation generally occurs from transitions amongst the n = 3 and n = 4 shells (visible transitions and quartz UV transitions occur to the n = 2 shell in the neutrals) for the impurity ions. Also the upper emitting level must not have an allowed transition to the ground state in order to avoid an unfavourable VUV branch. Thus, excitations of dipole, non-dipole and spin change type are all required up to the n = 4 shells. The low charge states and relatively high density in divertors mean that redistributive collisions also matter. Evidently, the spectral emission requirements and those for the generalized collisional–radiative calculation of ionization and recombination coefficients are closely connected [24]. Calculated local emissivities in specific lines are often expressed in terms of 'photon efficiencies' or 'ionizations per photon', since these allow immediate interpretation of observed signals as impurity fluxes [25]. It should be noted that collisional–radiative effects make the photon efficiencies sensitive to electron density as well as temperature. Electron temperature and density measurements are not readily available in divertor plasma regions and so sensitive line ratios are helpful. In more detailed studies of divertors, calculated local emissivities are incorporated in Monte Carlo models of the impurity ion population distributions for prediction of the detailed emission structure. These models are run in close association with neutral deuterium models [26, 22]. There is particular interest at this time in modification of emission by charge transfer in the deuterium rich environment. Excited deuterium (in the n = 2 or n = 3 shells) is an efficient donor here, especially to the higher n shells of the more highly ionized beryllium and boron ions (see the edge signal observed in CX spectroscopy studies using beams, Refs [27, 28]). Factors which influence the D^0 (n = 2) population are therefore important. In this respect, it is to be noted that the optical depth in the Lyman lines in cool high hydrogen density divertor plasma can become large. The implications are still to be appraised.

4. REQUIRED CROSS-SECTION DATA FOR HELIUM

Only fully ionized low and moderate mass ions in collision with He^0 need to be considered. Of principal importance are the D^+, T^+ fuel and the He^{+2} ash or added minority. Other relevant impurities are due to choices of plasma facing first wall materials, and to deposition and gettering strategies. This gives, in order of importance, C^{+6} (walls, X-point target plates, limiters, carbonization), Be^{+4} (JET X-point target plates, limiters and evaporation) and B^{+5} (boronization). The gettering procedures have reduced the importance of oxygen, but, nonetheless, O^{+8} must be included. Other species are of less concern. Titanium, iron and nickel are possible structural materials, neon and argon are useful added trace gases for diagnostics, and silicon is a possible impurity. A representative set through the second and third period which would act as a basis for interpolation is Ne^{+10}, Si^{+14}, Ar^{+18}, Fe^{+26}.

Concerning the energy ranges of cross-section data, since alpha particles are born by deuterium/tritium fusion at 880 keV/u, this energy sets the upper limit for He^0 ion/atom stopping cross-sections. The lower limit is set by the beam He^0 particles in collision with thermal plasma ions. A beam energy of ~ 30 keV/u (JET ^{4}He beams) and plasma ion temperatures up to 30 keV (15 keV/u for D^+) would properly set ~ 1 keV/u as the lower limit for ion/atom collision cross-sections. For ITER helium beams, which should certainly have particle energies of $\gtrsim$ 50 keV/u, a lower energy limit for cross-sections of ~ 10–20 keV/u is probably acceptable. Electron collisions contribute less to beam stopping. Electron temperatures from 1 keV up to 25 keV at the plasma core are most relevant. However, noting the additional interest of He I plasma edge and divertor emission for helium recycling and the helium inventory, the low energy range should be reduced to a few eV. Given the present state of e/He^0 data, it is appropriate now to recommend cross-sections complete in energy from threshold to infinity.

It is appropriate to make a broad statement of the minimum accuracy requirements in cross-section data,

although more specific assessments are made in later contributions. Typically, detector calibration, window transmission variation, plasma and viewing geometries, spectral feature isolation and uncertainties in temperature and density profiles limit the experimental uncertainty to >40%, so this is the acceptable accuracy for modelling prediction of the final observed quantities. Therefore, in beam driven diagnostics, a 30% error in calculation of beam attenuation and a 30% error in calculation of local particle production coefficients (e.g. He^0 by neutralizing) or photon effective emission coefficients (e.g. by single charge transfer in CX spectroscopy) are acceptable. Beam attenuation up to a factor of ten is typically encompassed in an experiment and, therefore, net stopping cross-sections at <10% accuracy are required. Individual acceptable cross-section tolerances are then in inverse proportion to their contribution. Impurity cross-sections scale at worst as Z^2 and so their acceptable tolerances are in inverse proportion to Z^2 times the fractional impurity abundance. Helium fractional abundance at up to 20% may be expected in fusion plasmas, but experimental test plasmas of pure helium are possible. Carbon and light impurities at <5% are anticipated. The contribution of each impurity to Z_{eff} is a helpful measure of its importance.

In presenting the following information, it has been convenient to allow some repetition of cross-sections so that the different areas can appear complete. A coding, (*1) - (*6), has been used to rank importance, with (*1) the most important. Also, a minimum required accuracy is suggested as a percentage, with an indication of its variation with energy. For beam stopping, the accuracy is based on the proportion of each individual cross-section's contribution and its being the sole source of error. This is of course subject to revision in the light of improvement of our cross-section knowledge and progress in modelling. The least acceptable accuracy is set at 100%. Impurity cross-section accuracies are assessed as though the impurity alone were contributing. A Z_{eff} based adjustment of these, as described above, is appropriate. For electron collisions, taking account of the many experimental measurements and theoretical calculations, a 20% accuracy is suggested as a reasonable aspiration at all energies for important transitions.

4.1. Alpha particle neutralization

This is the essential reaction between beam He^0 and the alpha particle produced by deuterium/tritium fusion which allows the neutral particle diagnostics to probe the alpha particle sources.

He^{+2} neutralization

(*1) $He^0(1\,^1S) + He^{+2} \rightarrow He^{+2} + He^0$: 20%

4.2. Beam and fusion He^0 stopping at low density

Most helium is in its ground state, so that the dominant stopping is by electron loss directly from the ground state. If the plasma density is very low so that excited helium populations are negligible, this is the only pathway.

Ground state single electron loss with primary species and impurities

(*1) $He^0(1\,^1S) + D^+ \rightarrow He^+ + D^+ + e$:
90% at E ~ 20 keV/u, 10% at E > 100 keV/u
(*1) $He^0(1\,^1S) + D^+ \rightarrow He^+ + D^0$:
10% at E ~ 20 keV/u, 40% at E > 100 keV/u
(*1) $He^0(1\,^1S) + He^{+2} \rightarrow He^+ + He^{+2} + e$:
100% at E ~ 20 keV/u, 20% at E > 100 keV/u
(*1) $He^0(1\,^1S) + He^{+2} \rightarrow He^{+1} + He^{+1}$:
20% at E ~ 20 keV/u, 20% at E > 100 keV/u
(*2) $He^0(1\,^1S) + X^{+z} \rightarrow He^+ + X^{+z} + e$:
100% at E ~ 20 keV/u, 50% at E > 100 keV/u
(*2) $He^0(1\,^1S) + X^{+z} \rightarrow He^{+1} + X^{+z-1}$:
10% at E ~ 20 keV/u, 20% at E > 100 keV/u

Note that X^{+z} denotes the fully ionized impurity.

With the data at this stage, an approximate stopping can be obtained. However, improvement at lower beam energies requires the following:

Ground state double electron loss with primary species and impurities

(*2) $He^0(1\,^1S) + D^+ \rightarrow He^{+2} + D^+ + e + e$: 100%
(*2) $He^0(1\,^1S) + D^+ \rightarrow He^{+2} + D^0 + e$: 100%
(*2) $He^0(1\,^1S) + He^{+2} \rightarrow He^{+2} + He^{+2} + e + e$: 100%
(*2) $He^0(1\,^1S) + He^{+2} \rightarrow He^{+2} + He^{+1} + e$: 100%
(*2) $He^0(1\,^1S) + He^{+2} \rightarrow He^{+2} + He^0$:
30% at E ~ 20 keV/u, 100% at E > 100 keV/u
(*3) $He^0(1\,^1S) + X^{+z} \rightarrow He^{+2} + X^{+z} + e + e$:
80% at E ~ 20 keV/u, 40% at E > 100 keV/u
(*3) $He^0(1\,^1S) + X^{+z} \rightarrow He^{+2} + X^{+z-1} + e$:
80% at E ~ 20 keV/u, 40% at E > 100 keV/u
(*3) $He^0(1\,^1S) + X^{+z} \rightarrow He^{+2} + X^{+z-2}$: 100%

Ground state ionization by electron impact

(*2) $He^0(1\,^1S) + e \rightarrow He^+ + e + e$: 20%

4.3. Beam and fusion He^0 stopping at moderate and high density

At plasma densities appropriate to ITER, impact excitation of helium from its ground state to excited states is sufficiently large for the latter populations to be non-negligible. Thus, electron loss from the excited states can occur before return to the ground state. This enhances the stopping. The metastable state ($1s2s\,^1S$ and $1s2s\,^3S$) populations are the most important in this respect, so cross-sections involved in their formation and destruction are of the first priority. Next in importance are other excited state populations up to an effective cut-off principal quantum shell, at which Lorentz electric field or collisional merging to the continuum occurs.

Ground state excitation to the n = 2 shell by primary species and impurities

(*2) $He^0(1\,^1S) + D^+ \rightarrow He^0(2\,^1S, 2\,^1P) + D^+$: 100%
(*2) $He^0(1\,^1S) + He^{+2} \rightarrow He^0(2\,^1S, 2\,^1P) + He^{+2}$: 100%
(*3) $He^0(1\,^1S) + X^{+z} \rightarrow He^0(2\,^1S, 2\,^1P) + X^{+z}$: 100%

Ground state excitation to the n = 2 shell by electrons

(*3) $He^0(1\,^1S) + e \rightarrow He^0(2\,^1S, 2\,^1P, 2\,^3S, 2\,^3P) + e$: 20%

It is to be noted that ion impact excitations are spin system preserving, while electron collisions allow exchange.

n = 2 state single electron loss with primary species, impurities and electrons

(*2) $He^0(2^{2S+1}L) + D^+ \rightarrow He^+ + D^+ + e$: 100%
(*2) $He^0(2^{2S+1}L) + D^+ \rightarrow He^+ + D^0$: 100%
(*2) $He^0(2^{2S+1}L) + He^{+2} \rightarrow He^+ + He^{+2} + e$: 100%
(includes inner electron ionization)
(*2) $He^0(2^{2S+1}L) + He^{+2} \rightarrow He^{+1} + He^{+1}$: 100%
(*3) $He^0(2^{2S+1}L) + X^{+z} \rightarrow He^+ + X^{+z} + e$: 100%
(includes inner electron ionization)
(*3) $He^0(2^{2S+1}L) + X^{+z} \rightarrow He^{+1} + X^{+z-1}$: 100%
(*3) $He^0(2\,^1S, 2\,^1P, 2\,^3S, 2\,^3P) + e \rightarrow He^+ + e + e$: 20%

Redistributive collisions within the n = 2 shell by primary species, impurities and electrons

(*2) $He^0(2^{2S+1}L) + D^+ \rightarrow He^0(2^{2S+1}L') + D^+$: 100%
(*2) $He^0(2^{2S+1}L) + He^{+2} \rightarrow He^0(2^{2S+1}L') + He^{+2}$: 100%
(*3) $He^0(2^{2S+1}L) + X^{+z} \rightarrow He^0(2^{2S+1}L') + X^{+z}$: 100%
(*3) $He^0(2^{2S+1}L) + e \rightarrow He^0(2^{2S'+1}L') + e$: 20%

With the data at this stage, the $2\,^1S$ state populations and enhanced stopping via the singlet side can be obtained approximately. The $2\,^3S$ state population is incorrect and requires the following reactions:

Ground state excitation to the 2 < n ≤ 4 shells by primary species and impurities

(*3) $He^0(1\,^1S) + D^+ \rightarrow He^0(n\,^1L) + D^+$: 100%
(*3) $He^0(1\,^1S) + He^{+2} \rightarrow He^0(n\,^1L) + He^{+2}$: 100%
(*4) $He^0(1\,^1S) + X^{+z} \rightarrow He^0(n\,^1L) + X^{+z}$: 100%

It is to be noted that excitation to $4\,^1F$ opens access to the triplet side through state mixing with $4\,^3F$.

Ground state excitation to the 2 < n ≤ 4 shells by electrons

(*3) $He^0(1\,^1S) + e \rightarrow He^0(n\,^1L, n\,^3L) + e$: 20%

2 < n ≤ 4 state single electron loss with primary species, impurities and electrons

(*3) $He^0(n^{2S+1}L) + D^+ \rightarrow He^+ + D^+ + e$: 100%
(*3) $He^0(n^{2S+1}L) + D^+ \rightarrow He^+ + D^0$: 100%
(*3) $He^0(n^{2S+1}L) + He^{+2} \rightarrow He^+ + He^{+2} + e$: 100%
(includes inner electron ionization)
(*3) $He^0(n^{2S+1}L) + He^{+2} \rightarrow He^{+1} + He^{+1}$: 100%
(*4) $He^0(n^{2S+1}L) + X^{+z} \rightarrow He^+ + X^{+z} + e$: 100%
(includes inner electron ionization)
(*4) $He^0(n^{2S+1}L) + X^{+z} \rightarrow He^{+1} + X^{+z-1}$: 100%
(*4) $He^0(n^{2S+1}L) + e \rightarrow He^+ + e + e$: 20%

Redistributive collisions between 2 ≤ n,n' ≤ 4 shells by primary species, impurities and electrons

(*3) $He^0(n^{2S+1}L) + D^+ \rightarrow He^0(n'^{2S+1}L') + D^+$: 100%
(*3) $He^0(n^{2S+1}L) + He^{+2} \rightarrow He^0(n'^{2S+1}L') + He^{+2}$: 100%
(*4) $He^0(n^{2S+1}L) + X^{+z} \rightarrow He^0(n'^{2S+1}L') + X^{+z}$: 100%
(*4) $He^0(n^{2S+1}L) + e \rightarrow He^0(n'^{2S'+1}L') + e$: 20%

Residual cross-sections up to n = 10 by primary species, impurities and electrons

(*5) $He^0(n) + D^+ \rightarrow He^0(n') + D^+$: 100%
(*5) $He^0(n) + He^{+2} \rightarrow He^0(n') + He^{+2}$: 100%
(*6) $He^0(n) + X^{+z} \rightarrow He^0(n') + X^{+z}$: 100%
(*5) $He^0(n) + e \rightarrow He^0(n') + e$: 20%

Spin system merging and ℓ-subshell mixing is large beyond n = 4, and merging with the continuum by field ionization occurs by n = 10 typically.

4.4. Beam emission spectroscopy

Spectral emission from the beams is an important opportunity for experimental verification of beam attenuation and of the correctness of the enhancements attributed to the finite plasma density. Exploitation of the scope of beam emission spectroscopy dictates that emission from helium excited states up to the n = 4 shell should be modelled carefully. For example, the transitions $4\,^1L - 2\,^1P$ are of particular interest since the forbidden components and the linear Stark shifts are of use for diagnostics. The overall atomic data requirements are the same as for beam stopping at moderate and high density. However, the priority and accuracy for processes populating and depopulating upper states of observable spectrum lines are altered. These are repeated here.

Ground state excitation to the $2 \leq n \leq 4$ shells by primary species and impurities

(*2) $He^0(1\,^1S) + D^+ \rightarrow He^0(n\,^1L) + D^+$: 30%
(*2) $He^0(1\,^1S) + He^{+2} \rightarrow He^0(n\,^1L) + He^{+2}$: 30%
(*2) $He^0(1\,^1S) + X^{+z} \rightarrow He^0(n\,^1L) + X^{+z}$: 30%

Ground state excitation to the $2 \leq n \leq 4$ shells by electrons

(*2) $He^0(1\,^1S) + e \rightarrow He^0(n\,^1L, n\,^3L) + e$: 20%

Initial estimates suggest that $4\,^1L - 2\,^1P$ on the singlet side and $4\,^3L - 2\,^3S$ on the triplet side should be studied experimentally as well as the transitions from the n = 3 shells.

$2 \leq n \leq 4$ stage single electron loss with primary species, impurities and electrons

(*2) $He^0(n^{2S+1}L) + D^+ \rightarrow He^+ + D^+ + e$:
40% at E ~ 20 keV/u, 40% at E > 100 keV/u
(*2) $He^0(n^{2S+1}L) + D^+ \rightarrow He^+ + D^0$: 100%
(*2) $He^0(n^{2S+1}L) + He^{+2} \rightarrow He^+ + He^{+2} + e$:
40% at E ~ 20 keV/u, 40% at E > 100 keV/u
(includes inner electron ionization)
(*2) $He^0(n^{2S+1}L) + He^{+2} \rightarrow He^{+1} + He^+$:
50% at E ~ 20 keV/u, 100% at E > 100 keV/u
(*3) $He^0(n^{2S+1}L) + X^{+z} \rightarrow He^+ + X^{+z} + e$:
40% at E ~ 20 keV/u, 30% at E > 100 keV/u
(includes inner electron ionization)
(*3) $He^0(n^{2S+1}L) + X^{+z} \rightarrow He^+ + X^{+z-1}$: 100%
(*3) $He^0(n^{2S+1}L) + e \rightarrow He^+ + e + e$: 20%

Redistributive collisions between $2 \leq n,n' \leq 4$ shells by primary species, impurities and electrons

(*2) $He^0(n^{2S+1}L) + D^+ \rightarrow He^0(n'^{2S+1}L') + D^+$:
30%
(*2) $He^0(n^{2S+1}L) + He^{+2} \rightarrow He^0(n'^{2S+1}L') + He^{+2}$:
30%
(*3) $He^0(n^{2S+1}L) + X^{+z} \rightarrow He^0(n'^{2S+1}L') + X^{+z}$:
30%
(*3) $He^0(n^{2S+1}L) + e \rightarrow He^0(n'^{2S'+1}L') + e$: 20%

The residual cross-sections of Section 4.3 are again required.

4.5. Charge exchange spectroscopy (CXS)

State selective single electron charge transfer from neutral helium beam atoms in their ground state to alpha particles forming excited states of He^{+1} is the initial concern. Subsequent He II emission, such as n = 4–3 at 4685 Å, is the CXS signal, to be contrasted with the neutral particle analyser signals. There is a further aspect, however, in that neutral helium beams may be usable in CXS for all light impurity densities. Consistency with impurity densities used for modelling beam stopping may then be sought.

State selective charge transfer from ground state to primary species

(*2) $He^0(1\,^1S) + He^{+2} \rightarrow He^+ + He^+(n\ell\,^2L)$: 30%
(*2) $He^0(1\,^1S) + D^+ \rightarrow He^+ + D(n\ell\,^2L)$: 30%

The first is the key reaction for CXS. The second is relevant for formation of the D^0 halo associated with the helium beams. For He, $1 \leq n \leq 6$, and for D, $1 \leq n \leq 4$, are relevant ranges.

State selective transfer ionization from ground state to primary species

(*4) $He^0(1\,^1S) + He^{+2} \rightarrow He^{+2} + He^+(n\ell\,^2L) + e$:
100%
(*4) $He^0(1\,^1S) + D^+ \rightarrow He^{+2} + D(n\ell\,^2L) + e$: 100%

These reactions tend to populate low n shells. They provide a correction of CXS using short wavelength transitions.

State selective charge transfer from metastables to primary species

(*3) $He^0(2\,^1S, 2\,^3S) + He^{+2} \rightarrow He^+ + He^{+1}(n\ell\,^2L)$: 50%
(*3) $He^0(2\,^1S, 2\,^3S) + D^+ \rightarrow He^+ + D(n\ell\,^2L)$: 50%

These reactions are most relevant at low beam energies and to CXS with visible lines, since the dominant receiving n shell is usually close to the line emitting n shell. Expectations for beam metastable populations suggest that this may be a significant correction. For He, $1 \leq n \leq 6$, and for D, $1 \leq n \leq 4$, are relevant ranges. Redistribution and ionizing collisions with the He^+ and D excited populations are required to complete the diagnostic modelling. These are not given explicitly here, since He^0 is the main focus.

State selective charge transfer from ground state and metastables to impurities

(*3) $He^0(1\,^1S) + X^{+z} \rightarrow He^+ + X^{+z-1}(n\ell\,^2L)$: 30%
(*3) $He^0(2\,^1S, 2\,^3S) + X^{+z} \rightarrow He^+ + X^{+z-1}(n\ell\,^2L)$: 50%

This allows a full CXS diagnostic for impurities using helium beams. The relevant range is $1 \leq n \leq 2z^{0.75}$. Redistribution and ionizing collisions with the X^{+z-1} excited populations are required to complete the diagnostic modelling. These are again not given explicitly here.

5. REQUIRED CROSS-SECTION DATA FOR BERYLLIUM AND BORON

5.1. Ionization state

A 20% accuracy is appropriate for all the cross-section data in this section. In recombination data, this accuracy applies to the composite zero density coefficient, that is without collisional radiative losses.

Direct ionization (ground and metastable) by electron impact

(*1) $B^0(2s^2 2p\,^2P) + e \rightarrow B^{+1}(2s^2\,^1S) + e + e$
(*1) $Be^0, B^{+1}(2s^2\,^1S) + e \rightarrow Be^{+1}, B^{+2}(2s^2S) + e + e$
(*1) $Be^{+1}, B^{+2}(2s^2S) + e \rightarrow Be^{+2}, B^{+3}(1s^2\,^1S) + e + e$
(*1) $Be^{+2}, B^{+3}(1s^2\,^1S) + e \rightarrow Be^{+3}, B^{+4}(1s^2S) + e + e$
(*1) $Be^{+3}, B^{+4}(1s^2S) + e \rightarrow Be^{+4}, B^{+5} + e + e$
(*1) $B^0(2s^2 2p\,^2P) + e \rightarrow B^{+1}(2s2p\,^3P) + e + e$
(*1) $B^0(2s2p^2\,^4P) + e \rightarrow B^{+1}(2s^2\,^1S) + e + e$
(*1) $B^0(2s2p^2\,^4P) + e \rightarrow B^{+1}(2s2p\,^3P) + e + e$
(*1) $Be^{+1}, B^{+2}(2s\,^2S) + e \rightarrow Be^{+2}, B^{+3}(1s2s\,^3S) + e + e$
(*1) $Be^{+2}, B^{+3}(1s2s\,^3S) + e \rightarrow Be^{+3}, B^{+4}(1s^2S) + e + e$

Metastable cross-coefficients by electron impact

(*1) $B^0(2s^2 2p\,^2P) + e \leftarrow B^0(2s2p^2\,^4P) + e$
(*1) $Be^0, B^{+1}(2s^2\,^1S) + e \leftarrow Be^0, B^{+1}(2s2p\,^3P) + e$
(*1) $Be^{+2}, B^{+3}(1s^2\,^1S) + e \leftarrow Be^{+2}, B^{+3}(1s2s\,^3S) + e$

Note that the direct coefficients as defined here include transfers from the ground state or the metastable state to excited states of the other spin system and cascade. The required accuracies of separate contributions are in proportion to their part of the total.

Radiative and dielectronic recombination at low density

(*1) $X^{+z}(g, m) + e \rightarrow X^{+z-1}(g', m') + h\nu$

For conciseness, X^{+z} denotes an arbitrary charge state of beryllium or boron. g, m and g′, m′ denote the ground state and the metastable state of the recombining and recombined systems. The specific reactions are not given explicitly, but initial and final states correspond to those in the section on direct ionization. Note that these represent the total zero density coefficients which include the sums over all excited states which cascade to the lowest level of the spin system and include alternative autoionizations. The individual component reactions to excited states are required explicitly for the finite density studies below, and their accuracies should be in proportion to their part of the total. The sums extend to very high n shells, but, there, asymptotic behaviour is well specified. The limits to accuracy are in the low level recombination and correct Auger channel opening.

Charge exchange recombination at low density

(*1) $X^{+z}(g, m) + D(1s) \rightarrow X^{+z-1}(g', m') + D^+$

Note that these are the total zero density coefficients which include the sums over all excited states cascading to the lowest level of the spin system, but they are much more restricted than the dielectronic sums.

Collisional-radiative contributions at finite density

(*2) $X^{+z-1}(g', m') + e \rightarrow X^{+z-1}(\{g,m\}\, n'\ell'^{2S'+1}L') + e\ (n' \leq 4)$: 20%

(*3) $X^{+z-1}(\{g,m\}\, n\ell^{2S+1}L) + e \rightarrow X^{+z-1}(\{g,m\}\, n'\ell'^{2S'+1}L') + e\ (n, n' \leq 4)$: 40%

(*3) $X^{+z-1}(\{g,m\}\, n\ell^{2S+1}L) + e \rightarrow X^{+z}(g,m) + e + e\ (n \leq 4)$: 40%

(*4) $X^{+z-1}(\{g,m\}\, n\ell^{2S+1}L) + e \rightarrow X^{+z-1}(\{g,m\}\, n'\ell'^{2S'+1}L') + e\ (n \leq 4, n' > 4)$: 40%

(*5) $X^{+z-1}(\{g,m\}\, n\ell^{2S+1}L) + e \rightarrow X^{+z-1}(\{g,m\}\, n'\ell'^{2S'+1}L') + e\ (12 > n > 4,\ 12 > n' > 4)$: 100%

(*5) $X^{+z-1}(\{g,m\}\, n\ell^{2S+1}L) + e \rightarrow X^{+z}(g,m) + e + e\ (12 > n > 4)$: 100%

(*5) $X^{+z-1}(\{g,m\}\, n^{2S+1}L) + e \rightarrow X^{+z-1}(\{g,m\}\, n'^{2S'+1}L') + e\ (n \geq 12,\ n' \geq 12)$: 100%

(*5) $X^{+z-1}(\{g,m\}\, n^{2S+1}L) + e \rightarrow X^{+z}(g,m) + e + e\ (n \geq 12)$: 100%

(*5) $X^{+z-1}(\{g,m\}\, n\ell^{2S+1}L) + Z_0 \rightarrow X^{+z-1}(\{g,m\}\, n'\ell'^{2S'+1}L') + Z_0\ (12 > n > 4,\ 12 > n' > 4)$: 100%

(*5) $X^{+z-1}(\{g,m\}\, n^{2S+1}L) + Z_0 \rightarrow X^{+z-1}(\{g,m\}\, n'^{2S'+1}L') + Z_0\ (n \geq 12,\ n' \geq 12)$: 100%

Z_0 denotes fully ionized species. These data are required for the finite density improvement in generalized collisional radiative modelling. They apply also to the sections below and are only repeated if higher accuracy is required. Note the changing angular resolution level on moving to higher n shells. Such $n\ell$ and n bundling while retaining spin systems is an approach of sufficient accuracy. For generalized collisional-radiative recombination and ionization coefficients, the bundle-n approach can be used, for corrections to the direct rates, down to the n = 2 shell and, for corrections to low level emissivities, down to the n = 4 shell. The extension to $n \sim 12$ is necessary for high n shell visible CXS where ℓ-mixing matters. The various possible parent states, denoted by g, m, must be treated as well as the different spin systems.

5.2. Measurement of total power and low resonance lines

(*1) $X^{+z-1}(g', m') + e \rightarrow X^{+z-1}(\{g,m\}\, n'\ell'^{2S'+1}L') + e\ (n' \leq 4)$: 20%

These cross-sections give the dominant spectral line power at zero density. Recombination contributions, which are much smaller, except for the helium-like and hydrogen-like ions at high temperatures, follow from the data in Section 5.1. Note that no distinction between the actual cascade paths need be made in the case of power.

5.3. Visible influx spectroscopy

(*1) $X^{+z-1}(g', m') + e \rightarrow X^{+z-1}(\{g,m\}\, n'\ell'^{2S'+1}L') + e\ (n' \leq 4)$: 20%

(*2) $X^{+z-1}(\{g,m\}\, n\ell^{2S+1}L) + e \rightarrow X^{+z-1}(\{g,m\}\, n'\ell'^{2S'+1}L') + e\ (n, n' \leq 4)$: 30%

This is a repetition of the collisional-radiative part of Section 5.1, but higher accuracy is necessary. These data allow the low level excitation and redistribution part of line emissivities to be obtained. For recombination contributions to emissivities and stepwise collisional radiative losses through higher levels the additional data of Section 5.1 are required. These are appropriate for highly transient and dense plasma conditions.

5.4. Charge exchange spectroscopy

State selective CX into excited shells for influx ions

(*1) $X^{+z}(g, m) + D(1s) \rightarrow X^{z-1}(\{g,m\}\, n\ell^{2S+1}L) + D^+$: 30%

(*1) $X^{+z}(g, m) + D(n = 2, 3) \rightarrow X^{z-1}(\{g,m\}\, n\ell^{2S+1}L) + D^+$: 50%

The redistributive collisional data required in Sections 5.2, 5.3 and 5.4 are the same.

Neutral helium beam induced CX

This is given in Section 4.5.

Neutral deuterium beam induced CX

(*1) $D^0(1s^2S) + X^{+z0} \rightarrow D^+ + X^{+z0-1}(n\ell^2L)$: 30%

X^{+z0} denotes the bare nucleus state of beryllium or boron. This allows a full CXS diagnostic for impurities using deuterium beams. The relevant range is $1 \leq n \leq 2z^{0.75}$. Redistributive collisional data are also required (see Section 4.5).

6. CONCLUSIONS

We have sought to lay down the set of atomic collision cross-section data required to model and support alpha particle diagnostics for ITER and other fusion experiments using neutral helium beams. However, we

have gone further, in that we have also addressed the data required in practice to support and validate such a diagnostic fully by associating it with CXS and with beam emission spectroscopy. We have also laid down the atomic data needs for beryllium and boron in divertor experiments. It is anticipated that the data will form the high quality input to comprehensive excited population, effective ionization and recombination coefficient and effective emissivity coefficient codes in the collisional-radiative sense. There remain some anxieties. As has been mentioned, fast neutral helium atoms in tokamak plasmas will experience a strong $\vec{v} \times \vec{B}$ electric field, establishing a Stark state structure. Whether this can alter the balance of atomic reactions significantly is largely unexplored. Also, assumptions of isotropic averages of collision cross-sections cannot really be sustained. We therefore anticipate some elaboration or at least clarification of these points.

REFERENCES

[1] THOMAS, P.R., J. Nucl. Mater. **176–177** (1990) 3.

[2] WINTER, J., ESSER, H.G., KONEN, L., et al., J. Nucl. Mater. **162–164** (1989) 713.

[3] HOGAN, J.T., HILLIS, D.L., Nucl. Fusion **31** (1991) 2181.

[4] REDI, M.H., COHEN, S.A., SYNAKOWSKI, E.J., Nucl. Fusion **31** (1991) 1689.

[5] JANEV, R.K., LANGER, W.D., EVANS, K., POST, D.E., Elementary Processes in Hydrogen-Helium Plasmas, Springer-Verlag, Berlin (1987).

[6] JANEV, R.K., HARRISON, M.F.A., DRAWIN, H.W., Nucl. Fusion **29** (1989) 109.

[7] SCHWEER, B., MANK, G., POSPIESZCZYK, A., et al., in Controlled Fusion and Plasma Physics (Proc. 18th Eur. Conf. Berlin, 1991), Vol. 15C, Part I, European Physical Society (1991) 361.

[8] MARCUS, F.B., ADAMS, J.M., BARTLETT, D.V., et al., Plasma Phys. Control. Fusion **34** (1992) 1371.

[9] TOBITA, K., KUSAMA, Y., NAKAMURA, H., et al., Nucl. Fusion **31** (1991) 956.

[10] KAMELANDER, G., SIGMAR, D.J., Phys. Scr. **45** (1992) 147.

[11] ERIKSSON, L.-G., HELLSTEN, T., BOYD, D.A., et al., Nucl. Fusion **29** (1989) 87.

[12] SUMMERS, H.P., HELLERMANN, M. von, BREGER, P., et al., Am. Inst. Phys. Conf. Proc. **251** (1991) 111.

[13] FONCK, R.J., DARROW, D.S., JAEHNIG, R.P., Phys. Rev., A **29** (1984) 3288.

[14] JOBES, F.C., REDI, M.H., ROQUEMORE, A.L., et al., Rev. Sci. Instrum. **61** (1990) 2981.

[15] FISHER, R.K., to be published in Rev. Sci. Instrum. (1992).

[16] PETROV, M.P., AFANASYEV, V.I., CORTI, S.A., GONDHALEKAR, A., "Measurement of ICRF driven minority ions in JET", presented at Int. Conf. on Plasma Physics, Innsbruck, 29 June - 3 July 1992, paper 1-46, I-151. KHUDOLEEV, A.V., AFANASYEV, V.I., CORTI, S.A., GONDHALEKAR, A., MAAS, A.C., PETROV, M.P., "Neutral particle analysis in the MeV range in JET", presented at Int. Conf. on Plasma Physics, Innsbruck, 29 June - 3 July 1992, paper 6-2, II-1031.

[17] HELLERMANN, M. von, MANDL, W., SUMMERS, H.P., et al., Plasma Phys. Control. Fusion **33** (1991) 1805.

[18] GILBODY, H.B., DUNN, K.F., BROWNING, R., LATIMER, C.J., J. Phys., B **4** (1971) 800; McCULLOUGH, R.W., GOFFE, T.V., GILBODY, H.B., J. Phys., B **11** (1978) 2333.

[19] TOBITA, K., ITOH, T., SAKASAI, A., et al., Plasma Phys. Control. Fusion **32** (1990) 429.

[20] HEMSWORTH, R., TRAYNOR, N., Int. Rep. JET-DN-(90)86, JET Joint Undertaking, Abingdon, Oxfordshire (1990); HOEKSTRA, R., de HEER, F.J., MORGENSTERN, R., personal communication, 1991.

[21] VAN DEN EYNDE, R.K., WEIBES, G., NIEMEYER, T., Physica **59** (1972) 401.

[22] STANGEBY, P.C., McCRACKEN, G.M., Nucl. Fusion **30** (1990) 1225.

[23] HELLERMANN, M. von, SUMMERS, H.P., to be published in Rev. Sci. Instrum. (1992).

[24] SUMMERS, H.P., DICKSON, W.J., BOILEAU, A., et al., Plasma Phys. Control. Fusion **34** (1991) 325.

[25] BEHRINGER, K., SUMMERS, H.P., DENNE, B., FORREST, M., STAMP, M.F., Plasma Phys. Control. Fusion **31** (1989) 2059.

[26] KEILHACKER, M., SIMONINI, R., TARONI, A., WATKINS, M.L., Nucl. Fusion **31** (1991) 535.

[27] BOILEAU, A., HELLERMANN M. von, HORTON, L.D., SPENCE, J., SUMMERS, H.P., Plasma Phys. Control. Fusion **31** (1989) 779.

[28] MATTIOLI, M., PEACOCK, N.J., SUMMERS, H.P., DENNE, B., HAWKES, N.C., Phys. Rev., A **40** (1989) 3886.

[29] SUMMERS, H.P., THOMAS, P., GIANNELLA, R., et al., Z. Phys. D, Suppl. **21** (1991) S17.

EXCITATION OF NEUTRAL HELIUM BY ELECTRON IMPACT

F.J. de HEER[1], R. HOEKSTRA[2], A.E. KINGSTON[3], H.P. SUMMERS
JET Joint Undertaking,
Abingdon, Oxfordshire,
United Kingdom

ABSTRACT. Experimental data for electron impact excitation of neutral helium in its ground state are reviewed critically. A preferred dataset is established and combined with theoretical close coupling approximation data below the ionization threshold and Born approximation data at high energy. Results are presented in figures and tables. Maxwell averaged collision strengths are also tolerated.

1. INTRODUCTION

A new assessment of electron impact cross-section data for excitation of helium from the $1\,^1S$ state is presented. This study was initiated in view of the expected use of $^3He^0$ and $^4He^0$ neutral heating beams on the JET tokamak. It is now motivated and sustained by the actuality of their use in the 1991 experimental campaign. The resulting new observations of charge exchange spectra, beam emission spectra, and thermal and recycling helium emission are of sufficient diagnostic quality to justify detailed atomic modelling of the effective emission and beam stopping processes. The studies are very relevant to the behaviour of slowing down alpha particles and helium ash in planned D/T fusion machines such as ITER and to beam based diagnostics of such plasmas.

Practically, the principal new contribution in this paper is the linkage of recent 29-state R-matrix calculations at low energies to reappraised experimental data at medium energies, and to the merging with asymptotic high energy behaviour.

The assessment of the data presented here must be seen as a continuation and revision of previous compilations of experimental and theoretical data [1–4]. The previous work also contains theoretical cross-sections for excitation from helium $2\,^1S$ and $2\,^3S$ metastable states. Compilation and analysis of the JET database for the metastables is still in progress and will be reported later.

The data are presented in the form of figures and tables of collision strengths Ω and Maxwell averaged rate parameters γ.

Permanent affiliations:
[1] FOM-Institute for Atomic and Molecular Physics, Amsterdam, The Netherlands.
[2] Kernfysisch Versneller Instituut, Groningen, The Netherlands.
[3] Department of Applied Mathematics and Theoretical Physics, The Queen's University of Belfast, Belfast, Northern Ireland, United Kingdom.

For a transition from an initial state i to a final higher excited state j, we have

$$\Omega_{ij} = w_i \left(\frac{E_i}{I_H}\right) \frac{\sigma_{i-j}}{\pi a_0^2}$$

where w_i is the statistical weight of the initial state i of the atom, σ_{i-j} is the excitation cross-section, and E_i is the energy of the free projectile electron with the atom in the initial state i. The Maxwell averaged rate parameter is

$$\gamma_{ij} = \int_0^\infty \Omega_{ij}(E_j) \exp(-E_j/kT_e)\, d(E_j/kT_e)$$

where E_j is the energy of the free electron, with the atom in the final state j, and T_e is the electron temperature. The other notation is conventional.

2. THEORETICAL DATA

Over the last ten years, the Queen's University group has conducted a series of R-matrix calculations of increasing complexity on neutral helium, culminating in the present 29-state study [5]. It is a low speed coupled calculation including all 29 terms of the n = 1–5 principal quantum shells. The successive calculations, for example for 19 states and 29 states, show excellent convergence of the detailed resonance structure associated with the various n-shell series. This is illustrated in Fig. 1 for the $1\,^1S - 2\,^1S$ transition. However, since the calculations do not include a complete representation of the omitted higher states and continuum states, the results are in error near and above the ionization threshold. This representation is analogous to that examined in detail for the H + e systems. Cross-sections above the ionization threshold (particularly for excitation to higher n-shells, ≥ 3) may be overestimated by factors of ≤ 2. The 29-state calculations have been executed at energies below the ionization threshold and are suitable for providing the low energy extension

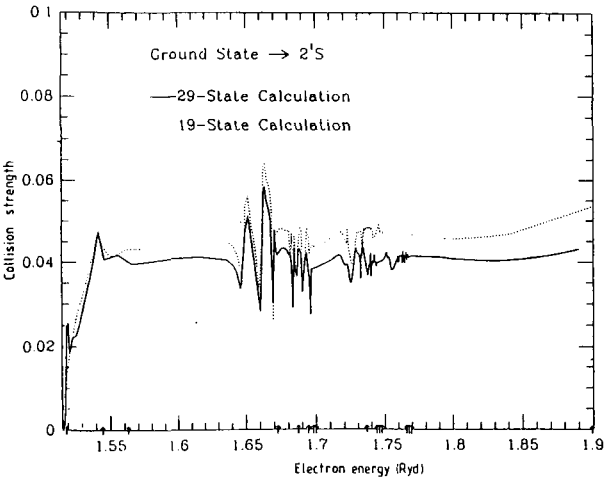

FIG. 1. Collision strength Ω versus electron impact energy from R-matrix calculations for the $1\,^1S - 2\,^1S$ excitation.

of the existing substantial body of experimental data above the ionization threshold. In the present investigation, the R-matrix data have to be merged with experimental measurements of energy resolution less than those of the resonance structure, and then quadratures have to be performed over appropriate Maxwellian (or in some cases non-Maxwellian) distribution functions. It is therefore appropriate to form interval averages, and it is these which are presented in the following figures and tabulations of collision strengths. Note also that adjustment is required for the differences between the theoretical bound state energies as used in the R-matrix codes and the exact observed energies. Conservatively, we have used R-matrix data up to the n = 4 shell only, since the n = 5 shell may be more strongly influenced by truncation.

At high energies, for non-spin changing transitions, the exact excitation cross-sections are expected to converge on those calculated in the first Born approximation. The accurate non-relativistic Born calculations of Bell et al. [6] are used to define the high energy limiting behaviour. Spin changing transitions are assumed to follow the $1/E^3$ behaviour suggested by Ochkur [7]. No precise high energy spin change calculations have been used in this work, but simply an extension of experimental data with the Ochkur slope.

3. EXPERIMENTAL DATA

The excitation cross-sections of the JET database are based on experiment in the region of about 30–2000 eV electron impact energy for singlet excitation, merging into the theoretical first Born cross-sections [6], and up to less high impact energies for triplet excitation, because the cross-section becomes very small and, according to the Ochkur approximation [7], decreases with the incident electron energy E as E^{-3}. Below 30 eV, an extrapolation is made towards the close coupling (29-states R-matrix) calculations [8] from the threshold up to the ionization energy of helium. Except for the metastable $2\,^1S$ and $2\,^3S$ states, most experimental data are from the photon emission cross-section measurements reviewed by Heddle and Gallagher [9]. For metastables the (integrated) cross-sections have been obtained by several groups, by making use of their angular differential scattering cross-sections for inelastic (energy loss selected) scattering of electrons (many of these data were reviewed by de Heer and Jansen [10]). Excitation of and cascade from $^{1,3}F$ levels have not been considered.

The following points are typical for the experimental data:

- Similarity in the σ or Ω dependence on E in a term series where the values are not too close to the threshold. The cross-section ratios at some sufficiently large value of E are equal to those in the first order (Born) theory. (For high principal quantum number n, $\sigma(n^*) \sim n^{*-3}$, with n^* being the effective principal quantum number.)
- At high energy, Ω becomes constant for non-spin changing optical forbidden transitions, i.e. $1\,^1S - n\,^1S$ and $1\,^1S - n\,^1D$.
- At high energies, $\Omega = \frac{4}{3} S_n \ln c_n E$ for optically allowed transitions, where c_n is a constant following from the first order Born theory and S_n is the optical line strength for the relevant $1\,^1S - n\,^1P$ transition.
- At high energies, cross-sections for spin forbidden transitions, $1\,^1S - n\,^3L$, become very small and, according to the Ochkur approximation [7], should decrease as E^{-3}.
- The main maximum in the cross-section is around 100 eV for $n\,^1P$ states, between 42 and 46 eV for $n\,^1D$ states, between 32 and 37 eV for $n\,^1S$ states, and between 26 and 30 eV for triplet states (see Ref. [11]).

The errors are generally smallest for *singlet states* (optical measurements) above about 40 eV, i.e. ~10%, and merge well into the theoretical Born cross-sections between 500 and 2000 eV (dependent on the azimuthal quantum number ℓ) claimed to be within 5%. Only for the $n\,^1D$ states is it necessary to choose a set of data that is different from those given by Heddle and

Text continued on page 26

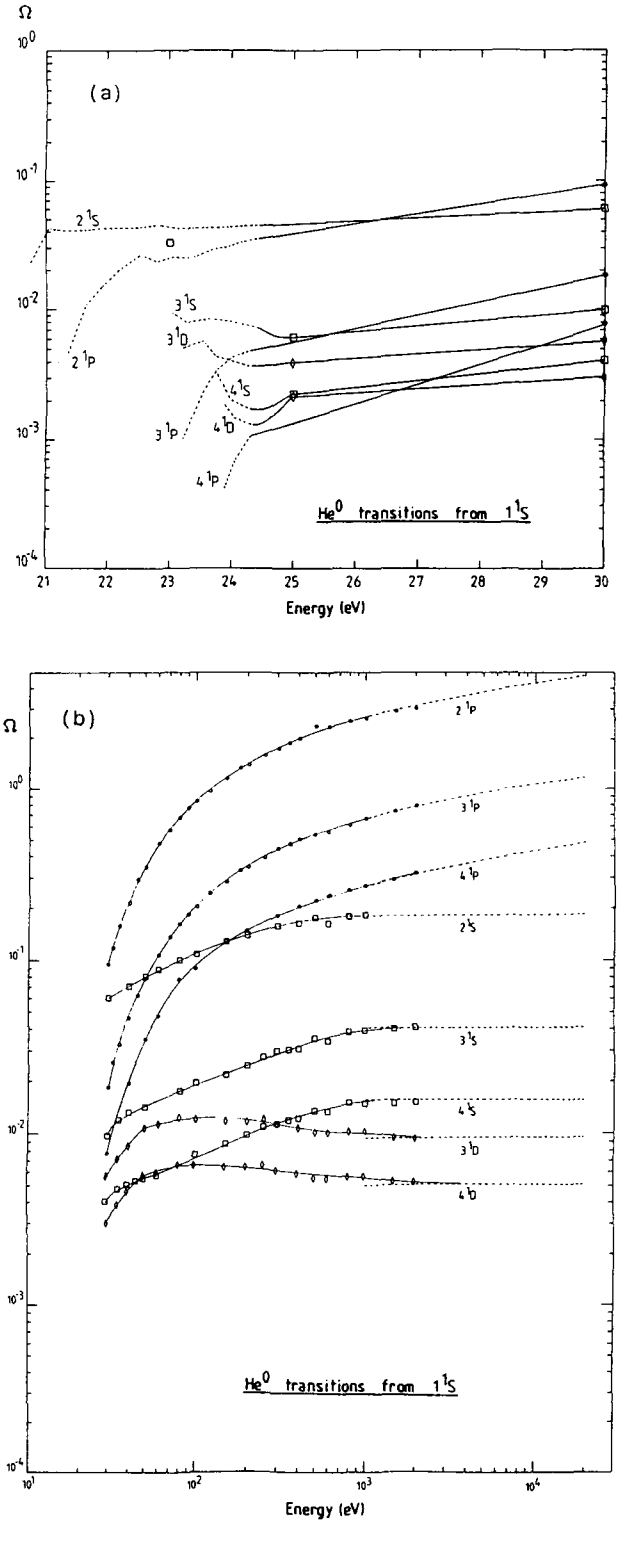

FIG. 2. Collision strengths versus electron impact energy for $1\,^1S - n\,^1L$ excitations (□ — $n\,^1S$, ○ — $n\,^1P$, ◇ — $n\,^1D$). (a) Low energy region up to 30 eV, showing the matching of experimental and R-matrix data. (b) Region above 30 eV, marking the experimental points (squares for s states, circles for p states), the preferred curves (solid lines) and the Born approximation (dotted lines).

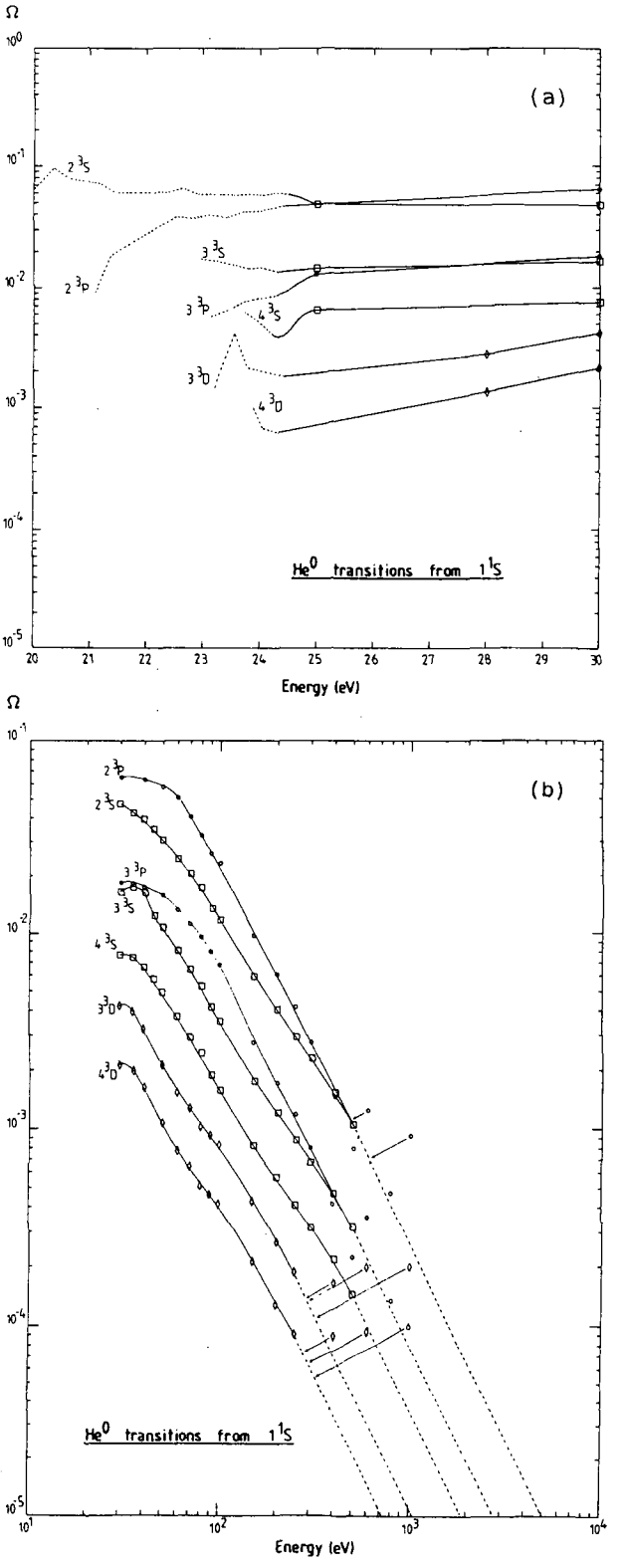

FIG. 3. Collision strengths versus electron impact energy for $1\,^1S - n\,^3L$ excitations (□ — $n\,^3S$, ○ — $n\,^3P$, ◇ — $n\,^3D$). (a) Low energy region up to 30 eV, showing the matching of experimental and R-matrix data. (b) Region above 30 eV, marking the experimental points (squares for s states, circles for p states), the preferred curves (solid lines) and extrapolations at higher energies, decreasing according to the Ochkur [7] approximation as E^{-2}.

TABLE I. PRIMARY CHOICES OF EXPERIMENTAL DATA AND ASSESSMENTS OF THE ACCURACY OF THE CROSS-SECTIONS OVER THE VARIOUS ENERGY INTERVALS

(a) $e + He(1\,^1S) \rightarrow e + He(n\,^1S)$

Excited state	Energy range	Method	Refs	Accuracy
$2\,^1S$	≤ 24.58 eV	R-matrix, 29-state close coupling	Berrington et al. [8]	<10%
	$30 \leq E \leq 100$ eV	Differential scattering integrated	Trajmar [12], Hall [13], Crooks [14]	~30%
	23 eV	Experiment, retarding potential difference	Brongersma et al. [15]	~30%
	$200 \leq E \leq 700$ eV	Differential scattering integrated	Dillon and Lassettre [16]	30-10%
$n\,^1S$ (n = 3, 4, 5, 6)	≤ 24.58 eV	R-matrix, 29-state close coupling up to n = 4	Berrington et al. [8]	<10%
	<50 eV	Optical experiment	Van Raan et al. [17], Zapesochnyi and Feltsan [18], normalized	30-10%
	50-2000 eV	Optical experiment benchmark	Van Zyl et al. [19] (Moussa et al. [20])	<10%
	>1000 eV	Born	Bell et al. [6]	

(b) $e + He(1\,^1S) \rightarrow e + He(n\,^1P)$

Excited state	Energy range	Method	Refs	Accuracy
$n\,^1P$ ($n < 4$)	≤ 24.58 eV	R-matrix, 29-state close coupling	Berrington et al. [8]	<10%
	30-2000 eV	Optical experiment	Westerveld et al. [21]	<10%
	>500 eV	Born	Bell et al. [6]	<5%
$4\,^1P$	≤ 24.58 eV	R-matrix, 29-state close coupling	Berrington et al. [8]	<10%
	40-3000 eV	Optical experiment	de Jongh [22], series III	<10%
	>500 eV	Born	Bell et al. [6]	<5%
$n\,^1P$	All energies	Optical experiment, empirical, analytical	Shemansky et al. [23]	
	30-2000 eV	Optical experiment	Donaldson et al. [24]	

TABLE I. (cont.)

(c) $e + He(1\,^1S) \rightarrow e + He(n\,^1D)$

Excited state	Energy range	Method	Refs	Accuracy
$4\,^1D$	≤24.58 eV	R-matrix, 29-state close coupling	Berrington et al. [8]	<10%
	50–100 eV	Optical experiment	Moussa et al. [20]	<20%
	≤50 eV	Optical experiment	Zapesochnyi and Feltsan [18], normalized	~30%
	100–2000 eV	Optical experiment	Van Raan et al. [17], normalized	<30%
	≥2000 eV	Born	Bell et al. [6]	<10%
$5\,^1D$	50–100 eV	Optical experiment	Moussa et al. [20]	<20%
	≤50 eV	Optical experiment	Zapesochnyi and Feltsan [18], normalized	~30%
	100–2000 eV	Optical experiment	Van Raan et al. [17], normalized	<30%
	≥2000 eV	Born	Bell et al. [6]	<10%
$3\,^1D$	≤24.58 eV	R-matrix, 29-state close coupling	Berrington et al. [8]	<10%
	80–100 eV	Optical experiment	Moussa et al. [20], adjusted by 1/15	<20%
	50–80 eV	$\sigma(4\,^1D)/1.9$		<20%
	≤50 eV	Optical experiment	Zapesochnyi and Feltsan [18], normalized	~30%
	100–2000 eV	$\sigma(4\,^1D)/1.82$		~30%
	≥2000 eV	Born	Bell et al. [6]	<10%
$6\,^1D$	≤2000 eV	$\sigma(5\,^1D)/1.72$		~30%
	≥2000 eV	Born	Bell et al. [6]	<10%

(d) $e + He(1\,^1S) \rightarrow e + He(n\,^3S)$

Excited state	Energy range	Method	Refs	Accuracy
$4\,^3S$	≤24.50 eV	R-matrix, 29-state close coupling	Berrington et al. [8]	<10%
	25–100 eV	Optical experiment	Van Raan et al. [17]	~30%
	100–500 eV	Optical experiment	Van Raan et al. [25], adjusted (×1.15)	≥30%
$2\,^3S$	<24.58 eV	R-matrix, 29-state close coupling	Berrington et al. [8]	<10%
	20–100 eV	Differential scattering integrated, retarding potential difference	Trajmar [12], Hall et al. [13], Crooks [14], Brongersma et al. [15]	~30%
	≥100 eV	$\sigma(4\,^3S)/0.14$		Uncertain
$3\,^3S$	<24.58 eV	R-matrix, 29-state close coupling	Berrington et al. [8]	<10%
	All energies	Interpolated between $\sigma(2\,^3S)$ and $\sigma(4\,^3S)$		
	30–100 eV			~30%
	>100 eV			Uncertain

Note: Johnston and Burrow [26] in their electron trap experiment find the peak for $2\,^3S$ at 20.35 eV to be 6.2×10^{-18} cm^2.

TABLE I. (cont.)

(e) $e + He(1\,^1S) \rightarrow e + He(n\,^3P)$

Excited state	Energy range	Method	Refs	Accuracy
$2\,^3P$	≤24.50 eV	R-matrix, 29-state close coupling	Berrington et al. [8]	<10%
	30–100 eV	Optical experiment, differential scattering integrated	Jobe and St. John [27], cascade corrected by de Heer and Jansen [10], Trajmar [12], Hall et al. [13], Crooks [14]	~30%
	>100 eV	Extrapolation $\sigma(2\,^3P) = 3.5 \times \sigma(3\,^3P)$		>30%
$3\,^3P$	≤24.58 eV	R-matrix, 29-state close coupling	Berrington et al. [8]	<10%
	≤40 eV	Optical experiment	Zapesochnyi and Feltsan [13], normalized	~30%
	40–100 eV	Optical experiment	Van Raan et al. [17]	~30%
	100–1500 eV	Optical experiment	Van Raan et al. [25], adjusted (×1.58)	>30%

Note: Not analysed data of Bogdanova and Yurgenson [28], and of Chutjian and Thomas [29].

(f) $e + He(1\,^1S) \rightarrow e + He(n\,^3D)$

Excited state	Energy range	Method	Refs	Accuracy
$4\,^3D$	≤24.50 eV	R-matrix, 29-state close coupling	Berrington et al. [8]	<10%
	25–35 eV	Optical experiment	Zapesochnyi and Feltsan [18], normalized	~30%
	35–100 eV	Optical experiment	McConkey and Woolsey [30]	~30%
	100–1000 eV	Optical experiment	Van Raan et al. [25], normalized	>30%
$3\,^3D$	≤24.58 eV	R-matrix, 29-state close coupling	Berrington et al. [8]	<10%
	<100 eV	$\sigma(3\,^3D) = 2\sigma(4\,^3D)$		~factor 2
	100–1000 eV	$\sigma(3\,^3D) = 2\sigma(4\,^3D)$		≥factor 2

Note: For $3\,^3D$ see also the theoretical work of Tully [31].

TABLE II. INTERVAL AVERAGED COLLISION STRENGTHS FROM THE 29-STATE R-MATRIX CALCULATIONS

(a) 29-state R-matrix, $1\,^1S - n\,^1S$ interval, averaged collision strengths

E (eV)	$2\,^1S$	E (eV)	$3\,^1S$	E (eV)	$4\,^1S$
2.08^1	2.23^{-2}	2.31^1	9.29^{-3}	2.38^1	3.22^{-3}
2.11^1	4.22^{-2}	2.34^1	8.01^{-3}	2.40^1	2.02^{-3}
2.13^1	4.06^{-2}	2.37^1	8.54^{-3}	2.43^1	1.76^{-3}
2.16^1	4.09^{-2}	2.40^1	8.19^{-3}		
2.19^1	4.24^{-2}	2.41^1	7.76^{-3}		
2.22^1	4.30^{-2}	2.44^1	7.41^{-3}		
2.25^1	4.27^{-2}				
2.28^1	4.53^{-2}				
2.31^1	4.24^{-2}				
2.34^1	4.24^{-2}				
2.37^1	4.32^{-2}				
2.39^1	4.35^{-2}				
2.42^1	4.51^{-2}				
2.45^1	4.51^{-2}				

(b) 29-state R-matrix, $1\,^1S - n\,^1P$ interval, averaged collision strengths

E (eV)	$2\,^1P$	E (eV)	$3\,^1P$	E (eV)	$4\,^1P$
2.13^1	4.64^{-3}	2.32^1	1.00^{-3}	2.39^1	4.03^{-4}
2.17^1	1.10^{-2}	2.36^1	2.42^{-3}	2.41^1	6.71^{-4}
2.19^1	1.54^{-2}	2.38^1	3.48^{-3}	2.43^1	1.07^{-3}
2.22^1	2.03^{-2}	2.40^1	4.37^{-3}		
2.25^1	2.63^{-2}	2.43^1	4.87^{-3}		
2.28^1	2.35^{-2}				
2.31^1	2.56^{-2}				
2.34^1	2.50^{-2}				
2.37^1	2.91^{-2}				
2.40^1	3.05^{-2}				
2.42^1	3.31^{2}				
2.45^1	3.56^{-2}				

(c) 29-state R-matrix, $1\,^1S - n\,^1D$ interval, averaged collision strengths

E (eV)	$3\,^1D$	E (eV)	$4\,^1D$
2.32^1	5.12^{-3}	2.39^1	1.88^{-3}
2.36^1	5.77^{-3}	2.41^1	1.50^{-3}
2.38^1	4.31^{-3}	2.43^1	1.33^{-3}
2.40^1	4.14^{-3}		
2.43^1	3.69^{-3}		

(d) 29-state R-matrix, $1\,^1S - n\,^3S$ interval, averaged collision strengths

E (eV)	$2\,^3S$	E (eV)	$3\,^3S$	E (eV)	$4\,^3S$
2.00^1	6.27^{-2}	2.30^1	1.72^{-2}	2.37^1	6.23^{-3}
2.03^1	9.67^{-2}	2.32^1	1.67^{-2}	2.40^1	5.06^{-3}
2.06^1	7.80^{-2}	2.36^1	1.53^{-2}	2.43^1	4.00^{-3}
2.09^1	7.40^{-2}	2.38^1	1.43^{-2}		
2.12^1	7.21^{-2}	2.41^1	1.47^{-2}		
2.15^1	6.11^{-2}	2.43^1	1.34^{-2}		
2.18^1	6.02^{-2}				
2.21^1	6.06^{-2}				
2.24^1	6.04^{-2}				
2.26^1	6.68^{-2}				
2.29^1	5.88^{-2}				
2.32^1	5.87^{-2}				
2.35^1	5.76^{-2}				
2.38^1	5.84^{-2}				
2.41^1	5.75^{-2}				
2.43^1	5.98^{-2}				
2.46^1	5.78^{-2}				

(e) 29-state R-matrix, $1\,^1S - n\,^3P$ interval, averaged collision strengths

E (eV)	$2\,^3P$	E (eV)	$3\,^3P$	E (eV)	$4\,^3P$
2.11^1	9.07^{-3}	2.31^1	5.73^{-3}	2.38^1	2.25^{-3}
2.14^1	1.87^{-2}	2.35^1	6.59^{-3}	2.40^1	2.14^{-3}
2.17^1	2.29^{-2}	2.37^1	7.58^{-3}	2.43^1	2.41^{-3}
2.19^1	2.69^{-2}	2.40^1	8.12^{-3}		
2.22^1	3.18^{-2}	2.43^1	8.48^{-3}		
2.26^1	3.84^{-2}				
2.28^1	3.70^{-2}				
2.31^1	3.93^{-2}				
2.34^1	3.79^{-2}				
2.38^1	4.21^{-2}				
2.40^1	4.21^{-2}				
2.42^1	4.46^{-2}				
2.45^1	4.66^{-2}				

(f) 29-state R-matrix, $1\,^1S - n\,^3D$ interval, averaged collision strengths

E (eV)	$2\,^3D$	E (eV)	$4\,^3D$
2.32^1	1.45^{-3}	2.39^1	9.85^{-4}
2.36^1	4.10^{-3}	2.41^1	6.79^{-4}
2.38^1	2.12^{-3}	2.43^1	6.33^{-4}
2.40^1	2.01^{-3}		
2.43^1	1.80^{-3}		

Gallagher [9] above 1000 eV, in order to have a better fit with the Born data, and therefore the error might not be 10% but <30% for these states. At low energies (<40 eV), the error may increase up to about 30%. For the $2\,^1S$ data (not optical) there is a problem. The cross-section ratio, which is usually almost constant in a term series above about 50 eV and equal to the Born ratio, increases for $\sigma(2\,^1S)/\sigma(3\,^1S)$ from 4.44 (Born at 1000 eV) to 5.98 (experiment at 100 eV). Therefore, the $2\,^1S$ data towards 100 eV may be considered as an upper limit, with an increased error of up to ~30%. This accuracy may also persist to lower energies.

Errors in the triplet state cross-sections are generally relatively large, because, in particular at high energies, secondary effects, such as collisional transfers, are difficult to eliminate in experiment. The effect is largest for $n\,^3D$ states. The various theories (distorted waves, Born, Oppenheimer, Ochkur, etc.) sometimes give no unique results. Some experimental data were missing (i.e. for $3\,^3S$) or showed severe scatter (i.e. for $3\,^3D$) and were estimated via cross-section ratios in the term series. Generally, below 100 eV the error is ~30% for all triplet levels, although for $3\,^3D$ it may be somewhat worse. Above 100 eV, there is an increasing uncertainty, and our choice, which often follows experiment (deviating from $\sigma \sim E^{-3}$), may be considered somewhat arbitrary. More experimental and theoretical study and analysis is needed in this region. Because these cross-sections become very small at higher energies, the impact on the beam stopping and the beam diagnostics will be small.

TABLE III. ASSESSED EXPERIMENTAL DATA

(a) Experimental $1\,^1S - n\,^1S$ collision strengths and collision strength ratios of (n)/(n + 1)

E (eV)	$2\,^1S$	(2)/(3)	$3\,^1S$	(3)/(4)	$4\,^1S$	(4)/(5)	$5\,^1S$	(5)/(6)	$6\,^1S$
2.30[1]	3.36^{-2}								
2.50[1]			6.06^{-3}	2.67	2.28^{-3}	2.66	8.56^{-4}	2.16	3.97^{-4}
3.00[1]	6.02^{-2}	6.13	9.80^{-3}	2.41	4.06^{-3}	2.31	1.76^{-3}	1.95	9.02^{-4}
3.50[1]			1.20^{-2}	2.48	4.83^{-3}	2.18	2.21^{-3}	1.91	1.16^{-3}
4.00[1]	7.05^{-2}	5.34	1.32^{-2}	2.50	5.08^{-3}	2.12	2.40^{-3}	1.89	1.27^{-3}
4.50[1]					5.38^{-3}	2.10	2.56^{-3}		
5.00[1]	8.10^{-2}	5.75	1.41^{-2}	2.53	5.56^{-3}	2.07	2.68^{-3}	1.89	1.42^{-3}
6.00[1]	8.87^{-2}				5.66^{-3}	2.14	2.65^{-3}	1.88	1.42^{-3}
8.00[1]	1.00^{-1}	5.74	1.74^{-2}	2.74	6.36^{-3}	2.22	2.86^{-3}	1.88	1.55^{-3}
1.00[2]	1.09^{-1}	5.79	1.95^{-2}	2.57	7.57^{-3}	2.46	3.50^{-3}*	1.88	1.86^{-3}
1.50[2]	1.29^{-1}	5.98	2.16^{-2}	2.46	8.76^{-3}	2.12	4.14^{-3}	1.98	2.08^{-3}
2.00[2]	1.40^{-1}	5.75	2.44^{-2}	2.46	9.89^{-3}	2.11	4.70^{-3}	2.01	2.34^{-3}
2.50[2]			2.74^{-2}	2.51	1.09^{-2}	2.09	5.22^{-3}	1.90	2.74^{-3}
3.00[2]	1.59^{-1}	5.31	2.98^{-2}	2.63	1.13^{-2}	1.96	5.79^{-3}	1.98	2.93^{-3}
3.50[2]			3.01^{-2}	2.56	1.18^{-2}	1.97	5.99^{-3}	1.95	3.07^{-3}
4.00[2]	1.64^{-1}	5.34	3.06^{-2}	2.53	1.21^{-2}	1.97	6.15^{-3}	1.93	3.18^{-3}
5.00[2]	1.77^{-1}	5.00	3.53^{-2}	2.59	1.36^{-2}	2.06	6.60^{-3}	1.86	3.55^{-3}
6.00[2]	1.62^{-1}	4.79	3.39^{-2}	2.57	1.32^{-2}	1.94	6.82^{-3}	1.82	3.74^{-3}
8.00[2]	1.79^{-1}	4.68	3.82^{-2}	2.53	1.51^{-2}	2.15	7.02^{-3}	1.88	3.74^{-3}
1.00[3]	1.81^{-1}	4.68	3.87^{-2}	2.63	1.47^{-2}	2.04	7.20^{-3}	1.80	4.00^{-3}
1.50[3]			3.94^{-2}	2.66	1.48^{-2}	1.96	7.56^{-3}	1.82	4.16^{-3}
2.00[3]			4.09^{-2}	2.70	1.51^{-2}	2.02	7.47^{-3}	1.86	4.03^{-3}

* Benchmark adjusted.

4. RESULTS

Figure 2 shows the non-spin changing collision strengths from the $1\,^1S$ state. Figure 2(a) is for the low energy region up to 30 eV, giving the matching of experimental and R-matrix data. Figure 2(b) is for the region above 30 eV, marking the experimental points, the preferred curves (solid lines) and the Born approximation (dotted lines). Figures 3(a) and 3(b) show the equivalent results for the spin changing collision strengths for $1\,^1S - n\,^3L$.

Table I summarizes the primary choices of experimental data together with assessments of the accuracy of the cross-sections over the various energy intervals. Table II contains the interval averaged collision strengths from the 29-state R-matrix calculations. The averaging is over approximately 0.02 Rydbergs. Table III gives the assessed experimental data, and Table IV presents the familiar Born results at high energy for completeness. Table V gives the Maxwell averaged collision strengths over an extended range of temperature. Since the detailed behaviour of the collision strength at the threshold is not available, it has been assumed to be linear in the threshold energy to the first tabulated point. The uncertainty associated with this is estimated to be $\leq 20\%$ at 1 eV and $\leq 1\%$ at 10 eV. A correction is introduced for the integral from the last tabulated point to infinity according to the transition type.

TABLE III. (cont.)

(b) Experimental $1\,^1S - n\,^1P$ collision strengths and collision strength ratios of (n)/(n + 1)

E (eV)	$2\,^1P$	(2)/(3)	$3\,^1P$	(3)/(4)	$4\,^1P$
3.00^1	9.40^{-2}	5.07	1.85^{-2}	2.39	7.77^{-3} [a]
3.20^1	1.18^{-1}	4.66	2.54^{-2}		
3.50^1	1.59^{-1}	4.89	3.25^{-2}		
4.00^1	2.15^{-1}	4.66	4.61^{-2}	2.36	1.96^{-2}
4.50^1	2.90^{-1}	4.64	6.24^{-2}		
5.00^1	3.43^{-1}	4.46	7.69^{-2}	2.21	3.48^{-2}
6.00^1	4.77^{-1}	4.40	1.08^{-1}	2.30	4.73^{-2}
7.00^1	5.71^{-1}	4.18	1.37^{-1}		
8.00^1	6.78^{-1}	4.18	1.62^{-1}	2.11	7.69^{-2}
9.00^1	7.66^{-1}	4.16	1.84^{-1}		
1.00^2	8.44^{-1}	4.14	1.04^{-1}	2.28	8.94^{-2}
1.20^2	9.66^{-1}	3.99	2.42^{-1}		
1.50^2	1.15^0	4.06	2.83^{-1}	2.22	1.28^{-1}
1.80^2	1.32^0	4.00	3.31^{-1}		
2.00^2	1.39^0	3.99	3.48^{-1}	2.33	1.49^{-1}
2.50^2	1.59^0	4.06	3.93^{-1}		
3.00^2	1.74^0	3.93	4.44^{-1}	2.45	1.81^{-1}
3.50^2	1.87^0	3.93	4.77^{-1}		
4.00^2	1.99^0	3.93	5.05^{-1}	2.46	2.05^{-1}
5.00^2	2.37^0 [b]	4.40	5.39^{-1}	2.44	2.21^{-1}
6.00^2	2.32^0 [c]	4.17	5.56^{-1} [c]	2.33	2.39^{-1} [c]
8.00^2	2.51^0 [c]	4.10	6.12^{-1} [c]	2.42	2.53^{-1} [c]
1.00^3	2.62^0	3.96	6.63^{-1}	2.48	2.67^{-1}
1.50^3	2.93^0	3.98	7.37^{-1}	2.53	2.91^{-1}
2.00^3	3.09^0	3.95	7.82^{-1}	2.46	3.18^{-1}

[a] Donaldson et al. 1972.
[b] Too high.
[c] de Jongh and Van Eck, VII ICPEAC 1971 Amsterdam.

TABLE III. (cont.)

(c) Experimental $1\,^1S$ – $n\,^1D$ collision strengths and collision strength ratios of (n)/(n + 1)

E (eV)	$3\,^1D$	(3)/(4)	$4\,^1D$	(4)/(5)	$5\,^1D$	(5)/(6)	$6\,^1D$
2.50^1	4.01^{-3}	1.83	2.19^{-3}	1.71	1.28^{-3}	1.72	7.44^{-4}
3.00^1	5.72^{-3}	1.87	3.06^{-3}	1.69	1.80^{-3}	1.72	1.05^{-3}
3.50^1	7.25^{-3}	1.85	3.92^{-3}	1.64	2.39^{-3}	1.72	1.39^{-3}
4.00^1	8.66^{-3}	1.86	4.65^{-3}	1.68	2.76^{-3}	1.72	1.60^{-3}
4.50^1	9.93^{-3}	1.90	5.23^{-3}	1.73	3.02^{-3}	1.72	1.76^{-3}
5.00^1	1.09^{-2}	1.90	5.77^{-3}	1.86	3.10^{-3}	1.72	1.80^{-3}
6.00^1	1.14^{-2}	1.90	6.02^{-3}	1.86	3.23^{-3}	1.72	1.87^{-3}
8.00^1	1.24^{-2}	1.89	6.58^{-3}	1.81	3.54^{-3}	1.72	2.06^{-3}
1.00^2	1.20^{-2}	1.82	6.61^{-3}	1.87	3.53^{-3}	1.72	2.05^{-3}
1.50^2	1.17^{-2}	1.82	6.45^{-3}	1.87	3.46^{-3}	1.72	2.01^{-3}
2.00^2	1.18^{-2}	1.82	6.48^{-3}	1.87	3.48^{-3}	1.72	2.02^{-3}
2.50^2	1.21^{-2}	1.82	6.64^{-3}	1.87			
3.00^2	1.12^{-2}	1.82	6.17^{-3}	1.82	3.38^{-3}	1.72	1.97^{-3}
4.00^2	1.07^{-2}	1.82	5.88^{-3}	1.77	3.33^{-3}	1.72	1.94^{-3}
5.00^2	1.01^{-2}	1.82	5.56^{-3}	1.77			
6.00^2	1.00^{-2}	1.82	5.51^{-3}	1.74	3.17^{-3}	1.72	1.80^{-3}
8.00^2	1.04^{-2}	1.82	5.72^{-3}	1.84	3.10^{-3}	1.72	1.80^{-3}
1.00^3	1.04^{-2}	1.82	5.73^{-3}	1.83	3.12^{-3}	1.72	1.81^{-3}
1.50^3	9.78^{-3}	1.82	5.38^{-3}	1.83	2.93^{-3}	1.72	1.70^{-3}
2.00^3	9.73^{-3}	1.82	5.35^{-3}	1.83	2.91^{-3}	1.72	1.69^{-3}

(d) Experimental $1\,^1S$ – $n\,^3S$ collision strengths and collision strength ratios of (n)/(n + 1)

E (eV)	$2\,^3S$ [a]	(2)/(3)	$3\,^3S$	(2)/(4)	$4\,^3S$
2.00^1	5.18^{-2}				
2.50^1	4.80^{-2}	3.29	1.46^{-2}	7.30	6.60^{-3}
3.00^1	4.76^{-2}	2.82	1.65^{-2}	6.25	7.67^{-3}
3.50^1	4.24^{-2}	2.41	1.75^{-2}	5.88	7.43^{-3}
4.00^1	3.94^{-2}	2.41	1.64^{-2}	5.88	6.65^{-3}
4.50^1	3.50^{-2}	2.82	1.24^{-2}	6.25	5.75^{-3}
5.00^1	3.09^{-2}	2.82	1.09^{-2}	6.25	4.93^{-3}
6.00^1	2.46^{-2}	3.01	8.02^{-3}	6.66	3.72^{-3}
7.00^1	2.05^{-2}	3.29	6.43^{-3}	7.14	2.92^{-3}
8.00^1	1.74^{-2}	3.29	5.28^{-3}	7.14	2.43^{-3}
9.00^1	1.35^{-2}	3.29	4.14^{-3}	7.14	1.88^{-3}
1.00^2	1.17^{-2}	3.29	3.51^{-3}	7.69	1.57^{-3}
1.50^2	5.89^{-3} [b]	3.29	1.75^{-3}	7.14	8.21^{-4}
2.00^2	4.01^{-3} [b]	3.29	1.20^{-3}	7.14	5.65^{-4}
2.50^2	2.92^{-3} [b]	3.29	8.77^{-4}	7.14	4.07^{-4}
3.00^2	2.28^{-3} [b]	3.29	6.77^{-4}	7.14	3.18^{-4}
4.00^2	1.54^{-3} [b]	3.29	4.68^{-4}	7.14	2.17^{-4}
5.00^2	1.04^{-3} [b]	3.29	3.13^{-4}	7.14	1.45^{-4}

[a] For $2\,^3S$, Johnston and Burrow [26] have a peak in the cross-section at 20.35 eV.

[b] 7.14 $\Omega(4\,^3S)$.

TABLE III. (cont.)

(e) Experimental $1\,^1S - n\,^3P$ collision strengths and collision strength ratios of (n)/(n + 1)

E (eV)	$2\,^3P$	(2)/(3)	$3\,^3P$
2.50^{1}			1.31^{-2}
3.00^{1}	6.52^{-2}	3.52	1.85^{-2}
3.50^{1}			1.84^{-2}
4.00^{1}	6.35^{-2}	3.58	1.77^{-2}
5.00^{1}	5.85^{-2}	3.65	1.60^{-2}
1.60^{1}	5.16^{-2}	3.86	1.34^{-2}
7.00^{1}	4.09^{-2}	3.62	1.13^{-2}
8.00^{1}	3.28^{-2}	3.45	9.49^{-3}
9.00^{1}	2.63^{-2}	3.30	7.97^{-3}
1.00^{2}	2.34^{-2}	3.46	6.81^{-3}
1.50^{2}	9.65^{-3}	3.5	2.76^{-3}
2.00^{2}	6.02^{-3}	3.5	1.70^{-3}
2.50^{2}	4.18^{-3}	3.5	1.19^{-3}
3.00^{2}	2.76^{-3}	3.5	8.02^{-4}
4.00^{2}	1.47^{-3}	3.5	4.18^{-4}
5.00^{2}	7.94^{-4}	3.5	2.21^{-4}
6.00^{2}	1.25^{-3}	3.5	3.51^{-4}
8.00^{2}	4.68^{-4}	3.5	1.34^{-4}
1.00^{3}	9.19^{-4}	3.5	2.51^{-4}

(f) Experimental $1\,^1S - n\,^3D$ collision strengths and collision strength ratios of (n)/(n + 1)

E (eV)	$3\,^3D$	(3)/(4)	$4\,^3D$
2.80^{1}	2.76^{-3}	2.0	1.38^{-3}
3.00^{1}	4.26^{-3}	2.0	2.13^{-3}
3.50^{1}	3.98^{-3}	2.0	1.99^{-3}
4.00^{1}	3.28^{-3}	2.0	1.64^{-3}
5.00^{1}	2.13^{-3}	2.0	1.06^{-3}
6.00^{1}	1.55^{-3}	2.0	7.77^{-4}
7.00^{1}	1.29^{-3}	2.0	6.43^{-4}
8.00^{1}	1.02^{-3}	2.0	5.08^{-4}
9.00^{1}	9.32^{-4}	2.0	4.66^{-4}
1.00^{2}	8.36^{-4}	2.0	4.18^{-4}
1.50^{2}	4.26^{-4}	2.0	2.13^{-4}
2.00^{2}	2.67^{-4}	2.0	1.30^{-4}
2.50^{2}	1.86^{-4}	2.0	9.19^{-5}
4.00^{2}	1.67^{-4}	2.0	9.02^{-5}
6.00^{2}	2.00^{-4}	2.0	9.53^{-5}
1.00^{3}	2.00^{-4}	2.0	1.00^{-5}

TABLE IV. BORN APPROXIMATION RESULTS AT HIGH ENERGY

(a) Born approximation $1\,^1S - n\,^1S$ collision strengths and collision strength ratios of (n)/(n + 1)

E (eV)	$2\,^1S$	(2)/(3)	$3\,^1S$	(3)/(4)	$4\,^1S$
1.00^{3}	1.80^{-1}	4.44	4.05^{-2}	2.61	1.55^{-2}
1.50^{3}	1.80^{-1}	4.44	4.06^{-2}	2.61	1.56^{-2}
2.00^{3}	1.81^{-1}	4.44	4.07^{-2}	2.61	1.56^{-2}
3.00^{3}	1.81^{-1}	4.44	4.08^{-2}	2.61	1.56^{-2}
4.00^{3}	1.81^{-1}	4.44	4.08^{-2}	2.61	1.56^{-2}
5.00^{3}	1.81^{-1}	4.44	4.08^{-2}	2.61	1.56^{-2}

(b) Born approximation $1\,^1S - n\,^1P$ collision strengths and collision strength ratios of (n)/(n + 1)

E (eV)	$2\,^1P$	(2)/(3)	$3\,^1P$	(3)/(4)	$4\,^1P$
7.00^{2}	2.45^{0}	4.05	6.05^{-1}	2.49	2.43^{-1}
1.00^{3}	2.70^{0}	4.05	6.67^{-1}	2.49	2.67^{-1}
1.50^{3}	2.99^{0}	4.05	7.37^{-1}	2.49	2.95^{-1}
2.00^{3}	3.19^{0}	4.06	7.87^{-1}	2.49	3.15^{-1}
3.00^{3}	3.48^{0}	4.06	8.57^{-1}	2.49	3.43^{-1}
5.00^{3}	3.84^{0}	4.06	9.45^{-1}	2.50	3.79^{-1}

(c) Born approximation $1\,^1S - n\,^1D$ collision strengths and collision strength ratios of (n)/(n + 1)

E (eV)	$3\,^1D$	(3)/(4)	$4\,^1D$
1.00^{3}	9.42^{-3}	1.88	5.01^{-3}
1.50^{3}	9.49^{-3}	1.88	5.05^{-3}
2.00^{3}	9.53^{-3}	1.88	5.08^{-3}
3.00^{3}	9.56^{-3}	1.88	5.09^{-3}
4.00^{3}	9.58^{-3}	1.88	5.11^{-3}
5.00^{3}	9.59^{-3}	1.88	5.10^{-3}

TABLE V. MAXWELL AVERAGED COLLISION STRENGTHS OVER AN EXTENDED TEMPERATURE RANGE

(a) Maxwell averaged $1\,^1S$ – $n\,^1L$ collision strengths

T (eV)	$2\,^1S$	$3\,^1S$	$4\,^1S$	$3\,^1D$	$4\,^1D$	$2\,^1P$	$3\,^1P$	$4\,^1P$
1.00^0	3.30^{-2}	6.69^{-3}	2.02^{-3}	4.11^{-3}	1.61^{-3}	1.64^{-2}	3.79^{-3}	1.48^{-3}
2.00^0	3.86^{-2}	7.01^{-3}	2.42^{-3}	4.32^{-3}	2.00^{-3}	2.61^{-2}	6.47^{-3}	2.70^{-3}
3.00^0	4.19^{-2}	7.13^{-3}	2.73^{-3}	4.58^{-3}	2.26^{-3}	3.62^{-2}	9.09^{-3}	3.90^{-3}
4.00^0	4.45^{-2}	7.21^{-3}	2.99^{-3}	4.86^{-3}	2.48^{-3}	4.68^{-2}	1.17^{-2}	5.11^{-3}
5.00^0	4.67^{-2}	7.32^{-3}	3.21^{-3}	5.13^{-3}	2.67^{-3}	5.78^{-2}	1.44^{-2}	6.33^{-3}
7.00^0	5.04^{-2}	7.64^{-3}	3.55^{-3}	5.67^{-3}	3.00^{-3}	8.07^{-2}	1.99^{-2}	8.84^{-3}
1.00^1	5.05^{-2}	8.30^{-3}	3.92^{-3}	6.38^{-3}	3.41^{-3}	1.16^{-1}	2.84^{-2}	1.27^{-2}
1.50^1	6.11^{-2}	9.43^{-3}	4.35^{-3}	7.30^{-3}	3.92^{-3}	1.74^{-1}	4.24^{-2}	1.91^{-2}
2.00^1	6.61^{-2}	1.04^{-2}	4.67^{-3}	7.99^{-3}	4.29^{-3}	2.30^{-1}	5.60^{-2}	2.53^{-2}
3.00^1	7.40^{-2}	1.21^{-2}	5.18^{-3}	8.91^{-3}	4.80^{-3}	3.32^{-1}	8.12^{-2}	3.67^{-2}
4.00^1	8.04^{-2}	1.34^{-2}	5.60^{-3}	9.49^{-3}	5.12^{-3}	4.22^{-1}	1.04^{-1}	4.66^{-2}
5.00^1	8.59^{-2}	1.45^{-2}	5.97^{-3}	9.88^{-3}	5.33^{-3}	5.03^{-1}	1.24^{-1}	5.54^{-2}
7.00^1	9.48^{-2}	1.62^{-2}	6.60^{-3}	1.04^{-2}	5.61^{-3}	6.43^{-1}	1.60^{-1}	7.04^{-2}
1.00^2	1.05^{-1}	1.83^{-2}	7.35^{-3}	1.07^{-2}	5.82^{-3}	8.16^{-1}	2.03^{-1}	8.83^{-2}
1.50^2	1.17^{-1}	2.08^{-2}	8.31^{-3}	1.09^{-2}	5.95^{-3}	1.04^0	2.59^{-1}	1.11^{-1}
2.00^2	1.25^{-1}	2.28^{-2}	9.05^{-3}	1.10^{-2}	5.98^{-3}	1.22^0	3.02^{-1}	1.28^{-1}
3.00^2	1.37^{-1}	2.57^{-2}	1.01^{-2}	1.09^{-2}	5.97^{-3}	1.48^0	3.65^{-1}	1.53^{-1}
4.00^2	1.44^{-1}	2.77^{-2}	1.08^{-2}	1.08^{-2}	5.93^{-3}	1.67^0	4.12^{-1}	1.72^{-1}
5.00^2	1.49^{-1}	2.92^{-2}	1.14^{-2}	1.07^{-2}	5.88^{-3}	1.81^0	4.48^{-1}	1.86^{-1}
7.00^2	1.56^{-1}	3.13^{-2}	1.22^{-2}	1.06^{-2}	5.80^{-3}	2.04^0	5.05^{-1}	2.08^{-1}
1.00^3	1.62^{-1}	3.33^{-2}	1.29^{-2}	1.04^{-2}	5.71^{-3}	2.28^0	5.66^{-1}	2.31^{-1}
2.00^3	1.71^{-1}	3.65^{-2}	1.40^{-2}	1.01^{-2}	5.51^{-3}	2.75^0	6.83^{-1}	2.77^{-1}
3.00^3	1.74^{-1}	3.77^{-2}	1.44^{-2}	9.98^{-3}	5.41^{-3}	3.03^0	7.50^{-1}	3.03^{-1}
4.00^3	1.76^{-1}	3.84^{-2}	1.47^{-2}	9.89^{-3}	5.35^{-3}	3.22^0	7.96^{-1}	3.21^{-1}
5.00^3	1.77^{-1}	3.89^{-2}	1.48^{-2}	9.84^{-3}	5.31^{-3}	3.36^0	8.30^{-1}	3.34^{-1}
7.00^3	1.78^{-1}	3.94^{-2}	1.50^{-2}	9.77^{-3}	5.25^{-3}	3.56^0	8.80^{-1}	3.54^{-1}
1.00^4	1.79^{-1}	3.98^{-2}	1.52^{-2}	9.72^{-3}	5.21^{-3}	3.77^0	9.30^{-1}	3.74^{-1}

REFERENCES

[1] JANEV, R.K., LANGER, W.D., EVANS, K., Jr., POST, D.E., Jr., Elementary Processes in Hydrogen–Helium Plasmas. Cross-sections and Reaction Rate Coefficients, Springer Verlag, Berlin (1987), in particular pages 70–114 and 244–249.

[2] FUJIMOTO, T., Semi-empirical Cross-sections and Rate Coefficients for Excitation and Ionization by Electron Collision and Photoionization of Helium, Rep. IPPJ-AM-8, Institute of Plasma Physics, Nagoya University, Nagoya (1978).

[3] ABRAMOV, V.A., VAINSHTEIN, L.A., KROTOVA, G.I., PIGUROV, A.Yu., Recommended Atomic Data for Hydrogen and Helium Plasma, Rep. INDC(CCP)-2861/GA, Nuclear Data Section, IAEA, Vienna (1988).

[4] BRANSDEN, B.H., McDOWELL, M.R.C., Phys. Rep. **46** (1979) 250.

[5] SAWEY, P.M.J., BERRINGTON, K.A., BURKE, P.G., KINGSTON, A.E., J. Phys., B (London). At. Mol. Opt. Phys. **23** (1990) 4321.

[6] BELL, K.L., KENNEDY, D.J., KINGSTON, A.E., J. Phys., B (London). At. Mol. Phys. **2** (1969) 26.

[7] OCHKUR, V., Sov. Phys. — JETP **10** (1964) 503.

[8] BERRINGTON, K.A., SAWEY, M., KINGSTON, A.E. (Department of Applied Mathematics and Theoretical Physics, The Queen's University of Belfast), personal communication, 1991.

[9] HEDDLE, D.W.O., GALLAGHER, J.W., Rev. Mod. Phys. **61** (1989) 221.

[10] de HEER, F.J., JANSEN, R.H.J., J. Phys., B (London). At. Mol. Phys. **10** (1977) 3741.

TABLE V. (cont.)

(b) Maxwell averaged $1\,^1S$ – $n\,^3L$ collision strengths

T (eV)	$2\,^3S$	$3\,^3S$	$4\,^3S$	$3\,^3D$	$4\,^3D$	$2\,^3P$	$3\,^3P$
1.00^0	6.27^{-2}	1.20^{-2}	5.09^{-3}	2.12^{-3}	7.13^{-4}	2.31^{-2}	7.87^{-3}
2.00^0	6.25^{-2}	1.34^{-2}	5.85^{-3}	2.31^{-3}	9.39^{-4}	3.18^{-2}	1.04^{-2}
3.00^0	6.06^{-2}	1.41^{-2}	6.25^{-3}	2.52^{-3}	1.11^{-3}	3.75^{-2}	1.20^{-2}
4.00^0	5.87^{-2}	1.45^{-2}	6.47^{-3}	2.68^{-3}	1.23^{-3}	4.15^{-2}	1.30^{-2}
5.00^0	5.70^{-3}	1.48^{-2}	6.58^{-3}	2.80^{-3}	1.32^{-3}	4.45^{-2}	1.38^{-2}
7.00^0	5.42^{-2}	1.50^{-2}	6.65^{-3}	2.93^{-3}	1.40^{-3}	4.84^{-2}	1.47^{-2}
1.00^1	5.07^{-2}	1.48^{-2}	6.54^{-3}	2.95^{-3}	1.43^{-3}	5.15^{-2}	1.52^{-2}
1.50^1	4.62^{-2}	1.40^{-2}	6.19^{-3}	2.84^{-3}	1.38^{-3}	5.30^{-2}	1.53^{-2}
2.00^1	4.25^{-1}	1.32^{-2}	5.79^{-3}	2.67^{-3}	1.31^{-3}	5.25^{-2}	1.50^{-2}
3.00^1	3.69^{-2}	1.16^{-2}	5.09^{-3}	2.36^{-3}	1.16^{-3}	4.95^{-2}	1.39^{-2}
4.00^1	3.27^{-2}	1.03^{-2}	4.53^{-3}	2.11^{-3}	1.03^{-3}	4.59^{-2}	1.28^{-2}
5.00^1	2.95^{-2}	9.27^{-3}	4.08^{-3}	1.90^{-3}	9.33^{-4}	4.25^{-2}	1.19^{-2}
7.00^1	2.47^{-2}	7.76^{-3}	3.42^{-3}	1.60^{-3}	7.85^{-4}	3.68^{-2}	1.02^{-2}
1.00^2	2.01^{-2}	6.29^{-3}	2.77^{-3}	1.30^{-3}	6.38^{-4}	3.05^{-2}	8.47^{-3}
1.50^2	1.54^{-2}	4.86^{-3}	2.13^{-3}	9.98^{-4}	4.90^{-4}	2.38^{-2}	6.60^{-3}
2.00^2	1.26^{-2}	4.03^{-3}	1.74^{-3}	8.14^{-4}	4.00^{-4}	1.95^{-2}	5.42^{-3}
3.00^2	9.35^{-3}	3.11^{-3}	1.29^{-3}	5.99^{-4}	2.94^{-4}	1.45^{-2}	4.01^{-3}
4.00^2	7.47^{-3}	2.62^{-3}	1.03^{-3}	4.76^{-4}	2.34^{-4}	1.15^{-2}	3.19^{-3}
5.00^2	6.23^{-3}	2.30^{-3}	8.57^{-4}	3.95^{-4}	1.94^{-4}	9.57^{-3}	2.66^{-3}
7.00^2	4.70^{-3}	1.92^{-3}	6.46^{-4}	2.96^{-4}	1.45^{-4}	7.18^{-3}	1.99^{-3}
1.00^3	3.45^{-3}	1.60^{-3}	4.74^{-4}	2.16^{-4}	1.06^{-4}	5.24^{-3}	1.46^{-3}
2.00^3	1.84^{-3}	1.11^{-3}	2.54^{-4}	1.14^{-4}	5.61^{-5}	2.77^{-3}	7.71^{-4}
3.00^3	1.26^{-3}	8.84^{-4}	1.74^{-4}	7.80^{-5}	3.83^{-5}	1.89^{-3}	5.26^{-4}
4.00^3	9.62^{-4}	7.41^{-4}	1.32^{-4}	5.92^{-5}	2.91^{-5}	1.43^{-3}	4.00^{-4}
5.00^3	7.77^{-4}	6.41^{-4}	1.07^{-4}	4.77^{-5}	2.34^{-3}	1.16^{-3}	3.22^{-4}
7.00^3	5.62^{-4}	5.08^{-4}	7.72^{-5}	3.44^{-5}	1.69^{-5}	8.33^{-4}	2.32^{-4}
1.00^4	3.97^{-4}	3.90^{-4}	5.46^{-5}	2.43^{-5}	1.19^{-5}	5.88^{-4}	1.64^{-4}

[11] ZAPESOCHNYI, I.P., Astron. Zh. **43** (1966) 954.

[12] TRAJMAR, S., Phys. Rev., A **8** (1973) 191.

[13] HALL, R.I., JOYEZ, O., MAZEAU, J., REINHARDT, J., SCHERMANN, C., J. Phys. (Les Ulis) **34** (1973) 827.

[14] CROOKS, G.B., Energy and Angular Distributions of Scattered and Ejected Electrons Produced by 50–800 eV Electrons in Helium, PhD Thesis, University of Nebraska, Lincoln (1972); CROOKS, G.B., DUBOIS, R.D., GOLDEN, D.E., RUDD, M.E., Phys. Rev. Lett. **29** (1972) 327.

[15] BRONGERSMA, H.H., KNOOP, F.W.E., BACK, N., Chem. Phys. Lett. **13** (1972) 16.

[16] DILLON, M.A., LASSETTRE, E.N., J. Chem. Phys. **62** (1975) 2373.

[17] Van RAAN, A.J.F., de JONGH, J.P., Van ECK, J., HEIDEMAN, H.G.M., Physica **53** (1971) 45.

[18] ZAPESOCHNYI, I.P., FELTSAN, P.V., Ukr. Fiz. Zh. **10** (1965) 1197.

[19] Van ZYL, B., DUNN, G.H., CHAMBERLAIN, G., HEDDLE, D.W.O., Phys. Rev., A **22** (1980) 1916.

[20] MOUSTAFA MOUSSA, H.R., de HEER, F.J., SCHUTTEN, J., Physica **40** (1969) 517.

[21] WESTERVELD, W.B., HEIDEMAN, H.G.M., Van ECK, J., J. Phys., B (London). At. Mol. Phys. **12** (1979) 115.

[22] de JONGH, J.P., Electron Excitation of Noble Gas Atoms Measured by Vacuum Ultraviolet Spectrometry, PhD Thesis, University of Utrecht (1971); de JONGH, J.P., Van ECK, J., ICPEAC Abstracts, North-Holland, Amsterdam (1971) 701.

[23] SHEMANSKY, D.E., AJELLO, J.M., HALL, D.T., FRANKLIN, B., Astrophys. J. **296** (1985) 774.

[24] DONALDSON, F.G., HENDER, M.A., McCONKEY, J.W., J. Phys., B (London). At. Mol. Phys. **5** (1972) 1192.

[25] Van RAAN, A.J.F., MOLL, P.G., Van ECK, J., J. Phys., B (London). At. Mol. Phys. **7** (1974) 950.
[26] JOHNSTON, A.R., BURROW, P.D., J. Phys., B (London). At. Mol. Phys. **16** (1983) 613.
[27] JOBE, J.D., St. JOHN, R.M., Phys. Rev. **164** (1967) 117.
[28] BOGDANOVA, I.P., YURGENSON, S.V., Opt. Spektrosk. **61** (1986) 241.
[29] CHUTJIAN, A., THOMAS, L.D., Phys. Rev. **11** (1975) 1583.
[30] McCONKEY, J.W., WOOLSEY, J.M., ICPEAC VI Abstracts (AMDUR, I., Ed.), MIT Press, Cambridge, MA (1969) 355.
[31] TULLY, J.A., J. Phys., B (London). At. Mol. Phys. **13** (1980) 4845.

PARAMETRIC REPRESENTATION OF ELECTRON IMPACT EXCITATION AND IONIZATION CROSS-SECTIONS FOR HELIUM ATOMS

T. KATO
National Institute for Fusion Science,
Nagoya, Japan

R.K. JANEV
International Atomic Energy Agency,
Vienna

ABSTRACT. The recommended cross-sections of de Heer et al. (this issue) for electron impact excitation of the $n\,^{1,3}L$ ($n \leq 4$–6) states of helium from its ground state have been represented by analytic expressions containing only four to five fitting parameters. The database for the transitions to triplet states has been extended in the high energy region by additional Born–Ochkur calculations. The available data for electron impact ionization of He ($1\,^1S$) and He ($2\,^{1,3}S$) have also been assessed and represented by analytic fits. The analytic fits represent the recommended data with an rms deviation well within the uncertainty of the data.

1. INTRODUCTION

An analytic representation of atomic cross-section data or reaction rate coefficients is always desirable from the point of view of their use in various application codes. This is particularly true when the amount of data to be introduced into an application (e.g. plasma modelling or diagnostics) code is large. Besides its practical advantages, analytic formatting of the data, if based on solid physical grounds, may also be useful for extrapolation purposes. In the ALADDIN database of the International Atomic Energy Agency, the atomic collision cross-sections are normally stored in form of analytic functions supplemented by the values of the corresponding fitting coefficients for each cross-section.

In the present paper we provide relatively simple and uniform analytic formulas for the recommended cross-sections for electron impact excitation of the first several singlet and triplet states of the helium atom from its ground state. The numerical cross-section database to which the proposed analytic expressions have been fitted is that of de Heer et al. [1]. For the transitions in the triplet term series, the recommended database of Ref. [1] has been extended to the high energy region (up to 5 keV) by new theoretical calculations in the Ochkur approximation provided by Shevelko [2]. In Section 2, the choice of the analytic expressions for the cross-sections and the determination of their fitting parameters are briefly discussed. In Section 3, the values of the fitting parameters are given and the quality and validity range of the fits is discussed.

2. ANALYTIC EXPRESSIONS FOR EXCITATION CROSS-SECTIONS

We represent the electron impact excitation cross-section σ_{ij} for the $i \rightarrow j$ transition in the usual form:

$$\sigma_{ij} = \frac{\Omega_{ij}(X)}{\omega_i E(Ry)} \pi a_0^2 \qquad (1)$$

where E is the incident electron density in Rydberg units, ω_i is the statistical weight of the initial state, $\Omega_{ij}(X)$ is the collision strength and $X = E/\Delta E_{ij}$ is the collision energy in threshold units (ΔE_{ij} is the excitation energy). As discussed in Ref. [1], the collision strength $\Omega_{ij}(X)$ at high values of X shows certain regular patterns for a given type of $i \rightarrow j$ transition: it tends to a constant for the spin conserving optically forbidden transitions, it is proportional to $\ln X$ for the optically allowed transitions and it is proportional to X^{-2} for the spin forbidden transitions. In the threshold region ($X \rightarrow 1$), $\Omega_{ij}(X)$ usually exhibits a sharp decrease for most of the transitions. In the intermediate region of X, $\Omega(X)$ can be expanded in inverse powers of X. Guided by these properties of $\Omega_{ij}(X)$ and following the earlier experience in analytic fitting of electron impact excitation cross-sections [3, 4], we have adopted the following expressions for $\Omega(X)$ to fit the recommended data of Ref. [1]:

$1\,^1S \rightarrow n\,^1S;\ n\,^1D$; $1\,^1S \rightarrow n\,^3P;\ n\,^3D$

$$\Omega(X) = \left(A_1 + \frac{A_2}{X} + \frac{A_3}{X^2} + \frac{A_4}{X^3}\right)\left(\frac{X-1}{X}\right)^{A_5} \qquad (2a)$$

TABLE I. VALUES OF THE FITTING PARAMETERS A_i IN Eqs (2) AND OF THE TRANSITION ENERGIES ΔE_{ij}

Transition $1s\,^1S \rightarrow$	ΔE_{ij} (eV)	A_1	A_2	A_3	A_4	A_5	rms (%)
$2s\,^1S$	20.61	1.8732(-1)[a]	-2.8806(-1)	1.3589(-1)	1.7397(-1)	5.4268(-1)	10.9
$3s\,^1S$	22.92	4.0898(-2)	-1.3324(-1)	2.2846(-1)	-1.1951(-1)	3.3456(-1)	6.0
$4s\,^1S$	23.67	1.5387(-2)	-4.6305(-2)	7.4398(-2)	-3.9669(-2)	1.7198(-1)	5.5
$5s\,^1S$	24.01	7.7808(-3)	-2.6702(-2)	4.9135(-2)	-2.7484(-2)	4.1853(-1)	4.0
$6s\,^1S$	24.19	4.2253(-3)	-1.5233(-2)	2.8548(-2)	-1.6014(-2)	4.4802(-1)	5.8
$2p\,^1P$	21.22	1.2306(-4)	-4.9534(-1)	6.1713(-1)	7.085(-1)[b]	6.0006(-1)	4.9
$3p\,^1P$	23.09	2.3265(-2)	-1.5645(-1)	1.8723(-1)	1.736(-1)[b]	7.9383(-1)	5.6
$4p\,^1P$	23.74	4.5198(-2)	-1.1197(-1)	8.6180(-2)	6.923(-2)[b]	7.7622(-1)	2.6
$3d\,^1D$	23.07	9.4306(-3)	2.6771(-2)	-6.8326(-2)	3.6579(-2)	3.6564(-2)	2.1
$4d\,^1D$	23.74	5.0543(-3)	1.7876(-2)	-4.3079(-2)	2.4534(-2)	2.1977(-1)	2.5
$5d\,^1D$	24.04	2.8630(-3)	6.4713(-3)	-1.5538(-2)	7.5518(-3)	3.4587(-2)	2.6
$6d\,^1D$	24.21	1.7551(-3)	1.9242(-3)	-4.4939(-3)	1.4452(-3)	1.7771(-3)	3.6
$2s\,^3S$	19.82	1.6077(-3)	5.3368(-1)	-1.0601	6.1023(-1)		15.1
$3s\,^3S$	22.72	1.4346(-4)	1.1585(-1)	-1.6744(-1)	6.6875(-2)		12.5
$4s\,^3S$	23.59	3.7705(-5)	4.6867(-2)	-5.9202(-2)	1.7539(-2)		11.6
$2p\,^3P$	20.96	6.0203(-6)	-2.0588(-3)	6.7094(-1)	-5.7470(-1)	4.6491(-1)	8.5
$3p\,^3P$	23.01	1.1608(-6)	-3.2505(-4)	1.4814(-1)	-1.3766(-1)	1.3179(-1)	9.2
$3d\,^3D$	23.07	9.2318(-10)	-4.2120(-6)	1.9195(-2)	-1.2276(-2)	3.0710(-1)	11.1
$4d\,^3D$	23.74	1.0935(-7)	2.166(-5)	1.0716(-2)	-3.9355(-3)	5.4484(-1)	1.0

[a] $a(-b) = a \times 10^{-b}$.

[b] Theoretical values.

$1\,^1S \rightarrow n\,^1P$

$$\Omega(X) = \left(A_1 + \frac{A_2}{X} + \frac{A_3}{X^2} + A_4 \ln X\right)\left(\frac{X-1}{X}\right)^{A_5} \tag{2b}$$

$1\,^1S \rightarrow n\,^3S$

$$\Omega(X) = \frac{1}{X}\left(A_1 + \frac{A_2}{X} + \frac{A_3}{X^2} + \frac{A_4}{X^3}\right) \tag{2c}$$

The number of terms in the above expansions has been chosen to achieve a prescribed accuracy of the fits for a given class of transitions (rms deviation of 10–12% in our case) with a minimum number of fitting parameters. The constant A_4 in Eq. (2b) has been fixed at its theoretical value, $A_4 = 4\omega_i f_{ij}/\Delta E_{ij}(\mathrm{Ry})$, where f_{ij} is the oscillator strength. Since no restriction has been imposed on the sign of the parameters A_2–A_4 in Eqs (2), the high energy E^{-3} behaviour of $\sigma_{ij}(E)$ for the spin forbidden transitions is not violated, at least up to 5 keV (the upper limit of the numerical data range). The function $[(X-1)/X]^{A_5}$ in Eqs (2a) and (2b) has been introduced to describe the threshold behaviour of $\Omega(X)$. Note that the threshold behaviour of the $1\,^1S \rightarrow n\,^3S$ cross-section is different from that for other transitions (i.e. it is finite at the threshold), and that A_5 may have very small values (or zero) for some transitions (see Table I).

In determining the fitting coefficients in Eqs (2) for the transitions to singlet states, we have used the recommended collision strength data from Tables II–IV of Ref. [1]. For the transitions to triplet states, we have used the data of these tables up to 300 eV for $n\,^3S$, 500 eV for $n\,^3P$ and 250 eV for $n\,^3D$. Since in the energy range 250–500 eV it cannot be expected that the cross-section for these transitions has an asymptotic E^{-3} behaviour, new cross-section calculations have been performed [2] within the Ochkur approximation for the energy range from 100 eV to 5 keV. The new theoretical

data have been normalized to the recommended data of Ref. [1] in the energy range of their mutual overlap (the correction factors being 1.92 for $n\,^3S$, 1.57 for $n\,^3P$ and 10 for $n\,^3D$), thus ensuring a correct behaviour of the recommended cross-sections at high energies. In some cases ($4\,^3S$, $3\,^3P$, $n\,^3D$) the normalization had to be performed in the energy range 200–300 eV in order to match the gradients of the two sets of data.

3. PARAMETRIZED EXCITATION CROSS-SECTIONS

The fitting of Eqs (2) to the above discussed numerical data sets has produced the values of fitting parameters A_1–A_5 shown in Table I. The rms deviation for each fit is also shown in the table. Most of the rms deviation comes from the region around and below the cross-section maximum. The rms values are well below the uncertainties of the original data. We mention once again that the parameter A_4 in Eq. (2b) has been fixed at its asymptotic value derived from the oscillator strength (see Section 2).

In order to illustrate the quality of the fits, we give in Figs 1–4 four typical examples, where both the original points (open circles) and the fitting curves (solid lines) are shown. The open triangles at E = 10 and 20 keV in Fig. 2 have been generated by using only the $A_4 \ln X$ term of Eq. (2b), which gives accurate values of the collision strength at these energies. The open triangles in Figs 3 and 4 are normalized theoretical data of Shevelko [2].

In Figs 5–10 we show all the considered excitation cross-sections as generated by Eqs (2) with the coefficients given in Table I. The accuracy of these cross-sections in the energy range up to 5 keV is the same as that for the original data. For the singlet term series the assessed cross-section accuracy is about 20–30% for $E < 40$ eV, 10–15% for $40\ \text{eV} \le E \le 500$ eV, and 5–10% for $E > 500$ eV. (Exceptions are $2\,^1S$ and $n\,^1D$, which in the intermediate energy range may have somewhat higher (~20–25%) uncertainty.) For the triplet term series, the assessed cross-section accuracy is about 30% (40% for $3\,^3D$) for $E < 100$ eV and possibly slightly higher for $E > 100$ eV. In view of the correct representation of the high energy cross-section behaviour by Eqs (2), one can use these expressions with the coefficients given in Table I to extend the recommended excitation cross-sections (within the same accuracy), at least up to several hundred keV. Above 1 MeV, the relativistic corrections to the cross-sections become significant.

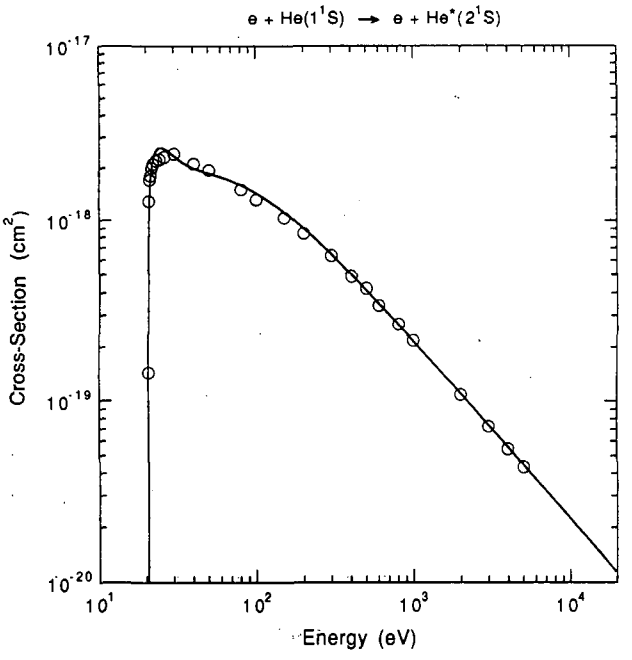

FIG. 1. Cross-section for $1\,^1S \rightarrow 2\,^1S$ excitation of He. Circles denote the recommended data from Ref. [1]; the solid line is the present analytic fit (Eq. (2) and Table I).

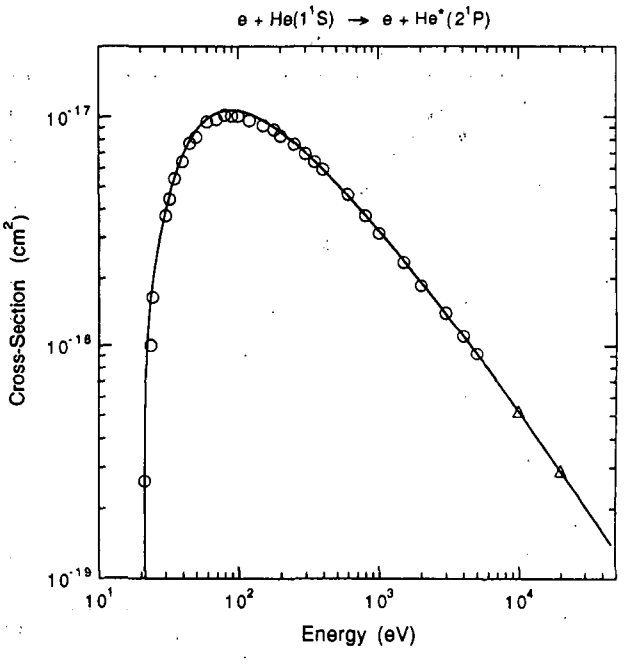

FIG. 2. Same as Fig. 1, but for the $1\,^1S \rightarrow 2\,^1P$ transition. The triangles denote data generated from the Born asymptotics.

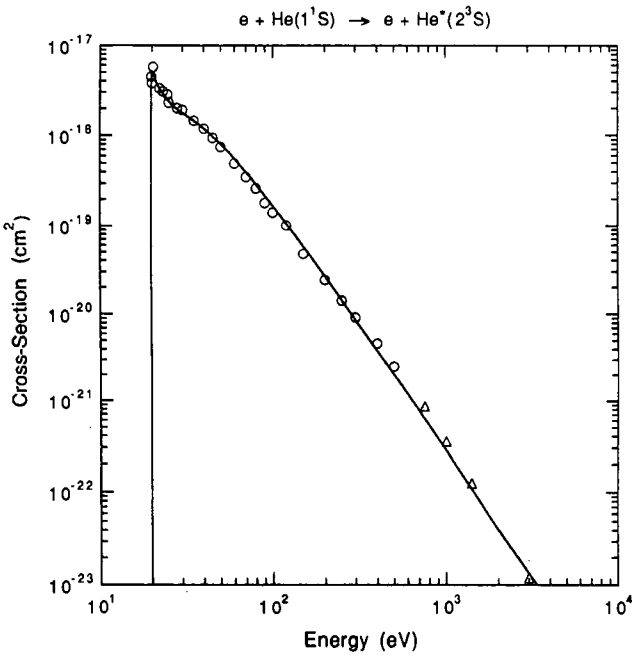

FIG. 3. Cross-section for $1\,^1S \rightarrow 2\,^3S$ excitation of He. Circles denote the recommended data from Ref. [1]; triangles denote normalized data from the Ochkur approximation. The solid line is the analytic fit of the data (Eq. (2) and Table I).

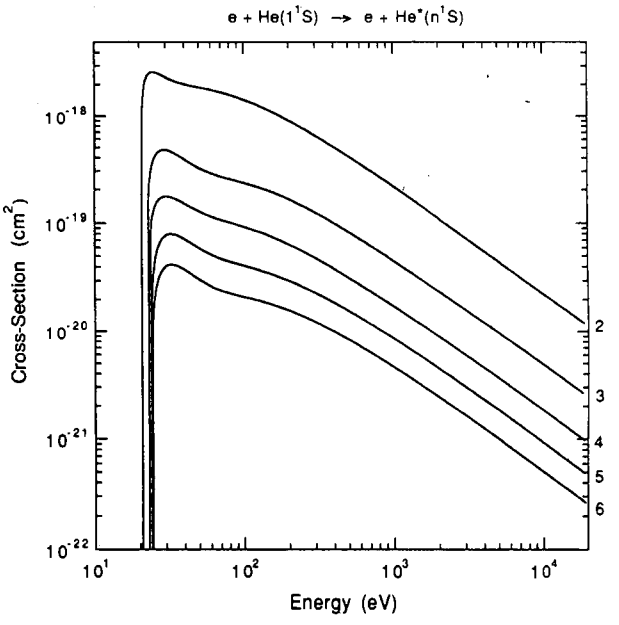

FIG. 5. Cross-sections for $1\,^1S \rightarrow n\,^1S$ excitation of He by electron impact generated by Eq. (2) with the values of the parameters A_i from Table I.

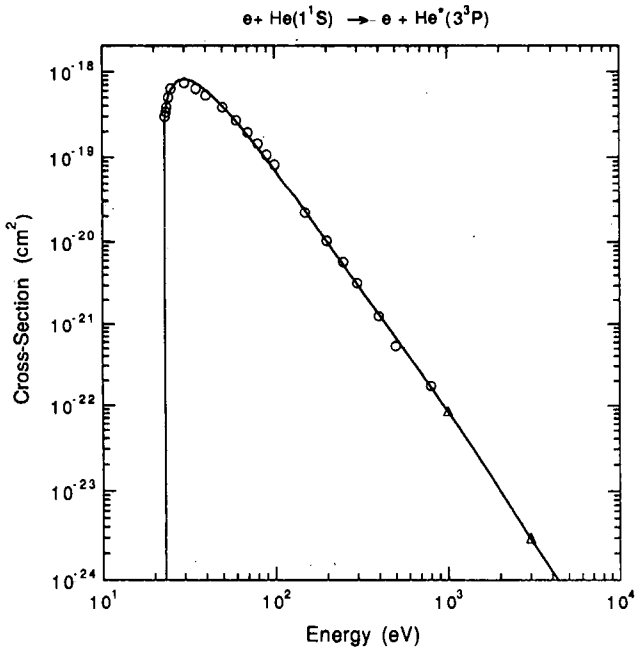

FIG. 4. Same as Fig. 3, but for the $1\,^1S \rightarrow 3\,^3P$ transition.

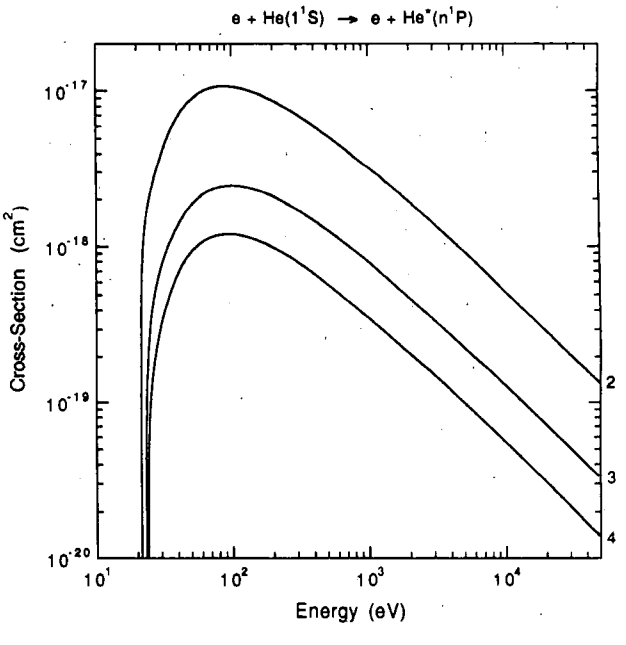

FIG. 6. Same as Fig. 5, but for $1\,^1S \rightarrow n\,^1P$ transitions.

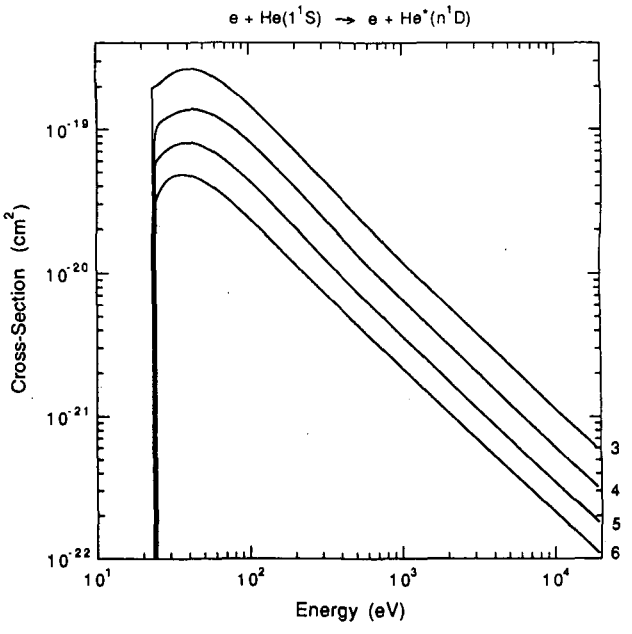

FIG. 7. Same as Fig. 5, but for $1^1S \rightarrow n^1D$ transitions.

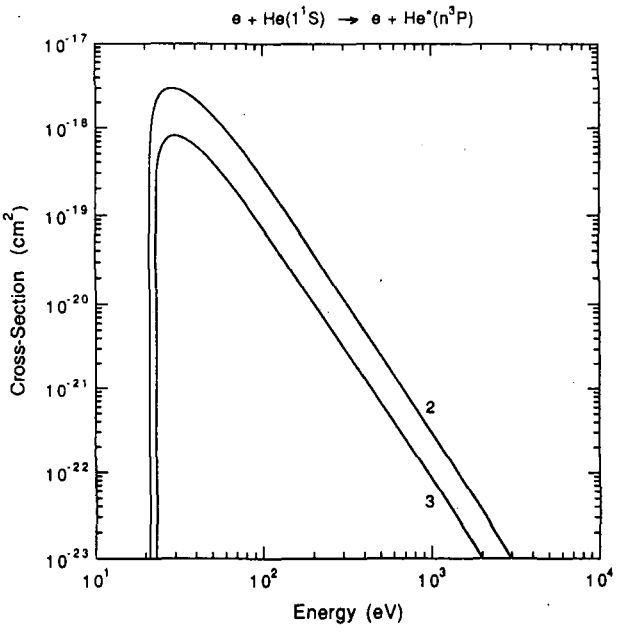

FIG. 9. Same as Fig. 5, but for $1^1S \rightarrow n^3P$ transitions.

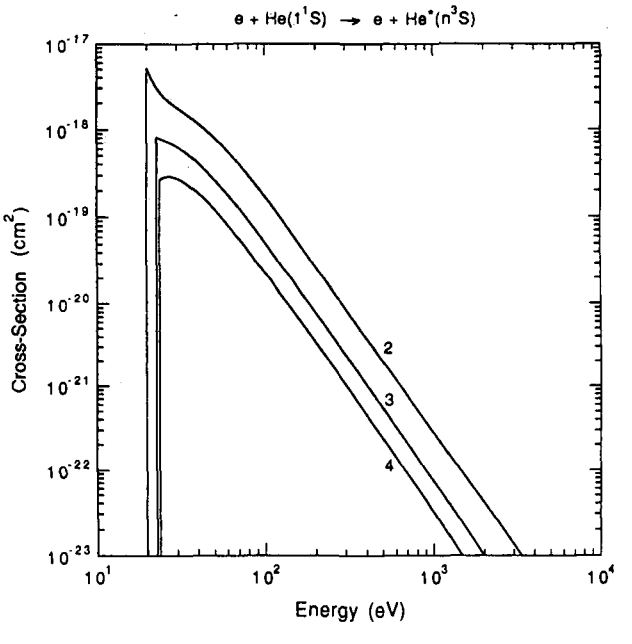

FIG. 8. Same as Fig. 5, but for $1^1S \rightarrow n^3S$ transitions.

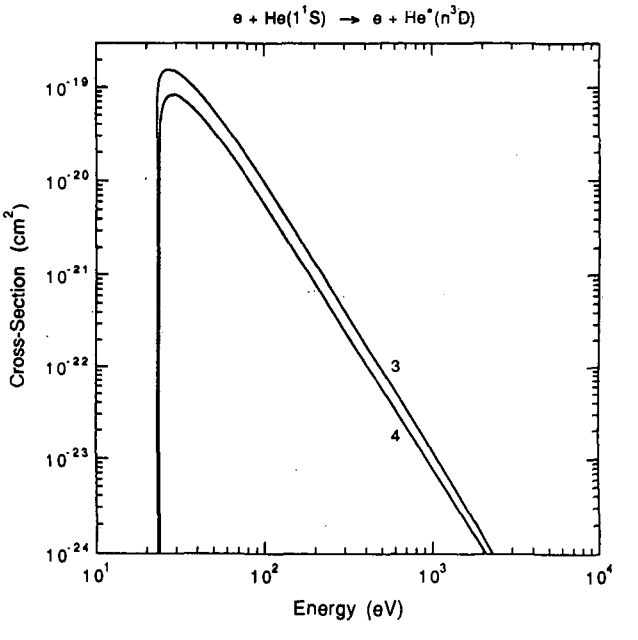

FIG. 10. Same as Fig. 5, but for $1^1S \rightarrow n^3D$ transitions.

We have checked the n^{-3} scaling of the cross-sections for all transitions considered. For the $1\,^1S \rightarrow n\,^1S$ and $1\,^1S \rightarrow n\,^1D$ transitions, we have found that for $n = 5$ and $n = 6$ this scaling is satisfied to within 10% at low energies and to 5% at high energies. For the $1\,^1S \rightarrow 3\,^1P$, $4\,^1P$ transitions, we found that the n^{-3} scaling is satisfied to within 15% at lower energies and to 3–5% in the energy region around and above the cross-section maximum. Therefore, within the accuracy of the data for $\sigma(4\,^1P)$ and $\sigma(6\,^1S; 6\,^1D)$, the cross-sections $\sigma(n\,^1P)$ for $n \geq 5$ and $\sigma(n\,^1S; n\,^1D)$ for $n \geq 7$ can be calculated from

$$\sigma(n\,^1P) = \left(\frac{4}{n}\right)^3 \sigma(4\,^1P) \qquad n \geq 5 \qquad (3a)$$

$$\sigma(n\,^1S; n\,^1D) = \left(\frac{6}{n}\right)^3 \sigma(6\,^1S; 6\,^1D) \quad n \geq 7 \qquad (3b)$$

For the $1\,^1S \rightarrow n\,^3S$ and $1\,^1S \rightarrow n\,^3P$ transitions, we have found that for $n = 3$ and $n = 4$ the n^{-3} scaling is satisfied to within 3–5% in the entire energy range considered, while for the $1\,^1S \rightarrow n\,^3D$ transitions ($n = 3, 4$) the scaling is satisfied only to within a 20% uncertainty (at lower energies) and a 40% uncertainty (at higher energies). To within these uncertainties, the excitation cross-sections for higher triplet states can be obtained from

$$\sigma(n\,^3P) = \left(\frac{3}{n}\right)^3 \sigma(3\,^3P) \qquad n \geq 4 \qquad (3c)$$

$$\sigma(n\,^3S; n\,^3D) = \left(\frac{4}{n}\right)^3 \sigma(4\,^3S; 4\,^3D) \quad n \geq 5 \qquad (3d)$$

4. IONIZATION CROSS-SECTIONS

The electron impact ionization cross-section data for ground state helium were previously assessed by Bell et al. [5], and the recommended cross-section was parametrized by the expression

$$\sigma\,[\mathrm{cm}^2] = \frac{10^{-13}}{IE}\left\{A_1 \ln(E/I) + \sum_{i=2}^{N} A_i \left(1 - \frac{I}{E}\right)^{i-1}\right\} \qquad (4)$$

where the collision energy E and ionization potential I are expressed in eV units and A_i are fitting coefficients. After this assessment was made, new experimental data were reported by Montague et al. [6] and Shah et al. [7]. Within their experimental uncertainty, the new data agree well with the recommended cross-section of Bell et al. The values of the parameters A_i in Eq. (4) are given in Table II. It should be noted that the coefficient A_1 can be related to the continuum oscillator strength $df/d\epsilon$ by

$$A_1 = 8.39 \times 10^{-2}\, I\,[\mathrm{eV}] \int_0^\infty \frac{1}{(E + \epsilon)} \frac{df}{d\epsilon}\, d\epsilon \qquad (5)$$

where ϵ is the energy of ejected electrons.

The ionization of $2\,^3S$ and $2\,^1S$ metastable states of helium has been studied theoretically by Briggs and Kim [8] and Taylor et al. [9, 10] within the Born approximation. We note that the theoretical cross-sections of Ref. [8] are larger than those of Refs [9, 10] by 60% for $2\,^3S$ and by 40% for $2\,^1S$. For $2\,^3S$, there also exist experimental cross-section measurements by Long and Geballe [11] and Dixon et al. [12], covering the energy range from the threshold up to 1 keV, and overlapping in the region 6–18 eV. The experimental data of Dixon et al. [12] agree well at high energies with the theoretical predictions of Briggs and Kim [8]. We have fitted these experimental data (the data of Long and Geballe [11] were taken only up to 10 eV) to the analytic expression (4) in which the coefficient A_1 has been fixed at its theoretical value 0.165 [8, 9]. The obtained values of the fitting coefficients A_2–A_5 are given in Table II. Figure 11 shows the experimental

TABLE II. VALUES OF THE FITTING PARAMETERS IN Eq. (4)

Transitions	I (eV)	A_1	A_2	A_3	A_4	A_5	A_6	rms (%)
He ($1\,^1S$) → He^+	24.58	0.572	-0.344	-0.523	3.445	-6.821	5.578	
He ($2\,^3S$) → He^+	4.77	0.165[a]	-0.29791	4.4626	- 9.4135	6.4685	—	8.5
He ($2\,^1S$) → He^+	3.99	0.2145	-0.38728	5.8013	-12.238	8.4090	—	
He ($1\,^1S$) → He^{2+}	78.98	1.3233(-6)[b]	+8.2077(-3)	-6.6759(-2)	+2.9780(-1)	-1.9248(-1)	—	10.5

[a] Theoretical value.

[b] a(-b) = a × 10^{-b}.

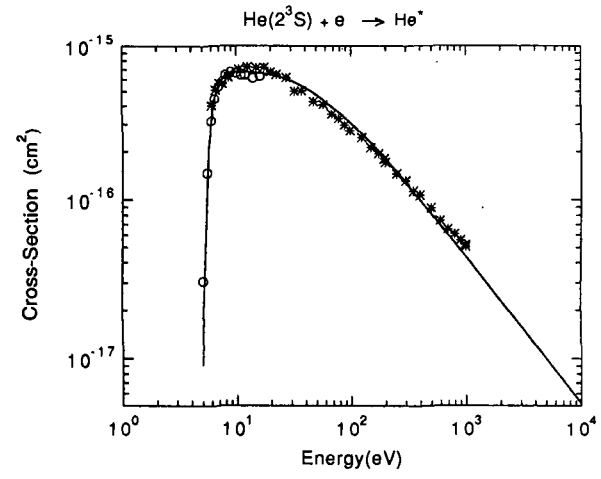

FIG. 11. Electron impact ionization cross-section for He ($2\,^3S$). The circles and stars denote the data from Ref. [11] and Ref. [12], respectively. The solid curve is the analytic fit to the data (Eq. (4)), with the parameter values given in Table II.

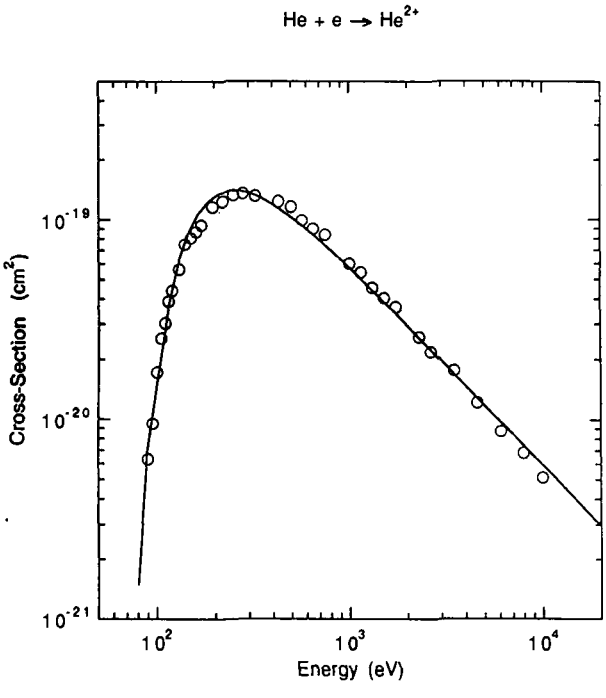

FIG. 12. Electron impact double ionization cross-section for He ($1\,^1S$). The circles denote experimental data from Ref. [7]; the solid curve is the fit of the data by Eq. (4).

data (symbols) and the cross-section obtained by the above described fitting procedure (full line).

For the ionization of He ($2\,^1S$), no experimental data are available. The theoretical calculations in Ref. [8] show that the cross-section ratio $\sigma(2\,^1S)/\sigma(2\,^3S)$ for energies above 100 eV is constant and close to 1.3, while Refs [9, 10] give a 15% higher value for this ratio. Judging from the variations of similar ratios for the excitation cross-sections (see Ref. [1]), one can expect that the extension of the value of 1.3 (which we adopt here) to lower energies should not introduce an uncertainty greater than 30%. Therefore, the parameters A_i for the $2\,^1S$ ionization cross-section shown in Table II have been obtained by multiplying the corresponding fitting coefficients for the $2\,^3S$ cross-section by 1.3.

Shah et al. [7] have also measured the electron impact double ionization cross-section of He($1\,^1S$) in the energy range from the threshold up to 10 keV. We have fitted these data (accuracy of about 10%) to the expression (4), and the obtained values of the fitting coefficients are given in Table II. The data and their fit are shown in Fig. 12.

ACKNOWLEDGEMENT

We are indebted to Dr. V.P. Shevelko from the Lebedev Institute, Moscow, for kindly providing the cross-sections for excitation of the triplet states of helium.

REFERENCES

[1] de HEER, F.J., HOEKSTRA, R., KINGSTON, A.E., SUMMERS, H.P., this issue, p. 19.
[2] SHEVELKO, V.P. (Lebedev Phys. Inst., Moscow), personal communication, 1991.
[3] ITIKAWA, Y., HARA, S., KATO, T., et al., At. Data Nucl. Data Tables **33** (1985) 149.
[4] KATO, T., NAKAZAKI, S., At. Data Nucl. Data Tables **42** (1989) 313.
[5] BELL, K.L., GILBODY, H.B., HUGHES, J.G., et al., At. Data Nucl. Data Tables **42** (1989) 313.
[6] MONTAGUE, R.G., HARRISON, M.F.A., SMITH, A.C.H., J. Phys., B **17** (1984) 3295.
[7] SHAH, M.B., ELLIOTT, D.S., McCALLION, P., GILBODY, H.B., J. Phys., B **21** (1988) 2756.
[8] BRIGGS, J.S., KIM, Y.K., Phys. Rev., A **3** (1971) 1342.
[9] TAYLOR, I.R., KINGSTON, A.E., BELL, K.L., J. Phys., B **12** (1979) 3093.
[10] TAYLOR, I.R., BELL, K.L., KINGSTON, A.E., J. Phys., B **13** (1980) 2983.
[11] LONG, D.R., GEBALLE, R., Phys. Rev., A **1** (1970) 260.
[12] DIXON, A.J., HARRISON, M.F.A., SMITH, A.C.H., J. Phys., B **9** (1976) 2617.

HELIUM EXCITATION IN HEAVY PARTICLE COLLISIONS

W. FRITSCH
Bereich Schwerionenphysik,
Hahn-Meitner-Institut Berlin,
Berlin, Germany

ABSTRACT. The database on helium excitation in heavy particle collisions is examined. A critical evaluation of existing data together with new calculations for specific transitions leads to recommended cross-section curves for the most important of these processes in fusion plasma applications.

1. INTRODUCTION

Helium atom excitation by heavy particle impact is one of the basic atomic collision processes. A number of experimental groups have investigated the H^+–He system in the 1960s and the early 1970s, concurrent with theoretical studies based on the Born approximation. Higher charged projectiles have been used in a series of experiments in the last five years. Theoretical work for strongly perturbed systems, i.e. higher charged or slow collision systems, has concentrated on hydrogen targets. Such work is still relevant to systems with helium targets in so far as it deals with the scaling properties of excitation cross-sections.

In this paper we review the status of present knowledge about electron excitation by A^{q+}–He collisions in the energy range of 10–1000 keV/amu — the range of primary interest for applications to processes in fusion plasmas. We also present results of calculations that have been performed within the close coupling scheme with atomic basis sets [1], for a few systems and transitions where the available information is discrepant or where there is no information at all. One particularly striking conflict has hitherto evaded notice and has been discovered, for H^+–He collisions, in the course of this work. It highlights the virtual neglect of low energy excitation processes by theory, for a variety of reasons [1], until very recently.

In Section 2, the H^+–He system is discussed. In Section 3, He excitation by higher charged projectiles, A^{q+} ($q > 1$), is considered, as well as the scaling properties of cross-sections with projectile charge. Details of the experimental results are presented by Anton et al. [2] in this issue. Section 4 presents theoretical results for excitation of pre-excited helium $He^*(2\,^1S)$ by heavy particle impact. A summary of the achievements and of missing information on these collision systems is given in Section 5.

2. EXCITATION IN H^+–He(^1S) COLLISIONS

The database of excitation cross-sections for H^+–He(^1S) collisions before 1972 has been reviewed by Thomas [3]. In the following, we will draw from that monograph, but include additional information which either has been published more recently or has been generated in the course of this work.

2.1. Excitation of n ^1S states

As has been discussed by Thomas [3], the measured cross-sections for population of the $4\,^1S$ state by Van den Bos et al. [4], Dodd and Hughes [5], Thomas and Bent [6], and Robinson and Gilbody [7] all agreee on the relative energy dependence in the respective overlapping energy regions (20–350 keV). On the other hand, the absolute magnitudes do not agree within the quoted errors.

At higher energies (200–1000 keV), Hasselkamp et al. [8] have addressed the problem of absolute normalization. The claimed absolute accuracy of their measured $4\,^1S$ excitation cross-section is 10%. Within this range of uncertainty, the data by Hasselkamp et al. agree, at the highest energy point of 1 MeV, with the result of the first Born approximation by Bell et al. [9]. Thus, it is possible to construct a consistent set of $4\,^1S$ cross-sections by taking the data of Hasselkamp et al. as a standard and renormalizing the other data accordingly. In Fig. 1, the resulting cross-sections are displayed; the original data from Refs [5], [6] and [7] have been multiplied by factors of 0.69, 1.74 and 1.39, respectively. The data by Van den Bos et al. [4] are consistent with those by Hasselkamp et al.

For excitation to the $5\,^1S$ state, it has been observed by Van den Bos et al. [4] that the ratio of cross-sections $\sigma(5\,^1S)/\sigma(4\,^1S)$ is, within 15%, the same in all experiments [4–7] at high energies and agrees with the Born

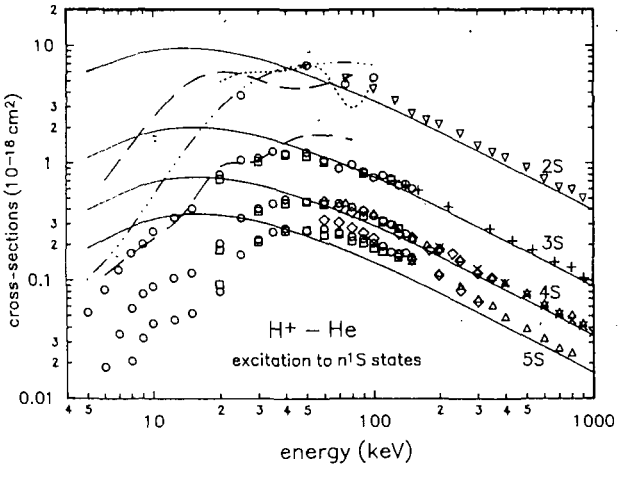

FIG. 1. Excitation cross-sections to $n\,^1S$ states in H^+–He collisions. Experimental data are by Van den Bos et al. [4] (circles for $3\,^1S$–$5\,^1S$), Dodd and Hughes [5] (squares), Thomas and Bent [6] (triangles), Robinson and Gilbody [7] (diamonds), Hasselkamp et al. [8] (×), Scharmann and Schartner [10] (+), and Kvale et al. [11] (circles for $2\,^1S$). All data are renormalized, as explained in the text, except for the data from Refs [8] and [11]. The calculated curves are from the Born approximation [9] (solid), from two-electron close coupling calculations with MO [12] (triple-dot-dashed line) and with AO [13] (dotted line) basis sets, and from the one-electron close coupling calculation (dashed lines) of this work. The inverted triangles designate an assessment of high energy $2\,^1S$ cross-sections by scaling the $4\,^1S$ cross-sections from Ref. [6], see text.

prediction. As a standard for $5\,^1S$ cross-sections, we have therefore taken the data by Thomas and Bent [6], multiplied by a factor of 1.6, which derives from the postulate that the cross-section ratio at high energies is the same as that in the Born approximation. The other data from Refs [4], [5] and [7] have then been renormalized to this chosen standard by adopting factors of 0.92, 0.83 and 1.74, respectively. The resulting cross-sections are displayed in Fig. 1. We note that the low energy data from Ref. [7] fall outside the trend of the other $5\,^1S$ cross-sections.

For excitation to the $3\,^1S$ state, we chose as standard the data by Scharmann and Schartner [10] as normalized by Thomas [3]. This again can be justified by the requirement that the cross-section ratio $\sigma(3\,^1S)/\sigma(4\,^1S)$ at high energy should be correctly predicted by the Born calculation. The data of Dodd and Hughes [5] agree with this standard at overlapping energies and the data of Van den Bos et al. [4] agree with it after renormalization with a factor of 0.74. The resulting cross-section curves are displayed in Fig. 1. For the $3\,^1S$–$5\,^1S$ states, a set of recommended cross-section curves may be deduced by straightforward graphical smoothing of the set of curves in Fig. 1.

Excitation to the $2\,^1S$ helium state is less well known. Figure 1 shows, besides the result of the Born approximation, the data by Kvale et al. [11], and the results of the close coupling calculations by Kimura and Lin [12] and by Slim et al. [13]. Surprisingly, the cross-sections from the two-electron MO calculation [12] seem to drop too fast with energy, compared to the trend of the $3\,^1S$–$5\,^1S$ cross-sections. The cross-sections from the two-electron AO model [13] display the expected trend at their low energy end, but there is a curious structure around 80 keV.

As part of this work, we have investigated He excitation in H^+–He collisions within the close coupling description and a one-electron potential model. Details of this work together with results for $n\,^1P$ states have been reported elsewhere [14]. In Fig. 1 we show results for $2\,^1S$ and $3\,^1S$ excitation. The calculated $3\,^1S$ excitation cross-sections are very close to the renormalized data curve in Fig. 1, except beyond 40 keV. Hence, one would expect that the calculated $2\,^1S$ cross-sections are also reasonably reliable; they certainly follow the undulatory trend of the other cross-section curves.

Clearly, the $2\,^1S$ cross-sections are the most uncertain in the $n\,^1S$ sequence. As recommended cross-sections, one may take, at high energies, the rescaled (by a factor of 11.6, see Fig. 1) $4\,^1S$ cross-sections from Ref. [6], following a suggestion by de Heer et al. [15]. At lower energies, the curve from this work is expected to be the most reliable one below 25 keV. These two curves may then be linked smoothly, approximately along the line suggested by the results from Ref. [13], but without the structure at 80 keV.

2.2. Excitation of $n\,^1P$ states

For the series of cross-sections to $n\,^1P$ states, Thomas [3] has identified the data by Van den Bos et al. [4], Thomas and Bent [6] and Scharmann and Schartner [10] as the most reliable. The latter data are now superseded by more recent measurements of Hasselkamp et al. [8] and Hippler and Schartner [16].

At high energies, the cross-sections measured by Hippler and Schartner [16] for $2\,^1P$–$4\,^1P$ states are considered reliable; above about 500 keV they agree with the results of the Born approximation [9]. The data by Thomas and Bent [6] for transitions to $3\,^1P$ and $4\,^1P$ states, after being renormalized with factors of 0.94 and 1.6, respectively, are consistent with those numbers. For the transition to the $5\,^1P$ state, the data from Ref. [6] have been normalized to the Born results [9] at high energies by applying a factor of 1.75. The data

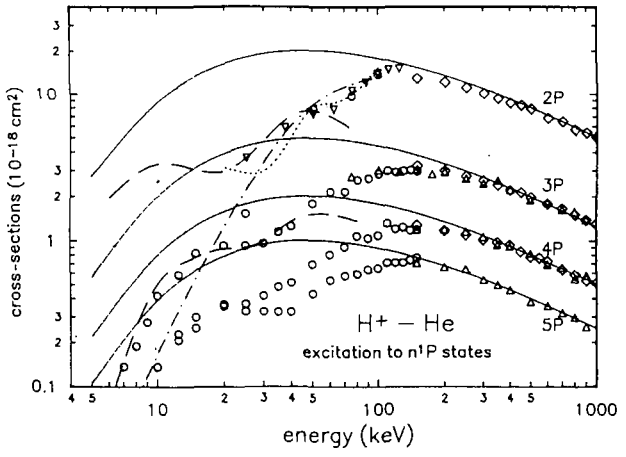

FIG. 2. Excitation cross-sections to n ^{1}P states in H^+-He collisions. For an explanation of the symbols, see caption to Fig. 1, except for the following: diamonds designate the data by Hippler and Schartner [16], inverted triangles the data by Park and Schowengerdt [17], and circles for the 2 ^{1}P state the data by Kvale et al. [11].

of Van den Bos et al. [4] can be brought to harmony with these results by applying factors of 0.75, 1.14 and 1.47 for the 3 ^{1}P, 4 ^{1}P and 5 ^{1}P states, respectively. Figure 2 shows the cross-sections which result from this procedure. As it turns out, the low energy 5 ^{1}P cross-sections by Van den Bos et al. appear to be too high. More reliable cross-sections for this state (and for higher-n states) are derived by scaling the 4 ^{1}P cross-sections, with factors which are derived from the ratio of Born cross-sections at 1000 keV.

For excitation to the 2 ^{1}P state at high energies, the data by Hippler and Schartner [16] are in good harmony with the Born results [9]. At lower energies, these data are consistent with the data by Park and Schowengerdt [17] and those by Kvale et al. [11], except at 25 keV where the latter data differ by more than a factor of two. The results calculated within the MO close coupling scheme by Kimura and Lin [12] appear to decrease much too fast with decreasing energy. The 2 ^{1}P cross-sections from the AO close coupling scheme by Slim et al. [13] are closer, at their low energy end, to what is expected from the trend of cross-sections for the higher-n states. In Fig. 2, these results are shown, together with the results from the one-electron close coupling scheme of this work (see also Ref. [14]). The present results for the 3 ^{1}P state agree closely with the renormalized data by Van den Bos et al. [4], up to an energy of 40 keV. We would assume that the calculated 2 ^{1}P cross-sections [14] are definitely more reliable than the MO results [12] below an energy of 30 keV. The two-electron close coupling scheme employed in Ref. [13] is expected, in principle, to yield better results than the one-electron close coupling scheme. Still, in view of the data [17], we would recommend a 2 ^{1}P cross-section curve which interpolates the data of Refs [16, 17] and continues, to lower energy, along the calculated results of this work and of Ref. [14].

2.3. Excitation of n ^{1}D states

As detailed by Thomas [3], the data by Van den Bos et al. [4], Thomas and Bent [6] and Scharmann and Schartner [10] are the most reliable for the n ^{1}D transitions. These data can be put to an absolute scale by adopting the data by Hasselkamp et al. [8] for 4 ^{1}D excitation as a standard and by postulating that the cross-section ratio in the n ^{1}D series at 1 MeV be the same as the ratio of model cross-sections from the Born approximation [9]. The renormalized cross-section data are displayed in Fig. 3. They have been derived by applying factors of 0.78, 1.7 and 1.92, respectively, to the 3 ^{1}D, 4 ^{1}D and 5 ^{1}D data from Ref. [10] (as cited in Ref. [3]), a factor of 1.72 to the 4 ^{1}D data from Ref. [6], and factors of 0.82, 0.90 and 1.12, respectively, to the 3 ^{1}D, 4 ^{1}D and 5 ^{1}D data from Ref. [4]. The calculated 3 ^{1}D excitation cross-sections from this work are also displayed in Fig. 3. They are seen to agree closely with the low energy data from Ref. [4]. At energies beyond 30 keV, these calculated results are not reliable, as has been observed also for the other transitions.

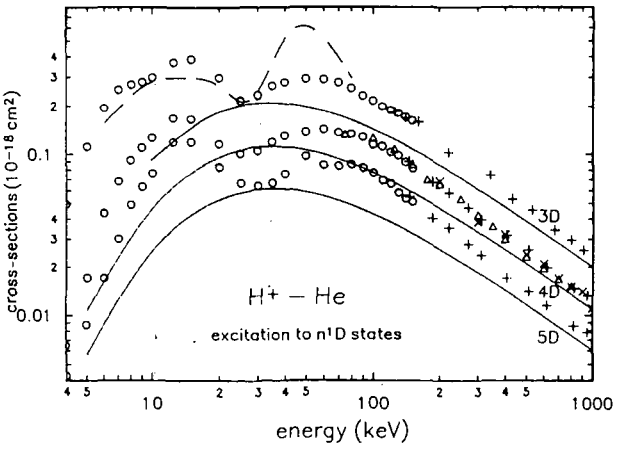

FIG. 3. Excitation cross-sections to n ^{1}D states in H^+-He collisions. For an explanation of the symbols, see caption to Fig. 1.

3. EXCITATION IN Z^{q+}–He(^{1}S) COLLISIONS

In the following discussion of He excitation by heavy ions (Z > 1) it is always understood that any effect of the projectile core can be neglected, except for screening of the projectile charge. This is generally true in not too slow collisions with a projectile in a high charge state. Helium excitation by He^+ projectiles is an extreme example for a case where core excitation and electron exchange cannot be discounted; such cases are not considered here.

Janev and Presnyakov [18] have shown that model np excitation cross-sections in Z^{q+}–H collisions lie on universal curves. The assumptions adopted in the 'dipole approximation close coupling' model of Ref. [18] have been shown later [19] to be rather severe. Improved calculated 2p excitation cross-sections scale only (with Z) at energies beyond the cross-section maximum. Another observation in Ref. [19], that cross-sections for H^+ projectiles may not lie on the otherwise universal curve, cannot be maintained after publication of the further improved, near-converged calculations for the He^2–H system [20]: the cross-sections for He^{2+} and H^+ impact (on H targets) lie on universal curves at high energies, while deviations occur at lower energies [20]. Typical deviations are by a factor of two, down to 10 keV/amu, but they may become larger at lower energies. It can be expected that such conclusions apply also to systems with helium targets.

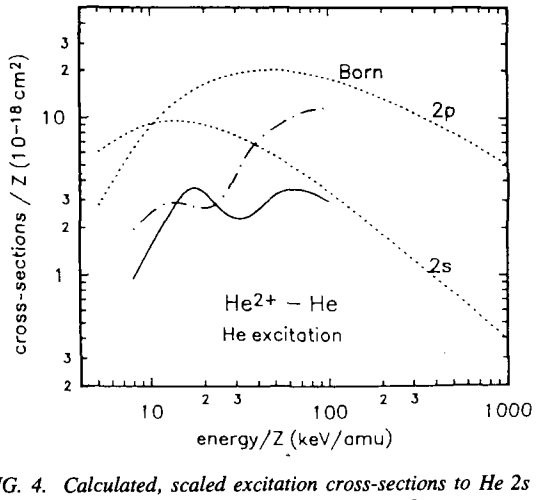

FIG. 4. Calculated, scaled excitation cross-sections to He 2s (full line) and 2p (dash-dotted line) states in He^{2+}–He collisions, this work. Dotted lines designate the scaled Born cross-sections from Ref. [9].

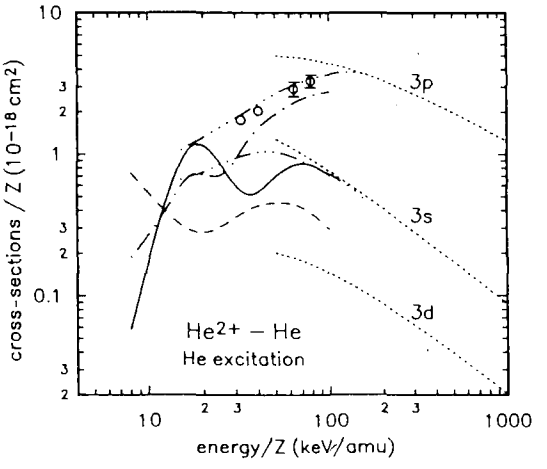

FIG. 5. Calculated, scaled excitation cross-sections to He 3s (full line), 3p (dash-dotted line) and 3d (dashed line) states in He^{2+}–He collisions, this work. Dotted lines designate the scaled Born cross-sections from Ref. [9] and open symbols the data for $3\,^1P$ excitation from Ref. [2]. Triple-dot-dashed lines designate the averaged, empirical universal curves from the data of Ref. [2].

In their review of the experimental situation, Anton et al. [2] arrive at similar conclusions for excitation to higher $n\,^1L$ states (n > 2), except that there is indication that cross-sections from proton impact do deviate from the otherwise universal curves in a systematic manner, even at higher energies, and increasingly so for higher-L or higher-n final states. Still, within a factor of two, there is agreement between the scaled cross-section curves for all projectiles.

For the purpose of this work, we have determined excitation cross-sections for He^2–He collisions within the close coupling scheme and a one-electron potential model for the active electron. In the atomic orbital basis we have included the n = 1–3 He^+ transfer states and the n = 2–4 excited states of He. Figure 4 shows the calculated, scaled excitation cross-sections to 2s and 2p He states. They seem to tie in smoothly with the Born cross-sections for the H^+–He system [9] at higher energies. At lower energies they show structures which are specific for this particular system. Such structures are known to occur in the H^+–H system [1], and recently they have also been observed in calculations for the He^{2+}–H system [20].

Figure 5 shows the calculated, scaled excitation cross-sections to the n = 3 He states from this work. Again, they seem to tie in smoothly with the (scaled) Born results at higher energies. The calculated cross-sections are also in harmony with the empirical

universal curves from the data set of Anton et al. [2] and, for the $3\,^1P$ state, with the available data [2] for this system. These data give no indication for the onset of structures at low energy, but they do not exclude it either. We note that, for higher-Z projectiles, cross-sections for individual systems may still show structures at low energy, while an averaged, universal curve does not. Low energy excitation certainly needs further investigation.

4. EXCITATION IN Z^{q+}-He($2\,^1S$) COLLISIONS

There are no data on collisions with excited helium, and, until very recently, there was only one theoretical assessment [21], within the dipole approximation close coupling model [18], of excitation cross-sections in H^+-He(n) collisions. As part of this work, we have determined $3\,^1L$ excitation cross-sections in H^+-He($2\,^1S$) collisions, within the close coupling method, in conjunction with a one-electron model for the active electron. The cross-section for $2\,^1P$ excitation has been determined with a two-electron description. Details have been reported elsewhere [22].

The calculated excitation cross-sections are shown in Fig. 6. The cross-section for the He $3\,^1D$ state is seen to be the largest one in the $3\,^1L$ manifold, in the considered energy range, but it is still much weaker than that in the DACC assessment [21] of the $3\,^1P$ cross-section. This indicates that the available DACC estimates [21] for the cross-sections in question are inadequate.

In the absence of other, independent information, it is still an open question how accurate the cross-sections from this work really are. The calculated $2\,^1P$ cross-section from a two-electron description is within 20% of another result derived with a one-electron model. It should be considered to be rather model insensitive and accurate to within 20%. The $3\,^1L$ cross-sections at low energy are certainly less reliable, and further work needs to be done. At higher energies, they tie in with other results derived within a two-state, two-electron description; in this case, an accuracy of about 20% may again be expected. At this point, cross-sections to higher-n states have to be constructed by applying n^{-3} scaling to the $3\,^1L$ cross-sections. This is, however, a particularly unsafe procedure at low energies. This is also true for applying σ/Z versus E/Z scaling for deriving cross-sections for higher-Z impact excitation.

No information is available for excitation from the He $2\,^3S$ state. Using the cross-sections for the corresponding singlet states would give a reasonable first guess.

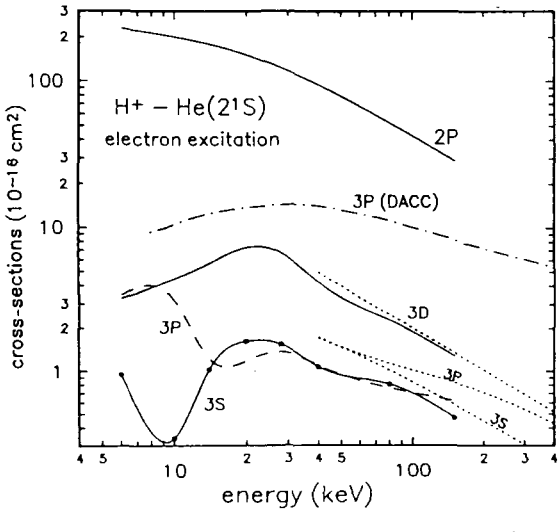

FIG. 6. Calculated excitation cross-sections for H^+-He($2\,^1S$) collisions. The dotted lines show results of two-electron, two-state calculations of this work and of Ref. [22] for the higher energies; the dash-dotted line shows the $3\,^1P$ excitation cross-section [21] of the dipole approximation close coupling model. The other curves show cross-sections for the $2\,^1P$ and $3\,^1L$ excited states from the multistate close coupling calculations of this work and of Ref. [22].

5. CONCLUSIONS

The database for excitation in H^+-He($1\,^1S$) collisions appears to be well established in the energy range 10–1000 keV, with accuracies estimated to be at the 10–20% level. Larger discrepancies remain for the $2\,^1L$ final states at low energy, and this work contains specific suggestions on recommended cross-section curves. These recommendations agree within a few per cent with the independent evaluation by de Heer et al. [15]. More work is needed to put these recommendations to a stringent test.

For the higher-Z projectiles, experimental work suggests universal cross-section curves, for a few transitions to $3\,^1L$–$5\,^1L$ states, for projectiles with $Z > 1$. Theoretical work on hydrogen targets suggests that excitation to the $2\,^1L$ states may be constructed from scaling the proton impact data. Uncertainties in these procedures are in the 30–50% range, with larger uncertainties applying at low energies or low projectile charge. For He^2 impact, we have calculated specific cross-sections for excitation to $2\,^1L$ and $3\,^1L$ states. Cross-sections for higher-n final states may be con-

structed from scaling of the $3\,^1L$ cross-sections, with the scaling factors being taken from the high energy behaviour of Born cross-sections. More work needs to be done in order to achieve a more accurate database.

Finally, there is now improved theoretical information about excitation in H^+–$He(2\,^1S)$ collisions. Scaling in both Z and the n quantum numbers of the final states may readily be applied for broadening of the database. More theoretical work is required for further improvements in the database.

ACKNOWLEDGEMENTS

The author is indebted to the participants of the IAEA meeting on the He beam database for α-particle diagnostics of fusion plasmas, June 1991, for their contributions and for discussions which led to improvements in the final form of this report, particularly to F.J. de Heer and K.-H. Schartner, and to the meeting organizer R.K. Janev. The independent evaluation by F.J. de Heer [15] has been very helpful in verifying the present work.

REFERENCES

[1] FRITSCH, W., LIN, C.D., Phys. Rep. **202** (1991) 1.
[2] ANTON, M., DETLEFFSEN, D., SCHARTNER, K.-H., this issue, p. 51.
[3] THOMAS, E.W., Excitation in Heavy Particle Collisions, Wiley-Interscience, New York (1972) 112ff.
[4] VAN DEN BOS, J., WINTER, G.J., de HEER, F.J., Physica **40** (1968) 357.
[5] DODD, J.G., HUGHES, R.H., Phys. Rev., A **135** (1964) 618.
[6] THOMAS, E.W., BENT, G.D., Phys. Rev. **164** (1967) 143.
[7] ROBINSON, J.M., GILBODY, H.B., Proc. Phys. Soc. (Lond.) **92** (1967) 589.
[8] HASSELKAMP, D., HIPPLER, R., SCHARMANN, A., SCHARTNER, K.-H., Z. Phys. **248** (1971) 254.
[9] BELL, K.L., KENNEDY, D.J., KINGSTON, A.E., J. Phys., B **1** (1968) 1037.
[10] SCHARMANN, A., SCHARTNER, K.-H., Z. Phys. **228** (1969) 254.
[11] KVALE, T.J., SEELY, D.G., BLANKENSHIP, D.M., et al., Phys. Rev., A **32** (1985) 1369.
[12] KIMURA, M., LIN, C.D., Phys. Rev., A **34** (1986) 176.
[13] SLIM, H.A., HECK, E.L., BRANSDEN, B.H., FLOWER, D.R., J. Phys., B **24** (1991) 1683.
[14] FRITSCH, W., Phys. Lett., A **160** (1991) 64.
[15] de HEER, F.J., HOEKSTRA, R., SUMMERS, H.P., this issue, p. 47.
[16] HIPPLER, R., SCHARTNER, K.-H., J. Phys., B **7** (1974) 618.
[17] PARK, J.T., SCHOWENGERDT, F.D., Phys. Rev., A **185** (1969) 152.
[18] JANEV, R.K., PRESNYAKOV, L.P., J. Phys., B **13** (1980) 4233.
[19] FRITSCH, W., SCHARTNER, K.-H., Phys. Lett., A **126** (1987) 17.
[20] FRITSCH, W., SHINGAL, R., LIN, C.D., Phys. Rev., A **44** (1991) 5686.
[21] JANEV, R.K., LANGER, W.D., EVANS, K., Jr., POST, D.E., Jr., Elementary Processes in Hydrogen-Helium Plasmas, Springer-Verlag, Berlin (1987).
[22] FRITSCH, W., Phys. Lett., A **158** (1991) 227.

NEW ASSESSMENT OF CROSS-SECTION DATA FOR HELIUM EXCITATION BY PROTONS

F.J. de HEER[1], R. HOEKSTRA[2,1], H.P. SUMMERS[3]
[1] FOM-Institute for Atomic and Molecular Physics,
Amsterdam,
The Netherlands
[2] Kernfysisch Versneller Instituut,
Groningen,
The Netherlands
[3] JET Joint Undertaking,
Abingdon, Oxfordshire,
United Kingdom

ABSTRACT. The paper presents a new assessment of cross-section data for excitation of He($1\,^1S$) by proton impact at energies higher than 10 keV (in a few cases 6 keV). Data for excitation to n ^{1}L states of He ($n \leq 4$, L = S, P and D) are given in tables. The data at high energy ($\sim$1000 keV) are linked to the first Born approximation, and data at low energies are linked in some cases to the close coupling atomic orbital results of Fritsch, who also made a critical evaluation of the cross-sections for excitation of helium by protons.

1. INTRODUCTION

A new assessment of proton impact cross-section data for excitation of helium from its $1\,^1S$ ground state is presented. As in the case of our studies of helium excitation by electron impact [1] and electron capture from helium by protons [2], this work was initiated in connection with the installation and recent use of ^{3}He and ^{4}He neutral heating beams on the JET tokamak [3]. The impact energy range covered extends to higher impact energies than the ones which are of direct interest for the present beam based diagnostics on JET (energies smaller than 200 keV) in order to be also of relevance to possible future helium beam based diagnostics. For ITER, neutral heating beams of a few hundreds of keV/amu are foreseen to closer match the velocity of fusion produced alpha particles [4].

Schematically, the processes studied here are given by

$$H^+ + He(1\,^1S) \rightarrow H^+ + He^*(n\,^1L) \qquad (1)$$

Except for the $2\,^1S$ state, the excited states decay under photon emission and so it is appropriate to study helium excitation by means of photon emission spectroscopy with measurement of absolute intensity. Therefore, this paper brings back into memory the often forgotten compilation by Thomas [5] of optical experiments in ion-atom collisions. Besides, it includes more recent work of this kind by Schartner's group, for example, Refs [6, 7]. As mentioned before, the $2\,^1S$ state of helium cannot be observed optically, and for the excitation of this state we have considered the energy loss experiments of Park's group [8, 9], who also measured the $2\,^1P$ excitation for which optical work has only been performed by Hippler and Schartner [7]. The most recent compilation of cross-section data has been provided by Barnett [10]. Our recommended cross-sections sometimes deviate from those given in that work.

Simultaneously with our study, Fritsch [11] has made a critical evaluation of existing data for helium excitation in heavy particle collisions, including proton impact, together with new calculations within the close coupling framework, with atomic basis sets applied to excitation of helium $2\,^1L$ and $3\,^1L$ levels. Our analysis of proton impact has many overlaps with the work of Fritsch and therefore we only give some complementary and relevant information, i.e. data tables of recommended excitation cross-sections.

2. RESULTS AND DISCUSSION

Compared with the compilation of Thomas [5], the principal new contribution in this paper is the inclusion of more recent experimental [6, 7, 9] and theoretical [11, 12] work. Generally, we confine ourselves to impact energies above 10 keV. In the article of Thomas we can see that the cross-sections obtained by the various

TABLE I. PRIMARY CHOICES OF EXPERIMENTAL AND THEORETICAL DATA

$H^+ + He(1\,^1S) \rightarrow H^+ + He(n\,^1L)$

Excited state	Energy range (keV)	Method	Refs	Accuracy
$2\,^1S$	6–28	AO	Fritsch [11]	~20%
	40–250	11.6 $\sigma(4\,^1S)$	Van den Bos et al. [14]	20–10%
	150–1000	11.6 $\sigma(4\,^1S)$	Hasselkamp et al. [6]	<10%
	>1000	Born	Bell et al. [13]	<5%
$3\,^1S$	10–150	Optical experiment, ×0.784	Van den Bos et al. [14]	30–10%
	200–1000	2.61 $\sigma(4\,^1S)$	Hasselkamp et al. [6]	<10%
	>1000	Born	Bell et al. [13]	<5%
$4\,^1S$	10–150	Optical experiment	Van den Bos et al. [14]	30–10%
	200–1000	Optical experiment	Hasselkamp et al. [6]	<10%
	>1000	Born	Bell et al. [13]	<5%
$2\,^1P$	6–28	AO	Fritsch [11]	~20%
	30–150	4.09 $\sigma(3\,^1P)$	Van den Bos et al. [14]	20–10%
	150–1000	Optical experiment	Hippler and Schartner [7]	<10%
	>500	Born	Bell et al. [13]	<5%
$3\,^1P$	10–150	Optical experiment, ×0.82	Van den Bos et al. [14]	30–10%
	150–1000	Optical experiment	Hippler and Schartner [7]	<10%
	>500	Born	Bell et al. [13]	<5%
$4\,^1P$	10–150	Optical experiment, ×1.25	Van den Bos et al. [14]	30–10%
	200–1000	Optical experiment	Hippler and Schartner [7]	<10%
	>1000	Born	Bell et al. [13]	<5%
$3\,^1D$	10–150	Optical experiment, ×0.8	Van den Bos et al. [14]	30–10%
	200–1000	1.88 $\sigma(4\,^1D)$	Hasselkamp et al. [6]	<10%
	>1000	Born	Bell et al. [13]	<5%
$4\,^1D$	10–150	Optical experiment, ×0.9	Van den Bos et al. [14]	30–10%
	200–1000	Optical experiment	Hasselkamp et al. [6]	<10%
	>1000	Born	Bell et al. [13]	<5%

Note: Fritsch [11] used the following correction factors in the case of the data of Van den Bos et al. [14]: 0.74 for $3\,^1S$, 0.75 for $3\,^1P$, 1.14 for $4\,^1P$, 1.47 for $5\,^1P$, 0.82 for $3\,^1D$, 0.9 for $4\,^1D$ and 1.12 for $5\,^1D$.

groups often show approximately the same energy dependence, but differ in absolute scale. Therefore, Thomas often applied a normalization procedure at one impact energy and then plotted the data again in one graph.

In order to establish an absolute scale, we generally give preference to the data of Schartner's group [6, 7] (for $2\,^1P$, $3\,^1P$ and $4\,^1L$ levels) between 150 and 1000 keV, because at high energies they merge very well with the data from the Born approximation. The corresponding cross-sections have been calculated by Bell et al. [13]. At these relatively high energies, we assume for the missing levels ($2\,^1S$, $3\,^1S$, $3\,^1D$ and $n\,^1L$ ($n \geq 4$)) that the cross-section ratios in a term series are independent of energy and have the same values as in the Born approximation. It appears experimentally that this ratio is even approximately constant down to about 40 keV. Thus, deviations are largest for the lower levels in a term series where the difference in excitation energy is relatively the largest. This can be seen in the low energy experimental data of Van den Bos et al. [14] and the calculations of Fritsch [11] and Slim et al. [12].

As noted before, data below 150 keV often differ in absolute scale and have to be normalized. In this work we have often given preference to the optical data of Van den Bos et al. [14] between 1 and 150 keV and fitted them to the high energy data of Hasselkamp et al. [6] and Hippler and Schartner [7], for the following two reasons: The energy dependence of the cross-

TABLE II. RECOMMENDED EXCITATION CROSS-SECTIONS (in units of 10^{-20} cm^2)

$H^+ + He(1\,^1S) \rightarrow H^+ + He(n\,^1L)$

E (keV)	$2\,^1S$	$3\,^1S$	$4\,^1S$	$2\,^1P$	$3\,^1P$	$4\,^1P$	$3\,^1D$	$4\,^1D$
6	71.1			194.5			19.5	
8							27.0	
10	241	27.4	8.82	331.3	45.5	14.8	29.9	12.6
12.5		36.1	10.4				37.1	16.7
14	460			311.4				
15		43.1	11.5		89.3	32.5	38.7	16.5
17.5								13.5
20	598	84.6	20.6	295.3	101	40.0	29.9	11.6
25		112	33.8		100	40.0	21.8	10.2
28	536			428				
30		116	40.8	425	104	45.6	23.4	10.4
35			44.8	512	125	52.5	26.7	11.9
40	567	128	48.9	556	136	56.3	32.0	13.1
50	547	131	47.1	793	194	75.0	29.3	13.7
60	520	112	44.8	954	234	87.5	29.1	14.2
70	523	94.7	45.1	958	234	98.7	27.9	13.6
80	483	102.6	41.7	1152	282	117	25.8	13.3
90	451	89.3	38.9	1183	289	114	23.3	12.8
100	407	90.8	35.1	1273	311	119	21.6	11.4
110	372	83.0	32.1	1340	328	144	20.0	11.2
120	343	77.8	29.6	1306	320	131	18.9	10.3
130	317	67.6	27.3	1333	326	135	18.1	9.81
140	287	69.8	24.7	1350	330	129	17.1	8.91
150	256	63.7	22.1	1287	323	130	16.1	8.19
200	219	49.3	18.9	1211	299	117	12.8	6.0
300	145	32.6	12.5	1006	256	101	7.1	3.8
400	110	24.8	9.5	864	220	93	6.0	3.2
500	87	19.6	7.5	787	197	77	4.5	2.4
600	69.6	15.7	6.0	682	178	72	3.9	2.1
700	59.2	13.3	5.1	647	165	63	3.2	1.7
800	53.4	12.0	4.6	568	150	58	2.8	1.5
1000	41.8	9.4	3.6	505	129	51	2.1	1.1
				Born cross-section (Bell et al. [13])				
1000	39.2	8.83	3.38	502.6	124.2	49.9	2.035	1.08
1500							1.374	0.732
2000	19.78	4.46	1.71	304.2	75.1	30.1	1.037	0.552
3000	13.23	2.98	1.14	223.6	55.1	22.1	0.696	
4000	9.94	2.24	0.857	178.8	44.1	17.7	0.524	
5000	7.96	1.79	0.686	150.0	37.0	14.8	0.420	

sections of Van den Bos et al. [14] is close to the average of various data sets, as shown by Thomas [5], and in several cases their absolute scale agrees within experimental errors with that of Schartner's group [6, 7]. The scaling factors for the data of Van den Bos used in the fitting procedure are mostly close to those of Fritsch [11], but they deviate in a few cases, as indicated below.

The experimental energy loss measurements of Kvale et al. [9], giving cross-sections for $2\,^1S$ and $2\,^1P$ at 25, 50, 75 and 100 keV, generally confirm the consistency of our procedure.

Table I summarizes the primary choices of experimental and theoretical data, together with the assessments of the accuracy of the cross-sections over the various energy intervals. Table II summarizes the recommended cross-sections for excitation to the different He($n\,^1L$) levels, where $n \leq 4$ and L = S, P and D from the He($1\,^1S$) ground state. For $n > 4$, we recommend to extrapolate the cross-sections with the same ratios as in the Born approximation at 100 keV (see Ref. [13], where these cross-sections are tabulated up to $7\,^1S$, $6\,^1P$ and $6\,^1D$). For higher n values, one may extrapolate according to the n^{*-3} proportionality, where n^* is the effective principal quantum number. All these extrapolated cross-sections have approximately similar errors as the corresponding n = 4 levels at comparable impact energies.

Excitation to the $n\,^1F$ (G, H, ...) levels is relatively small and negligible.

3. CONCLUSIONS

As was also pointed out by Fritsch [11], the excitation cross-sections for H^+ - He($1\,^1S$) collisions are generally well established, particularly in the energy range relevant for nuclear fusion applications, i.e. for more than 10 keV impact energy. The higher the impact energy, the more accurate were the cross-sections obtained experimentally and theoretically. Generally, near 1000 keV, the theoretical Born values are expected to be within 5%. At lower impact energies, optical experiments give data accurate to 10% down to about 150 keV, and, at still lower energies, the scaled experimental data are expected to have uncertainties of 10–30% from 100 keV down to 10 keV. Close coupling extended atomic orbital calculations have been used to predict missing experimental data for $2\,^1S$ and $2\,^1P$ at low energies [11] which appear to be consistent with experiment for $3\,^1S$, $3\,^1P$ and $3\,^1D$ below about 30 keV.

ACKNOWLEDGEMENTS

This work is part of the research programme of the Stichting voor Fundamenteel Onderzoek der Materie (FOM), which is financially supported by the Nederlandse Organisatie voor Wetenschappelijk Onderzoek (NWO). Via an Article 14 Contract with JET, the work is also part of the research programme of the association agreement between FOM and Euratom, with financial support of NWO.

REFERENCES

[1] de HEER, F.J., HOEKSTRA, R., KINGSTON, A.E., SUMMERS, H.P., this issue, p. 19.
[2] HOEKSTRA, R., SUMMERS, H.P., de HEER, F.J., this issue, p. 63.
[3] SUMMERS, H.P., HELLERMANN, M. von, de HEER, F.J., HOEKSTRA, F., this issue, p.7.
[4] JANEV, R.K., Comments At. Mol. Phys. **26** (1991) 83.
[5] THOMAS, E.W., Excitation in Heavy Particle Collisions, Wiley-Interscience, New York (1971).
[6] HASSELKAMP, D., HIPPLER, R., SCHARMANN, A., SCHARTNER, K.-H., Z. Phys. **248** (1971) 254.
[7] HIPPLER, R., SCHARTNER, K.-H., J. Phys., B (London). At. Mol. Phys. **7** (1974) 618.
[8] PARK, J.T., SCHOWENGARDT, F.D., Phys. Rev., A **185** (1969) 152.
[9] KVALE, T.J., SEELY, D.G., BLANKENSHIP, D.M., et al., Phys. Rev., A **34** (1986) 176.
[10] BARNETT, C.F. (Ed.), Atomic Data for Fusion, Vol. 1, ORNL-6086/VI, Oak Ridge National Laboratory, Oak Ridge, TN (1990).
[11] FRITSCH, W., this issue, p. 41.
[12] SLIM, H.A., HECK, E.L., BRANSDEN, B.H., FLOWER, D.R., J. Phys., B (London). At. Mol. Opt. Phys. **24** (1991) 1683.
[13] BELL, K.L., KENNEDY, D.J., KINGSTON, A.E., J. Phys., B (London). At. Mol. Phys. **1** (1968) 1037.
[14] VAN DEN BOS, J., WINTER, C.J., de HEER, F.J., Physica **40** (1968) 357.

HEAVY ION IMPACT EXCITATION OF HELIUM: EXPERIMENTAL TOTAL CROSS-SECTIONS

M. ANTON, D. DETLEFFSEN, K.-H. SCHARTNER
I. Physikalisches Institut,
Justus-Liebig-Universität Giessen,
Giessen, Germany

ABSTRACT. The paper presents a collection of total cross-sections for the excitation of n ^{1}P, n ^{1}S and n ^{1}D levels of helium by projectiles with charges between $1e_0$ and $12e_0$ and for specific energies between 35 and 800 keV/u. Earlier results are included. The cross-sections are shown to fulfil a scaling relation with respect to projectile charge and velocity for $q \geq 2$. Mean curves through the experimental data are derived with an averaging procedure.

1. INTRODUCTION

The mean free path of fast neutral particles such as helium in plasmas can be reduced by the presence of highly charged impurity ions [1, 2]. Their influence results mainly from multistep processes producing excited He atoms in the first step and ionization out of the excited state in the second step. Calculations of the mean free path considering such multistep processes make use of a scaling relation of the total excitation processes which was based in its first derivation on a close coupling dipole approximation for hydrogen excitation [3, 4] but which can also be derived classically [5]. Recently, detailed theoretical studies of the excitation of He have been presented [6] and only one experimental investigation of the subject existed up to now [5]. A second set of data is published here, with more attention given to the lower specific energies.

2. EXPERIMENTAL

The excitation process under consideration reads schematically

$$A^{q+} + He \rightarrow A^{q+} + He^*$$

where * stands for 3 ^{1}P, 4 ^{1}P, 3 ^{1}S, 4 ^{1}S, 5 ^{1}S, 3 ^{1}D, 4 ^{1}D and 5 ^{1}D. Partially stripped projectiles with charge q were used. For the determination of the cross-sections the optical method was applied. The apparatus used by us is different from the one used in the first investigation [5]; it was originally designed to determine cross-sections for the five magnetic substates of the He–4 ^{1}D level [7]. It consists of a differentially pumped gas target which ensures single collision conditions. The observed fluorescence light is visible and the wavelengths range from ≈430 nm to 505 nm. Interference filters and polarization foils within a telescopic lens system were used. For details of the experimental set-up and procedure (e.g. cascade correction) the reader is referred to Refs [5] and [7], respectively.

The cross-sections published in Ref. [5] were measured using O^{6+}, Ne^{7+}, Cr^{15+}, Ni^{16+}, Ge^{18+}, Xe^{24+}, U^{33+}, Bi^{45+} at 1.4 MeV/u, Si^{6+} between 143 and 1000 keV/u, $Si^{3+,4+,8+,10+}$ at 500 keV/u, Cu^{5+} between 63.5 and 365 keV/u and $Cu^{6+,8+,10+,12+}$ at 444 keV/u. The experiments for 1.4 MeV/u were carried out at the linear heavy ion accelerator UNILAC at the Gesellschaft für Schwerionenforschung, Darmstadt [8]. In our case, we used $Si^{3+,6+,8+}$ between 150 and 800 keV/u, Cu^{q+} between 63.5 and 254 keV/u, He^{++} between 40 and 160 keV/u and H^+ between 35 and 250 keV/u. The cross-sections for He^{++} and H^+ impact were measured with a 400 kV accelerator, while the Cu and Si ions were produced in a 4 MV tandem accelerator. The ion beams from both accelerators could be focused into the same target. All experiments with Si, Cu, He and H ions were carried out at the Dynamitron Tandem Laboratorium, Bochum. The absolute cross-sections given in Ref. [5] were obtained by normalization on reliable published cross-sections for electron impact excitation which are cited in Ref. [5]. The new data were obtained by normalization on cross-sections for proton impact excitation of He. 1 MeV protons from the tandem accelerator were used to normalize the cross-sections for Cu and Si impact. The cross-sections for H^+ and He^{++} impact, measured with the 400 keV accelerator, were normalized on the proton impact cross-sections at 200 keV.

3. CROSS-SECTIONS

The scaled excitation cross-sections are presented in Figs 1–7, where we plot $\sigma/q = f(v^2/q)$, with q denoting the projectile charge and v the projectile velocity. This scaling relation is the one mentioned in the introduction (Refs [3, 5]). In Figs 2, 3, 4, 6 and 7 the data for Si^{q+} impact from Ref. [5] are included for comparison. The cross-sections for excitation of the $3\,^1S$ and $3\,^1D$ level (Figs 1 and 5) have not been published so far [9] and, to our knowledge, no other data for these levels and for $q \geq 2$ are available. The dashed line in the figures is a guiding line through the recommended cross-sections for proton impact [10].

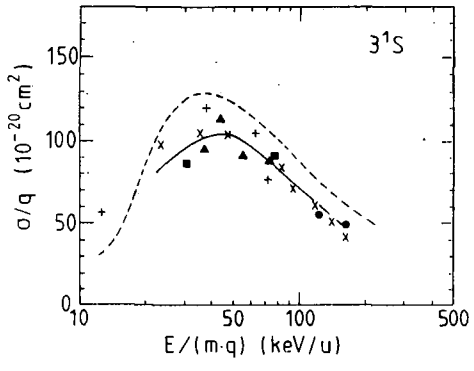

FIG. 1. Scaled excitation cross-section σ/q for the $3\,^1S$ state as a function of the scaled specific energy E/mq: ■ — Ge^{18+}, Bi^{45+}; ▲ — Cu^{q+} ($6 \leq q \leq 10$); + — Cu^{5+}; × — Si^{6+}; ● — Si^{q+} ($3 \leq q \leq 10$) from Ref. [9]; full line: average curve through data for $q \geq 2$ (see text); dashed line: average curve through recommended H^+ data from Ref. [10].

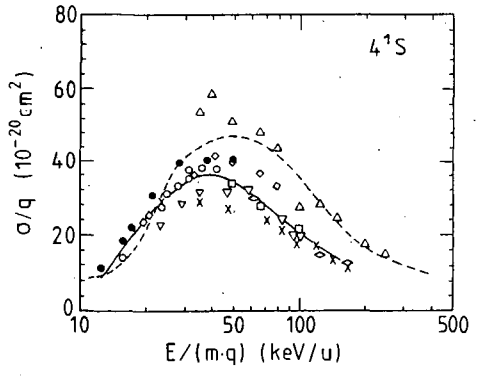

FIG. 2. Scaled excitation cross-section σ/q for the $4\,^1S$ state as a function of the scaled specific energy E/mq: × — Si^{6+}; ◆ — Si^{q+} ($3 \leq q \leq 10$) (from Ref. [9]); △ — H^+; ◇ — He^{++}; □ — Si^{3+}; ▽ — $Si^{6+,8+}$; ● — Cu^{5+}; ○ — Cu^{q+} ($6 \leq q \leq 10$); full line: average curve through data for $q \geq 2$ (see text); dashed line: average curve through recommended H^+ data from Ref. [10].

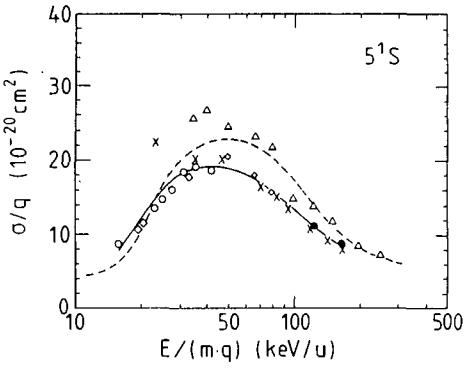

FIG. 3. Scaled excitation cross-section σ/q for the $5\,^1S$ state as a function of the scaled specific energy E/mq: × — Si^{6+}; ● — Si^{q+} ($3 \leq q \leq 10$) (from Ref. [9]); △ — H^+; ◇ — He^{++}; □ — Si^{3+}; ▽ — $Si^{6+,8+}$; ○ — Cu^{q+} ($6 \leq q \leq 10$); full line: average curve through data for $q \geq 2$ (see text); dashed line: average curve through recommended H^+ data from Ref. [10].

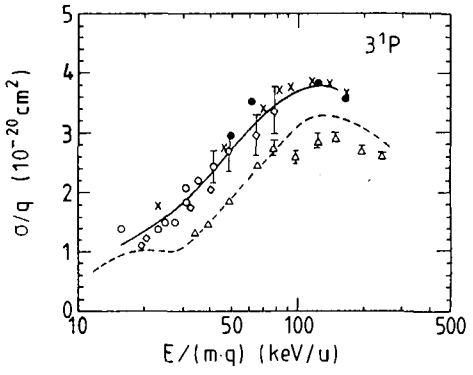

FIG. 4. As Fig. 3, but excitation of the $3\,^1P$ state. Error bars give the maximum statistical error.

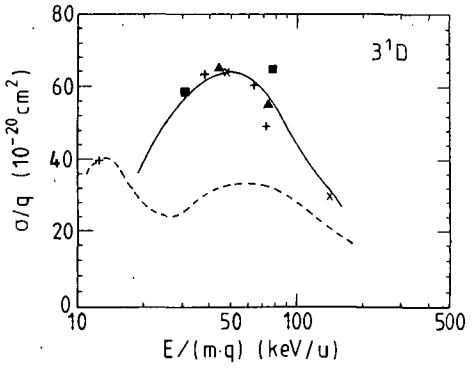

FIG. 5. As Fig. 1, but excitation of the $3\,^1D$ state.

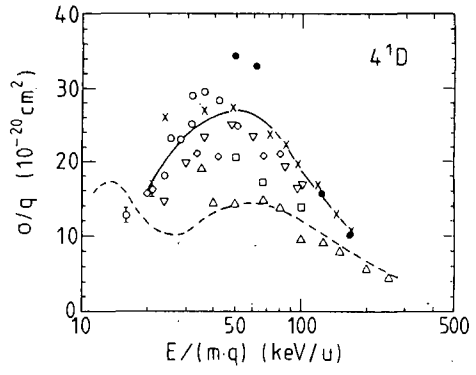

FIG. 6. As Fig. 3, but excitation of the $4\,^1D$ state.

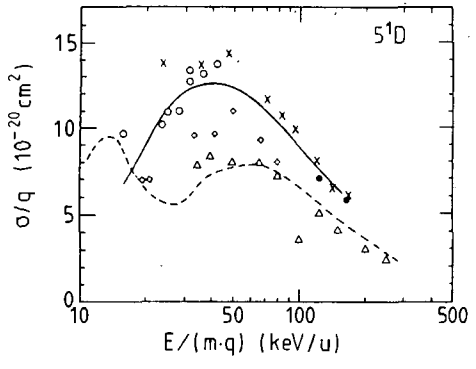

FIG. 7. As Fig. 3, but excitation of the $5\,^1D$ state.

There is good agreement between our heavy ion data and the Si cross-sections from Ref. [5] within the error bars of the absolute cross-sections. These are estimated to be 30%, where the contribution of the statistical error is 10–15% in the case of He^{++} impact and 5% in all other cases. In some cases, e.g. for the $4\,^1S$ and $5\,^1S$ levels, the cross-sections for proton impact show deviations of about 20% from the recommended energy dependence for energies below 50 keV. The cross-section value for 100 keV proton impact is certainly systematically too low for all levels and should be disregarded. In all cases, only the proton impact data seem to differ significantly from the scaled data with $q \geq 2$. This deviation is systematic in the sense that the cross-sections for proton impact excitation exceed the scaled cross-sections for heavy ion impact for the $n\,^1S$ levels, while they are smaller for the $n\,^1D$ and $n\,^1P$ levels. The largest difference is observed for the $n\,^1D$ levels. The experimental conditions did not allow to study finer details, for example the convergent behaviour of the scaled cross-sections as a function of q, if this exists.

The experimental cross-sections are consistent with the assumption that the shape of the scaling function f is the same within each $n\,^1L$ series, with L = S,P,D. Moreover, a $\sigma_n \sim n^{-3}$ relation is valid.

For a simpler use of the presented experimental results in calculations of the neutral beam stopping we derived smooth curves through all data points with $q \geq 2$. These curves were obtained by calculating first a weighted mean, x_{mean}, y_{mean}, of six to nine adjacent experimental values, with $x_i = (E/mq)_i$ and $y_i = (\sigma/q)_i$. The reciprocal values of the relative statistical errors Δy_i of the scaled cross-sections were taken as weighting factors:

$$x_{mean} = \left(\sum \frac{1}{\Delta y_i} x_i\right) \Big/ \left(\sum \frac{1}{\Delta y_i}\right)$$

$$y_{mean} = \left(\sum \frac{1}{\Delta y_i} y_i\right) \Big/ \left(\sum \frac{1}{\Delta y_i}\right)$$

It has to be stressed that for both x and y the weight was $1/\Delta y_i$. At the low and high energy end of the data sets, additional average values were calculated from

TABLE I. AVERAGED VALUES FOR THE SCALED EXCITATION CROSS-SECTION σ/q GIVEN BY THE AVERAGING AND INTERPOLATING PROCEDURE DESCRIBED IN THE TEXT

E/mq (keV/u)	σ/q (10^{-20} cm^2)						
	$3\,^1S$	$4\,^1S$	$5\,^1S$	$3\,^1P$	$3\,^1D$	$4\,^1D$	$5\,^1D$
15	65.7	14.2	6.99	106	25.8	10.9	6.30
20	74.7	24.2	11.9	132	38.6	16.3	8.89
30	93.6	33.4	17.9	181	56.4	23.8	12.1
40	103.2	36.1	19.0	227	62.1	26.2	12.6
50	102.9	34.2	18.9	269	64.0	27.0	12.4
60	96.6	31.1	18.2	302	62.8	26.5	11.8
70	88.9	28.1	17.0	327	59.3	25.0	11.0
80	82.1	25.3	15.8	345	54.5	23.0	10.3
90	76.3	22.8	14.6	359	49.1	20.7	9.55
100	71.2	20.6	13.5	369	44.1	18.6	8.90
110	66.6	18.7	12.4	377	40.1	16.9	8.30
120	62.4	17.0	11.4	381	37.0	15.6	7.76
130	58.4	15.7	10.6	382	34.1	14.4	7.27
140	54.5	14.6	9.85	379	31.8	13.4	6.84
150	50.7	13.7	9.25	374	29.2	12.3	6.45
160	46.8	12.8	8.67	367	26.3	11.1	6.07

three points each. Finally, the mean values were connected by a natural cubic spline [11]. The procedure was tested using Monte Carlo simulated data. The good agreement between the model functions underlying the simulated data and the averaged curves supported the use of the procedure described above. Nevertheless, it was not applied to the $3\,^1D$ level because of the small number of experimental data points. In this case, the full line in Fig. 5 was obtained from the result for the $4\,^1D$ level in Fig. 6 using the $\sigma_n \sim n^{-3}$ relation.

The results are presented in Table I. Without losing accuracy, the curves for the $3\,^1P$, the $4\,^1S$ and the $4\,^1D$ levels might be used as basic curves, while the scaled cross-sections for all other levels can be calculated using the $\sigma_n \sim n^{-3}$ relation.

Summarizing, we have presented total cross-sections for the excitation of $n\,^1S$, $n\,^1P$ and $n\,^1D$ levels of He by highly charged ions. The scaling relation $\sigma_n/q = f_n(v^2/q)$ has been shown to hold within 30% for $2 \leq q \leq 12$ and for scaled specific energies E/mq between 20 and 150 keV/u. Smooth curves for the functions f_n have been derived to simplify the use of the cross-sections in calculations of the neutral beam stopping in plasmas.

For scaled specific energies E/mq below 20 keV/u, the cross-sections are probably *not* in accordance with the scaling relation. Fritsch et al. [4, 12] showed that for the excitation of atomic hydrogen, scaled cross-sections for σ/q for different charge states q obtained with close coupling calculations differ by more than a factor of two in this E/mq range. The first Born approximation is generally believed to be an adequate theory for scaled specific energies E/mq higher than 200 keV/u, but it is in accordance with the scaling relation only for dipole forbidden transitions.

REFERENCES

[1] BOLEY, C.B., JANEV, R.K., POST, D.E., Phys. Rev. Lett. **52** (1984) 534.

[2] KOROTKOV, A.A., this issue, p. 79.

[3] JANEV, R.K., PRESNYAKOV, L.P., J. Phys., B. **13** (1980) 4233.

[4] FRITSCH, W., SCHARTNER, K.-H., Phys. Lett., A **126** (1987) 17.

[5] REYMANN, K., SCHARTNER, K.-H., SOMMER, B., TRÄBERT, E., Phys. Rev., A **38** (1988) 2290.

[6] RODRÍGUEZ, V.D., MIRAGLIA, J.E., J. Phys., B (London). At. Mol. Phys. **23** (1990) 3629.

[7] ANTON, M., SCHARTNER, K.-H., HASSELKAMP, D., SCHARMANN, A., Z. Phys., D **18** (1991) 53.

[8] ANTON, M., SCHARTNER, K.-H., Sci. Rep. GSI **90-1**, Gesellschaft für Schwerionenforschung, Darmstadt (1990) 139.

[9] REYMANN, K., Experimente zur Anregung von Heliumatomen durch hochgeladene Ionen im Bereich mittlerer und hoher Projektilgeschwindigkeiten, PhD thesis, University of Giessen (1989).

[10] FRITSCH, W., this issue, p. 41.

[11] PRESS, W.H., FLANNERY, B.P., TEUKOLSKY, S.A., VETTERLING, W.T., Numerical Recipes: The Art of Scientific Computing, Cambridge University Press, New York (1986).

[12] FRITSCH, W., SHINGAL, R., LIN, C.D., Phys. Rev., A **44** (1991) 5686.

REVIEW OF EXPERIMENTAL DATA ON ELECTRON CAPTURE AND IONIZATION FOR COLLISIONS OF PROTONS AND MULTIPLY CHARGED IONS WITH HELIUM ATOMS AND IONS

H.B. GILBODY
Department of Pure and Applied Physics,
The Queen's University of Belfast,
Belfast, Northern Ireland, United Kingdom

ABSTRACT. Cross-sections relating to electron capture, transfer ionization and pure ionization in collisions of protons and multiply charged ions with helium are considered in terms of both the available experimental data and scaling relations. The data on charge transfer in collisions between He^+ ions and other simple ions are also discussed. The possible influence of fast metastable atoms in collision processes involving helium beams is considered in terms of the available experimental data.

1. INTRODUCTION

Accurate cross-section data for collision processes involving both electron capture and ionization are required for a better understanding of helium atom beam penetration into fusion plasmas and for schemes relevant to alpha particle diagnostics. The energies of primary interest are in the range 10–1000 keV/u. Recommended data for some of these processes based on an evaluation of both experimental results and theoretical predictions have been given by Barnett [1] for ions of hydrogen, helium and lithium in collisions with helium atoms. Electron capture data for other multiply charged ions have been compiled by Huber and Kahlert [2].

In this short review, the experimental data on cross-sections for electron capture and ionization in collisions of helium atoms with ions are considered. Protons and fully stripped ions are of primary interest, although partially stripped ions may also be important in the context of impurities. The available data apply mainly to helium atoms in the ground state, although there have been some measurements relating to the formation and collisional destruction of fast metastable atoms. Some relevant data on collisions of helium ions with positive ions are also considered.

2. COLLISIONS WITH GROUND STATE HELIUM ATOMS

2.1. Identification of the processes

The following processes involving ground state helium atoms are considered:

One-electron capture

$$X^{q+} + He \rightarrow X^{(q-1)+} + He^+ \quad (1)$$

with the cross-section ${}_{q0}\sigma_{(q-1)1}$ which includes all final ground and excited product states.

Two-electron capture

$$X^{q+} + He \rightarrow X^{(q-2)+} + He^{2+} \quad (2)$$

with the cross-section ${}_{q0}\sigma_{(q-2)2}$ for capture into bound states of $X^{(q-2)+}$.

Transfer ionization

$$X^{q+} + He \rightarrow X^{(q-1)+} + He^{2+} + e \quad (3)$$

with the cross-section ${}_{q0}\sigma_{(q-1)2}$ which could include contributions from processes involving two-electron capture into states which undergo autoionization.

Pure single ionization

$$X^{q+} + He \rightarrow X^{q+} + He^+ + e \quad (4)$$

with the cross-section ${}_{q0}\sigma_{q1}$.

Pure double ionization

$$X^{q+} + He \rightarrow X^{q+} + He^{2+} + 2e \quad (5)$$

with the cross-section ${}_{q0}\sigma_{q2}$.

2.2. Experimental methods

For many years, a variety of experimental techniques (see for example Massey and Gilbody [3]) have been used to obtain data on these processes. However, few of the methods used can provide data on all the individual processes (1)–(5). In the widely used

beam/static gas target approach, in which the primary X^{q+} ion beam is passed through a thin helium target, studies of the yields of either the fast $X^{(q-1)+}$ or the $X^{(q-2)+}$ product ions can provide total cross-sections for either one- or two-electron capture with an accuracy within 10%. In the condenser plate method, which has been used in a number of different variants, measurements of the yields of slow ions and electrons from a well defined path length in the target gas provide only total cross-sections for slow ion or electron production which require careful interpretation. Some of the most careful measurements of this type have been carried out by Rudd et al. [4], but discrepancies of up to about 50% between the results of different investigators are not unusual.

In a different experimental approach, first used by Afrosimov et al. [5], slow product ions are extracted from a well defined target region, charge analysed and then counted in delayed coincidence with the charge analysed products arising from the same collision events. In this way, it is possible in principle to determine separate cross-sections for all the individual processes. More recently, Shah and Gilbody [6, 7] have developed a crossed beam method in which slow product ions arising from the crossed beam region are extracted with high efficiency, analysed by time-of-flight mass spectrometry and counted in coincidence with either the electrons or the charge analysed fast ion collision products from the same events. This method, originally developed for studies of collisions involving hydrogen atoms, has since been applied to stable targets including helium [8, 9]. Measurements must be normalized to well established cross-sections, and in this way cross-sections for the individual processes (1)–(6) have been determined with estimated accuracies well within 10%.

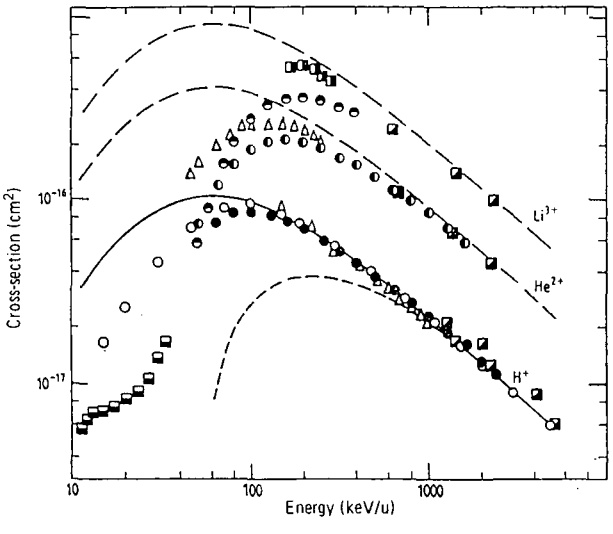

FIG. 1. Cross-sections $_{q0}\sigma_{q1}$ for single ionization of helium by H^+, He^{2+} and Li^{3+} ions together with other relevant data.
Coincidence measurements of $_{q0}\sigma_{q1}$: ●, ◐, ○ — Shah and Gilbody [8] for H^+, He^{2+} and Li^{3+} impact; ◪ — Knudsen et al. [10] for H^+, He^{2+} and Li^{3+} impact; ◘ — Afrosimov et al. [11] for He^{2+} impact.
Condenser plate measurements of total cross-sections σ_e for electron production: ○ — Rudd et al. [4] for H^+ impact; △ — Puckett et al. [12] and Puckett and Martin [13] for He^{2+} and H^+ impact; ◘ — Pivovar et al. [14] for Li^{3+} impact.
Theory for $_{q0}\sigma_{q1}$: ——, — — — $_{q0}\sigma_{q1}$ calculated by Bell and Kingston [15] using the Born approximation.
Electron impact ionization: —— cross-sections for single ionization by equivelocity electrons measured by Montague et al. [16].
(Figure adapted from Ref. [8]).

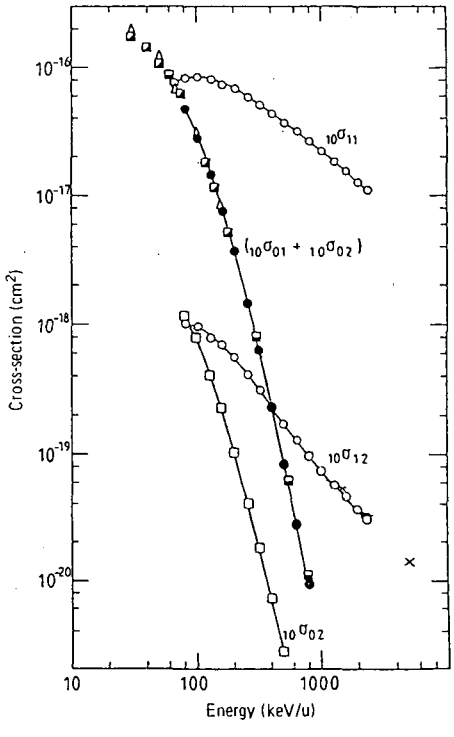

FIG. 2. Cross-sections for ionization and electron capture in collisions of protons with helium.
Coincidence measurements: ○ — $_{10}\sigma_{11}$ and $_{10}\sigma_{12}$, Shah and Gilbody [8]; × — $_{10}\sigma_{12}$, Knudsen et al. [10]; ● $(_{10}\sigma_{01} + _{10}\sigma_{02})$, Shah and Gilbody [8]; □ — $_{10}\sigma_{02}$, Shah and Gilbody [8].
Condenser plate and beam-static gas measurements: △ — $(_{10}\sigma_{01} + _{10}\sigma_{02})$, Rudd et al. [4]; ◘ — $(_{10}\sigma_{01} + _{10}\sigma_{02})$, Toburen et al. [21]; ◪ — $(_{10}\sigma_{01} + _{10}\sigma_{02})$, Stier and Barnett [22].
(Figure adapted from Ref. [8]).

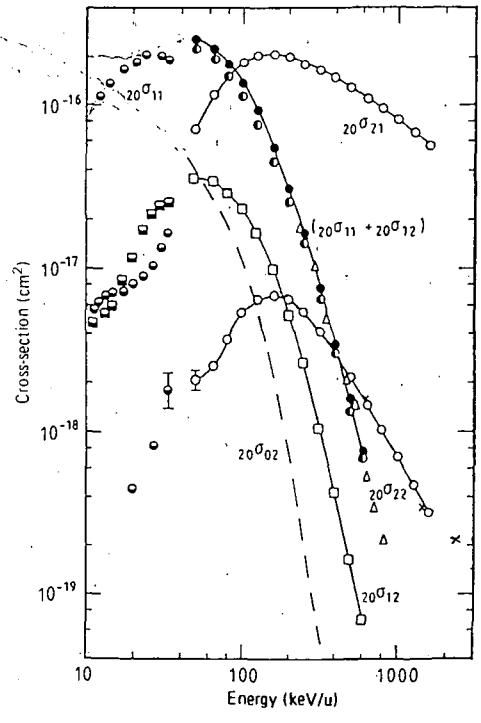

FIG. 3. Cross-sections for ionization and electron capture in collisions of He^{2+} ions with helium.
Coincidence measurements: ○ — $_{20}\sigma_{21}$ and $_{20}\sigma_{22}$, Shah and Gilbody [8]; × — $_{20}\sigma_{22}$, Knudsen et al. [10]; ◘, ◒ — $_{20}\sigma_{21}$, $_{20}\sigma_{22}$, $_{20}\sigma_{11}$ and $_{20}\sigma_{12}$, Afrosimov et al. [11]; ◐ — $_{20}\sigma_{11}$, Shah and Gilbody [8]; ● — $(_{20}\sigma_{11} + _{20}\sigma_{02})$, Shah and Gilbody [8]. Beam-static gas measurements: △ — $(_{20}\sigma_{11} + _{20}\sigma_{12})$, Hvelplund et al. [23]; —— —— $_{20}\sigma_{02}$, recommended values, Barnett et al. [24].
(Figure adapted from Ref. [8]).

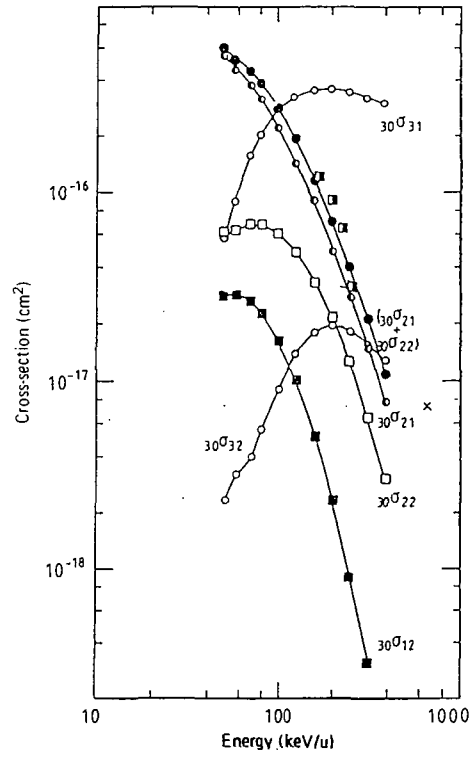

FIG. 4. Cross-sections for ionization and electron capture in collisions of Li^{3+} ions with helium.
Coincidence measurements: ○ — $_{30}\sigma_{31}$ and $_{30}\sigma_{32}$, Shah and Gilbody [8]; × — $_{30}\sigma_{32}$, Knudsen et al. [10]; □ — $_{30}\sigma_{22}$, Shah and Gilbody [8]; ■ — $_{30}\sigma_{12}$, Shah and Gilbody [8]; ◐ — $_{30}\sigma_{21}$, Shah and Gilbody [8]; ● — $(_{30}\sigma_{21} + _{30}\sigma_{22})$, Shah and Gilbody [8]. Beam-static gas measurements: ◧ — $(_{30}\sigma_{21} + _{30}\sigma_{22})$, Pivovar et al. [14].
(Figure adapted from Ref. [8]).

2.3. Experimental data

Cross-sections for the individual processes (1)–(5) for H^+, He^{2+} and Li^{3+} impact have been measured experimentally, but results are sparse for more highly charged primary ion species. The most comprehensive and accurate data for H^+, He^{2+} and Li^{3+} impact have been obtained by Shah and Gilbody [8] at energies in the range 50–2400 keV/u. Additional measurements by Shah et al. [9] for H^+ and He^{2+} extend the data down to energies of 9 keV/u and 6 keV/u, respectively.

Figure 1 shows the cross-sections $_{q0}\sigma_{q1}$ for single ionization of helium by H^+, He^{2+} and Li^{3+} impact based on coincidence counting studies together with total electron production cross-sections σ_e based on the condenser plate technique. The values of σ_e include contributions from processes (3) and (5) as well as from process (4) and are therefore expected to be larger than the corresponding values of $_{q0}\sigma_{q1}$. Single ionization cross-sections calculated using the Born approximation, also included for comparison, indicate that the predicted Z^2 scaling (where Z is the atomic number of the fully stripped primary ion) of cross-sections only appears reasonable at high velocities which increase as Z increases. Cross-sections for single ionization by equivelocity electrons can be seen to become equal to the corresponding cross-sections for proton impact at high velocities, as predicted by the Born approximation. At the lower impact velocities where the Born approximation is in poor accord with experiment, calculations by Fainstein et al. [17], based on the continuum-distorted-wave-eikonal-initial-state model (not shown) for H^+, He^{2+} and Li^{3+} impact, are found to provide a much better description of the experimental data.

In Figs 2, 3 and 4, cross-sections for the electron capture and ionization channels (1)–(5) are shown for H^+, He^{2+} and Li^{3+} impact. In all cases the main contribution to He^+ formation at high energies is provided by the single ionization cross-section $_{q0}\sigma_{q1}$, while at

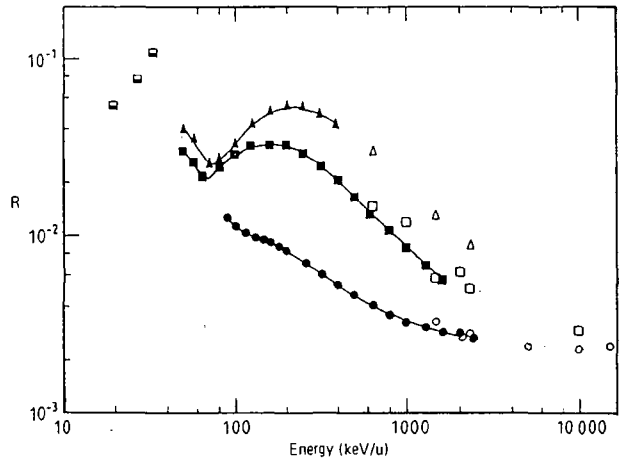

FIG. 5. Ratio $R = {}_{q0}\sigma_{q2}/{}_{q0}\sigma_{q1}$ of the double to single ionization cross-sections for helium bombarded by H^+, He^{2+} and Li^{3+} ions.
●, ■, ▲ — H^+, He^{2+}, Li^{3+} impact, Shah and Gilbody [8];
○, □, △ — H^+, He^{2+}, Li^{3+} impact, Knudsen et al. [10];
◘ — He^{2+} impact, Afrosimov et al. [11].
(Figure adapted from Ref. [8]).

low energies the simple one-electron capture cross-section ${}_{q0}\sigma_{(q-1)1}$ is dominant. The total cross-sections for one-electron capture which comprise the sum $({}_{q0}\sigma_{(q-1)1} + {}_{q0}\sigma_{(q-1)2})$ can be seen to contain contributions from the transfer-double ionization process (3) which increases as q increases.

The double ionization cross-sections ${}_{q0}\sigma_{q2}$ in Figs 2, 3 and 4 can be seen to maximize at about the same velocity as the corresponding single ionization cross-sections ${}_{q0}\sigma_{q1}$, but they are at least an order of magnitude smaller and decrease more rapidly at higher velocities. Figure 5 presents the values of the cross-section ratio $R = {}_{q0}\sigma_{q2}/{}_{q0}\sigma_{q1}$ for double to single ionization. At high velocities, the values of R appear to decrease towards a common velocity independent limit which is consistent with the 'shake off' mechanism of double ionization described by McGuire [18]. At lower velocities, below 100 keV/u, where a molecular description of the collision is appropriate, the values of R are rising to a second maximum.

Data for primary ions of higher q are sparse, but McGuire et al. [19] have considered experimentally measured cross-sections for both single and double ionization by ions which include C^{6+}, Fe^{15+}, Kr^{18+}, Fe^{20+}, U^{36+}, Gd^{37+} and U^{44+} at a fixed energy of 1.4 MeV/u. For charge states $q \leq 6$, the single ionization cross-sections are consistent with the q^2 scaling predicted by the first Born approximation. The departure from q^2 scaling for $q > 6$ is shown to be well described by the Glauber approximation. The ratio R of the double to single ionization cross-sections increases as approximately q^2 up to $q = 6$, but for $q > 6$ the divergence for q^2 scaling is believed to reflect the failure of the Born approximation rather than the direct ionization mechanism corresponding to direct Coulomb ionization of both electrons by the projectile.

Olson et al. [20] have compared experimental data for both ionization and electron capture at an energy of 1 MeV/u for q up to 50; their theoretical predictions are based on the classical trajectory Monte Carlo (CTMC) method. These calculations have been found to provide a reasonable description of both single and double ionization and of the total cross-section $({}_{q0}\sigma_{q-1)1} + {}_{q0}\sigma_{(q-1)2})$ for one-electron capture.

The resonant two-electron capture process for collisions of He^{2+} with He is of special interest. In Fig. 3, only the cross-sections ${}_{20}\sigma_{02}$ recommended by Barnett et al. [24], based on available data in the range 30–270 keV/u, are shown. Although there have been many experimental measurements at energies ranging from 0.001 to 170 keV/u (see compilation by Huber and Kahlert [2]), discrepancies by up to 50% between some of these results indicate the need for additional, more accurate measurements. In Fig. 6 the cross-sections ${}_{20}\sigma_{02}$ for two-electron capture are shown for impact energies which extend down to 0.9 keV/u. The data can be seen to be satisfactorily described by the

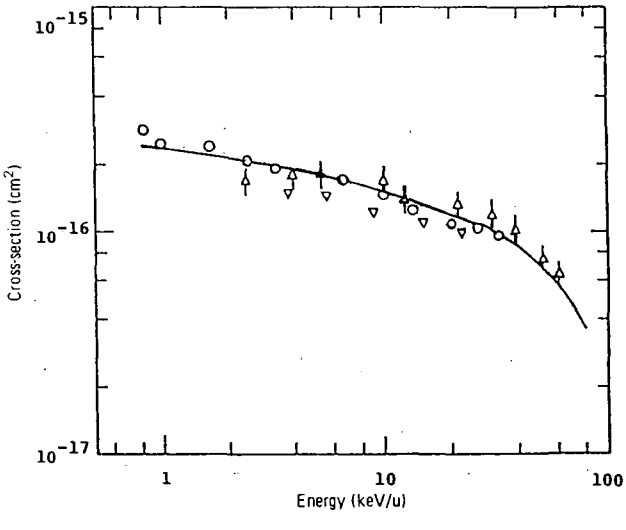

FIG. 6. Cross-sections for two-electron capture by He^{2+} ions in collisions with helium.
Experimental data: ○ — Afrosimov et al. [11, 25].
△ — Berkner et al. [26]; ▽ — Bayfield and Khayrallah [27].
Theory: —— Travelling molecular orbital method, Kimura [28].
(Figure adapted from Ref. [28]).

calculations of Kimura [28] based on the molecular orbital method. Low energy cross-sections are large and exceed the corresponding cross-sections $_{20}\sigma_{11}$ for one-electron capture at energies below 13 keV/u.

2.4. Cross-section scaling relations

It is useful to consider the extent to which scaling relations can be used to describe the available experimental data so that these may then be used to predict approximate values of unknown cross-sections.

Experimental data are most extensive for the total cross-sections $\sigma_c = ({}_{q0}\sigma_{(q-1)1} + {}_{q0}\sigma_{(q-1)2})$ for one-electron capture, and a number of different scaling procedures have been considered. Figure 7 shows the

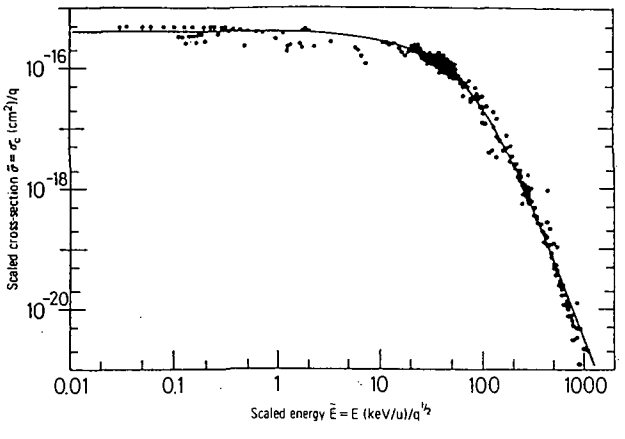

FIG. 7. Reduced cross-sections $\tilde{\sigma}$ for one-electron capture by multiply charged ions (with $q \geq 5$) in collisions with helium, plotted against reduced energy $\tilde{E}$. The curve is a fit to the experimental data.
(Figure adapted from Ref. [29]).

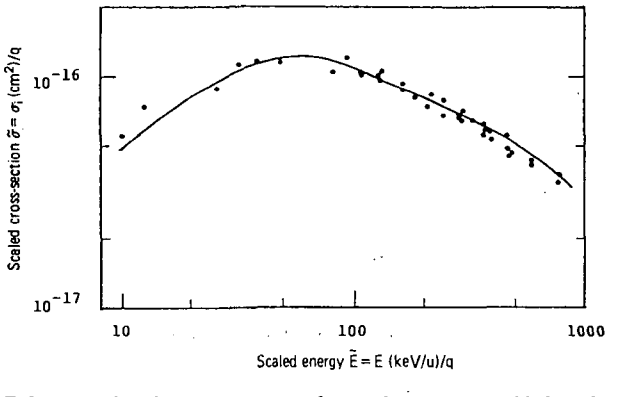

FIG. 8. Reduced cross-sections $\tilde{\sigma}$ for single ionization of helium by ion impact, plotted against reduced energy $\tilde{E}$. The curve is a fit to the experimental data.
(Figure adapted from Ref. [29]).

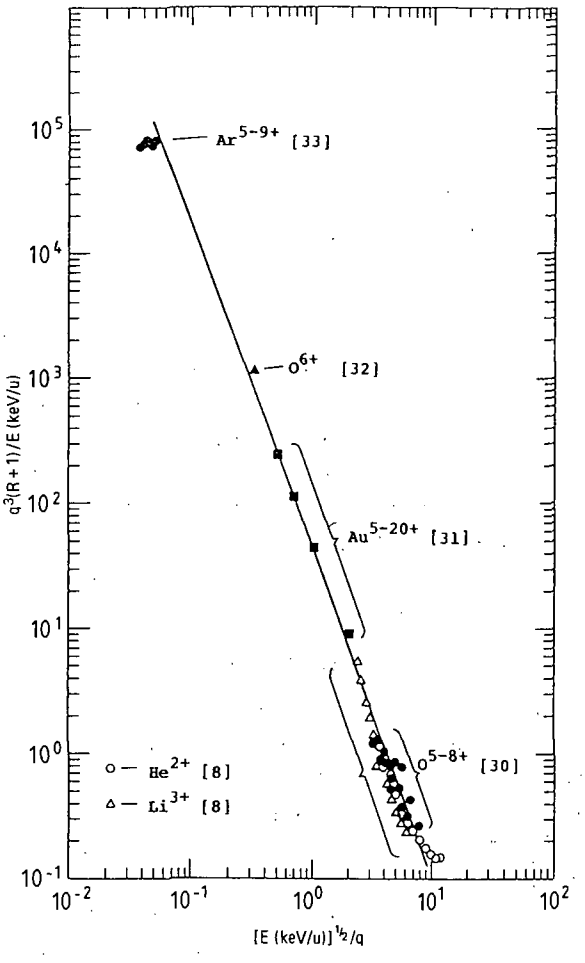

FIG. 9. Scaling relation (see text) for transfer ionization cross-sections $_{q0}\sigma_{(q-1)2}$ in collisions with helium.
(Figure adapted from Ref. [30]).

relation used by Janev and Hvelplund [29] in which a reduced cross-section $\tilde{\sigma} = \sigma_c/q$ is plotted against a reduced impact energy $\tilde{E} = E/q^{1/2}$ for experimental data with $q \geq 5$. The results are described reasonably well by a single universal curve giving the reduced cross-section as

$$\tilde{\sigma} = \sigma_0(\tilde{v})\, q^{\alpha(\tilde{v})}$$

where the reduced velocity $\tilde{v} = v/q^{1/4}$, and σ_0 and α are fitting parameters.

Figure 8 shows a similar scaling relation used by Janev and Hvelplund [29] to describe the cross-sections $\sigma_i = {}_{q0}\sigma_{q1}$ for single ionization. In this case, when reduced ionization cross-sections $\tilde{\sigma}_i = \sigma_i/q$ are plotted against reduced energy $\tilde{E} = E(keV/u)/q$, the results are also well described by a single universal curve.

Figure 9 shows a scaling relation applied by Tanis et al. [30] to the cross-sections $_{q0}\sigma_{(q-1)2}$ for transfer ionization. In this case the ratio $R + 1 = ({}_{q0}\sigma_{(q-1)2} + \sigma_c)/\sigma_c$

is considered. A plot of $q^3(R + 1)/E(keV/u)$ against the reduced velocity $E(keV/u)^{1/2}/q$ can be seen to provide a reasonable straight line fit to the experimental data consistent with

$$R + 1 = 40/E^{0.3}q^{0.4}$$

3. COLLISIONS WITH HELIUM IONS

A number of experimental studies of collisions involving He^+ ions with other positive ions have been carried out using fast intersecting beam techniques. Such experiments are difficult, but they can provide absolute cross-sections with an accuracy within 10% without the need for normalization to other data. A review of some of the experimental data has been given by Salzborn [34].

Data for the electron capture and ionization process

$$H^+ + He^+ \rightarrow H + He^{2+} \quad (6)$$

$$H^+ + He^+ \rightarrow H^+ + He^{2+} + e \quad (7)$$

are available for centre of mass energies in the range 4–400 keV and are shown in Figs 10 and 11. In these experiments, the cross-sections $\sigma(He^{2+})$ for He^{2+} production from the sum of processes (6) and (7) are measured. The cross-sections σ_c for the charge transfer process (6) can also be separately determined using coincidence counting techniques. Ionization cross-sections for process (7) are then obtained from the difference $\sigma_i = (\sigma(He^{2+}) - \sigma_c)$.

The results of different experiments for $\sigma(He^{2+})$ and σ_c can be seen to be in satisfactory general accord. The uncertainties in σ_i are understandably larger than for both $\sigma(He^{2+})$ and σ_c. It is evident that at energies below about 40 keV, $\sigma_c \simeq \sigma(He^{2+})$. At higher centre of mass energies, σ_i increases in relative importance, and above about 180 keV, $\sigma_i \simeq \sigma(He^{2+})$. Theoretical descriptions of processes (6) and (7) have been discussed in a recent review by Fritsch and Lin [40].

Similar experimental data (see Ref. [34]) are available for the processes

$$He^+ + He^+ \rightarrow He + He^{2+} \quad (8)$$

$$He^+ + He^+ \rightarrow He^+ + He^{2+} + e \quad (9)$$

within the centre of mass energy range 11–113 keV.

Cross-sections for the resonant charge transfer process

$$^3He^{2+} + {}^4He^+ \rightarrow {}^3He^+ + {}^4He^{2+} \quad (10)$$

measured in the centre of mass energy range 10 eV to 20 keV [41] provide only lower limits to the true cross-sections, since the angular acceptance of the product detectors in these experiments was too small. However, more recently, Melchert et al. [42] have measured cross-sections for process (10) in the centre of mass energy range 4–200 keV, with an accuracy within 10%. At 4 keV, the cross-section is 4.6×10^{-16} cm^2 and then decreases with increasing energy in the manner predicted by the calculations of Dickinson and Hardie [43].

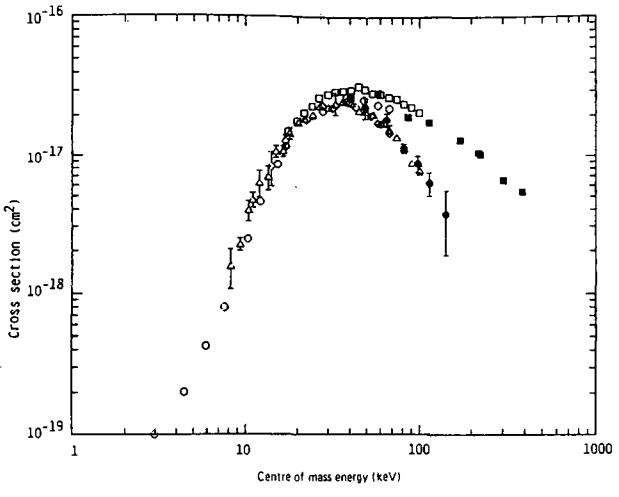

FIG. 10. Charge transfer in H^+–He^+ collisions.
Total cross-sections $\sigma(He^{2+})$ for He^{2+} production:
○ — Peart et al. [35] (not all data points are shown);
□ — Rinn et al. [36]; ■ — Angel et al. [37].
Charge transfer cross-sections σ_c:
△ — Rinn et al. [38]; ● — Watts et al. [39].
Statistical uncertainties shown are at the 90% confidence level.

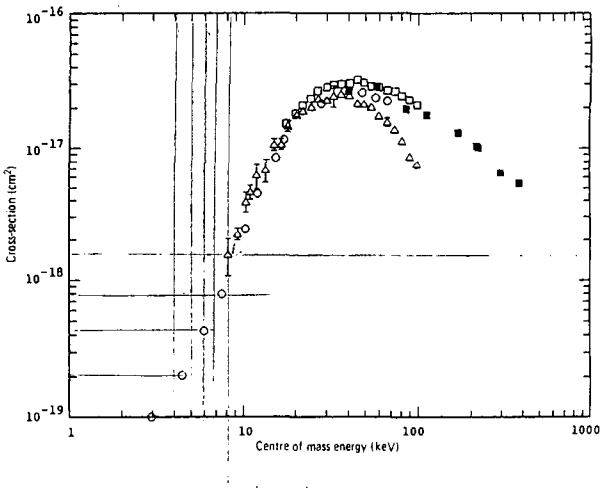

FIG. 11. Ionization in H^+–He^+ collisions.
Total cross-sections $\sigma(He^{2+})$ for He^{2+} production:
○ — Peart et al. [35] (not all data points are shown);
□ — Rinn et al. [36]; ■ — Angel et al. [37].
Ionization cross-sections σ_i:
△ — Rinn et al. [38]; ● — Watts et al. [39].
Statistical uncertainties shown are at the 90% confidence level.

4. PROCESSES INVOLVING THE FORMATION AND COLLISIONAL DESTRUCTION OF FAST METASTABLE HELIUM ATOMS

Data on charge changing collision process are important for a proper understanding of the production and penetration of fast helium beams. The following processes are relevant, with cross-sections denoted by σ_{if}, where i and f are the respective initial and final charge states of the fast helium beams.

Electron capture

σ_{10}: $He^+ + X \rightarrow He + X^+$ (11)

σ_{20}: $He^{2+} + X \rightarrow He + X^{2+}$ (12)

Electron loss

σ_{12}: $He^+ + X \rightarrow He^{2+} + X(\Sigma) + e$ (13)

σ_{01}: $He + X \rightarrow He^+ + X(\Sigma) + e$ (14)

σ_{02}: $He + X \rightarrow He^{2+} + X(\Sigma) + 2e$ (15)

where $X(\Sigma)$ denotes all final bound and continuum states of the target species X. Recommended cross-sections for these processes in targets of He and H_2 over a wide energy range have been given in the compilation by Barnett [1]. However, the analysis of such processes can be complicated by the presence of long lived metastable $He(2\,^3S) + He(2\,^1S)$ atoms (denoted by He^*) in the beams (see Wittkower et al. [44]). The most important processes to consider are the following:

σ_{10^*}: $He^+ + X \rightarrow He^* + X^+$ (16)

σ_{0^*1}: $He^* + X \rightarrow He^+ + X(\Sigma) + e$ (17)

A beam attenuation technique first developed by Gilbody and collaborators (see review [45]) and subsequently used by others has provided estimates of cross-sections for processes (16) and (17) in a variety of different target gases. In this method the fraction f of He^* atoms present in a beam of fast helium atoms (formed by charge transfer neutralization) is determined from careful studies of the rate of attenuation of the helium atom beam as a result of passage through a gas as the target thickness is increased. Under the conditions of the experiment it was assumed that the attenuation of the helium ground state and of the He^* metastable components of the beam were determined primarily by σ_{01} and σ_{0^*1}, respectively. In this way, Gilbody et al. [46] estimated that for a helium target the cross-sections σ_{0^*1} for process (17) in the energy range 25–350 keV were between six and five times larger than the corresponding cross-sections σ_{01} for ground state atoms.

The fraction f of metastable atoms formed by one-electron capture by He^+ ions in passage through a gas target depends strongly on both target species and target thickness. Gilbody et al. [47] showed that, for a 'thin' helium target (corresponding to single collision conditions) the measured fractions f increased from about 2.5% at 20 keV to about 12.8% at 200 keV. However, for a 'thick' helium target (where both charge state and excited state equilibrium had been attained) the measured fractions f were not more than 1% over the same energy range. This fraction was lower than any other thick target species investigated.

It is important to point out that in the simple analysis used by Gilbody et al. [46] the possible influence of collisions involving excitation or de-excitation of helium atoms is assumed to be relatively small. The experimental data of Blair et al. [48] indicate that the cross-sections σ_{00^*} for excitation of helium by ground state atoms are comparatively small. If the cross-sections σ_{0^*0} for de-excitation are not small enough to be neglected, it can be shown that the attenuation technique provides an apparent fraction f_{app} rather than a true metastable fraction f, where

$$f_{app} = \frac{f(\sigma_{0^*1} - \sigma_{01})}{(\sigma_D - \sigma_{01})}$$

in which $\sigma_D = (\sigma_{0^*1} + \sigma_{0^*0})$. Thus, the measured fractions f_{app} strictly provide a lower limit to the true metastable fraction. The neglect of σ_{0^*0} also implies that, where this process is significant, the measured cross-sections σ_{10^*} and σ_{0^*1} for processes (16) and (17) without taking this into account require correction. The available evidence (see McCullough et al. [49]) suggests that corrections to measured values of f should be small at energies above about 50 keV.

Values of σ_{0^*0} have been deduced by Pedersen et al. [50] from curve fitting procedures using beams with high metastable fractions, but the accuracy of these measurements is very difficult to assess. They have also measured a metastable fraction of 14 ± 2% for a helium atom beam prepared by electron capture neutralization of He^+ in a thick helium target. This result seems inexplicably at variance with the values of less than 1% obtained by Gilbody et al. [47] for energies below 200 keV and with any reasonable estimates of both σ_{0^*0} and σ_{00^*} which should be considered in a full analysis.

Studies of He^* formation in two-electron capture by He^{2+} ions in collisions with H_2 have been carried out by Dunn et al. [51] at an energy of 50 keV/u. They

obtained the cross-section $\sigma_{20^*} = (3.6 \pm 0.5) \times 10^{-18}$ cm^2 and were able to satisfactorily account for the dependence of the measured metastable fraction on target thickness in terms of relevant charge changing collision cross-sections. There are no measurements for other target gases.

REFERENCES

[1] BARNETT, C.F., Atomic Data for Fusion, Vol. 1, Rep. ORNL-6086/VI, Oak Ridge National Laboratory, Oak Ridge, TN (1990).

[2] HUBER, B.A., KAHLERT, H.J., Total Cross Sections for Electron Capture by Multiply Charged Ions in H, H_2 and He, Rep. 82-05-104, Ruhr University, Bochum (1982).

[3] MASSEY, H.S.W., GILBODY, H.B., Electronic and Ionic Impact Phenomena, Vol. 4, Clarendon Press, Oxford (1974).

[4] RUDD, M.E., DUBOIS, R.D., TOBUREN, L.H., RATCLIFFE, C.A., GOFFE, T.V., Phys. Rev., A **28** (1983) 3244.

[5] AFROSIMOV, V.V., MAMAEV, Ya.A., PANOV, M.N., UROSHEVICH, B., FEDORENKO, V.V., Sov. Phys. — Tech. Phys. **12** (1967) 394.

[6] SHAH, M.B., GILBODY, H.B., J. Phys., B (Lond.). At. Mol. Phys. **14** (1981) 2361.

[7] SHAH, M.B., GILBODY, H.B., J. Phys., B (Lond.). At. Mol. Phys. **15** (1982) 3441.

[8] SHAH, M.B., GILBODY, H.B., J. Phys., B (Lond.). At. Mol. Phys. **18** (1985) 899.

[9] SHAH, M.B., McCALLION, P., GILBODY, H.B., J. Phys. B. Atom. Mol. Opt. Phys. **22** (1989) 3037.

[10] KNUDSEN, H., ANDERSON, L.H., HVELPLUND, P., et al., J. Phys., B (Lond.). At. Mol. Phys. **17** (1984) 3545.

[11] AFROSIMOV, V.V., LEIKO, G.A., MAMAEV, Yu.A., PANOV, M.N., Sov. Phys. — JETP **40** (1975) 661.

[12] PUCKETT, L.J., TAYLOR, G.O., MARTIN, D.W., Phys. Rev. **178** (1969) 271.

[13] PUCKETT, L.J., MARTIN, D.W., Phys. Rev., A **1** (1970) 1432.

[14] PIVOVAR, L.I., LEVCHENKO, Yu.Z., KRIVONOSOV, G.A., Sov. Phys. — JETP **32** (1971) 11.

[15] BELL, K.L., KINGSTON, A.E., J. Phys., B (Lond.). At. Mol. Phys. **2** (1969) 635.

[16] MONTAGUE, R.G., HARRISON, M.F.A., SMITH, A.C.H., J. Phys., B (Lond.). At. Mol. Phys. **17** (1974) 3295.

[17] FAINSTEIN, P.D., PONCE, V.H., RIVAROLA, R.D., Phys. Rev., A **36** (1987) 3639.

[18] McGUIRE, J.H., Phys. Rev. Lett. **49** (1982) 1153.

[19] McGUIRE, J.H., MULLER, A., SCHUCH, B., et al., Phys. Rev., A **35** (1987) 2479.

[20] OLSON, R.E., WETMORE, A.E., McKENZIE, M.L., J. Phys., B (Lond.). At. Mol. Phys. **19** (1986) L629.

[21] TOBUREN, L.H., NAKAI, M.Y., LANGLEY, R.A., Phys. Rev. **171** (1968) 114.

[22] STIER, P.M., BARNETT, C.F., Phys. Rev. **103** (1956) 896.

[23] HVELPLUND, P., HEINEMEIER, J., HORSDAL-PEDERSEN, E., SIMPSON, F.R., J. Phys., B (Lond.). At. Mol. Phys. **9** (1976) 491.

[24] BARNETT, C.F., RAY, J.A., RICCI, E., et al., Atomic Data for Controlled Fusion Research, Vol. 1, Rep. ORNL-5206, Oak Ridge National Laboratory, Oak Ridge, TN (1977).

[25] AFROSIMOV, V.V., BASALAEV, A.A., LEIKO, G.A., PANOV, M.N., Sov. Phys. — JETP **47** (1978) 837.

[26] BERKNER, K.H., PYLE, R.V., STEARNS, J.W., WARREN, J.C., Phys. Rev. **166** (1968) 44.

[27] BAYFIELD, J.E., KHAYRALLAH, G.A., Phys. Rev., A **11** (1975) 920.

[28] KIMURA, M., J. Phys. B, At. Mol. Opt. Phys. **21** (1988) L19.

[29] JANEV, R.K., HVELPLUND, P., Comments At. Mol. Phys. **11** (1981) 75.

[30] TANIS, J.A., CLARK, M.W., PRICE, R., FERGUSON, S.M., OLSON, R.E., Nucl. Instrum. Methods Phys. Res., Sect. B **23** (1987) 167.

[31] DAMSGAARD, H., HAUGEN, H.K., HVELPLUND, P., KNUDSEN, H., Phys. Rev., A **27** (1983) 112.

[32] STOLTERFOHT, N., HAVENER, C.C., PHANEUF, R.A., et al., Phys. Rev. Lett. **57** (1986) 74.

[33] COCKE, C.L., DUBOIS, R., GRAY, T.J., JUSTIANO, E., CAN, C., Phys. Rev. Lett. **46** (1981) 1671.

[34] SALZBORN, E., J. Phys., Colloq. **1** (1989) 207.

[35] PEART, B., RINN, K., DOLDER, K., J. Phys., B (Lond.). At. Mol. Phys. **16** (1983) 1461.

[36] RINN, K., MELCHERT, F., RINK, K., SALZBORN, E., J. Phys., B (Lond.). At. Mol. Phys. **19** (1986) 3717.

[37] ANGEL, G.C., DUNN, K.F., SEWELL, E.C., GILBODY, H.B., J. Phys., B (Lond.). At. Mol. Phys. **11** (1978) L49.

[38] RINN, K., MELCHERT, F., RINK, K., SALZBORN, E., J. Phys., B (Lond.). At. Mol. Phys. **8** (1985) 3783.

[39] WATTS, M.F., DUNN, K.F., GILBODY, H.B., J. Phys., B. (Lond.). At. Mol. Phys. **19** (1986) L355.

[40] FRITSCH, W., LIN, C.D., Phys. Rep. **202** (1991) 2.

[41] PEART, B., DOLDER, K., J. Phys., B (Lond.). At. Mol. Phys. **12** (1979) 4155.

[42] MELCHERT, F., KRÜDENER, S., SCHULZE, R., et al., in Physics of Electronic and Ionic Collisions (Proc. 17th Int. Conf. Brisbane, 1991), I.O.P. Publishing (1991) 571.

[43] DICKINSON, A.D., HARDIE, D.J.W., J. Phys., B (Lond.). At. Mol. Phys. **12** (1979) 4147.

[44] WITTKOWER, A.B., LEVY, G., GILBODY, H.B., Proc. Phys. Soc. **91** (1967) 862.

[45] GILBODY, H.B., Inst. Phys. Conf. Ser. **38** (1978) 156.

[46] GILBODY, H.B., DUNN, K.F., BROWNING, R., LATIMER, C.J., J. Phys., B (Lond.). At. Mol. Phys. **3** (1970) 1105.

[47] GILBODY, H.B., DUNN, K.F., BROWNING, R., LATIMER, C.J., J. Phys., B (Lond.). At. Mol. Phys. **4** (1971) 800.

[48] BLAIR, W.G.F., McCULLOUGH, R.W., SIMPSON, F.R., GILBODY, H.B., J. Phys., B (Lond.). At. Mol. Phys. **6** (1973) 1265.

[49] McCULLOUGH, R.W., GOFFE, T.V., GILBODY, H.B., J. Phys., B (Lond.). At. Mol. Phys. **11** (1978) 2333.

[50] PEDERSEN, E.H., HEINEMEIER, J., LARSEN, L., MIKKELSEN, J.V., J. Phys., B (Lond.). At. Mol. Phys. **13** (1980) 1167.

[51] DUNN, K.F., GILMORE, B.J., SIMPSON, F.R., GILBODY, H.B., J. Phys., B (Lond.). At. Mol. Phys. **11** (1978) 1797.

CHARGE TRANSFER IN COLLISIONS OF PROTONS WITH HELIUM

R. HOEKSTRA[1,2], H.P. SUMMERS[3], F.J. de HEER[2]
[1] Kernfysisch Versneller Instituut,
Groningen,
The Netherlands
[2] FOM-Institute for Atomic and Molecular Physics,
Amsterdam,
The Netherlands
[3] JET Joint Undertaking,
Abingdon, Oxfordshire,
United Kingdom

ABSTRACT. In the energy range of 3×10^2 to 5×10^5 eV/amu, data for total and state selective electron capture in collisions of protons with helium have been evaluated critically. From this investigation, a set of recommended data has been constructed which are part of the atomic database in JET and which, therefore, are used for modelling of helium beam stopping and related diagnostics. Motivation for the assessment of the cross-sections is presented and the corresponding uncertainties are inferred.

1. INTRODUCTION

Recently, in the Joint European Torus (JET) the neutral beam injector assemblies have been upgraded such that He beams can be injected, as well as the D beams used previously. In the plasma, these neutral beams are stopped by ionizing and/or charge changing collisions. Photon emission spectroscopy of light in the visible spectral range, emitted by plasma particles following electron capture from the He beam and by collisionally excited He beam atoms, is being assessed as a tool to measure plasma quantities such as, for example, the ion temperature and the impurity densities. This type of diagnostic has been used successfully in combination with the neutral D heating beams (Boileau et al. [1] and von Hellermann et al. [2]).
To be able to fully develop the potentialities of this method, it is necessary to know accurately the absolute cross-sections for the basic charge transfer, excitation and ionization processes. These cross-sections have to be known in the energy range of approximately 1–100 keV/amu. This range is defined by the energy of the He beams, at present up to 53 keV/amu and 30 keV/amu for ^{3}He and ^{4}He beams, respectively, and the energy distribution of the plasma ions. For future machines such as ITER, the energy range of interest extends towards higher energies, since, to match the velocity of the fusion produced α-particles, diagnostic beams with energies of a few hundreds of keV/amu are foreseen (see, for example, this issue and Ref. [3]).

In this paper we review and recommend total and state selective cross-sections for electron capture by protons, the most abundant plasma species. Schematically, the charge transfer processes are given by

$$H^+ + He \rightarrow H(n\ell) + He^+ \qquad (1)$$

Throughout the paper, the emphasis will be on experimental data for processes (1); this is possible because the processes have been studied extensively over the whole energy range of plasma fusion interest, $\sim 10^3$–10^6 eV/amu (Refs [4–43]). Notwithstanding the fact that recently recommended cross-sections have been presented by Barnett [44], here referred to as the Redbook, we have again investigated the status of the available data. The investigation was motivated by the large differences between theory and experiment at energies below 10^4 eV/amu, the publication of new elaborate experimental and theoretical data in the energy range of 10^4–10^5 eV/amu and some inconsistencies in the ratio of the recommended 3ℓ and 2ℓ cross-sections given in the Redbook.

In the following sections we discuss the cross-sections for total electron capture and those for state selective charge transfer into states with $n \leq 3$, and present the corresponding recommended cross-sections in graphical and tabular form.

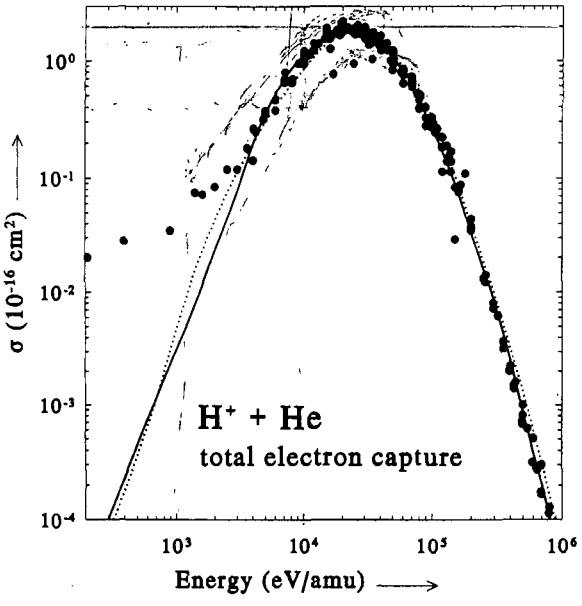

FIG. 1. Total one-electron capture cross-sections in H^+-He collisions. Experiment: Refs [4-19]. Recommended data: ····· Redbook [44], —— this work.

2. ASSESSMENT OF RECOMMENDED CROSS-SECTIONS

2.1. Total cross-sections for electron capture

The experimental data for total charge transfer in collisions of protons with helium are presented in Fig. 1. Because of the good agreement between the different data sets and the large amount of data, we have indicated all results by the same symbol. Unfortunately, many of these data were only presented in graphical form by the authors. Whenever possible, we have used for these data the numerical values given in the data compilation of Wu et al. [45], which includes results up to March 1986, and otherwise we have extracted them directly from the figures. It is seen that at energies above $\sim 5 \times 10^3$ eV/amu the recommended curves closely follow the experiments, whereas at lower impact energies they strongly deviate from the experimental data. At these lower energies we have decided not to follow the trend in the experimental

TABLE I. RECOMMENDED CROSS-SECTIONS (in units of 10^{-18} cm^2) FOR ELECTRON CAPTURE IN H^+-He COLLISIONS

E (keV/amu)	σ(tot)	σ(2s)	σ(2p)	σ(3s)	σ(3p)	σ(3d)
0.3	0.01	0.001	0.0056			
0.5	0.045	0.0029	0.0155			
0.7	0.11	0.0054	0.031			
1	0.31	0.011	0.062	0.00165	0.0027	0.0016
2	2.28	0.044	0.24	0.0066	0.011	0.0065
3	7.6	0.095	0.475	0.015	0.024	0.015
5	35	0.24	1.02	0.041	0.068	0.041
7	70	0.49	1.6	0.081	0.132	0.081
10	114	0.88	2.25	0.16	0.27	0.16
20	178	2.7	3.6	0.57	0.75	0.23
30	170	4.6	3.45	1.42	1.1	0.2
50	107	6.8	2.0	2.1	0.65	0.11
70	62	5.5	1.1	1.7	0.34	0.045
100	27	3.0	0.55	0.85	0.16	0.015
200	3.3	0.39	0.075	0.11	0.021	0.0012
300	0.82	0.08	0.015	0.024	0.004	0.0002
500	0.087	0.01	0.0012	0.003		

data (mainly from Stedeford and Hasted [4] and from Hasted as quoted by Allison [5]) but to follow the trend in the theoretical results of Kimura [46] and Kimura and Lin [47]. There are two arguments to justify this choice:

(i) Although charge transfer mainly populates the H(1s) ground state, it is still a highly endothermic process. Therefore, it may be expected that the cross-sections decrease strongly with decreasing impact energy, which is not the case for the experimental results (see Fig. 1). Furthermore, it is noted that the population of excited H states has to proceed via couplings with the molecular orbital, corresponding, at infinity, to the H(1s) ground state. Since, as can be seen in the next section (Fig. 3), the theoretical results of Kimura and Lin [47] for capture into such a state, H(2p), are in good agreement with the most sophisticated experimental results, it is likely that theory is also rather reliable for capture into H(1s).

(ii) Experimentally, the conditions were such that the residual gas pressure was about 1% of the pressure of the He target [4]. Failure to properly account for the interaction with the residual gas yields an extra apparent cross-section of a few times 10^{-18} cm^2 since cross-sections for electron capture from gases such as H_2, N_2, Ar and O_2 [4–6] are of the order of a few times 10^{-16} cm^2. From these numbers it is also clear that the purity of the helium gas admitted to the target cell is of great importance. Therefore, electron capture from small fractions of 'impurity' gases may well explain the magnitude of the experimental cross-sections at the lower impact energies.

Values of our recommended cross-sections are presented in Table I. At energies between 4×10^3 and 3×10^5 eV/amu, the uncertainties are expected to be smaller than 20%. At higher energies, the uncertainty increases only slightly, up to ~30% at 8×10^5 eV/amu, but at lower impact energies the uncertainty may be considerably larger; we estimate a factor of two at 10^3 eV/amu and an even larger factor at still lower impact energies.

2.2. Cross-sections for electron capture into H(2ℓ) states

The data for electron capture into H(2s) and H(2p) are shown in Figs 2 and 3, respectively. Excluding for electron capture into H(2p) the results of Hippler et al. [29] and Van Zyl et al. [33], we see from Fig. 3 that at impact energies below 10^4 eV/amu the other data exhibit the same trend as the total charge transfer

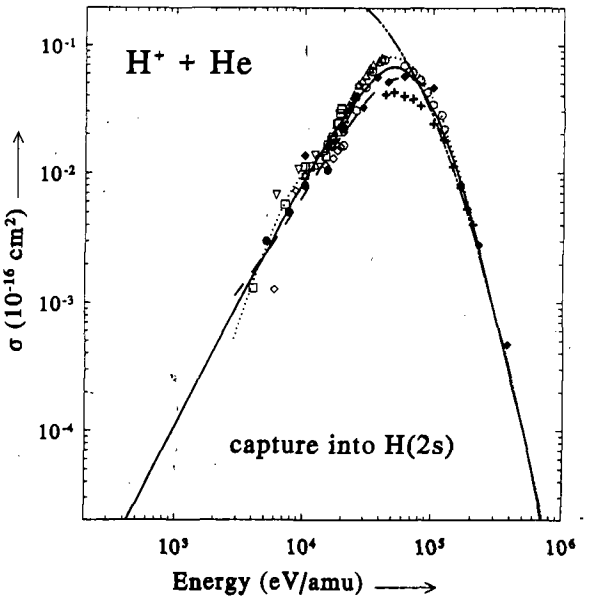

FIG. 2. Cross-sections for electron capture into H(2s) in H^+–He collisions. Experiment: ▽ Jaecks et al. [22], △ Andreev et al. [24], + Ryding et al. [21], ◇ Fitzwilson and Thomas [23], ○ Hughes et al. [26], □ Crandall and Jaecks [20], ◆ Rodbro and Andersen [27] and ● Hippler et al. [25]. Theory: --- Kimura and Lin [47], -·-·-· Belkič [48]. Recommended data: ····· Redbook [44], —— this work.

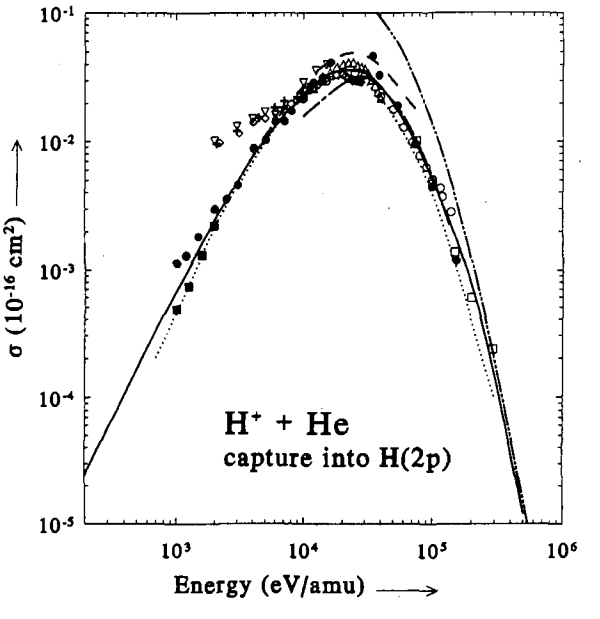

FIG. 3. Cross-sections for electron capture into H(2p) in H^+–He collisions. Experiment: ▽ Risley et al. [31], △ Andreev et al. [24], + Gaily et al. [32], ◇ Pretzer et al. [30], ○ Hughes et al. [26], □ Hippler et al. [28], ■ Van Zyl et al. [33] and ● Hippler et al. [29]. Theory: --- Kimura and Lin [47], -·-·-· Belkič [48] and —·— Slim et al. [49]. Recommended data: ····· Redbook [44], —— this work.

cross-sections (see Fig. 1), i.e. compared to theory, a less steep decrease with decreasing energy. Again, this may be due to charge changing collisions with the background gas. However, in this case there is a second process that may significantly contribute to the observed H(2p) cross-sections, namely excitation of the neutrals in the H beam (a small fraction of the proton beam may be neutralized during transport to the collision centre). The cross-section for H(2p) excitation in H–He collisions is relatively large, $\sim 5 \times 10^{-17}$ cm^2 (Birely and McNeal [50]), more than two orders of magnitude larger than the one for charge transfer into H(2p) in proton–He collisions. Since Hippler et al. [29] and Van Zyl et al. [33] corrected for these effects, we recommend to follow their results below 10^4 eV/amu. The AO–MO results of Kimura and Lin [47] are in good agreement with these experimental data. Our recommended cross-sections below 3×10^3 eV/amu are an extrapolation of the AO–MO results and are based on the E^2 dependence derived by Rapp and Francis [51] for endothermic electron capture processes. As can be seen from Fig. 3, the scaling describes well the results between 1 and 3×10^3 eV/amu. At high energies (above 2×10^5 eV/amu), the energy dependence of our recommended curve is defined by the theoretical results of Belkič [48].

The procedure for the assessment of the cross-sections for capture into H(2s) has been the same as that for capture into H(2p); below 3×10^3 eV/amu we extrapolated the curve by means of the E^2 dependence and at high energies we used the results of Belkič [48] as a guideline. Note from Fig. 2 that, especially around the cross-section maximum, the status of the experimental results is not optimal.

For the recommended H(2s) and H(2p) electron capture cross-sections shown in Figs 2 and 3 and presented in Table I we expect that in the energy range of approximately 2×10^3 to 2×10^5 eV/amu the uncertainties are about 30% and 20% for H(2s) and H(2p), respectively. At lower and higher energies the data are less certain.

2.3. Cross-sections for electron capture into H(3ℓ) states

The data for electron capture into H(3s), H(3p) and H(3d) are shown in Figs 4, 5 and 6, respectively. Besides the results dating from the 1970s [14, 31, 34–39], there are recent results stemming from experimental work directed towards the determination of the full density matrices for charge transfer into H(3ℓ) states [40, 41]. These latter measurements define

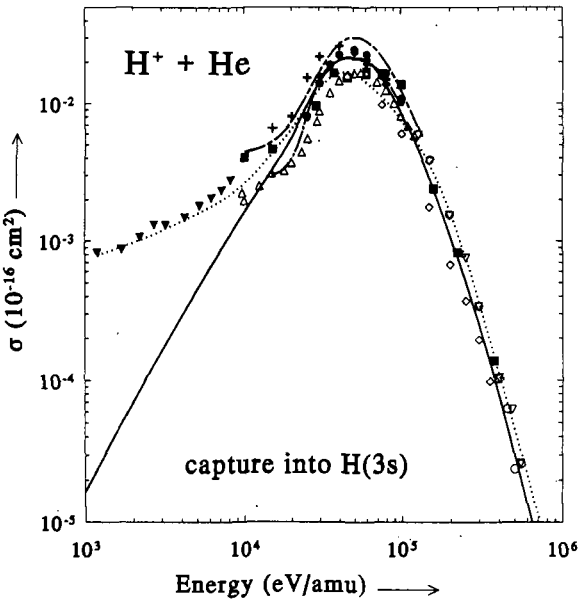

FIG. 4. Cross-sections for electron capture into H(3s) in H^+–He collisions. Experiment: ▽ Dawson and Loyd [37], ▼ Ford and Thomas [36], △ Hughes et al. [34], + Lenormand [39], ◇ Edwards and Thomas [38], ○ Conrads et al. [35], ■ Rodbro and Andersen [27], ◆ Brower and Pipkin [41] and ● Ashburn et al. [40]. Theory: –·–·– Shingal and Lin [52] and — — Slim et al. [49]. Recommended data: ····· Redbook [44], —— this work.

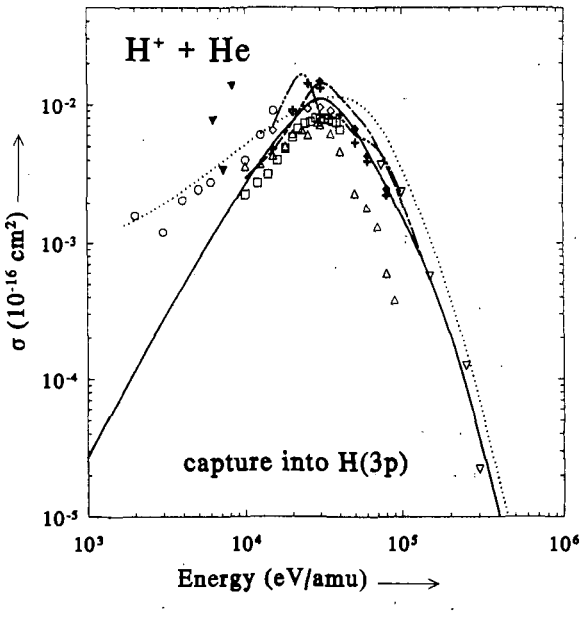

FIG. 5. Cross-sections for electron capture into H(3p) in H^+–He collisions. As in Fig. 4, except for ○ Risley et al. [31] and ◇ de Heer et al. [14].

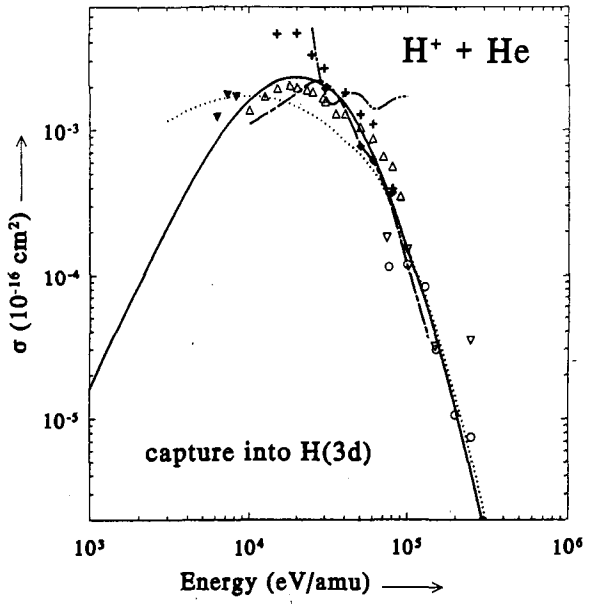

FIG. 6. Cross-sections for electron capture into H(3d) in H^+–He collisions. As in Fig. 4.

TABLE II. BALMER-α EMISSION CROSS-SECTIONS (in units of 10^{-21} cm^2)

E (keV/amu)	Our scaling	Van Zyl et al. [42]
1.25	5.5	6 ± 3
2	14.2	16 ± 6

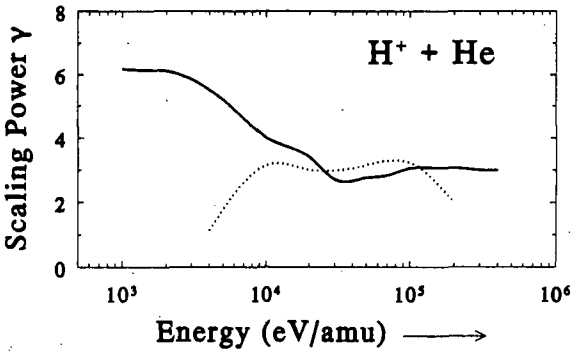

FIG. 7. Scaling power γ ($n^{-\gamma}$) determined from the total n = 2 and n = 3 cross-sections. ····· Redbook [44], —— this work.

mainly the shape and magnitude of our recommended cross-sections around the cross-section maxima. In this energy range, ~ 10^4 to 10^5 eV/amu, the uncertainties in the 3s and 3p cross-sections are expected not to exceed 30%, but the ones in the 3d cross-sections may be as large as 50%. However, in this respect it has to be noted that the cross-section for electron capture into H(3d) is approximately one order of magnitude smaller than the ones for H(3s) and H(3p).

At impact energies lower than 10^4 eV/amu we have again used the E^2 scaling of Rapp and Francis [51] to extrapolate our recommended curve. This curve deviates strongly from the one given in the Redbook [44] which follows the trend in the experimental data of Ford and Thomas [36] and of Conrads et al. [35]. Support of our extrapolated curves is presented by the Balmer-α measurements of Van Zyl et al. [42]. Table II shows a comparison of their Balmer-α cross-sections and the ones constructed from our 3ℓ cross-sections. The Balmer-α cross-section is related to the 3ℓ cross-sections via the respective branching ratios of these 3ℓ states, i.e. the Balmer-α cross-section is equal to σ(3s) + 0.12 σ(3p) + σ(3d). From Table II it is obvious that there is good agreement between the experimental data [42] and the ones determined from our recommended cross-sections.

To interpret as accurately as possible the photon emission spectra, it is important to know the cascade contributions from high-n levels to the line under observation. The high-n electron capture cross-sections are generally estimated from scalings of the type $n^{-\gamma}$ (see, for example, Spence and Summers [53]). In high energy approximations based on the available density of states in the ion, γ becomes equal to 3. However, at lower impact energies it has been noted that the high-n cross-sections are relatively smaller (see, for example, von Hellermann et al. [2] and Hoekstra et al. [54] for the case of electron capture in He^{2+}–H collisions). To get an impression of the scaling power γ for H^+–He collisions, Fig. 7 shows γ determined from the n = 2 and n = 3 recommended cross-sections of the Redbook [44] and of the present work. It is seen that, going up from an energy of 10^3 eV/amu, the present value of γ decreases from ~6 to 2.6 at 3.5 × 10^4 eV/amu and reaches the expected value of about 3 at ~ 10^5 eV/amu. At high energies the difference between the present work and the Redbook arises mainly from the fact that the 3s cross-sections given in Ref. [44] are larger (see Fig. 4).

3. CONCLUSIONS

The database for electron capture in collisions of protons with helium has been investigated. For impact energies of 3 × 10^2 to 5 × 10^5 eV/amu, we have determined a set of recommended cross-sections for

total electron capture and state selective electron capture into H(2ℓ) and H(3ℓ) states. At energies above $\sim 10^5$ eV/amu and especially below 10^4 eV/amu, the present assessment differs from the one given in the Redbook compilation [44]. At the low energy side, we are fairly confident about our recommendation because of the good agreement with the Balmer-α measurements of Van Zyl et al. [42]. At the high energy side, the cross-sections are supported by the fact that the scaling power γ ($n^{-\gamma}$ scaling) reaches neatly the expected high energy value of 3.

ACKNOWLEDGEMENTS

This work is part of the research programme of the Stichting voor Fundamenteel Onderzoek der Materie (FOM), which is financially supported by the Nederlandse Organisatie voor Wetenschappelijk Onderzoek (NWO). Via an article 14 contract with JET, the work is also part of the research programme of the association agreement between FOM and Euratom with financial support by NWO.

REFERENCES

[1] BOILEAU, A., HELLERMANN, M. von, HORTON, L.D., SUMMERS, H.P., Plasma Phys. Control. Fusion **31** (1989) 779.

[2] HELLERMANN, M. von, MANDL, W., SUMMERS, H.P., BOILEAU, A., HOEKSTRA, R., de HEER, F.J., FRIELING, G.J., Plasma Phys. Control. Fusion **33** (1991) 1805.

[3] JANEV, R.K., Comments At. Mol. Phys. **26** (1991) 83.

[4] STEDEFORD, J.B.H., HASTED, J.B., Proc. R. Soc. (London), Ser. A **227** (1955) 466.

[5] ALLISON, S.K., Rev. Mod. Phys. **30** (1958) 1137.

[6] STIER, P.M., BARNETT, C.F., Phys. Rev., A **103** (1956) 896.

[7] de HEER, F.J., SCHUTTEN, J., MOUSTAFA, H., Physica **32** (1966) 1766.

[8] BARNETT, C.F., STIER, P.M., Phys. Rev., A **109** (1958) 385.

[9] WILLIAMS, J.F., DUNBAR, D.N., Phys. Rev., A **149** (1966) 62.

[10] WILLIAMS, J.F., Phys. Rev., A **157** (1967) 97.

[11] AFROSIMOV, V.V., IL'IN, R.N., Sov. Phys.-Tech. Phys. **5** (1960) 661.

[12] WELSH, L.M., BERKNER, K.H., KAPLAN, S.N., PYLE, R.V., Phys. Rev. **158** (1967) 85.

[13] COLLI, L., CRISTOFORI, F., FRIGERIO, G.E., SONA, P.G., Phys. Lett. **3** (1962) 62.

[14] de HEER, F.J., VAN ECK, J., KISTEMAKER, J., in Ionization Phenomena in Gases (Proc. 6th Conf. Paris, 1963), Vol. 1, Centre de Documentation Universitaires, Paris (1963) 73.

[15] RUDD, M.E., DUBOIS, R.D., TOBUREN, L.H., RATCLIFFE, C.A., GOFFE, T.V., Phys. Rev., A **28** (1983) 3244.

[16] DAHL, P., J. Phys., B (London), At. Mol. Phys. **18** (1985) 1181.

[17] SHAH, M.B., GILBODY, H.B., J. Phys., B (London), At. Mol. Phys. **18** (1985) 899.

[18] SHAH, M.B., McCALLION, P., GILBODY, H.B., J. Phys., B (London), At. Mol. Opt. Phys. **22** (1989) 3037.

[19] SCHWAB, W., BAPTISTA, G.P., JUSTINIANO, E., SCHUCH, R., VOGT, H., WEBER, E.W., J. Phys., B (London). At. Mol. Phys. **20** (1987) 2825.

[20] CRANDALL, D.H., JAECKS, D., Phys. Rev., A **4** (1971) 2271.

[21] RYDING, S., WITTKOWER, A.B., GILBODY, H.B., Proc. Phys. Soc. **89** (1966) 547.

[22] JAECKS, D.H., VAN ZYL, B., GEBALLE, R., Phys. Rev., A **137** (1965) 340.

[23] FITZWILSON, R.L., THOMAS, E.W., Phys. Rev., A **3** (1971) 1305.

[24] ANDREEV, E.P., ANKUDINOV, V.A., BOBASHEV, S.V., Sov. Phys.-JETP. **23** (1966) 375.

[25] HIPPLER, R., PLOTZKE, O., HARBICH, W., MADEHEIM, H., KLEINPOPPEN, H., LUTZ, H.O., Z. Phys., D **18** (1991) 61.

[26] HUGHES, R.H., STOKES, E.D., CHOE, S.S., KING, T.J., Phys. Rev., A **4** (1971) 1453.

[27] RODBRO, M., ANDERSEN, F.D., J. Phys., B (London). At. Mol. Phys. **12** (1979) 2883.

[28] HIPPLER, R., HARBICH, W., FAUST, M., LUTZ, H.O., DUBÉ, L., J. Phys., B (London). At. Mol Phys. **19** (1986) 1507.

[29] HIPPLER, R., HARBICH, W., MADEHEIM, H., KLEINPOPPEN, H., LUTZ, H.O., Phys. Rev., A **35** (1987) 3139.

[30] PRETZER, D., VAN ZYL, B., GEBALLE, R., in Physics of Electron and Atomic Collisions (Proc. 3rd Int. Conf. London, 1963), North-Holland, Amsterdam (1963) 618.

[31] RISLEY, J.S., de HEER, F.J., KERKDIJK, C.B., J. Phys., B (London). At. Mol. Phys. **11** (1978) 1759.

[32] GAILY, T.D., JAECKS, D.H., GEBALLE, R., Phys. Rev. **167** (1968) 81.

[33] VAN ZYL, B., GEALY, M.W., NEUMANN, H., Phys. Rev., A **35** (1987) 4551.

[34] HUGHES, R.H., STIGERS, C.A., DOUGHTY, B.M., STOKES, E.D., Phys. Rev., A **1** (1970) 1424.

[35] CONRADS, R.J., NICOLS, T.W., FORD, J.C., THOMAS, E.W., Phys. Rev., A **7** (1973) 1928.

[36] FORD, J.C., THOMAS, E.W., Phys. Rev., A **5** (1972) 1649.

[37] DAWSON, H.R., LOYD, D.H., Phys. Rev., A **9** (1974) 166.

[38] EDWARDS, J.L., THOMAS, E.W., Phys. Rev., A **2** (1970) 2346.

[39] LENORMAND, J., J. Phys. (Les Ulis) **37** (1976) 699.

[40] ASHBURN, J.R., CLINE, R.A., Van der BURGT, P.J.M., WESTERVELD, W.B., RISLEY, J.S., Phys. Rev., A **41** (1990) 2407.

[41] BROWER, M.C., PIPKIN, F.M., Phys. Rev., A **39** (1989) 3323.

[42] VAN ZYL, B., GEALY, M.W., NEUMANN, H., Phys. Rev., A **33** (1986) 2333.
[43] ANDREEV, E.P., ANKUDINOV, V.A., BOBASHEV, S.V., Sov. Phys.-JETP. **25** (1967) 232.
[44] BARNETT, C.F. (Ed.), Atomic Data for Fusion, Vol. 1, Collisions of H, Hg, He, Li Atoms and Ions with Atoms and Molecules, Rep. ORNL-6086/V1, Oak Ridge Natl. Lab., Oak Ridge, TN (1990).
[45] WU, W.K., HUBER, B.A., WIESEMANN, K., At. Data Nucl. Data Tables **40** (1988) 58.
[46] KIMURA, M., Phys. Rev., A **31** (1955) 2158.
[47] KIMURA, M., LIN, C.D., Phys. Rev., A **34** (1986) 176.
[48] BELKIČ, D., Phys. Rev., A **37** (1988) 55.
[49] SLIM, H.A., HECK, E.L., BRANSDEN, B.H., FLOWER, D.R., J. Phys., B (London). At. Mol. Opt. Phys. **24** (1991) 1683.
[50] BIRELY, J.H., McNEAL, R.J., Phys. Rev., A **5** (1972) 257.
[51] RAPP, D., FRANCIS, W.F., J. Chem. Phys. **37** (1963) 2631.
[52] SHINGAL, R., LIN, C.D., J. Phys., B (London). At. Mol. Opt. Phys. **24** (1991) 963.
[53] SPENCE, J., SUMMERS, H.P., J. Phys., B (London). At. Mol. Phys. **19** (1986) 3749.
[54] HOEKSTRA, R., de HEER, F.J., MORGENSTERN, R., J. Phys., B (London). At. Mol. Opt. Phys. **24** (1991) 4025.

CROSS-SECTION SCALING FOR ONE- AND TWO-ELECTRON LOSS PROCESSES IN COLLISIONS OF HELIUM ATOMS WITH MULTIPLY CHARGED IONS

R.K. JANEV
International Atomic Energy Agency,
Vienna

ABSTRACT. Using well established classical and quantum mechanical models for the mechanisms governing one- and two-electron processes in low and high energy collisions of helium atoms with multiply charged ions, simple scaling relationships are derived for the cross-sections of one-electron loss, double electron capture with transfer ionization and two-electron loss processes over a wide energy range. The parameters in these scaling relationships are determined from the available experimental data. The cross-section scaling of one- and two-electron loss processes from excited helium atoms is also discussed.

1. INTRODUCTION

One-electron loss (or electron removal), resulting from either single-electron capture or single-electron ionization of helium atoms colliding with ions, is the major process determining the penetration of an energetic neutral helium beam in a fusion plasma. The linear dependence of the electron loss cross-section on the ionic charge q at low collision energies (where the process is dominated by the electron capture mechanism) and its quadratic q-dependence at high energies (where ionization dominates) make this beam attenuation process even more important if the plasma contains multiply charged impurity ions. The overall effect is a linear increase of the beam stopping cross-section with the effective plasma ion charge Z_{eff} [1]. In the case of a low energy neutral helium beam, the two-electron transition processes leading to two-electron removal (double electron capture, transfer ionization and double ionization) can also contribute to the attenuation of the beam intensity. As we shall see in Section 4, this contribution may amount to 25–30% in the low energy total beam stopping cross-section and, therefore, the two-electron loss process should be included in the calculations of beam attenuation kinetics.

The purpose of the present article is to derive scaling relationships for the cross-sections of one- and two-electron loss processes:

$$A^{q+} + He \rightarrow A^{(q-1)+} + He^{+} \qquad (c) \qquad (1a)$$

$$A^{q+} + He \rightarrow A^{q+} + He^{+} + e \qquad (i) \qquad (1b)$$

$$A^{q+} + He \rightarrow A^{(q-2)+} + He^{2+} \qquad (2c) \qquad (2a)$$

$$A^{q+} + He \rightarrow A^{(q-1)+} + He^{2+} + e \qquad (ti) \qquad (2b)$$

$$A^{q+} + He \rightarrow A^{q+} + He^{2+} + 2e \qquad (2i) \qquad (2c)$$

where A^{q+} is an ion in charge state q, generally higher than q = 5. We note that the double capture (2c) and transfer ionization (ti) channels of the two-electron loss process (2) are strongly coupled when q is high; the two-electron capture in reaction (2a) may lead to the formation of a doubly excited state of the $A^{(q-2)+}$ ion which can autoionize and thus contribute to the transfer ionization channel (2b).

Our derivation of scaling relationships for processes (1) and (2) will be based on well established theoretical models for the reaction channels at both low and high collision energies, and on determining the numerical constants in these models from the available experimental data. In the intermediate energy region, where for some of the reaction channels in reactions (1) and (2) simple theoretical models do not exist, we shall apply an appropriate interpolation procedure allowing for a few fitting parameters. These parameters are then determined from experimental data.

2. ONE-ELECTRON LOSS CROSS-SECTION SCALING

The one-electron cross-section scaling in collisions of helium atoms with multiply charged ions has been discussed previously [2], purely on the basis of classical models for electron capture at low energies (the over-barrier electron transition model) and for ionization at high energies (the binary encounter approximation, BEA). The exact results of these models have been linked by an interpolation function containing no empirical parameters. The obtained cross-section scaling formula has reproduced the results of the corresponding fit to the scaled electron loss data from extensive classical trajectory Monte Carlo (CTMC)

calculations [3] to within 7% (i.e. well within their statistical uncertainty). The agreement of this scaling formula with the experimental data was found to be within 30% below 300 × q keV/u, and increasingly worse at higher values of the product Eq. The latter is an obvious consequence of the failure of CTMC (or BEA) models to describe the ionization events at larger impact parameters (which, as is well known, generate the E^{-1} lnE term in the first Born approximation for ionization).

Using the low energy asymptotics ($\sigma^<$) of the electron removal cross-section of the classical over-barrier model [4] and the high energy asymptotics ($\sigma^>$) of the ionization cross-section in the three-state dipole close coupling (DCC) model [5], we have

$$\sigma_{1c}^{<} \simeq \sigma_{+}^{<} = aq$$
$$\sigma_{1i}^{>} \simeq \sigma_{+}^{>} = \frac{bq^2}{E} \ln (cE/q) \tag{3}$$

where a, b and c are constants. Further, introducing the scaled quantities

$$\tilde{\sigma} = \sigma/q \text{ and } \tilde{E} = E/q \tag{4}$$

one finds that $\tilde{\sigma}$ depends only on $\tilde{E}$, i.e.

$$\tilde{\sigma}_{+}^{<} = a$$
$$\tilde{\sigma}_{+}^{>} = b\tilde{E}^{-1} \ln(c\tilde{E}) \tag{5}$$

We note that the high energy DCC asymptotics (3) of the single-ionization cross-section shows a departure from the first Born behaviour, consistent with the result of the eikonal initial state-continuum distorted wave approximation (EIS-CDWA) [6].

The classical over-barrier model provides an approximate expression for the constant a in Eq. (5), expressed in terms of the first ionization potential of the atom [7, 8]. However, we shall determine a as the mean value of the reduced experimental cross-sections $\tilde{\sigma}$ given in Ref. [9] (q = 11–31, $\tilde{E}$ = 0.03 keV/u) and Ref. [10] (q = 6, $\tilde{E}$ = 0.01–0.325 keV/u). The mean value, a = 3.8 × 10^{-16} cm^2, represents the data with an rms deviation of about 15%. The constants b and c in Eq. (5) can be determined from the high energy recommended ionization cross-section data on C^{q+} + He and O^{q+} + He (q ≥ 4) given in Ref. [11] and compiled from various experimental sources. The experimental data used in the fits are shown in Fig. 1 in the reduced parameter representation.

The scaled electron loss cross-section in the intermediate reduced energy range can be represented by the following interpolation formula:

$$\tilde{\sigma}_{+} = \frac{A\,B \ln(e + C\tilde{E}_{100})}{B + D\tilde{E}_{100}^{\beta} + A\tilde{E}_{100}} \quad [10^{-16}\ cm^2] \tag{6}$$

$$\tilde{E}_{100} = \frac{\tilde{E}}{100} = \frac{E[keV/u]}{100q}$$

where e = 2.71828 ... is the base of the natural logarithm, the constants A, B and C are related to a, b and c, respectively, and the constants D and β can be determined from the experimental electron loss data for the Li^{3+} + He [12] and A^{q+} + He (q = 4–8) [13, 14] systems in the intermediate $\tilde{E}$ region ($\tilde{E}$ = 10–100 keV/u). The values of A, B, C, D and β, determined in the above described way, are

$$A = 3.80,\ B = 2.28,\ C = 2.15 \times 10^{-2},$$
$$D = 3.088,\ \beta = 0.2578 \tag{7}$$

We note that for $\tilde{E} \gtrsim 100$ keV/u, the experimental electron loss data of Ref.[12] for the H^+ + He and He^{2+} + He systems can also be scaled by Eq. (6) (see Fig. 1). The scaled cross-section generated by Eq. (6) with the coefficients (7) is also shown in Fig. 1. It represents the data with an accuracy of 20–30% in the energy region $\tilde{E}$ < 1 keV/u, 10–20% in the range $\tilde{E} \simeq$ 1–30 keV/u and better than 10% for $\tilde{E} \gtrsim 30$ keV/u.

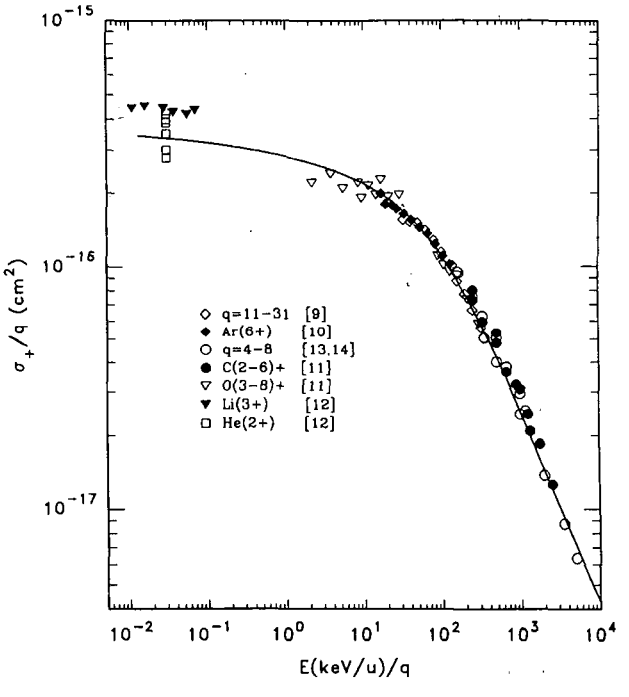

FIG. 1. Scaled one-electron loss cross-section in A^{q+} + He collisions, as a function of reduced energy. The solid line represents the result of Eq. (6) with the coefficient given by Eq. (7). The symbols are experimental data for various ions taken from the references indicated in the legend.

3. CROSS-SECTION SCALINGS FOR TWO-ELECTRON PROCESSES

The two-electron loss in collisions of helium atoms with multicharged ions includes several processes (see Eq. (2)), each of which is governed by different mechanisms at low, intermediate and high energies. It is also clear that the inter-electron correlation should play a more pronounced role in these processes than in the case of single-electron transition processes. In order to construct a scaling relationship for the two-electron loss cross-section, one should first consider the scaling properties of the cross-sections for the individual processes (2a)-(2c).

3.1. Transfer ionization

We consider here only the proper transfer ionization channel (2b), i.e. ignoring the contribution to its cross-section from the two-electron capture into an auto-ionizing, doubly excited state. In Section 3.2 we combine the transfer ionization and the two-electron capture to derive a scaling relation for the sum of their cross-sections.

In order to reveal the energy- and q-dependences of the transfer ionization cross-section σ_{ti} at high and low energies, we point out that for high q the single-electron ionization at high energies is the dominant collision process, while single-electron capture is the dominant (quasi-resonant) collision process at low energies. Therefore, within an independent particle model, the probability of the two-electron capture and ionization process in a given energy region is essentially determined by the probability of the less probable of the two single-electron transitions. Mediating the transfer ionization as a two-step process, it follows that at high collision energies its probability is determined by the capture of the second target electron, after the ionization of the first one has already taken place in the first step of the process. At low (adiabatic) energies, the probability of transfer ionization is determined by the ionization of the second electron, after the capture of the first one in an earlier stage of the collision has been completed. Within this two-step model of the process, the high energy behaviour of σ_{ti} should be $\sim q^3/E^{3.5}$, according to the Bohr-Lindhard classical model [15], or $\sim q^3/E^4$, according to the binary encounter approximation [16]. At low energies, the BEA model for the ionization of the second target electron [16] gives $\sigma_{ti} \sim (q/E)^2(1 - cq^{0.5}/E)$ where c = const. Introducing reduced quantities

$$\tilde{\sigma}_{ti} = \frac{\sigma}{q} \quad \text{and} \quad \tilde{E} = \frac{E}{q^{0.5}} \tag{8}$$

the BEA transfer ionization cross-sections at low and high energies can be put in the scaled form

$$\tilde{\sigma}_{ti}^{<} = \frac{a}{\tilde{E}^2}(1 - c/\tilde{E}) \simeq \frac{a}{\tilde{E}^2}\exp(-c/\tilde{E})$$
$$\tilde{\sigma}_{ti}^{>} = \frac{b}{\tilde{E}^4} \tag{9}$$

Since the experimental data on σ_{ti} always contain a contribution from the autoionization of doubly excited states formed by the two-electron capture reaction (2a), we determine the constants a, b and c in Eqs (9) from the CTMC results for the A^q + He systems [17], where A^{q+} is a fully stripped ion with q = 6, 8, 10 and 14. Indeed, all CTMC data, available for the above ions in the energy interval from 100 to 1000 keV/u, when scaled according to Eq. (8), fall on one curve, with an asymptotic behaviour in accordance with Eqs (9) (see Fig. 2). We note that in these CTMC calculations a 'split-shell' model for the two electrons in the helium atom has been used, which 'individualizes' the electrons by equating their binding

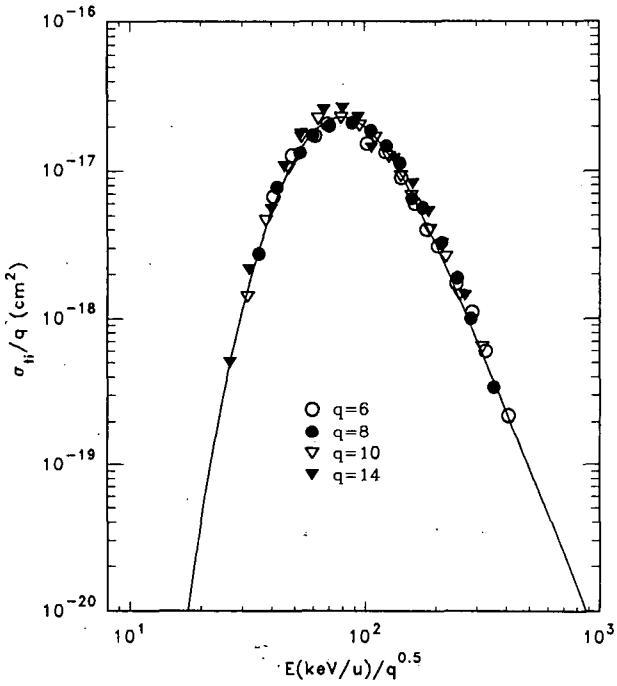

FIG. 2. Scaled transfer ionization cross-section in collisions of He atoms with fully stripped ions of charge q ≥ 6, as a function of reduced energy. The solid line is a fit of the results of classical trajectory Monte Carlo calculations [17] (symbols) as given by Eqs (10) and (11).

energies with the first and the second ionization potentials, respectively. Such a 'split-shell' two-electron atomic model is consistent with the picture of the two-step collision dynamics outlined at the beginning of this Section.

The interpolation expression which connects the asymptotics (9) in the intermediate region of $\tilde{E}$ has the form

$$\tilde{\sigma}_{ti} = \frac{AB \times 10^{-16}\ [cm^2]}{B\tilde{E}_{100}^2 \exp(C/\tilde{E}_{100}) + D\tilde{E}_{100} + A\tilde{E}_{100}^4} \qquad (10)$$

$$\tilde{E}_{100} = \frac{E[keV/u]}{100q^{0.5}}$$

with the constants A, B and C, related to a, b and c of Eq. (9) and determined as described above, having the values

$$A = 5.8965,\ B = 0.600,\ C = 2.241,\ D = 6.15 \qquad (11)$$

The cross-section generated by Eq. (10) is given in Fig. 2 by the solid line and represents all CTMC data of Ref. [17] for $q \geq 6$, with an accuracy of about 5%. The scaled cross-section has a maximum at $\tilde{E} \simeq 80$ keV/u. We note that the scaling relationship (10) significantly differs from the semi-empirical one proposed by Tanis et al. [18] (see also Ref. [19]).

3.2. Two-electron capture and transfer ionization

Two-electron capture and transfer ionization at low collision energies and for high projectile charges are strongly coupled processes, and it is convenient to consider them together, as a two-electron release from the target. The two-electron release at low energies can be described as a two-step process (sequential release of the first and the second electron), the overall probability of which is determined by the second step [7]. Within an extended classical over-barrier transition model [7, 8], one finds that the characteristic internuclear distance for the release of the second electron is $R_{2c} \simeq 2q^{0.5}/I_2$, where I_2 is the second ionization potential (in atomic units). Therefore, the cross-section for two-electron release at low energies, given by the extended classical over-barrier model, is

$$\sigma_{2r}^{<} = aq \qquad a = \text{const.} \qquad (12)$$

For sufficiently high values of q, this low energy behaviour of σ_{2r} has indeed been experimentally observed (see, for example, Refs [7, 8]). For a helium target, the value of the constant a can be determined from the experimental data of Ref. [9] ($E = 0.03 \times q$ keV/u, q = 11–29), and Ref. [10] (q = 6, E = 0.07–1.5 keV/u), giving $a = 1.37 \times 10^{-16}$ cm^2.

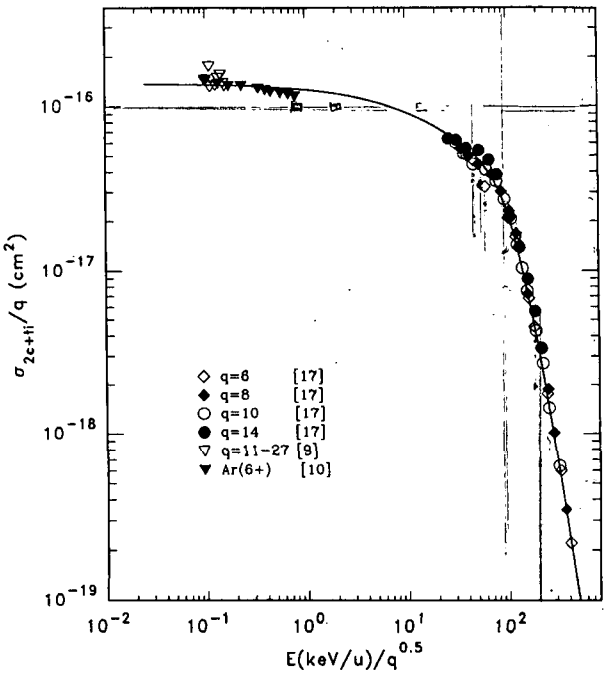

FIG. 3. Scaled cross-section for double capture and transfer ionization in collisions of He with multiply charged ions, as a function of reduced energy. The symbols on the left hand side are experimental data from Refs [9, 10] and the symbols on the right hand side are the results of classical trajectory Monte Carlo calculations [17] for q = 6–14. The solid line is the analytic fit of the data given by Eqs (14) and (15).

At high energies ($E > 80q^{0.5}$ keV/u), the two-electron release is determined by the transfer ionization, the cross-section of which decreases more slowly than that for two-electron capture. Indeed, the CTMC two-electron capture cross-sections of Ref. [17] for $E \geq 100q^{0.5}$ keV/u ($q \geq 6$) can all be put into a scaled form (within an accuracy of 5–10%):

$$\tilde{\sigma}_{2c}^{>} = \frac{\sigma_{2c}}{q} = \frac{5.8 \times 10^{-18}\ cm^2}{\tilde{E}_{100}^{4.5}} \qquad (13)$$

$$\tilde{E}_{100} = \frac{E[keV/u]}{100q^{0.5}}$$

and are at least an order of magnitude smaller than the values of $\tilde{\sigma}_{ti}$ for $\tilde{E} \geq 200$ keV/u. In the region $E < 200\ q^{0.5}$ keV/u, the CTMC two-electron capture cross-sections continue to preserve the scaling $\tilde{\sigma}_{2c} = \sigma_{2c}/q$ and $\tilde{E} = E/q^{0.5}$.

On the basis of the above discussion and the expressions (12) and (9) (for $\tilde{\sigma}_{ti}^{>}$), we represent the scaled cross-section $\tilde{\sigma}_{2c+ti} = \sigma_{2c+ti}/q$ for the combined process of double electron capture and transfer ionization in the form

$$\tilde{\sigma}_{2c+ti} = \frac{A\,B \times 10^{-16}\ [cm^2]}{B + D\tilde{E}_{100}^{\beta} + A\tilde{E}_{100}^{4}} \qquad (14)$$

$$\tilde{E}_{100} = \frac{E[keV/u]}{100q^{0.5}}$$

where the constants A, B, D and β have the values

$$A = 1.37,\ B = 0.64,\ D = 1.77,\ \beta = 0.75 \qquad (15)$$

The constants D and β have been determined from the CTMC $\tilde{\sigma}_{2c+ti}$ data in the region $\tilde{E} < 200$ keV/u and from experimental data of Ref. [10] for $E \gtrsim 0.3$ keV/u, while A and B have been determined from the corresponding asymptotic regions. The data used in these fits are shown in Fig. 3, together with the cross-section generated by Eq. (14) with the coefficients (15) (solid line). We note that Eq. (14) represents these data with an rms of about 10%.

3.3. Two-electron loss

The cross-section for two-electron loss is the sum of the cross-sections of all channels in reaction (2), i.e.

$$\sigma_{++} = \sigma_{2c} + \sigma_{ti} + \sigma_{2i} = \sigma_{2c+ti} + \sigma_{2i} \qquad (16)$$

Since, at low energies, σ_{2c+ti} gives the main contribution to σ_{++} and, at high energies, double ionization is the dominant two-electron loss channel, we need to find an appropriate high energy scaling for σ_{2i} which should be consistent with the scaling of σ_{2c+ti} at low energies.

The two-electron ionization at high energies is governed by three different basic mechanisms, the role of which in the ionization process depends on the collision energy and the ionic charge q (i.e. the ratio of ion–electron and electron–electron interactions) (see, for example, Refs [20, 21] and references therein). The shake-off mechanism includes only one projectile-electron interaction, leading to ionization, while the ejection of the other electron is the result of the sudden change of the atomic self-consistent field. This first-order process gives a high energy behaviour, $\sigma_{2i,0}^{>} \sim q^2E^{-1}\ \ln E$. The other mechanisms describe second-order processes, such as projectile–electron and electron–electron interaction, each leading to electron ejection ($\sigma_{2i,1}^{>} \sim q^2E^{-1}\ \ln E$), projectile interaction with each of the electrons ($\sigma_{2i,2}^{>} \sim q^4/E^2$), and a coherent interference of these two processes ($\sigma_{2i,3}^{>} \sim q^3/E^{3/2}$). The ionization mechanisms (2i,1), (2i,2) and (2i,3) can also be related with the role of inter-electronic correlations in the process. In the mechanism (2i,1), the projectile–electron interaction is weaker (low q) than the electron–electron interaction, and because of the strong correlation effects the ionization of one of the electrons leads also to ionization of the other. In the process (2i,2) the situation is reversed: the projectile-electron interaction is much stronger (high q) than the electron–electron interaction, and the correlation effects do not play any role in the ionization of each of the electrons (independent particle model). In the process (2i,3) the two interactions are of the same order of magnitude. The ratio r_c of projectile–electron and electron–electron interactions ($r_c = q$, in atomic units) thus appears as an independent parameter in the collision dynamics. Having in mind the above expressions for $\sigma_{2i,1-3}^{>}$, an appropriate reduced energy variable for $\sigma_{2i}^{>}$ would be (within a logarithmic accuracy) $\tilde{E} = E/q^2$. Indeed, the experimental data with $q \gtrsim 4$ from various sources [22–25] do demonstrate such a scaling. This variable, however, is not convenient from the view point of connecting $\sigma_{2i}^{>}$ with $\sigma_{2c+ti}^{<}$ through an interpolation expression, since $\sigma_{2c+ti}^{<}$ explicitly depends on q. On the other hand, the expressions for $\sigma_{2i,0}^{<}$ and $\sigma_{2i,1}^{>}$ suggest that the reduced variable $\tilde{E} = E/q$ does allow (at least within a logarithmic accuracy) $\sigma_{2i}^{>}$ and $\sigma_{2c+ti}^{<}$ to be connected through the intermediate energy region by introducing the scaled cross-sections $\tilde{\sigma}_{2i}^{>} = \sigma_{2i}^{>}/q$ and $\tilde{\sigma}_{2c+ti}^{<} = \sigma_{2c+ti}/q$. By using these variables, the asymptotic forms of $\tilde{\sigma}_{++} = \sigma_{++}/q$ at low and high reduced energies are

$$\tilde{\sigma}_{++}^{<} \simeq \tilde{\sigma}_{2c+ti}^{<} = a$$

$$\tilde{\sigma}_{++}^{>} \simeq \tilde{\sigma}_{2i}^{>} = \frac{b}{\tilde{E}^2}\,\xi(q,\tilde{E})$$

$$\tilde{E} = E/q \qquad (17)$$

where $\xi(q,\tilde{E})$ is a function which for $\tilde{E}/q \gg 1$ should satisfy the condition $\xi(q,\tilde{E}) = q$ (i.e. in this limit $\sigma_{2i}^{>} = \sigma_{2i,2}^{>}$). We may impose another condition on $\xi(q,\tilde{E})$, such that for $\tilde{E}/q \ll 1$, $\xi(q,\tilde{E}) \simeq (q\tilde{E})^{1/2}$, so that in this limit $\sigma_{2i}^{>} = \sigma_{2i,3}^{>}$. Thus, the function $\xi(q,\tilde{E})$ can be regarded as describing the role of inter-electron correlations in the collision. The ratio $\nu = \tilde{E}/q = \tilde{E}/r_c$ describes the relative role of the reduced kinetic energy and the reduced potential interaction in the ionization process. The transition from the $\sigma_{2i,2}^{>}$ behaviour to the $\sigma_{2i,3}^{>}$ behaviour usually takes place for relatively small variations of the ratio $\tilde{E}/q$, which suggests the following exponential form for $\xi(q,\tilde{E})$

$$\xi(q,\tilde{E}) = q\ \{1 - \exp[-\gamma(\tilde{E}/q)^{1/2}]\} \qquad (18)$$

where γ is a constant. The choice of the $\tilde{\sigma}_{2i}^{>}$ asymptotics in the form of Eqs (17) and (18) appears to be an adequate one, since with two fitting parameters (b and γ) it successfully describes a large variety of

experimental data [22–25] in the region $\tilde{E} > 200$ keV/u, and for q varying between q = 4 and q = 92. The interpolation formula linking the asymptotics (17) can be chosen in the form

$$\tilde{\sigma}_{++} = \frac{A\,B \times 10^{-16}\ [cm^2]}{B + D\,\xi^{1/2}\tilde{E}_{100}^{\beta} + A\xi^{-1}\tilde{E}_{100}^{2}} \qquad (19)$$

$$\tilde{E}_{100} = \frac{E[keV/u]}{100q}$$

where the constants have the values

$$A = 1.37,\ B = 0.08,\ D = 0.035,$$
$$\beta = 0.2,\ \gamma = 0.9 \qquad (20)$$

The constants D and β have been determined from experimental data [23] and recent CTMC data [26] in the reduced range $\tilde{E} \simeq 2.5$–100 keV/u. The experimental and CTMC data used in determining the fitting coefficients in Eq. (19) are shown in Fig. 4, together with the scaled cross-sections calculated from Eq. (19) for q = 6, 36 and 90. The accuracy of the scaling formula (19) is within 10–20% and is probably somewhat worse (20–30%) in the range $\tilde{E} = 0.3$–30 keV/u, where only the CTMC data were used as the basis for fitting.

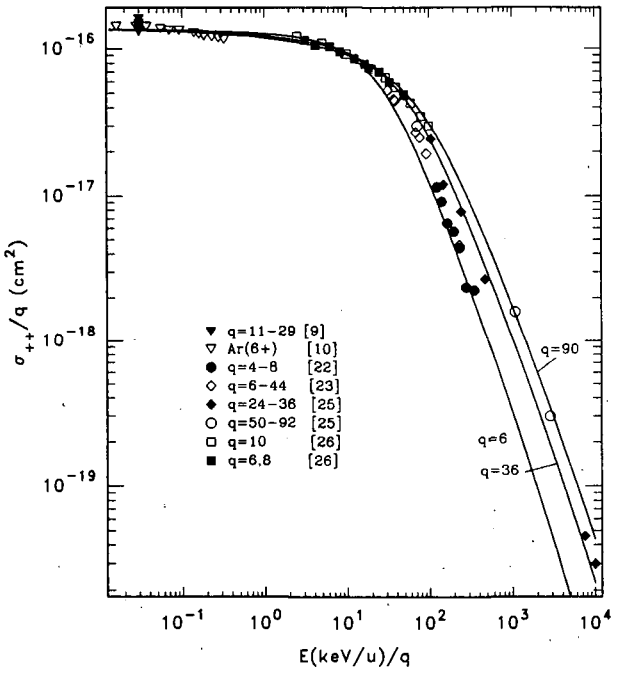

FIG. 4. Scaled two-electron loss cross-section in collisions of He with multiply charged ions of q ≥ 6, as a function of reduced energy. The symbols represent experimental data and results of classical trajectory Monte Carlo calculations from the references indicated. The solid lines denote results obtained from Eq. (19) for q = 6, 36 and 90.

4. ION PRODUCTION CROSS-SECTION

From the point of view of neutral beam attenuation kinetics in a fusion plasma, the relevant total cross-section for ion production (or atom loss from the beam) in collisions of beam atoms with plasma impurity ions is

$$\sigma_{i,p} = \sigma_{+} + \sigma_{++} \qquad (21)$$

Since both σ_+ and σ_{++} are scaled with the same reduced energy ($\tilde{E} = E/q$), the corresponding scaled cross-sections $\tilde{\sigma}_+ = \sigma_+/q$ and $\tilde{\sigma}_{++} = \sigma_{++}/q$ can be summed directly. For the low-$\tilde{E}$ and high-$\tilde{E}$ limits of $\tilde{\sigma}_{i,p} = \sigma_{i,p}/q$, one then obtains (see Eqs (5) and (17))

$$\tilde{\sigma}_{i,p}^{<} = \tilde{a}$$
$$\tilde{\sigma}_{i,p}^{>} \simeq \tilde{\sigma}_{+}^{>} = b\tilde{E}^{-1}\ln(c\tilde{E}) \qquad (22)$$

where $\tilde{a}$ is the sum of the a-constants in Eqs (5) and (17), and b and c are the same constants as in Eq. (5). For $\tilde{\sigma}_{i,p}^{>}$ it has been taken into account that $\tilde{\sigma}_{++}^{>} \ll \tilde{\sigma}_{+}^{>}$. Using for the interpolation expression of $\tilde{\sigma}_{i,p}$ in the intermediate region the same form as for $\tilde{\sigma}_+$ (Eq. (6)), we have

$$\tilde{\sigma}_{i,p} = \frac{\tilde{A}B\ln(e + C\tilde{E}_{100})}{B + D\tilde{E}_{100}^{\beta} + \tilde{A}\tilde{E}_{100}}\ [10^{-16}\ cm^2] \qquad (23)$$

$$\tilde{E}_{100} = \frac{E[keV/u]}{100q}$$

with

$$\tilde{A} = 5.17,\ B = 2.82,\ C = 2.15 \times 10^{-2},$$
$$D = 2.426,\ \beta = 0.25 \qquad (24)$$

Comparing the value of $\tilde{A}$ with that for A in Eq. (20), we see that the contribution of $\tilde{\sigma}_{++}$ to $\tilde{\sigma}_{i,p}$ in the low energy limit is 27%. When the reduced energy is increased, the contribution of $\tilde{\sigma}_{++}$ to $\tilde{\sigma}_{i,p}$ decreases gradually, and at $\tilde{E} \simeq 100$ keV/u it amounts to about 10–20%, depending on q.

5. ELECTRON LOSS FROM EXCITED STATES

In view of the important role of multistep processes in the attenuation kinetics of an energetic neutral beam in a plasma (the collision times of excited beam atoms are comparable with their radiative lifetimes), the electron loss from excited beam atoms due to collisions with plasma impurities is also needed in beam stopping calculations. For a helium neutral beam this is a par-

ticularly important process, since the first excited states $He^*(2\,^{1,3}S)$ and $He^*(2\,^3P)$ are metastable. Moreover, depending on the method of its preparation, the initial He beam may contain fractions of the long lived $He^*(2\,^{1,3}S)$ metastable atoms.

If the binding energy of an excited atom $He^*(1s, n\,^{2S+1}L)$ is $I_0 = -1/2n_0^2$, then, on the basis of classical arguments, one has the following scalings for low energy electron capture and high energy ionization of excited atoms:

$$\sigma_{1c}^{<}(n) \sim n_0^4$$
$$\sigma_{1i}^{>}(n) \sim \frac{n_0^2}{E} \sim \frac{n_0^4}{n_0^2 E} \tag{25}$$

These relations, together with Eqs (4), suggest the following reduced quantities for the single electron loss [2]:

$$\tilde{\sigma}_+ = \frac{\sigma_+}{q n_0^4} \quad \text{and} \quad \tilde{E} = \frac{n_0^2 E}{q} \tag{26}$$

While the n_0^4 scaling of the electron capture cross-section has been widely demonstrated to be valid for any value of n [27], it is not expected to be valid for the ionization of the lowest excited states (since Eq. (25) for $\sigma_{1i}^{>}$ in its quantum version, besides the binding energy contains also a dipole matrix element for coupling with the continuum which also depends on n). Indeed, when one tries to calculate $\sigma_{1i}^{>}$ for the $He^*(2\,^3S)$ atom by scaling the $H^+ + He(1\,^1S)$ high energy ionization cross-section with the use of Eq. (26), one finds that the obtained cross-section is about two times larger than the cross-section obtained by scaling the experimental electron impact ionization cross-section for $He^*(2\,^3S)$ [28]. For this reason, we determine the high energy asymptotics for the $\sigma_{1i}^{>}(2\,^3S)$ cross-section from the scaled electron impact experimental ionization cross-section of $He(2\,^3S)$, while the low energy asymptotics of $\sigma_{1c}^{<}(2\,^3S)$ can be derived from the n_0^4 scaled $\sigma_{1c}^{<}(1\,^1S)$, cross-section

$$\sigma_{1c}^{<}(2\,^3S) = \left[\frac{n_0(2\,^3S)}{n_0(2\,^1S)}\right]^4 \sigma_{1c}^{<}(1\,^1S)$$
$$= 26.584\ \sigma_{1c}^{<}(1\,^1S) \tag{27}$$

Using the asymptotic forms (5) for the reduced electron loss cross-section $\tilde{\sigma}_+(2\,^3S) = \sigma_+(2\,^3S)/q$, we write its interpolation expression as

$$\tilde{\sigma}_+(2\,^3S) = \frac{A\,B\ln(e + C\tilde{E}_{10})}{B + A\tilde{E}_{10}}\ [10^{-16}\ cm^2] \tag{28}$$

$$\tilde{E}_{10} = \frac{E[keV/u]}{10q}$$

with the constants A, B and C determined as described above, having the values

$$A = 101,\ B = 56,\ C = 1 \times 10^{-2} \tag{29}$$

The accuracy of Eq. (28) in the high energy region ($\tilde{E} \gtrsim 100$ keV/u) should be close to that of the original data (15–20%), and within 20–30% in the region $\tilde{E} \lesssim 1$ keV/u, where the scaling (27) is certain. In the intermediate energy range, the uncertainty of Eq. (28) is about 30–40%.

Using the scaling relations (26) and the cross-section $\tilde{\sigma}_+(2\,^3S)$, one can calculate the reduced electron loss cross-sections for any excited state $n\,^{2S+1}L$ of helium,

$$\tilde{\sigma}_+(n\,^{2S+1}L;\ \underline{\tilde{E}_{10}}) = \underline{\epsilon}^2 \tilde{\sigma}_+(2\,^3S;\ \epsilon\tilde{E}_{10}) \tag{30}$$

where

$$\epsilon = \left[\frac{n_0(2\,^3S)}{n_0(n\,^{2S+1}L)}\right]^2 = \frac{I(n\,^{2S+1}L)}{I(2\,^3S)} \tag{31}$$

$I(n\,^{2S+1}L)$ being the ionization potential of $He^*(n\,^{2S+1}L)$.

The two-electron loss process in collisions of excited helium atoms with ions has a cross-section which is of the same order of magnitude as that for ground state helium atoms and therefore can be ignored in the beam attenuation kinetics.

6. CONCLUDING REMARKS

Using the available experimental data and the numerical results of classical trajectory Monte Carlo calculations, as well as simple and well established models for one- and two-electron transition processes in ion–atom collisions, we have derived scaled cross-sections for the one-electron loss, transfer ionization, double capture plus transfer ionization and two-electron loss processes in collisions of multiply charged ions with helium atoms. The presented semi-empirical fits are valid in a wide range of variation of the reduced energy parameter. Only in the case of two-electron loss it was not possible to comprise the energy charge and the ionic charge into one scaled variable. The reason for this is the variety of second-order physical mechanisms contributing to the high energy double ionization in different domains of the energy–ionic charge parametric space. Apart from the usual reduced energy parameter $\tilde{E} = E/q$ (for one-electron ionization), in the case of double ionization the ratio $r_c(=q)$ of ion–electron and electron–electron interactions appears as another independent parameter. In a reduced $\tilde{\sigma} = \sigma_{2i}/q$ cross-section representation, the existence of two independent parameters in the problem leads to the

appearance of the 'correlation' function $\xi(q,\tilde{E})$ in $\sigma_{2i}^{\geq}$ (see Eq. (17)). The accuracy of the semi-empirically derived scaling formulas is within the uncertainties of the experimental data used in the determination of the fitting constants.

The cross-section scaling for one-electron loss from excited helium atoms, discussed in Section 5, should also be of sufficient accuracy for the calculations of helium beam attenuation.

REFERENCES

[1] BOLEY, C.D., JANEV, R.K., POST, D.E., Phys. Rev. Lett. **52** (1984) 534.

[2] JANEV, R.K., Phys. Rev., A **28** (1983) 1810.

[3] OLSON, R.E., Phys. Rev., A **18** (1978) 2464.

[4] GROZDANOV, T.P., J. Phys., B. At. Mol. Phys. **13** (1980) 3835.

[5] JANEV, R.K., PRESNYAKOV, L.P., J. Phys., B. At. Mol. Phys. **13** (1980) 4233.

[6] FAINSTEIN, P.D., PONCE, V.H., RIVAROLA, R.D., J. Phys., B. At. Mol. Opt. Phys. **23** (1990) 1481.

[7] JANEV, R.K., PRESNYAKOV, L.P., Phys. Rep. **70** (1981) 1.

[8] BARANY, A., et al., Nucl. Instrum. Methods Phys. Res., Sect. B **9** (1985) 397.

[9] ANDERSSON, H., ASTNER, G., CEDERQUIST, H., J. Phys., B. At. Mol. Opt. Phys. **21** (1988) L188.

[10] MULLER, A., SALZBORN, E., Phys. Lett., A **59** (1976) 19.

[11] JANEV, R.K., PHANEUF, R.A., HUNTER, H.T., At. Data Nucl. Data Tables **40** (1988) 249.

[12] SHAH, M.B., GILBODY, H.B., J. Phys., B. At. Mol. Phys. **18** (1985) 899.

[13] HVELPLUND, P., HAUGEN, H.K., KNUDSEN, H., Phys. Rev., A **22** (1980) 1930.

[14] KNUDSEN, H., HAUGEN, H.K., HVELPLUND, P., Phys. Rev., A **23** (1981) 597.

[15] BOHR, N., LINDHARD, J., K. Dan. Vidensk. Selsk., Mat.-Fys. Medd. **28** (1854) 1.

[16] CHATTERJEE, S.N., PRASAD, S., ROY, B.N., J. Phys., B. At. Mol. Opt. Phys. **21** (1988) 1209.

[17] WETMORE, A.E., OLSON, R.E., Phys. Rev., A **38** (1988) 5563.

[18] TANIS, J.A., CLARK, M.W., PRICE, R., et al., Nucl. Instrum. Methods Phys. Res., Sect. B **23** (1987) 167.

[19] GILBODY, H.B., this issue, p. 55.

[20] McGUIRE, J.H., Phys. Rev. Lett. **49** (1982) 1153.

[21] ANDERSEN, L.H., HVELPLUND, P., KNUDSEN, H., et al., Phys. Rev., A **36** (1987) 3612.

[22] KNUDSEN, H., ANDERSEN, L.H., HVELPLUND, P., et al., J. Phys., B. At. Mol. Phys. **17** (1984) 3545.

[23] McGUIRE, J., MULLER, A., SCHUCH, B., et al., Phys. Rev., A **35** (1987) 2479.

[24] COCKE, C.L., Phys. Rev., A **20** (1979) 749.

[25] BERG, H., ULLRICH, J., BERNSTEIN, E., et al., J. Phys., B. At. Mol. Opt. Phys. **25** (1992) 3655.

[26] KATSONIS, K., MAYNARD, G. (Université Paris-Sud, Orsay), personal communication, 1992.

[27] JANEV, R.K., Phys. Lett., A **160** (1990) 67.

[28] DIXON, A.J., HARRISON, M.F.A., SMITH, A.C.H., J. Phys., B. At. Mol. Phys. **9** (1976) 2617.

SENSITIVITY OF NEUTRAL HELIUM BEAM STOPPING IN FUSION PLASMAS TO ATOMIC COLLISION CROSS-SECTIONS

A.A. KOROTKOV
A.F. Ioffe Physico-Technical Institute,
Russian Academy of Sciences,
St. Petersburg, Russia

ABSTRACT. It is shown that the enhancement of the helium beam stopping cross-section in a fusion plasma due to multistep collision processes is determined mostly by the rate of the population of highly excited singlet states ($n \geq 4$). The major atomic processes are the dipole transitions from the ground state by proton and electron impact, including transitions to the levels lying above the Lorentz ionization limit. The contribution of metastable states is about 10% in the equilibrium case. The effect of multistep collision processes on the helium beam attenuation is large at integrated line plasma densities above 10^{16} cm^{-2} as expected for next generation tokamaks.

1. INTRODUCTION

The enhancement of neutral beam attenuation in a plasma due to multistep atomic processes has a strong impact on the design of neutral beam injection systems for heating, current drive and diagnostics of fusion plasmas [1]. This phenomenon has been thoroughly analysed for neutral hydrogen beams [2]. It is also of interest to investigate the role of multistep processes in the stopping of neutral helium beams. Helium beams have already been successfully used for plasma heating on JET [3], and they represent a very attractive means of active charge exchange diagnostics for fusion alpha particles [4].

In the study of helium beam stopping in fusion plasmas, it is necessary to establish the main dependences of beam stopping cross-sections on the plasma parameters and to elucidate the role of particular collision processes in the enhancement of beam stopping. For this purpose, we have performed extensive beam stopping cross-section calculations by varying the cross-sections for the relevant collision processes and the effective beam energy (E/Z) between 20 and 1000 keV/u (Z is the impurity ion charge).

We consider a plasma consisting of electrons, hydrogen ions (deuterons or tritons) and impurity ions (He^{2+}, C^{6+}, O^{8+}, Fe^{24+}) with parameters typical for present day and next generation tokamaks: $n_e = 10^{13}$–10^{15} cm^{-3}, T = 1–10 keV, B = 2–5 T, Z_{eff} = 1–3. The influence of the magnetic $\vec{B}$ field and the Lorentz ($\vec{\mathcal{E}} = \vec{v}_0 \times \vec{B}$) field on the energies of the excited states and their radiative life times and spin state mixing is also taken into account ($\vec{v}_0$ is the atom velocity).

2. METHOD OF CALCULATION

2.1. Beam stopping cross-section and description of atomic states

The total beam stopping cross-section σ_s can be expressed as $\sigma_s = \sigma_s^0 + \sigma_{ad}$, where σ_s^0 and σ_{ad} designate the beam stopping cross-sections for the ground state and the excited beam atoms, respectively. (Initially, all beam atoms are in the ground state.) The beam stopping cross-section due to multistep processes can be calculated with the formula

$$\sigma_{ad} = \left[\sum_{k=1}^{k_m} (I_k - I_0) N_k + \sum_{k>k_m} K_{1k} \right] \Big/ v_0 \left(1 + \sum_{k=1}^{k_m} N_k \right) \quad (1)$$

where N_k is the population of the state k relative to the ground state population, I_k is the rate coefficient for electron loss from the state k due to ionization and charge exchange (I_0 corresponds to σ_s^0), K_{ik} is the rate coefficient for excitation (de-excitation) from the state i to the state k, and k_m is the maximum state number determined by the Lorentz field ionization limit.

The excited state populations N_k are determined from the set of coupled equations of the stationary radiative collisional model [5] using the atomic physics database presented in Section 3.

Only singly excited electronic states are considered in the beam attenuation kinetics. For the states with principal quantum number $n \leq 4$, the multiplet structure is taken into account. The wave functions

$$\Psi_{1s,nk} = \sum_{\ell jm} C^k_{n\ell jm} \Psi^0_{1s,n\ell jm}$$

and energies of the state E_k are determined by diagonalizing the energy matrix with the field-free states:

$$\langle n\ell' j' m' \,|W|\, n\ell jm\rangle = (E - E^0_{n\ell' j' m'})\,\delta_{\ell' j' m' \ell jm} + \langle n\ell' j' m' \,|V|\, n\ell jm\rangle \quad (2)$$

$$V = V^{\mathcal{E}} + V^{B}$$

$$V^{\mathcal{E}}_z = v_0 B z$$

$$V^{B}_y = \mu_0 B (M_y + S_y)$$

where M_y and S_y are respectively the components of the total angular momentum and the spin operators perpendicular to the magnetic field $\vec{B}$ (taken along the Z-axis), μ_0 is the Bohr magneton and $\vec{v}_0$ is assumed to be perpendicular to $\vec{B}$.

The approximate field-free wave functions, characterized by quantum numbers $n\ell jm$ of the outer electron, have been taken in the form $\Psi^0_{1s,n\ell jm} = u_{1s}(1)\,\varphi_{n\ell jm}(2)$, where $\varphi_{n\ell jm}$ is the hydrogen wave function.

For $n \leq 7$, $\ell < 4$, we use $E^0_{n\ell}$ from Ref. [6]. For $n \leq 7$, $\ell \geq 4$, $E^0_{n\ell}$ was calculated by taking into account the Rydberg corrections from the first order perturbation theory [7]. The field-free fine structure was taken into consideration for the triplet states. The states with $n > 7$ are considered to be hydrogen-like states. It is assumed that the ℓ-states for $n \geq 5$ are completely mixed.

2.2. Singlet–triplet spin state mixing

The excitation of helium triplet states in high temperature plasmas ($T \geq 1$ keV) has some important features. The rates of the spin changing transitions induced by electron impact become much lower than those for spin conserving transitions. Under such conditions, the relativistic mixing of singlet–triplet states becomes an important mechanism contributing to the triplet state population. The basis wave functions which take this mixing into account have the form

$$\Phi(n\ell\ {}^1L_\ell) = -b_{n\ell}\Psi^0_{1s,n\ell}({}^3L_\ell) + a_{n\ell}\Psi^0_{1s,n\ell}({}^1L_\ell)$$
$$\Phi(n\ell\ {}^3L_\ell) = a_{n\ell}\Psi^0_{1s,u\ell}({}^3L_\ell) + b_{n\ell}\Psi^0_{1s,n\ell}({}^1L_\ell) \quad (3)$$

where $a_{n\ell}$ and $b_{n\ell}$ are the mixing coefficients, $a^2_{n\ell} + b^2_{n\ell} = 1$.

The mixing coefficients for a free atom are obtained by diagonalizing the energy matrix with the pure LS states using a spin orbit operator of the form suggested in Ref. [8].

The calculations show that singlet and triplet states with $n \geq 5$, $\ell \geq 5$ are completely mixed ($a^2_{n\ell} = b^2_{n\ell} = 0.5$), but the states with $\ell < 4$ are nearly pure.

In the calculations we have also taken into account the additional spin state mixing when occasional degeneration of the singlet and triplet states occurs owing to the motional Stark effect. In this case

$$b^2_{n\ell} = \xi/(1+\xi) \quad (4)$$

where

$$\xi = \frac{4\,(E^{ss}_{n\ell})^2}{(\Delta E_{n\ell} + \sqrt{(\Delta E_{n\ell})^2 + 4\,(E^{ss}_{n\ell})^2})^2}$$

$$\Delta E_{n\ell} = \begin{cases} \Delta E^p_{n\ell} - \Gamma & \Delta E^p_{n\ell} \geq \Gamma \\ 0 & \Delta E^p_{n\ell} < \Gamma \end{cases}$$

$$E^{ss}_{n\ell}\ [\text{a.u.}] = 2.7 \times 10^{-5}\,[n^3(2\ell+1)\sqrt{\ell(\ell+1)}]^{-1}$$

Here, $E^{ss}_{n\ell}$ is the matrix element for mixing of the pure singlet ${}^1L_\ell$ and triplet ${}^3L_\ell$ states, $\Delta E^p_{n\ell}$ is the energy gap between these states taking into account the Stark and Zeeman effects in the plasma, and Γ is the sum of collisional and radiative widths of the states.

Figure 1 shows the total population of the singlet and triplet helium states for three plasma densities as a function of beam energy (or, equivalently, the Lorentz field strength $\mathcal{E}[\text{V/cm}] = 1.09 \times 10^4 \sqrt{E\,(\text{keV})}$). It can be seen that the spin state mixing results in a several-fold increase of triplet state populations. The maxima and minima in the triplet state populations in Fig. 1 correspond to the energy level crossings of the states in $3\ {}^1D$ and $3\ {}^3D$ multiplets due to the Stark effect. The increase in the collision width Γ with increasing plasma density results in additional degeneration of the states and, thus, promotes the spin state mixing.

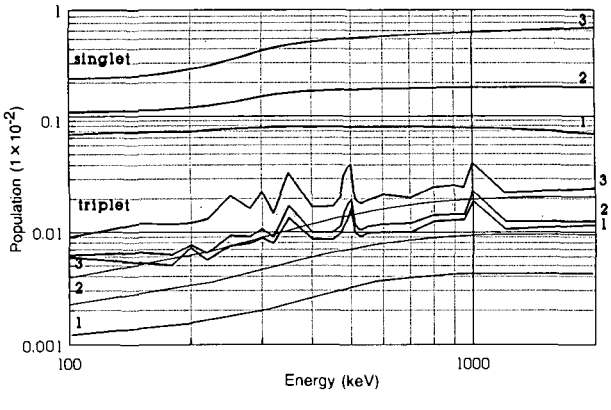

FIG. 1. Total population of singlet and triplet excited states versus helium beam energy for three values of plasma density: 1 — $n_e = 10^{13}$ cm^{-3}, 2 — $n_e = 10^{14}$ cm^{-3}, 3 — $n_e = 10^{15}$ cm^{-3} ($Z_{eff} = 1$, $T = 10$ keV, $B = 5$ T). Thin curves are for the case without spin state mixing.

3. ATOMIC PHYSICS DATABASE

Here we give a brief description of the atomic physics database used for calculation of the coefficients in the equations of the radiative collisional model and in Eq. (1). The method of calculating the rate coefficients for collisional and radiative transitions between the multiplet states, allowing for spin state mixing, is described in the Appendix.

3.1. Proton impact processes

$$H^+ + He(1s^2\,{}^1S) \rightarrow H^+ + He(1s, n\ell\,{}^1L) \quad n \geq 2 \tag{5a}$$

$$H^+ + He(1s, n\ell\,{}^{1,3}L) \rightarrow H^+ + He(1s, m\ell'\,{}^{1,3}L) \quad m \geq n \geq 2 \tag{5b}$$

$$H^+ + He(1s, n\ell\,{}^{1,3}L) \rightarrow H(\Sigma m) + He^+(\Sigma k) \quad n \geq 2,\ m,k \geq 1 \tag{5c}$$

$$H^+ + He(1s, n\ell\,{}^{1,3}L) \rightarrow H^+ + He^+(\Sigma m) + e \quad n \geq 2,\ m \geq 1 \tag{5d}$$

For the process (5a) the experimental cross-sections recommended by de Heer et al. [9] are used for $n = 2, 3, 4$ and $\ell = 0, 1, 2$. The cross-sections for $n > 4$ are calculated from the relation

$$\sigma(1s^2\,{}^1S \rightarrow 1s, n\ell\,{}^1L) = (4/n)^3\,\sigma(1s^2\,{}^1S \rightarrow 1s, 4\ell\,{}^1L)$$

For the process (5b) the analytic expression from the two-state dipole-approximation close-coupling (DACC) theory [10] is used.

In calculating the electron loss induced by the Lorentz field, ($\sum_{k>k_m} K_{ik}$), we have summed over all levels above the ionization limit using the n^{-3} scaling for the oscillator strengths of the levels with $n > 12$.

The cross-section of the process [5c], and the similar process for an impurity ion with charge Z, is estimated from the relation (see Ref. [5])

$$\sigma_{cx}^{(Z)}(E/m) = (1/2\,I_n)^2\,Z^{1.07}\,\sigma_{cx}^{u}(\tilde{E}/m) \tag{6}$$

where $\tilde{E} = E/(2\,Z^{0.464}\,I_n)$, σ_{cx}^{u} is the function fitted to the experimental data for hydrogen presented in Ref. [11], I_n is the electron binding energy in the state n, and m is the mass of the ion per nucleon.

The cross-section of reaction (5d) is described by the approximation of Rudd et al. [12] which gives results close to the Lotz formula [13] generalized for proton impact.

3.2. Electron impact processes

$$e + He(1s^2\,{}^1S) \rightarrow e + He(1s, n\ell\,{}^1L) \quad n \geq 2 \tag{7a}$$

$$e + He(1s^2\,{}^1S) \rightarrow e + He(1s, n\ell\,{}^3L) \quad n \geq 2 \tag{7b}$$

$$e + He(1s, n\ell\,{}^{1,3}L) \rightarrow e + He(1s, m\ell'\,{}^{1,3}L) \quad m \geq n \geq 2 \tag{7c}$$

$$e + He(1s, n\ell\,{}^{1,3}L) \rightarrow e + He(1s, m\ell'\,{}^{3,1}L) \quad m \geq n \geq 2 \tag{7d}$$

$$e + He(1s, n\ell\,{}^{1,3}L) \rightarrow e + He^+(\Sigma m) + e \quad n \geq 2 \tag{7e}$$

For the cross-sections of dipole transitions (reactions (7a), (7c)) the semi-empirical formula of Seaton, with the Gaunt factor given in Ref. [14], has been used in the calculations. The cross-section for the process (7a) is fitted to the experimental data [15] for $n = 2, 3$. The rate coefficients for non-dipole and spin-changing transitions are described by the approximations of Ref. [16], based on the normalized Born cross-sections. The cross-section of reaction (7e) is estimated by the Lotz formula [13].

3.3. Collisions of helium with impurities

For the estimation of the impurity impact excitation (de-excitation) and ionization cross-sections of helium (reactions similar to (5a), (5b), (5d)), we have used the scaling relation (see Refs [17, 18])

$$\sigma_Z(E/m) = Z\,\sigma_p(E/Z/m) \tag{8}$$

where σ_p is the cross-section for the corresponding proton impact process. The cross-section for charge exchange from the excited state is described by relation (6).

All inverse, de-excitation processes have been calculated from the direct ones by using the detailed balance principle. The rate coefficients ($I, K = \langle \sigma v \rangle$) in Eq. (1) have been calculated on the assumption of a Maxwellian velocity distribution of plasma particles and taking into account the beam velocity in the case of ion collisions.

The electron loss cross-section for the helium ground state in a pure hydrogen plasma is obtained from the experimental data presented in Ref. [12] and by using the Lotz formula, fitted to the experimental data [19].

The ionization cross-section for the helium ground state by impurity ion impact is estimated from the scaling relation (8), but the charge exchange cross-section is estimated from the scaling suggested in Ref. [17].

4. RESULTS AND DISCUSSION

4.1. Major atomic processes

The enhancement of the helium stopping cross-section due to multistep collisions, $\delta_s = \sigma_{ad}/\sigma_s^0$, is presented in Fig. 2.

Despite the large number of atomic processes included in the calculations, only a limited number of them determine the value of the effect considered. According to

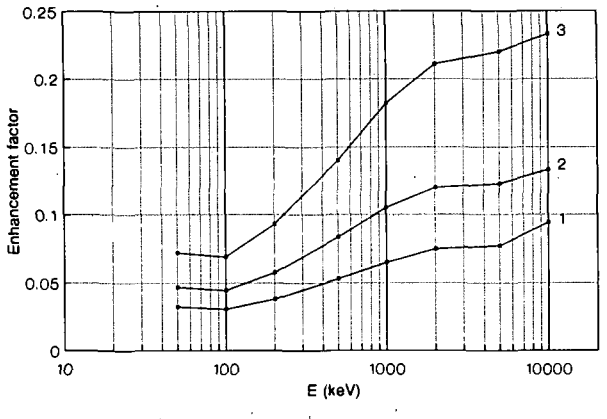

FIG. 2. Energy dependence of the factor δ_s for three values of plasma density: 1 — $n_e = 10^{13}$ cm^{-3}, 2 — $n_e = 10^{14}$ cm^{-3}, 3 — $n_e = 10^{15}$ cm^{-3} (T = 10 keV, B = 5 T, He:C:O:Fe = 5.0:1.5:0.5:0.05).

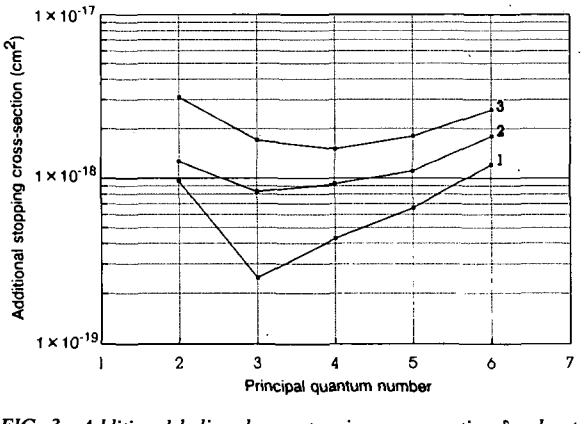

FIG. 3. Additional helium beam stopping cross-section δ_{ad} due to electron loss from excited beam atoms versus the principal quantum number, for three values of plasma density: 1 — $n_e = 10^{13}$ cm^{-3}, 2 — $n_e = 10^{14}$ cm^{-3}, 3 — $n_e = 10^{15}$ cm^{-3} (E = 200 keV, Z_{eff} = 1, T = 10 keV, B = 5 T).

TABLE I. SENSITIVITY OF δ_s TO COLLISION PROCESSES*

Process	k_i	Δ_i
Excitation by protons		
(1) $1s^2\ ^1S \rightleftharpoons 1snp\ ^1P$		
n = 2	0.06	20%
n = 3	0.15	
n = 4	0.1	
(2) $1s^2\ ^1S \rightarrow 1s2s\ ^1S$	0.05	30%
(3) $n \rightleftharpoons m$, $n,m \geq 2$		
All transitions	0.08	factor of two
$2 \rightleftharpoons 3$	0.02	
$3 \rightleftharpoons 4$	0.03	
Excitation by electrons		
(4) $1s^2\ ^1S \rightleftharpoons 1snp\ ^1P$		
n = 2	0.02	10%
n = 3	0.06	
Excitation by protons and electrons		
(5) $n \rightarrow m$, $m > n_L$		
(a) All transitions for n = 1	0.3	30%
(b) All transitions for $n \geq 4$	0.04	factor of two
Excitation by impurity ions		
(6) $1s^2\ ^1S \rightleftharpoons 1sn\ell\ ^1L$	0.05	40%
Ionization by protons and electrons		
(7) All excited states	0.1	30%
Ionization by impurity ions		
(8) All excited states	0.05	40%

* Data valid at $E \geq 50$ Z, keV/u, $n_e \approx 10^{14}$ cm^{-3}, $Z_{eff} = 2$; Δ_i is the existing uncertainty of the experimental data on the cross-sections or the accuracy of the approximations used; k_i is the relative change of δ_s resulting from doubling the rate coefficients of the corresponding processes.

Fig. 1, at a plasma temperature of T ≈ 10 keV the singlet states determine nearly 90% of δ_s. This allows us to restrict our analysis of the contributions of individual processes to δ_s only to collisions within the singlet spin system. This analysis shows that the major contribution to δ_s is due to the electron loss from highly excited states with $n \geq 4$. According to Fig. 3, this contribution amounts to 60–80%, depending on the

plasma density. Since the probability for an electron to be lost from the highly excited state is close to unity, δ_s is weakly sensitive to the corresponding electron loss mechanism, namely to particle impact ionization, charge exchange and particle impact excitation from these states to the levels which are subject to Lorentz field ionization. On the other hand, δ_s turns out to be most sensitive to the collisions determining the population of highly excited states and, in the first place, to the excitation from the ground state to the low lying excited states ($n \leq 4$) through which the highly excited states are populated.

The sensitivity of δ_s to the relevant atomic processes has been determined quantitatively by varying the rate coefficients in the equations of the radiative collisional model and in Eq. (1). The relative changes (k_i) of δ_s resulting from doubling the rate coefficients of various processes are given in Table I. This table shows that δ_s is more sensitive to the dipole allowed transitions from the ground state than to the forbidden transition $1s^2 \rightarrow 1s2s\ ^1S$ which determines the metastable state population. Further, δ_s is more sensitive to the $1s^2 \rightarrow 1s3p\ ^1P$, $1s4p\ ^1P$ transitions than to $1s^2 \rightarrow 1s2p\ ^1P$ because of the short radiative lifetime of this state. The factor δ_s is also very sensitive to the excitation from the ground state to the levels with $n > 5$, which may be directly ionized by the Lorentz field.

It should be emphasized that because of the importance of highly excited states in the enhanced beam stopping it is necessary to include a large number of states in the calculations. Our calculations have shown that convergence of the results can be reached only when all the states with $n \leq 12$ are included.

4.2. Contribution of metastable states

The 2^1S state has an extremely high population in the plasma (about 40% of the total excited state population at $n_e \approx 10^{14}$ cm^{-3}). However, its contribution to σ_{ad} is not so high ($\approx 10\%$) (Fig. 4). The reason for this is a very strong dependence of the electron loss cross-section on the principal quantum number of the excited state (for direct ionization, $\sigma_s^n \sim n^2$, but for highly excited states, $\sigma_s^n \sim n^3$, due to the Lorentz field ionization). On the other hand, the role of the 2^1S state as a 'donor' of electrons for highly excited states is nearly the same as that of the 2^1P state because of the closeness of their populations at $n_e \approx 10^{14}$ cm^{-3} (Fig. 5).

Figure 5 shows that the population of the 2^3S metastable state is much smaller than that of 2^1S and decreases when the plasma density increases. Such

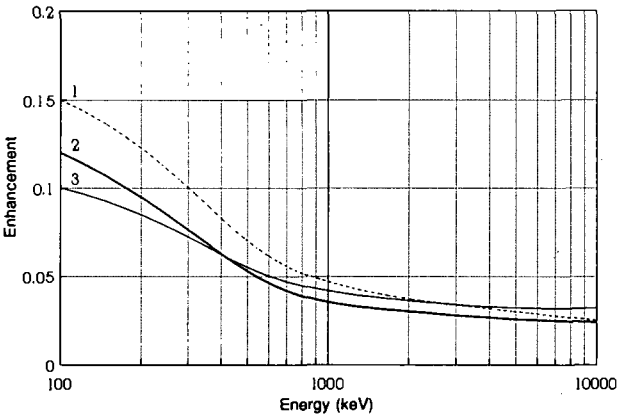

FIG. 4. Contribution of the $2\ ^1S$ state to σ_{ad} as a function of beam energy for three values of plasma density: 1 — $n_e = 10^{13}$ cm^{-3}, 2 — $n_e = 10^{14}$ cm^{-3}, 3 — $n_e = 10^{15}$ cm^{-3} ($Z_{eff} = 1$, $T = 10$ keV, $B = 5$ T).

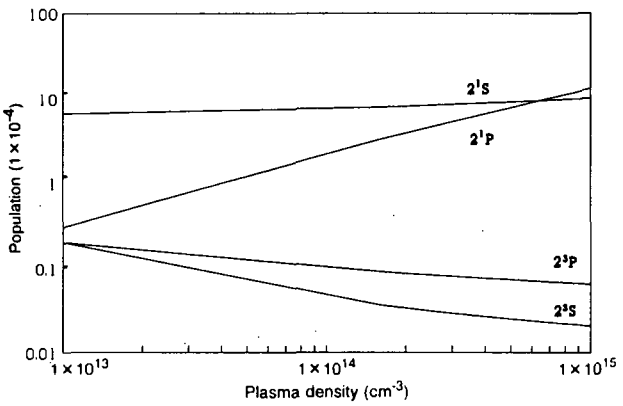

FIG. 5. Relative population of the excited helium states with $n = 2$ versus plasma density ($E = 200$ keV, $Z_{eff} = 1$, $T = 10$ keV, $B = 5$ T).

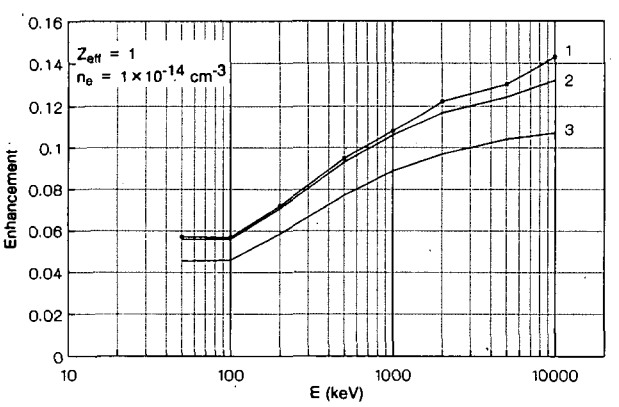

FIG. 6. Energy dependence of δ_s for various values of the principal quantum number (n_L) determining the Lorentz field ionization limit: 1 — for n_L calculated by Eq. (9), 2 — for n_L increased by one, 3 — without Lorentz ionization ($T = 10$ keV, $B = 5$ T).

behaviour can be explained if one takes into account that the 2^3S state is populated mostly by radiative transitions from higher excited states whose population is nearly independent of the plasma density, but the decay rate of the 2^3S state is proportional to n_e (at $n_e \leq 10^{14}$ cm^{-3}).

4.3. Sensitivity of δ_s to Lorentz field ionization

The sensitivity of δ_s to Lorentz field ionization has been tested by variation of the principal quantum number (n_L) determining the field ionization limit [5]:

$$n_L = 17.2/(E^{0.125} B^{0.25}) \quad (9)$$

where E is in units of keV/u and B is in tesla.

According to Fig. 6, δ_s is weakly sensitive to this process. The reason for this is that even without Lorentz ionization, the probability for an electron to be lost from the highly excited state is close to unity.

5. CONCLUDING REMARKS

The above analysis shows that the enhancement of the neutral helium beam in a plasma is mainly due to the excitation of helium atoms to highly excited states ($n \geq 4$) by multistep collisions through the low lying singlet states followed by the inevitable electron loss. The contribution of triplet states to δ_s is small, despite the additional spin state mixing caused by the energy degeneration of multiplet states due to the motional Stark effect. The contribution of metastable states (mainly the 2^1S state) to δ_s is about 10%. Therefore, the major atomic processes involved in helium beam stopping in a plasma are: dipole allowed transitions from the ground state to 2^1P, 3^1P, 4^1P states, and transitions from these states to the highly excited states. Direct excitation from the ground state to the levels lying above the Lorentz ionization limit is also important.

According to the present calculations, the enhancement of the helium beam stopping cross-section due to multistep collision processes is about four times smaller than that for a hydrogen beam at the same velocity [2]. The reasons for this are the smaller values of the cross-sections for excitation from the helium ground state and the larger radiative decay probabilities. Nevertheless, the multistep collision processes become important for helium beam stopping in plasmas with an integrated line density $n_e a > 10^{16}$ cm^{-2} as expected for the next generation tokamaks (ITER, BPX) and for reactor level devices. The most serious requirement on the accuracy of δ_s ($\approx 20\%$) arises in the analysis of neutralized alpha particle fluxes [4]. The atomic physics database used in the present calculations cannot fulfil this requirement. The conclusions from the data presented in Table I are as follows:

(1) More accurate cross-sections for helium excitation from the ground state to states with $n > 5$ by proton impact are required, particularly for $E \leq 100$ keV/u, where the n^{-3} scaling is not justified;
(2) The accuracy of the DACC theory for proton impact induced transitions between excited singlet states has to be critically assessed, since it is the only available theory which allows these processes to be included in the multilevel numerical calculations;
(3) A higher (20%) accuracy is required for the cross-sections for ionization by proton impact from the states with $n = 2, 3$, because this is the dominant electron loss process for these states;
(4) The relevance of two-electron transition processes, including inner-shell processes of excited helium atoms, should be more closely investigated and included in the computational scheme, if necessary.

The conclusion drawn in the present study regarding the role of metastable states is related to the equilibrium population of the excited states. The real situation may differ from this case if the initial helium beam in the injector has a considerable fraction of metastable states (especially 2^3S). In this case, a non-stationary radiative collisional model must be used in the beam attenuation calculations.

Direct measurement of the effect of helium beam stopping enhancement in experiments on beam attenuation in a plasma is very complicated because of the insufficient line plasma density of present day tokamaks [20]. It is, therefore, more reasonable to test the calculated excited state populations by spectroscopic methods. Improvement of the computer code using spectroscopic data on helium beam emission in a plasma seems to be a proper way to attain the required accuracy of the beam stopping cross-section.

Appendix

In order to derive the cross-section for a collision induced transition or the probability of a radiative transition between the multiplet states on the basis of available experimental data or theoretical calculations for the $n\ell \rightarrow n'\ell'$ transition, we sum the corresponding

quantities over the expansion coefficients of the final state and average them over the expansion coefficients of the initial state. For example, for the process (5a) we have

$$\sigma_{1k} = \sum_{\ell} \frac{\sigma(1s^1\,{}^1S \rightarrow 1s, n\ell\,{}^1L)}{2(2\ell+1)} B_{n\ell} \sum_{jm} |C^k_{n\ell jm}|^2$$

where $B_{n\ell} = 1 - \beta_{n\ell}$ for transitions within the singlet system and $B_{n\ell} = \beta_{n\ell}$ for transitions to states of the triplet system, with $\beta_{n\ell} = b^2_{n\ell} = b^2_{n\ell}$ (see Eq. (4)).

The oscillator strength for a dipole allowed transition is expressed in terms of the radiative transition probability A_{km} ($k > m$):

$$f_{k'k} = 3.11 \times 10^{-11} A_{kk'}/(\Delta E_{k'k})^2$$

(ΔE in atomic units)

$$A_{kk'} = (\Delta E_{k'k})^3 \sum_{\ell,\ell'} \frac{2\ell+1}{\ell_{max}} B^{n'\ell'}_{n\ell} \sum_{\substack{jm \\ j'm'}} (D^{kk'})^{n'\ell'j'm'}_{n\ell jm}$$

$$(D^{kk'})^{n'\ell'j'm'}_{n\ell jm} = |C^k_{n\ell jm}\, C^{k'}_{n'\ell'j'm'}|^2\, (\chi^{j'm'}_{jm})^2$$

where $\chi^{j'm'}_{jm}$ is the angular part of the hydrogenic dipole matrix element [21], and $n\ell jm$ correspond to the upper state. For transitions within one spin system,

$$B^{n'\ell'}_{n\ell} = (1 - \alpha_1\beta_{n\ell})(1 - \alpha_1\beta_{n'\ell'})\, A_1 + \alpha_2^2 \beta_{n\ell}\beta_{n'\ell'} A_2$$

while for transitions between states of different spin systems,

$$B^{n'\ell'}_{n\ell} = (1 - \alpha_1\beta_{n\ell})\,\alpha_1\beta_{n'\ell'} A_1 + \alpha_2\beta_{n\ell}(1 - \alpha_2\beta_{n'\ell'}) A_2$$

$$A_{1,2} = A_{1,2}(1s, n\ell;\ 1s, n'\ell')/(\Delta E^0_{1,2})^3$$

where $A_1(1s, n\ell;\ 1s, n'\ell')$ and ΔE^0_1 are respectively the probability and the energy of the dipole radiative transition ($n\ell \rightarrow n'\ell'$) between the states of the spin system considered for field-free atoms without spin state mixing; $A_2(1s, n\ell;\ 1s, n'\ell')$ and ΔE^0_2 have the same meaning, but for other spin systems; $\alpha_i = 1$ if A_i corresponds to the singlet system and $\alpha_i = 1/3$ if A_i corresponds to the triplet system ($i = 1, 2$). For $n = n'$ ($n \leq 5$, $n' \leq 3$) and $n = n'$ ($n \leq 3$) we have used the tabulated values for $A(1s, n\ell;\ 1s, n'\ell')$ of Ref. [21]. For the other transitions we have used the hydrogenic values, taking into account the change of the energies ΔE^0.

ACKNOWLEDGEMENTS

The author is grateful to Drs. A.I. Kislyakov and M.P. Petrov for continuous support and to M.S. Samsonov for assistance with mathematical programs. The author also wishes to thank Dr. H.P. Summers for useful remarks. Special thanks are due to Dr. R.K. Janev for detailed critical analysis of the work.

REFERENCES

[1] ITER Concept Definition, Vol. 2, IAEA, Vienna (1989) 35.
[2] JANEV, R.K., BOLEY, C.D., POST, D.E., Nucl. Fusion **29** (1989) 2125.
[3] MARCUS, F.B., ADAMS, J.M., BARTLETT, D.V., et al., in Controlled Fusion and Plasma Physics (Proc. 18th Eur. Conf. Berlin, 1991), Vol. 15C, Part I, European Physical Society (1991) 45.
[4] AFANASIEV, V.I., IZVOZCHIKOV, A.B., KISLYAKOV, A.I., et al., Ion Component Diagnostics on ITER by Means of Atomic Beams, Internal Letter, ITER-IL-PH-7-0-26, Max-Planck-Institut für Plasmaphysik, Garching (1990).
[5] KOROTKOV, A.A., SAMSONOV, M.S., Light Atom Beam Stopping Cross Sections in Fusion Plasmas due to Effective Charge and Electron Loss through Excited States, Preprint 1351, Ioffe Institute, Leningrad (1989).
[6] MOORE, Ch.E., Atomic Energy Levels, Rep. NSRDS-NBS35, Vol. 1, National Bureau of Standards, Washington, DC (1991).
[7] BETHE, H.G., SALPETER, E.E., Quantum Mechanics of One- and Two-Electron Atoms, Springer Verlag, Berlin (1957).
[8] SPENCE, J., SUMMERS, H.P., J. Phys., B **19** (1986) 3749.
[9] de HEER, F.J., HOEKSTRA, R., SUMMERS, H.P., this issue, p. 47.
[10] JANEV, R.K., PRESNYAKOV, L.P., J. Phys., B **13** (1980) 4233.
[11] RYUFUKU, H., WATANABE, T., Phys. Rev., A **20** (1979) 1828.
[12] RUDD, M.E., DuBOIS, R.D., TOBUREN, L.H., et al., Phys. Rev., A **28** (1983) 3244.
[13] LOTZ, W., Z. Physik **232** (1970) 101.
[14] GITKOV, A.G., MARCHENKO, V.S., YAKOVENKO, S.I., Radiative Losses for Typical Impurities in Fusion Plasmas during Neutral Beam Injection, Preprint 3278/6, I.V. Kurchatov Institute of Atomic Energy, Moscow (1980) (in Russian).
[15] WESTERVELD, W.B., HEIDEMAN, H.G.M., VAN ECK, J., J. Phys., B **12** (1979) 115.
[16] ABRAMOV, V.A., VAINSHTEIN, L.A., KROTOVA, G.I., PIGAROV, A.Y., Recommended Atomic Data for Hydrogen and Helium Plasmas, Rep. INDC (CCP)-286/GA, IAEA, Vienna (1988).
[17] JANEV, R.K., HVELPLUND, P., Comments. At. Mol. Phys. **11** (1981) 75.
[18] ANTON, M., DETLEFFSEN, D., SCHARTNER, K.-H., this issue, p. 51.

[19] NAGY, P., SKUTLARTZ, A., SCHMIDT, V., J. Phys., B **13** (1980) 1249.

[20] TOBITA, K., ITOH, T., SAKASAI, A., et al., Plasma Phys. Control. Fusion **32** (1990) 429.

[21] SOBEL'MAN, I.I., Atomic Spectra and Radiative Transitions, Springer Verlag, Berlin (1979).

RECOMMENDED DATA FOR ELECTRON IMPACT EXCITATION OF Be^{q+} AND B^{q+} IONS

K.A. BERRINGTON
Department of Applied Mathematics and Theoretical Physics,
Queen's University of Belfast,
Belfast, United Kingdom

R.E.H. CLARK*
Los Alamos National Laboratory,
Los Alamos, New Mexico,
United States of America

ABSTRACT. A report on electron impact excitation data for ionized beryllium and boron is given. Collision strengths from new R-matrix and distorted wave calculations for these ions are presented as graphs, showing the effect of resonances at low energies. At higher energies, the collision strengths from the distorted wave calculation are fitted to simple functions of energy for each transition, and these fits are tabulated for excitation from the ground state to the n = 2 and n = 3 excited states in each ion.

1. INTRODUCTION

Collisional data for beryllium and boron atoms and ions have recently attracted attention because of the use of these elements as plasma facing materials in fusion plasma experiments. These data were the subject of a recent Consultants' Meeting of the International Atomic Energy Agency, summarized by Janev (1991) [1].

This paper concentrates on electron impact excitation of Be and B atoms and ions. There are few experimental data on these processes, and even the theoretically calculated data are somewhat limited; in some cases, data are only available as isoelectronic interpolations or as Born approximations. In the course of the present review it was realized that new calculations were needed in order to make sound recommendations. Two sets of calculations were made: an R-matrix calculation giving a detailed description of the low energy behaviour of the cross-section, including resonances structures, and a distorted wave calculation extending the energy range to the higher temperatures found in plasmas. Details of these calculations can be obtained from Berrington (1991) [2] and Clark (1991) [3].

Section 2 summarizes the excitation data for each ionization stage of B and Be, arranged in isoelectronic sequences, for transitions from the ground state to excited states with principal quantum numbers n = 2 and 3. The new R-matrix and distorted wave calculations are presented in figures and tables in Section 2 and discussed further in Section 3.

2. ELECTRON EXCITATION DATA FOR EACH IONIZATION STAGE OF B AND Be

Each isoelectronic sequence is treated separately in the following subsections. A summary of the existing data is given, followed by a presentation of the new R-matrix and distorted wave calculations.

In the R-matrix calculations, target states with $n \leq 4$ were included in the scattering wave function for the H, He and Li isoelectronic ions and for Be I; $n \leq 3$ for B I and B II. Channel coupling, resonances and electron exchange are explicitly included. These calculations should be highly accurate at low energies. However, since the cross-section typically varies rapidly with energy owing to the presence of resonances in this energy region, it is not practical to tabulate the cross-section as a function of energy in this paper; the R-matrix results are therefore presented only graphically.

The distorted wave method is less elaborate than the R-matrix calculation and is computationally easier to extend to higher energies. Here, the cross-section varies smoothly with energy, and it is convenient to fit the dimensionless collision strength for each transition as a function of electron impact energy in threshold units

* The work at Los Alamos was performed under the auspices of the United States Department of Energy.

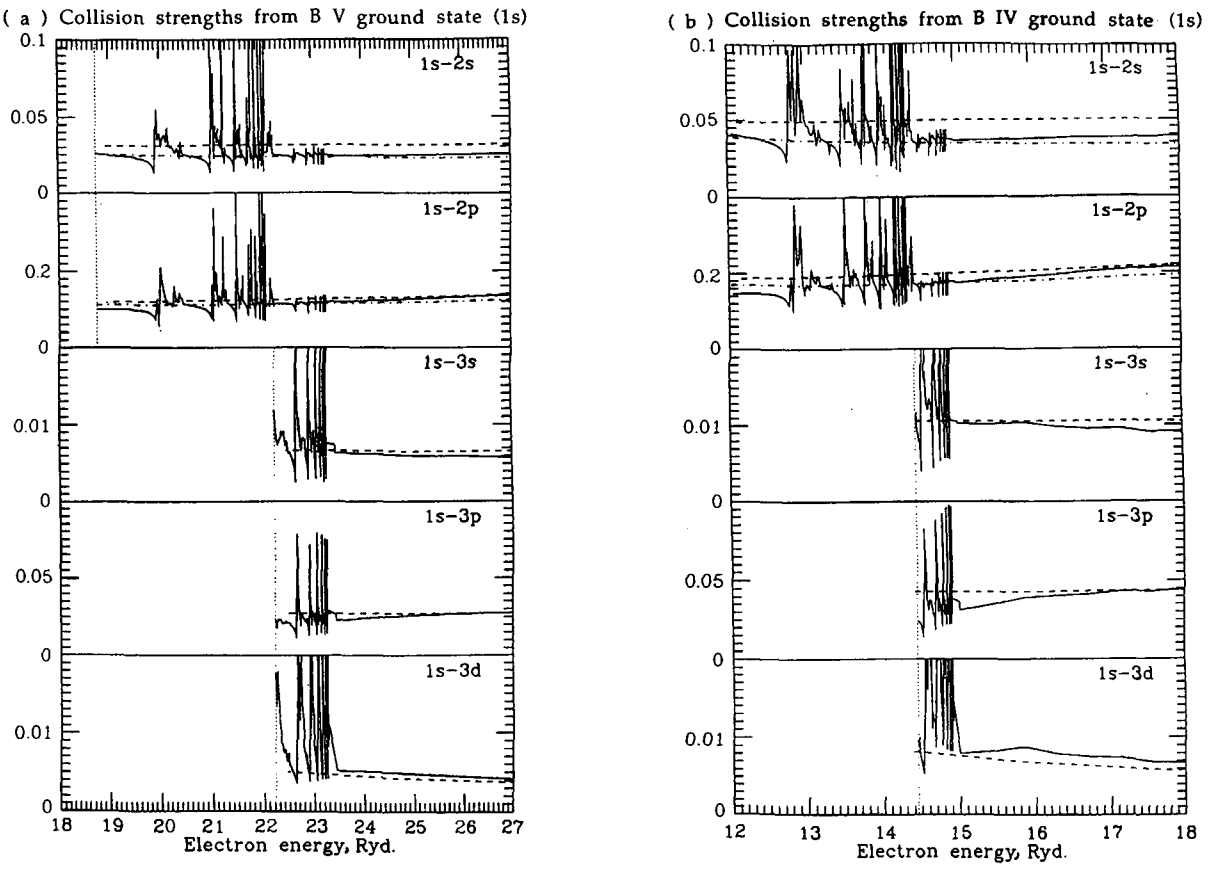

FIG. 1. Collision strength at low electron impact energies for H-like B V (a) and Be IV (b) from the $1s^2S$ ground state to n = 2 and n = 3 states. —— R-matrix calculation of Berrington (1991) [2]; --- distorted wave calculation of Clark (1991) [3]; -·-·- interpolation formula of Callaway (1983) [4]. The vertical dotted line indicates the threshold energy.

TABLE I. ELECTRON IMPACT EXCITATION OF H-LIKE B V AND Be IV, INITIALLY IN THE $1s^2S$ GROUND STATE*

Final state	ΔE (Ryd)	Eq.	c_1	c_2	c_3	c_4	d
B V							
2s	18.75	(2)	3.5472×10^{-2}	-1.3462×10^{-2}	1.7578×10^{-2}	-1.1211×10^{-2}	0.4
2p	18.75	(1)	1.8701×10^{-1}	-1.1167×10^{-2}	8.8277×10^{-2}	-1.1496×10^{-2}	-0.5
3s	22.22	(2)	7.0341×10^{-3}	-2.2149×10^{-3}	-6.9848×10^{-3}	3.3224×10^{-2}	2.2
3p	22.22	(1)	2.9989×10^{-2}	7.7586×10^{-3}	9.1920×10^{-3}	-1.0019×10^{-3}	-0.7
3d	22.22	(2)	5.4840×10^{-3}	-7.3865×10^{-3}	-8.8475×10^{-4}	1.1088×10^{-2}	0.2
Be IV							
2s	12.00	(2)	5.5410×10^{-2}	-1.9679×10^{-2}	2.7694×10^{-2}	-1.7670×10^{-2}	0.3
2p	12.00	(1)	2.9169×10^{-1}	-1.5513×10^{-2}	1.2366×10^{-1}	-1.7218×10^{-2}	-0.6
3s	14.22	(2)	1.1002×10^{-2}	-3.8931×10^{-3}	7.2631×10^{-3}	-3.7649×10^{-3}	0.2
3p	14.22	(1)	4.6823×10^{-2}	1.2072×10^{-2}	1.4784×10^{-2}	-1.6191×10^{-3}	-0.7
3d	14.22	(2)	8.5752×10^{-3}	-1.1344×10^{-2}	-2.3511×10^{-3}	1.8862×10^{-2}	0.2

* Fit parameters in Eqs (1-3) for collision strengths based on distorted wave calculations, for impact energies to 100 × threshold (ΔE Ryd).

($x = k_i^2/\Delta E$, where k_i^2 is the incident electron energy and ΔE is the threshold energy; Rydberg units for energy are used in this paper). Three different forms of fit are used, depending on the high energy behaviour of the collision strength:

$$\Omega_{if} = c_1 \ln(x) + c_2 + c_3/(x+d) + c_4/(x+d)^2 \quad (1)$$

$$\Omega_{if} = c_1 + c_2/(x+d) + c_3/(x+d)^2 + c_4/(x+d)^3 \quad (2)$$

$$\Omega_{if} = c_1/(x+d)^2 + c_2/(x+d)^3 + c_3/(x+d)^4 + c_4/(x+d)^5 \quad (3)$$

where Ω_{if} is the collision strength for a transition from the initial state i to the final state f; $c_1 \ldots c_4$ are obtained from a least squares fit procedure, and d is varied in steps of 0.1 from -0.9 to 3 to find the best fit. The distorted wave collision strength is fitted for x = 1.01–100, with an error generally less than 20% above x = 2.

If the cross-section is required, it may be determined from

$$\sigma(i \rightarrow f) = \Omega_{if} \frac{\pi a_0^2}{w_i k_i^2} \quad (4)$$

where w_i is the statistical weight of the initial state and a_0 is the Bohr radius.

2.1. H-like ions: Be IV and B V

For 1s → 2s and 1s → 2p the Callaway (1983) [4] formulas for the collision strength are recommended; these are fits to accurate close-coupling pseudo-state calculations for the isoelectronic sequence, though no explicit calculations were made for Be IV and B V. Resonances are not included in Callaway's formulas, but they may have only a small effect on the collision rate. The accuracy is judged to be 5%.

For more general n → n′ transitions, the Sampson and Zhang (1988) [5] formulas obtained from Coulomb–Born calculations were found by Clark (1990) [6] to agree with distorted wave results to 10% except at low energies where the uncertainty is up to 25%.

Figure 1 shows the behaviour of the low energy collision strength for B V and Be IV from the new R-matrix and distorted wave calculations (Berrington, 1991 [2], Clark, 1991 [3]), and from the interpolation formulas of Callaway (1983) [4]. The disagreements are of the order of 10% (greater for 1s → 2s), and represent the accuracy of the new calculations. Table I presents fits to the distorted wave collision strengths at higher energies, using Eqs (1-3).

2.2. He-like ions: Be III and B IV

For Be III, Pradhan et al. (1981) [7, 8] provide good low energy data by explicitly including resonances in a distorted wave calculation, and these data are recommended. There is some uncertainty regarding the high energy tail which they used to calculate their tabulated collision rates; distorted wave calculations of either Badnell (1985) [9] or Clark (1991) [3] can be used above four times the threshold energy.

There are no previous elaborate calculations for B IV at low energies (i.e. with resonances and channel coupling which can have significant effects on the collision rate). The new R-matrix calculation for B IV (Berrington, 1991 [2]) is therefore recommended, together with the new distorted wave cross-sections (Clark, 1991 [3]) at higher energies.

Figure 2 shows the behaviour of the low energy collision strength for B IV and Be III from the new calculations. Table II presents fits to the distorted wave collision strengths at higher energies, using Eqs (1-3).

2.3. Li-like ions: Be II and B III

For Be II, close coupling calculations by Mitroy and Norcross (1988) [10] and Parpia et al. (1986, 1987) [11, 12] represent attempts to calculate the 2s − 2p cross-section with high precision, and their data are recommended as the best ones available from theory. However, there is a persistent disagreement with the experiment of Taylor et al. (1980) [13].

There have been no elaborate calculations specifically for B III. Cochrane and McWhirter (1983) [14] presented easy to use $\bar{g}$ fits for the isoelectronic sequence based on close coupling calculations of the collision rates. These calculations generally ignored resonances, which can make significant contributions to the excitation cross-section of $n \geq 3$ states at low energies. The new R-matrix calculation is therefore recommended (Berrington, 1991 [2]), together with the new distorted wave calculation at high energies (Clark, 1991 [3]).

Figure 3 shows the behaviour of the low energy collision strength for B III and Be II from the new calculations, together with some sample points from the experimental measurement for Be II, showing the puzzling ~5–10% discrepancy. Table III presents fits to the distorted wave collision strengths at higher energies, using Eqs (1-3).

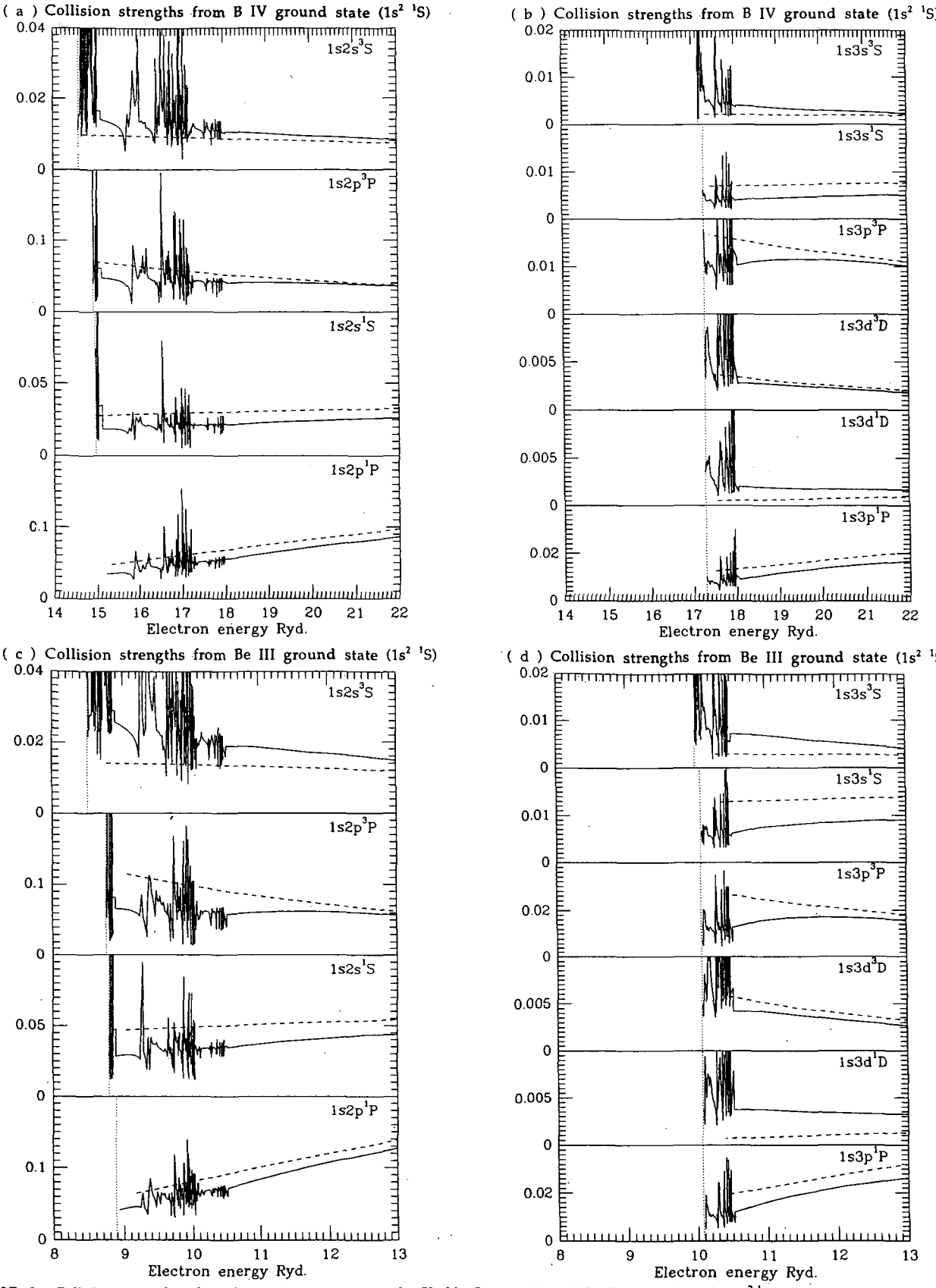

FIG. 2. Collision strength at low electron impact energies for He-like B IV (a, b) and Be III (c, d) from the $1s^2\,{}^1S$ ground state to n = 2 and n = 3 states. —— R-matrix calculation of Berrington (1991) [2]; --- distorted wave calculation of Clark (1991) [3]. The vertical dotted line indicates the threshold energy.

TABLE II. ELECTRON IMPACT EXCITATION OF He-LIKE B IV AND Be III, INITIALLY IN THE $1s^2\,{}^1S$ GROUND STATE*

Final state	ΔE (Ryd)	Eq.	c_1	c_2	c_3	c_4	d
B IV							
$1s2s\,{}^3S$	14.563	(3)	5.8727×10^{-2}	-4.9199×10^{-2}	4.2780×10^{-2}	-7.5930×10^{-2}	0.8
$1s2s\,{}^1S$	14.882	(2)	4.6147×10^{-2}	-2.0415×10^{-2}	-2.7955×10^{-2}	-4.1693×10^{-4}	0.9
$1s2p\,{}^3P$	14.886	(3)	5.3483×10^{-2}	6.3383×10^{-1}	-1.3753	9.8438	1.8
$1s2p\,{}^1P$	15.075	(1)	2.0123×10^{-1}	-1.8726×10^{-2}	4.9070×10^{-2}	1.7764×10^{-3}	-0.2
$1s3s\,{}^3S$	17.150	(3)	9.8930×10^{-3}	-8.4724×10^{-3}	5.6143×10^{-3}	-6.6947×10^{-3}	0.5
$1s3p\,{}^3P$	17.237	(3)	1.1209×10^{-2}	1.0960×10^{-1}	-2.0520×10^{-1}	1.3002	1.5
$1s3s\,{}^1S$	17.239	(2)	1.2252×10^{-2}	-1.1294×10^{-2}	7.7677×10^{-3}	-8.6367×10^{-3}	0.8
$1s3d\,{}^3D$	17.275	(2)	3.3524×10^{-6}	-3.4958×10^{-6}	7.6724×10^{-4}	3.2158×10^{-3}	0.0
$1s3d\,{}^1D$	17.276	(2)	4.8902×10^{-3}	-4.7826×10^{-3}	-9.3858×10^{-3}	1.0481×10^{-2}	0.4
$1s3p\,{}^1P$	17.292	(1)	4.4981×10^{-2}	-5.5536×10^{-3}	3.8828×10^{-2}	1.6431×10^{-2}	1.6
Be III							
$1s2s\,{}^3S$	8.6862	(3)	1.0256×10^{-1}	-6.2494×10^{-2}	2.9814×10^{-2}	-1.8705×10^{-1}	0.9
$1s2s\,{}^1S$	8.9214	(2)	7.7062×10^{-2}	-3.7116×10^{-2}	-4.6958×10^{-2}	4.6782×10^{-4}	1.0
$1s2p\,{}^3P$	8.9321	(3)	9.6372×10^{-2}	3.8681×10^{-1}	8.6681×10^{-1}	-3.1354×10^{-1}	1.0
$1s2p\,{}^1P$	9.0587	(1)	3.2037×10^{-1}	-4.1553×10^{-2}	7.5127×10^{-2}	-1.7864×10^{-3}	-0.3
$1s3s\,{}^3S$	10.208	(3)	1.6762×10^{-2}	-8.6117×10^{-3}	4.2874×10^{-3}	-2.4125×10^{-2}	0.7
$1s3p\,{}^3P$	10.274	(3)	1.9913×10^{-2}	7.2259×10^{-2}	1.0569×10^{-1}	-2.2079×10^{-2}	0.8
$1s3s\,{}^1S$	10.275	(2)	2.2344×10^{-2}	-2.6918×10^{-2}	2.9254×10^{-2}	-3.1527×10^{-2}	1.1
$1s3d\,{}^3D$	10.300	(2)	1.4736×10^{-6}	1.6500×10^{-6}	1.0110×10^{-3}	5.1732×10^{-3}	0.0
$1s3d\,{}^1D$	10.301	(2)	7.3003×10^{-3}	-5.8825×10^{-3}	-1.8145×10^{-2}	1.8798×10^{-2}	0.4
$1s3p\,{}^1P$	10.312	(1)	7.9051×10^{-2}	-2.4375×10^{-2}	1.1117×10^{-1}	4.9127×10^{-2}	2.0

* Fit parameters in Eqs (1-3) for collision strengths based on distorted wave calculations, for impact energies to 100 × threshold (ΔE Ryd).

2.4. Be-like ions: Be I and B II

For neutral beryllium the R-matrix calculation of Fon et al. (1922) [15] is recommended, together with the new distorted wave calculation (Clark, 1991 [3]) at high energies. Similarly, for B II the new R-matrix calculation (Berrington, 1991 [2]) is recommended, together with the new distorted wave calculation (Clark, 1991 [3]) at higher energies. It should be noted that this distorted wave calculation is probably less accurate for neutrals than for ions.

Figure 4 shows the behaviour of the low energy collision strength for B II and Be I for these calculations. Table IV presents fits to the distorted wave collision strengths at higher energies, using Eqs (1-3).

2.5. B-like ions: B I

The R-matrix calculation of Nakazaki and Berrington (1991) [16] is the only elaborate calculation at low energies, and the new distorted wave calculation (Clark, 1991 [3]) can be used at higher energies. The calculations differ by small or large (factors of two) amounts, depending on the transition. Given the disagreement with experiment (Kuchenev and Smirnov, 1981 [17]) by factors of three to five, the accuracy of the recommended data for neutral boron may be low.

Figure 5 shows the behaviour of the low energy collision strength of B I for these calculations. Table V presents fits to the distorted wave collision strengths at higher energies, using Eqs (1-3).

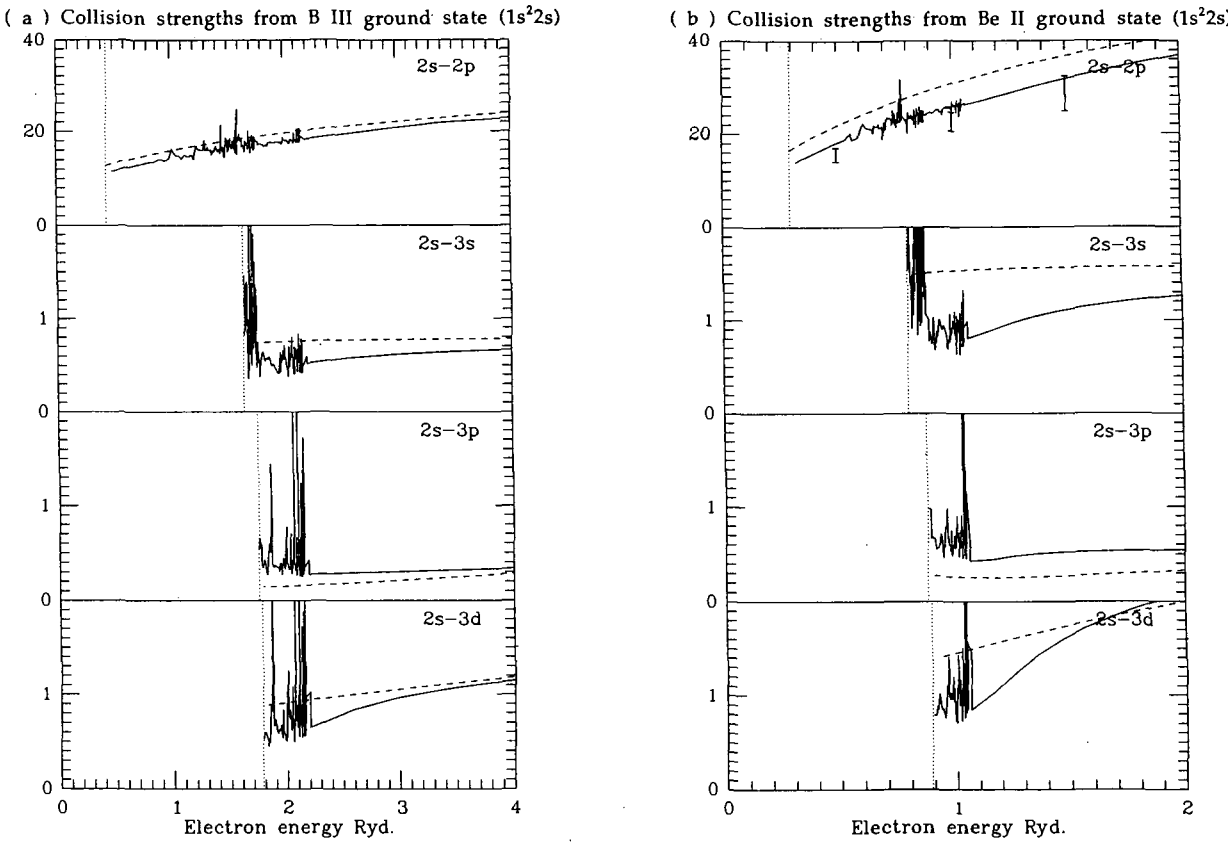

FIG. 3. Collision strength at low electron impact energies for Li-like B III (a) and Be II (b) from the $1s^2 2s\ ^2S$ ground state to n = 2 and n = 3 states. — R-matrix calculation of Berrington (1991) [2]; --- distorted wave calculation of Clark (1991) [3]; I, three sample points (with error bars) from the experiment of Taylor et al. (1980) [13]. The vertical dotted line indicates the threshold energy.

TABLE III. ELECTRON IMPACT EXCITATION OF Li-LIKE B III AND Be II, INITIALLY IN THE $1s^2 2s\ ^2S$ GROUND STATE

Final state	ΔE (Ryd)	Eq.	c_1	c_2	c_3	c_4	d
B III							
2p	0.4394	(1)	8.1593	4.6488	1.3259×10	-4.9607×10^{-1}	0.6
3s	1.6607	(2)	7.8867×10^{-1}	1.4986×10^{-1}	-6.4630×10^{-1}	-1.7578×10^{-1}	1.6
3p	1.7773	(1)	7.0194×10^{-1}	-7.9128×10^{-1}	1.3732	4.1912×10^{-2}	0.5
3d	1.8058	(2)	1.9674	-2.0828	-4.9508	9.2604	1.3
Be II							
2p	0.2908	(1)	1.6021×10	1.0650×10	-9.4842	4.8231×10	1.2
3s	0.8179	(2)	1.5483	2.0293×10^{-1}	-3.8016×10^{-1}	3.1506×10^{-2}	0.3
3p	0.8934	(1)	7.3977×10^{-1}	-8.5105×10^{-1}	1.4918	1.0411×10^{-1}	0.4
3d	0.9090	(2)	3.4170	-3.2721	-1.3238×10	2.2063×10	1.5

* Fit parameters in Eqs (1–3) for collision strengths based on distorted wave calculations, for impact energies to 100 × threshold (ΔE Ryd).

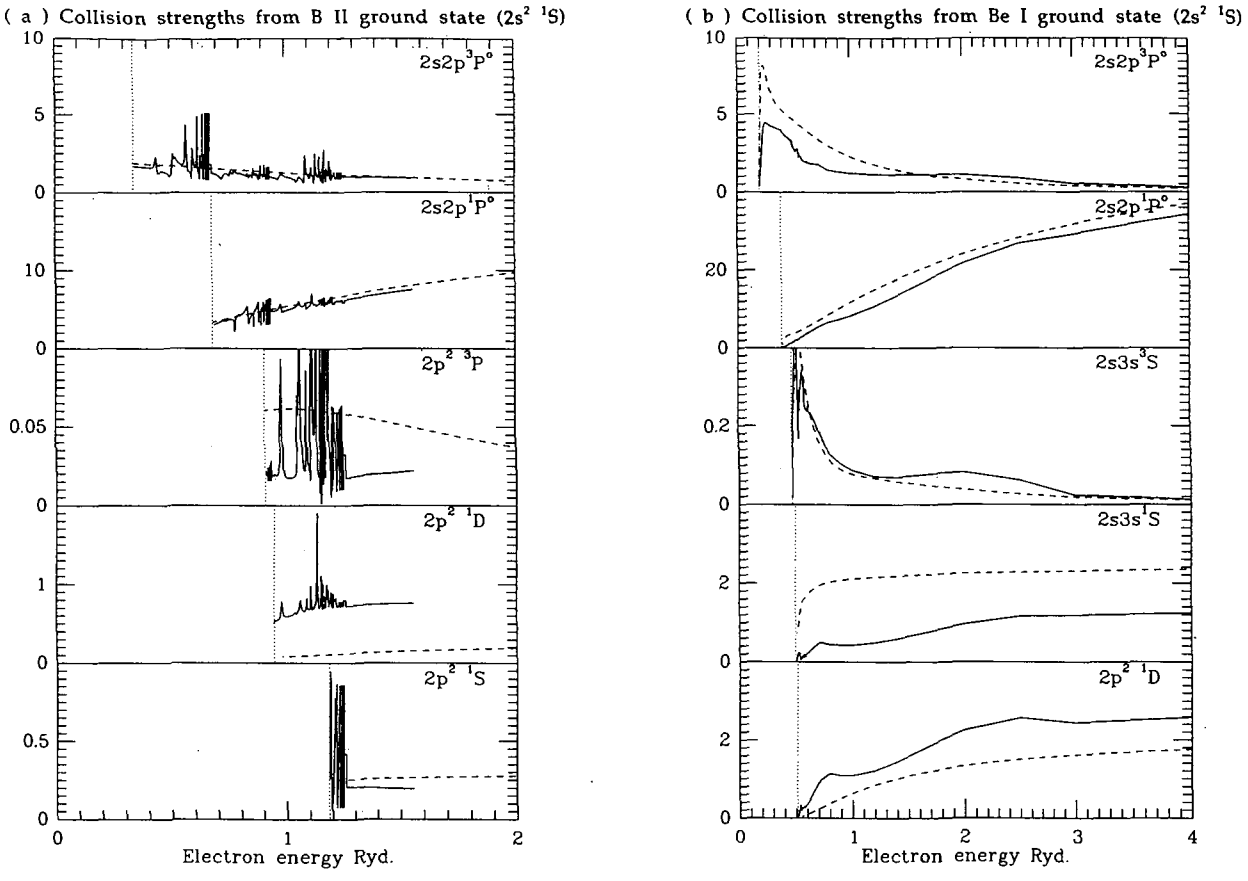

FIG. 4. Collision strength at low electron impact energies for Be-like B II (a) and Be I (b) from the $1s^2 2s^2\,{}^1S$ ground state to the five lowest excited states. — R-matrix calculations of Berrington (1991) [2] and of Fon et al. (1992) [15]; --- distorted wave calculation of Clark (1991) [3]. The vertical dotted line indicates the threshold energy.

3. DISCUSSION

The figures show that the new R-matrix and distorted wave calculations can differ significantly at low impact energies, with a tendency for better agreement at higher energies. This is because autoionizing resonances and channel coupling, important at low energies, are included in the R-matrix calculation but not in the distorted wave calculation; additionally, the target wave functions are different in the two calculations. In general, the R-matrix calculation should provide the most accurate data available, though in practice the energy range is limited by computer resources. At higher energies, the less computationally demanding distorted wave calculation should yield accurate cross-sections, which may be obtained from the fits presented here in the tables. At intermediate energies, near and above the ionization threshold, both calculations may have a systematic error due to the omission of coupling to the continuum. This error is difficult to quantify, given the lack of experiments and suitable theory, but is likely to be greater for neutral Be and B than for their ions.[1]

[1] Computer files of cross-sections from the new calculations described here can be obtained from the authors, including details of the low energy resonance structure, data for more highly excited final states, and data for excitation from metastable and excited initial states.

TABLE IV. ELECTRON IMPACT EXCITATION OF Be-LIKE B II AND Be I, INITIALLY IN THE $1s^2 2s^2\ ^1S$ GROUND STATE*

Final state	ΔE (Ryd)	Eq.	c_1	c_2	c_3	c_4	d
B II							
$2s2p\ ^3P$	0.3349	(3)	7.7421×10	-3.5890×10	-1.6191×10^3	4.0815×10^3	3.0
$2s2p\ ^1P$	0.6760	(1)	6.8643	3.0258	-6.7660	1.5490×10	1.1
$2p^2\ ^3P$	0.9007	(3)	2.0646×10^{-3}	2.2601	-4.7606	2.4002	0.7
$2p^2\ ^1D$	0.9724	(2)	4.2518×10^{-1}	-3.1026×10^{-1}	-4.3714	2.9311	2.7
$2p^2\ ^1S$	1.1827	(2)	3.1998×10^{-1}	-9.0022×10^{-2}	2.8988×10^{-2}	-1.8010×10^{-1}	0.8
$2s3s\ ^3S$	1.1884	(3)	3.2277×10^{-1}	-4.9663×10^{-1}	2.7498×10^{-1}	-5.2171×10^{-2}	-0.3
$2s3s\ ^1S$	1.2631	(2)	7.6921×10^{-1}	-1.5518×10^{-1}	5.1145×10^{-2}	-8.2870×10^{-3}	-0.5
$2s3p\ ^3P$	1.3210	(3)	3.0684×10^{-1}	3.7237	-1.0202×10	8.9270×10	3.0
$2s3p\ ^1P$	1.3259	(1)	4.2424×10^{-1}	-4.9301×10^{-1}	7.1616×10^{-1}	3.1699×10^{-2}	0.4
$2s3d\ ^3D$	1.3811	(3)	1.2574×10^{-1}	1.4351×10	-1.2839×10^2	6.8394×10^2	3.0
$2s3d\ ^1D$	1.4247	(2)	1.3230	-1.7864	-6.5375×10^{-1}	1.2882	0.4
Be I							
$2s2p\ ^3P$	0.1930	(3)	1.1065×10^2	-3.5585×10^2	4.7227×10^2	-2.2698×10^2	0.0
$2s2p\ ^1P$	0.3890	(1)	1.9222×10	-9.0615	5.3705	-6.9732×10^{-1}	-0.8
$2s3s\ ^3S$	0.4784	(3)	8.9572×10^{-1}	-1.9274	1.6108	-4.3148×10^{-1}	-0.5
$2s3s\ ^1S$	0.5035	(2)	2.5406	-1.6804	2.3451	-1.2149	-0.4
$2p^2\ ^3P$	0.5393	(3)	1.4125×10^{-3}	1.6215	6.1904	-1.4025×10	0.9
$2s3p\ ^3P$	0.5423	(3)	7.6196×10^{-1}	5.6079×10^{-1}	-4.1751	3.4902	0.1
$2p^2\ ^1D$	0.5479	(2)	2.1956	-3.2808	-7.5291×10^{-2}	1.1805	0.1
$2s3p\ ^1P$	0.5585	(2)	2.2153	-6.2005	-3.8947	-7.2683×10^{-1}	3.0
$2s3d\ ^3D$	0.5714	(3)	8.0307×10^{-2}	1.2390×10	-1.1406×10^2	7.2571×10^2	3.0
$2s3d\ ^1D$	0.6175	(2)	2.3242×10^{-1}	-3.7998×10^{-1}	-2.1050×10^{-1}	9.0500×10^{-1}	0.2

* Fit parameters in Eqs (1-3) for collision strengths based on distorted wave calculations, for impact energies to 100 × threshold (ΔE Ryd).

TABLE V. ELECTRON IMPACT EXCITATION OF B-LIKE B I, INITIALLY IN THE $1s^2 2s^2 2p\ ^2P$ GROUND STATE*

Final state	ΔE (Ryd)	Eq.	c_1	c_2	c_3	c_4	d
B I							
$2s2p^2\ ^4P$	0.2542	(3)	2.6569×10^2	1.7484×10^3	-1.8657×10^4	3.8502×10^4	3.0
$2s^2 3s\ ^2S$	0.3610	(1)	5.0914	-2.1377	2.9169	-4.8593×10^{-1}	-0.8
$2s^2 3p\ ^2P$	0.4396	(2)	3.8322	1.1374	-1.5199	9.2315×10^{-1}	-0.6
$2s2p^2\ ^2D$	0.4546	(1)	7.3214	1.0544×10	-2.1932×10	2.2758×10	0.0
$2s^2 3d\ ^2D$	0.4964	(1)	1.4097×10	-2.8940	2.6487	-1.4584×10^{-1}	-0.9
$2s2p^2\ ^2S$	0.5587	(1)	5.5264	4.5967	-1.0361×10	7.1815	-0.3
$2s2p^2\ ^2P$	0.6548	(1)	2.6986×10	3.0837	-2.3908×10	2.1048×10	-0.2

* Fit parameters in Eqs (1-3) for collision strengths based on distorted wave calculations, for impact energies to 100 × threshold (ΔE Ryd).

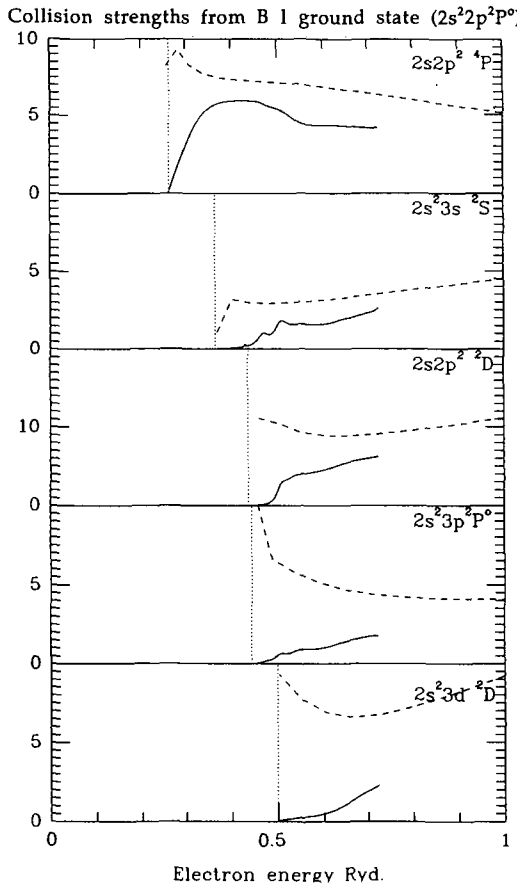

FIG. 5. Collision strength at low electron impact energies for B-like B I from the $1s^22s^22p^2P^0$ ground state to the five lowest excited states. — R-matrix calculation of Nakazaki and Berrington (1991) [16]; --- distorted wave calculation of Clark (1991) [3]. The vertical dotted line indicates the threshold energy.

REFERENCES

[1] INTERNATIONAL ATOMIC ENERGY AGENCY, Consultants' Meeting on Atomic Data Base for Be and B, 10–12 June 1991, INDC(NDS)-254 (JANEV, R.K., Ed.), IAEA, Vienna (1991).

[2] BERRINGTON, K.A., Computer files of data available from the Belfast Atomic Data Bank (1991); to be published.

[3] CLARK, R.E.H., Computer files of data available in the ALADDIN format of the IAEA, Rep. LA-UR-91-1932, Los Alamos National Laboratory, Los Alamos, NM (1991).

[4] CALLAWAY, J., Phys. Lett., A **96** (1983) 26.

[5] SAMPSON, D.H., ZHANG, H., Astrophys. J. **335** (1988) 516.

[6] CLARK, R.E.H., Astrophys. J. **354** (1990) 382.

[7] PRADHAN, A.K., NORCROSS, D.W., HUMMER, D.G., Astrophys. J. **246** (1981) 1031.

[8] PRADHAN, A.K., NORCROSS, D.W., HUMMER, D.G., Phys. Rev., A **23** (1981) 619.

[9] BADNELL, N.R., J. Phys., B **28** (1985) 955.

[10] MITROY, J., NORCROSS, D.W., Phys. Rev., A **37** (1988) 3755.

[11] PARPIA, F.A., NORCROSS, D.W., Da PAIXAO, F.J., Phys. Rev., A **34** (1986) 4777.

[12] PARPIA, F.A., NORCROSS, D.W., Da PAIXAO, F.J., Phys. Rev., A **36** (1987) 1510.

[13] TAYLOR, P.O., PHANEUF, R.A., DUNN, G.H., Phys. Rev., A **22** (1980) 435.

[14] COCHRANE, D.M., McWHIRTER, R.W.P., Phys. Scr. **28** (1983) 25.

[15] FON, W.C., BERRINGTON, K.A., BURKE, P.G., HIBBERT, A., J. Phys., B **25** (1992) 507.

[16] NAKAZAKI, S., BERRINGTON, K.A., J. Phys., B **24** (1991) 4263.

[17] KUCHENEV, A.N., SMIRNOV, Yu.M., Opt. Spektrosk. **51** (1981) 210.

ELECTRON IMPACT IONIZATION OF Be AND B ATOMS AND IONS

D.L. MOORES
Department of Physics and Astronomy,
University College London,
London,
United Kingdom

ABSTRACT. The best available data on electron impact ionization cross-sections of B and Be ions have been selected and are presented in simple parametric form. Tables of the fitting parameters are included.

1. INTRODUCTION

Data on cross-sections for ionization of atomic systems by electron impact can be derived from three principal sources: semi-empirical methods and formulas, ab initio theory and experimental measurements. In the first category we have the Seaton formula [1] (which is only valid near threshold), the exchange classical impact parameter method [2], the infinite-z scaling method of Golden and Sampson (applicable to highly charged ions) [3], the formula of Percival [4] (for hydrogenic ions), and the formulas of Lotz [5] (probably the most widely used) and of Burgess and Chidichimo [6] (including an estimate of the excitation-autoionization contribution).

Ab initio theoretical methods include the Coulomb-Born and the distorted wave methods with exchange, which are the most elaborate and become increasingly accurate with increasing charge on the ion, as well as the Born and Bethe-Born approximations (which should be valid at very high impact energies, provided accurate target wave functions have been used), and a range of classical [7] and semi-classical methods.

For complex ions it may be necessary to include not just inner-shell processes but also contributions from indirect processes such as excitation-autoionization and resonant excitation-double autoionization.

It should be pointed out that no reliable theoretical method capable of yielding accurate data for ions of low charge at low energies has been developed.

On the experimental side, the crossed beam technique is capable of producing accurate results. Methods based on plasma spectroscopy measure rate coefficients rather than cross-sections, but in many cases they yield data of uncertain precision. For very highly charged systems, electron beam ion trap methods are beginning to be used.

Estimates of unknown cross-sections can be obtained by making use of the fact that for a given isoelectronic sequence the reduced cross-section

$$Q_R(X) = I^2 Q(X) \tag{1}$$

(where I is the ionization energy, Q(X) is the ionization cross-section in cm^2, and X is the incident energy divided by I) varies slowly as a function of Z. This technique is referred to as scaling.

The high energy behaviour of the cross-section can be fixed by making use of the fact that, for large X,

$$XQ(X) = A \ln X + B \tag{2}$$

where

$$A = 4 \int_I^\infty \frac{df}{d\epsilon} \frac{d\epsilon}{\epsilon} \tag{3}$$

with $df/d\epsilon$ being the differential dipole continuum oscillator strength of the ion, and B is independent of X.

In this report, the cross-sections have been parametrized either in the form

$$XQ(X) = A \ln X + \frac{C_0}{X} \ln X + \sum_{i=1}^{N} C_i \left(1 - \frac{1}{X}\right)^i \tag{4}$$

or in the form

$$XQ(X) = A \ln X + \sum_{i=0}^{N} \frac{\alpha_i}{X^i} \tag{5}$$

where C_i and α_i are constants with no special physical interpretation, merely having the role of fitting parameters. We now discuss the recommended data for each isoelectronic sequence in turn.

TABLE I. PARAMETERS OF Eq. (4) FOR ELECTRON IMPACT IONIZATION OF Be^{q+} AND B^{q+} IONS

Species	I (eV)	A	C_0	C_1	C_2	C_3	C_4	C_5	Remarks*	Accuracy
Be V	340.22	1.5275-19	—	2.1678-19	-4.9163-19	2.2145-18	-2.8808-18	1.6432-18		12%
Be IV	217.71	3.7027-19	—	4.9003-19	-1.0595-18	4.8960-18	-6.2381-18	3.6395-18		12%
B IV	259.37	6.8418-19	—	-9.7357-20	4.0760-20	5.7328-18	-8.4384-18	4.9724-18		12%
Be III	153.89	1.9435-18	—	-2.7656-19	1.1579-19	1.6285-17	-2.3971-17	1.4125-17		12%
B III	37.93	8.4971-18	—	9.6681-18	1.5560-17	-1.0150-17	-2.1487-17	5.3676-17		30%
Be II	18.21	3.3039-17	—	9.0589-17	-8.8416-17	3.4311-16	-4.1859-16	2.6885-16		30%
B II	25.15	3.9682-17	-3.0639-16	3.6726-16	-1.1683-16				(a)	30%
	20.53	4.2350-17	-2.7128-16	3.5826-16	-1.1887-17				(b)	40%
	26.52	1.9621-17	-1.2940-16	1.5677-16	-5.1186-17				(c)	40%
Be I	9.32	2.8896-16	-2.2311-15	2.6743-15	-8.5077-16				(a)	30%
	6.60	4.0978-16	-2.6249-15	3.4665-15	-1.1501-15				(b)	40%
	13.28	7.8250-17	-5.1599-16	6.2520-16	-2.0413-16				(c)	40%

* (a) $2s^2\,{}^1S \rightarrow 2s\,{}^2S$; (b) $2s2p\,{}^3P \rightarrow 2s\,{}^2S$; (c) $2s2p\,{}^3P \rightarrow 2p\,{}^2P$.

2. RECOMMENDED IONIZATION CROSS-SECTIONS

H-like ions B V and Be IV

Bell et al. [8] recommended results based on a scaling of Younger's [9] distorted wave exchange calculations for C VI. The scaled curve agreed well with Younger's calculation for Ne X. The formulas of Lotz [5], Golden and Sampson [3] and Percival [4] gave results roughly 10% higher. New calculations [10] using a relativistic distorted wave method (relativistic effects were in fact negligible) were carried out specifically for B V and Be IV. Similar calculations for Ne X were in close agreement with those by Younger.

These calculations for $X \leq 5$ were merged with the Born calculation of Peach [11] above $X = 150$ and fitted to Eq. (4), and these results provide the recommended data. The parameters are given in Table I. The accuracy of these cross-sections should be better than 12%.

For ionization from states other than the ground state the formulas of Golden and Sampson [3] should be used.

He-like ions Be III, B IV

For ground state ionization of B IV, Bell et al. [8] point out the good agreement between a crossed beam experiment, distorted wave exchange calculations and a semi-empirical formula. We recommend a cross-section based on these data for $X \leq 5$, merged with Peach's calculation [11] above $X = 150$. Be III data are to be obtained by scaling the B IV data using Eq. (1). Parameters obtained from fitting to Eq. (4) are given in Table I; the estimated accuracy is 12%.

For the ionization out of metastable states $1s2s\,{}^{1,3}S$, Coulomb-Born exchange calculations have been performed by Attaourti et al. [12] for the isoelectronic C, N, O ions. Their results for O differ by 25% from the results of a calculation by Moores and Tully [13] using the code COBION [14].

The results shown in Table II have been obtained by scaling the C V results of Attaourti et al. [12] and merging with the Burgess and Chidichimo [6] formula above $X = 150$. The estimated accuracy is 30%.

Li-like ions Be II and Be III

Falk and Dunn [15] have carried out a crossed beam measurement for Be II. Their fit, which includes 1s ejection and a small excitation-autoionization contribution, fails to match the Born approximation, however at very high energy.

Instead, we recommend the calculations of Younger [16] at low energies merged with those of Peach [11] above $X = 150$. The combined inner-shell and excitation-autoionization contributions are less than the estimated 30% accuracy. A similar procedure was employed for B III. The parameters of the fits are given in Table I.

TABLE II. PARAMETERS OF Eq. (4) FOR ELECTRON IMPACT IONIZATION FROM METASTABLE STATES $2\,^1S$, $2\,^3S$ OF He-LIKE IONS

Species	State	I (eV)	A	C_0	C_1	C_2	Accuracy
B IV	$2\,^1S$	56.4	1.4870-17	3.0520-17	-3.1517-17	1.4244-17	30%
Be III	$2\,^1S$	32.0	4.6194-17	9.4808-17	9.7908-17	4.4244-17	30%
B IV	$2\,^3S$	60.8	9.7412-18	-1.6292-17	1.4620-17	-1.2500-17	30%
Be III	$2\,^3S$	35.3	2.8908-17	-4.8347-17	4.3384-17	-3.7093-17	30%

TABLE III. PARAMETERS OF Eq. (5) FOR ELECTRON IMPACT IONIZATION OF B I

Species	I (eV)	A	α_0	α_1	α_2	α_3	α_4	α_5	Remarks*	Accuracy
B I	8.30	4.2820-16	1.1049-15	-2.6816-15	8.3591-16	3.4155-15	4.1763-15	1.5015-16	(a)	Factor of two
	12.93	3.4867-16	1.3375-16	6.7887-16	-8.4807-16	-9.3416-16	2.5971-15	-1.3600-15	(b)	Factor of two
	17.40	6.4165-17	2.4614-17	1.0032-16	-1.5607-16	-1.7191-16	4.7795-16	-2.5028-16	(c)	Factor of two

* (a) $2s^22p\,^2P \rightarrow 2s^2\,^1S$; (b) $2s^22p\,^2P \rightarrow 2s2p\,^3P$; (c) $2s^22p\,^2P \rightarrow 2s2p\,^1P$.

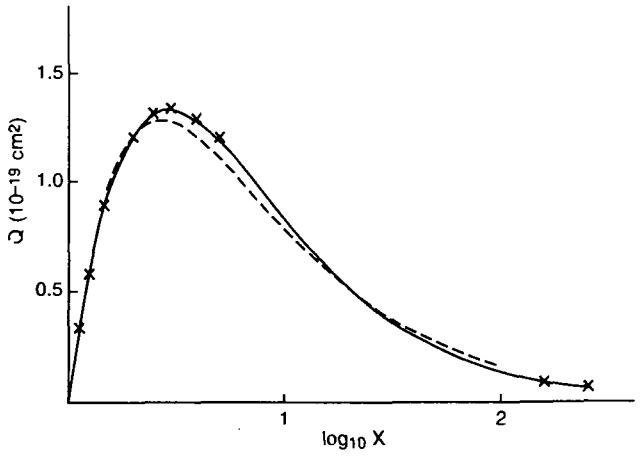

FIG. 1. Electron impact ionization cross-sections for B V versus log X. The full line is the recommended cross-section of the present evaluation (Eq. (4) and Table I); the dashed line represents the cross-section earlier recommended by Bell et al. [8], and the crosses are the cross-section values used in the fitting.

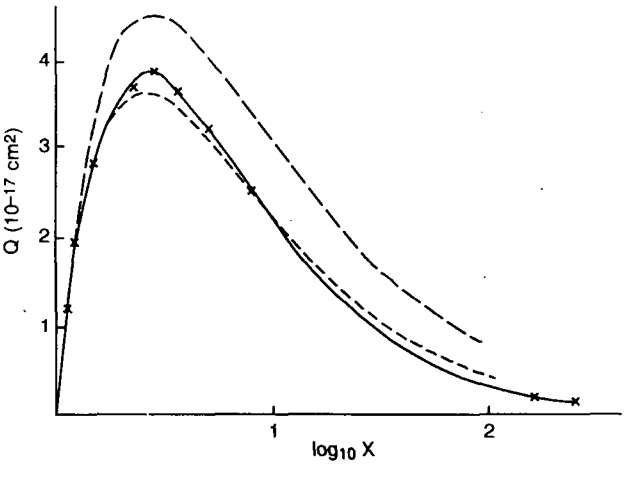

FIG. 2. Electron impact ionization cross-sections for Be II versus log X. The long-dashed curve represents the data of Falk and Dunn [15].

Be-like ions Be I and B II

The formulas given by Younger [17] for more highly charged Be-like ions cannot be extrapolated below Z = 6. However, reasonable results can be obtained by scaling Younger's C III results. This applies equally to ionization from the $2s^2$ and $2s2p\,^3P$ states. Parameters obtained by fitting to Eq. (4) are shown in Table I. The accuracy is 30–40%.

Neutral B

This cross-section is the least well known. For lack of anything better, we recommend a result obtained by scaling the C II calculation of Moores [18]. Parameters obtained from a fit to Eq. (5) are given in Table III for ejection of 2s and 2p electrons. The cross-sections may be regarded as being only accurate to within about a factor of two.

Figures 1 and 2 show the recommended cross-sections for B V and Be II, respectively, resulting from the present data assessment study. They are compared with the earlier recommendations of Bell et al. [8].

REFERENCES

[1] SEATON, M.J., Planet. Space Sci. **12** (1964) 55.
[2] BURGESS, A., in Proc. Symp. Atomic Collisions in Plasmas, Rep. 4818, UKAEA, Culham (1964) 63.
[3] GOLDEN, L.A., SAMPSON, D.G., J. Phys., B. **10** (1977) 2229; **13** (1981) 385.
[4] PERCIVAL, I.C., Nucl. Fusion **6** (1966) 182.
[5] LOTZ, W., Astrophys. J., Suppl. Ser. **14** (1967) 207; Z. Phys. **216** (1968) 241.
[6] BURGESS, A., CHIDICHIMO, M.C., Mon. Not. R. Astron. Soc. **203** (1983) 1269.
[7] McGUIRE, E.J., Phys. Rev., A **3** (1971) 267.
[8] BELL, K., GILBODY, H.B., HUGHES, J.G., Atomic and Molecular Data for Fusion, Part I, UKAEA Rep. CLM-R216, HMSO, London (1982).
[9] YOUNGER, S.M., Phys. Rev., A **22** (1980) 1425.
[10] MOORES, D.L., Presented at IAEA Consultants Meeting on Atomic Database for Be and B, June 1991, Rep. INDC(NDS)-254, compiled by R.K. JANEV (1991).
[11] PEACH, G., Presented at IAEA Consultants Meeting on Atomic Database for Be and B, June 1991, Rep. INDC(NDS)-254, compiled by R.K. JANEV (1991).
[12] ATTAOURTI, Y., MAKHOUTE, A., DEFRANCE, P., Phys. Scr. **43** (1991) 578.
[13] MOORES, D.L., TULLY, J. (Observatoire de la Côte d'Azur, Nice), personal communication, 1987.
[14] JAKUBOWICZ, H., MOORES, D.L., J. Phys., B **14** (1981) 3733.
[15] FALK, R.A., DUNN, G.H., Phys. Rev., A **27** (1983) 754.
[16] YOUNGER, S.M., Phys. Rev., A **22** (1980) 111.
[17] YOUNGER, S.M., Phys. Rev., A **24** (1981) 1278.
[18] MOORES, D.L., J. Phys., B **5** (1972) 286.

DIELECTRONIC RECOMBINATION RATE COEFFICIENTS FOR IONS OF THE Be AND B ISONUCLEAR SEQUENCES

M.S. PINDZOLA, N.R. BADNELL
Department of Physics,
Auburn University,
Auburn, Alabama
United States of America

ABSTRACT. Dielectronic recombination rate coefficients for all ions of the Be and B isonuclear sequences are calculated in the zero density limit using a multiconfiguration, intermediate coupling approximation for atomic structures.

The appearance of low-Z metals in current tokamak fusion experiments has prompted the IAEA to extend its atomic database to cover these materials. In this paper we calculate dielectronic recombination (DR) rate coefficients for all atomic ions of the beryllium and boron isonuclear sequences. The zero density rates generated here need to be incorporated into the solution of the collisional-dielectronic population rate equations [1] from which level populations, ionization balance and power loss can be determined for a finite density plasma.

The energy averaged dielectronic recombination cross-section for a given initial state i through an intermediate state j is given by

$$\bar{\sigma}_d(i \rightarrow j) = \frac{(2\pi a_0 I)^2}{E_c \Delta E_c} \cdot \frac{\omega(j)}{2\omega(i)} \times \frac{\tau_0 \sum_k A_r(j \rightarrow k) \sum_\ell A_a(j \rightarrow i, E_c \ell)}{\sum_h \left[A_r(j \rightarrow h) + \sum_\ell A_a(j \rightarrow h, E_c \ell) \right]} \quad (1)$$

where E_c is the energy of the continuum, which is fixed by the position of the resonances, I is the ionization potential of hydrogen and ΔE_c is the bin width. $\omega(j)$ is the statistical weight of the (N + 1) electron doubly excited state, $\omega(i)$ is the statistical weight of the N-electron target ion, and $(2\pi a_0)^2 \tau_0 = 2.6741 \times 10^{-32}$ cm^2·s. The dielectronic recombination rate coefficient can be written in terms of the energy averaged cross-section as

$$\alpha_d(i) = \left[\frac{4\pi a_0^2 I}{k_B T} \right]^{3/2} \frac{1}{(2\pi a_0 I)^2 \tau_0} \times \sum_j E_c \Delta E_c \bar{\sigma}_d(i \rightarrow j) \exp(-E_c / k_B T) \quad (2)$$

where $(4\pi a_0^2)^{3/2} = 6.6011 \times 10^{-24}$ cm^3. Many-body perturbation theory is used to evaluate both the radiative (A_r) and the autoionization (A_a) rates for the many intermediate levels j in the energy range of interest. The atomic structure computer code SUPERSTRUCTURE [2], based on Thomas-Fermi-Dirac-Amaldi (TFDA) wave functions, was extensively modified to calculate multiconfiguration, intermediate coupling autoionization rates. The resulting computer code AUTOSTRUCTURE [3, 4] calculates multiconfiguration, intermediate coupled DR cross-sections, Eq. (1), and rate coefficients, Eq. (2), for low n explicitly and for high n by extrapolating radial wave functions using quantum defect theory.

For dielectronic recombination in B^+, we consider the following reaction pathways ($1s^2$ core):

$$(2s^2 + 2p^2)\,{}^1S_0 + k\ell_c \rightarrow 2s2p({}^3P_{2,1,0}, {}^1P_1)n\ell \quad (3)$$

$$2s2p({}^3P_{2,1,0}, {}^1P_1)n\ell \rightarrow \begin{cases} (2s^2 + 2p^2)\,{}^1S_0 n\ell + \hbar\omega \\ (2s^2 + 2p^2)\,{}^1S_0 + k\ell_c \\ 2s2p({}^3P_{2,1,0}, {}^1P_1) + k'\ell_c' \end{cases} \quad (4)$$

where we sum the above processes up to n = 1000 and ℓ = 12. The DR rate coefficients for B^+ from 10^4 K to 10^8 K are given in Table II.

For dielectronic recombination in Be^+ and B^{2+}, we consider the following reaction pathways ($1s^2$ core):

$$2s\,{}^2S_{1/2} + k\ell_c \rightarrow 2p({}^2P_{3/2,1/2})n\ell \quad (5)$$

$$2p({}^2P_{3/2,1/2})n\ell \rightarrow \begin{cases} 2s\,{}^2S_{1/2} n\ell + \hbar\omega \\ 2s\,{}^2S_{1/2} + k\ell_c \\ 2p({}^2P_{3/2,1/2}) + k'\ell_c' \end{cases} \quad (6)$$

where we sum the above processes up to n = 1000 and ℓ = 12. The DR rate coefficients for Be^+ and B^{2+}

TABLE I. Be DIELECTRONIC RECOMBINATION RATE COEFFICIENTS

$\log_{10}$ [T(K)]	Be^+ α (10^{-11} cm^3/s)	Be^{2+} α (10^{-11} cm^3/s)	Be^{3+} α (10^{-11} cm^3/s)
4.0	0.62872		
4.1	1.15464		
4.2	1.74627		
4.3	2.26130		
4.4	2.58738		
4.5	2.68276		
4.6	2.57202		
4.7	2.31695		
4.8	1.98634		
4.9	1.63721		
5.0	1.30790		
5.1	1.01920		
5.2	0.77871		
5.3	0.58570	0.00184	0.00125
5.4	0.43508	0.00531	0.00574
5.5	0.32002	0.01151	0.01811
5.6	0.23354	0.01987	0.04222
5.7	0.16937	0.02858	0.07727
5.8	0.12222	0.03556	0.11649
5.9	0.08785	0.03942	0.15046
6.0	0.06295	0.03986	0.17182
6.1	0.04500	0.03746	0.17789
6.2	0.03210	0.03321	0.17035
6.3	0.02286	0.02812	0.15332
6.4	0.01626	0.02295	0.13136
6.5	0.01156	0.01819	0.10821
6.6	0.00821	0.01408	0.08641
6.7	0.00582	0.01071	0.06732
6.8	0.00413	0.00802	0.05142
6.9	0.00293	0.00594	0.03867
7.0	0.00208	0.00436	0.02872
7.1	0.00147	0.00317	0.02112
7.2	0.00104	0.00230	0.01541
7.3		0.00166	0.01118
7.4		0.00119	0.00807
7.5			0.00580
7.6			0.00415
7.7			0.00297
7.8			0.00212
7.9			0.00151
8.0			0.00107

from 10^4 K to 10^8 K are given in Tables I and II, respectively.

For dielectronic recombination in Be^{2+} and B^{3+}, we consider the following reaction pathways:

$$1s^2\,{}^1S_0 + k\ell_c \rightarrow 1s2\bar{\ell}({}^3S_1, {}^1S_0, {}^3P_{2,1,0}, {}^1P_1)n\ell \tag{7}$$

$$\begin{aligned} 1s2\bar{\ell}({}^3S_1, {}^1S_0, {}^3P_{2,1,0}, {}^1P_1)n\ell \rightarrow\ & 1s^2\,{}^1S_0 2\bar{\ell} + \hbar\omega \\ \searrow\ & 1s^2\,{}^1S_0 n\ell + \hbar\omega \\ \searrow\ & 1s^2\,{}^1S_0 + k\ell_c \\ \searrow\ & 1s2\bar{\ell}({}^3S_1, {}^1S_0, {}^3P_{2,1,0}, {}^1P_1) \\ & + k'\ell'_c \end{aligned} \tag{8}$$

where we sum the above processes up to n = 100 and ℓ = 5. The DR rate coefficients for Be^{2+} and B^{3+} from 10^4 K to 10^8 K are given in Tables I and II, respectively. For B^{3+}, the peak DR rate coefficient (at 1.6×10^6 K) calculated by Chen [5] is about 8% lower than the value given in Table II.

For dielectronic recombination in Be^{3+} and B^{4+}, we consider the following reaction pathways:

$$1s^2S_{1/2} + k\ell_c \rightarrow 2\bar{\ell}({}^2S_{1/2}, {}^2P_{3/2,1/2})n\ell \tag{9}$$

$$\begin{aligned} 2\bar{\ell}({}^2S_{1/2}, {}^2P_{3/2,1/2})n\ell \rightarrow\ & 1s^2S_{1/2}2\bar{\ell} + \hbar\omega \\ \searrow\ & 1s^2S_{1/2}n\ell + \hbar\omega \\ \searrow\ & 1s^2S_{1/2} + k\ell_c \\ \searrow\ & 2\bar{\ell}\,{}^2S_{1/2}, {}^2P_{3/2,1/2} + k'\ell'_c \end{aligned} \tag{10}$$

where we sum the above processes up to n = 100 and ℓ = 5. The DR rate coefficients for Be^{3+} and B^{4+} from 10^4 K to 10^8 K are given in Tables I and II, respectively.

In conclusion, we have generated zero density DR rate coefficients for all atomic ions of the Be and B isonuclear sequences. The rates generated here are the first step in the solution of the collisional-dielectronic population rate equations for a finite density plasma. The overall accuracy of the DR rates is judged to be about 20%, because of approximations in the atomic structure and the neglect of contributions from higher excitations.

ACKNOWLEDGEMENTS

This work was supported by the United States Department of Energy, Office of Fusion Energy, under Contract No. DE-FG05-86ER53217 with Auburn University.

TABLE II. B DIELECTRONIC RECOMBINATION RATE COEFFICIENTS

$\log_{10}$ [T(K)]	B^+ α (10^{-11} cm^3/s)	B^{2+} α (10^{-11} cm^3/s)	B^{3+} α (10^{-11} cm^3/s)	B^{4+} α (10^{-11} cm^3/s)
4.0	0.00171	0.22968		
4.1	0.01272	0.56034		
4.2	0.05879	1.16283		
4.3	0.18535	1.98648		
4.4	0.43052	2.85670		
4.5	0.78384	3.56351		
4.6	1.17568	3.96259		
4.7	1.51149	4.01867		
4.8	1.71906	3.78663		
4.9	1.77367	3.36497		
5.0	1.69369	2.85402		
5.1	1.52082	2.33252		
5.2	1.30046	1.85090		
5.3	1.06968	1.43469		
5.4	0.85312	1.09155		
5.5	0.66394	0.81827	0.00353	0.00152
5.6	0.50674	0.60624	0.01061	0.00652
5.7	0.38083	0.44497	0.02387	0.01959
5.8	0.28271	0.32418	0.04247	0.04411
5.9	0.20783	0.23479	0.06266	0.07863
6.0	0.15160	0.16926	0.07959	0.11620
6.1	0.10991	0.12156	0.08972	0.14781
6.2	0.07929	0.08705	0.09195	0.16680
6.3	0.05699	0.06219	0.08735	0.17110
6.4	0.04083	0.04434	0.07813	0.16267
6.5	0.02918	0.03157	0.06661	0.14558
6.6	0.02081	0.02245	0.05466	0.12416
6.7	0.01482	0.01595	0.04351	0.10192
6.8	0.01054	0.01133	0.03381	0.08116
6.9	0.00749	0.00804	0.02578	0.06309
7.0	0.00532	0.00570	0.01936	0.04811
7.1	0.00378	0.00404	0.01436	0.03613
7.2	0.00268	0.00286	0.01055	0.02680
7.3	0.00190	0.00203	0.00769	0.01969
7.4	0.00135	0.00144	0.00558	0.01436
7.5		0.00102	0.00402	0.01041
7.6			0.00289	0.00751
7.7			0.00207	0.00539
7.8			0.00148	0.00386
7.9			0.00105	0.00276
8.0				0.00197

REFERENCES

[1] BURGESS, A., SUMMERS, H.P., Astrophys. J. **157** (1969) 1007.

[2] EISSNER, W., JONES, M., NUSSBAUMER, N., Comput. Phys. Commun. **8** (1974) 270.

[3] BADNELL, N.R., J. Phys., B **19** (1986) 3827.

[4] BADNELL, N.R., PINDZOLA, M.S., Phys. Rev., A **39** (1989) 1685.

[5] CHEN, M.H., Phys. Rev., A **38** (1988) 6430.

STATUS AND CRITICAL ASSESSMENT OF THE DATABASE FOR COLLISIONS OF Be^{q+} AND B^{q+} IONS WITH H, H_2 AND He

R.A. PHANEUF
University of Nevada-Reno,
Reno, Nevada, United States of America

R.K. JANEV
International Atomic Energy Agency,
Vienna

H. TAWARA
National Institute for Fusion Science,
Nagoya University,
Nagoya, Japan

M. KIMURA
Argonne National Laboratory,
Argonne, Illinois, United States of America

P.S. KRSTIC
Institute of Physics,
Theoretical Physics Department,
Belgrade, Yugoslavia

G. PEACH
University College London,
London, United Kingdom

M.A. MAZING
P.N. Lebedev Physical Institute,
Moscow, Russia

ABSTRACT. The available cross-section database for charge exchange, excitation and ionization in collisions of Be^{q+} and B^{q+} ions with H, H_2 and He is critically reviewed. Reference to data sources containing cross-sections of high accuracy is given. The gaps in the database for these collisional systems have been identified, as well as the reactions for which the existing data information is of inadequate accuracy.

1. INTRODUCTION

From the perspective of applications in fusion energy research, the relevant heavy particle collision processes involving Be^{q+} and B^{q+} ions are charge exchange, excitation and ionization in collisions with H, H_2 and He. The collision energy range considered is 10 to 10^6 eV per nucleon. The lower energies are relevant to modelling and diagnostics of the edge or scrape-off plasma, while the higher energies are important for diagnostics and energy deposition in the plasma using energetic neutral beams of H or He. Collisions between Be and B impurity atoms and ions themselves are considered to occur too infrequently to play a significant role in such plasma devices. Heavy particle collisions are most often studied experimentally by passing energetic ion beams through gaseous targets. Therefore, in the following discussion, Be or B ions will be referred to as the projectile and H, H_2 or He as the target.

The available data information for charge exchange, excitation and ionization in collisions of Be^{q+} and B^{q+} ions with H, H_2 and He are summarized in Table I, where E refers to experimental data and T to theoretical data. For excitation and ionization collisions, the subscripts t and p refer to target and projectile, respectively. For electron capture collisions involving He or H_2, the subscripts 1 and 2 refer to the transfer of one or two electrons, respectively.

TABLE I. AVAILABILITY OF DATA FOR COLLISIONS OF Be^{q+} AND B^{q+} IONS WITH H, H_2 AND He

Target (t)	H					H_2					He				
Projectile (p)	TC	SSC	ANG	EX	ION	TC	SSC	ANG	EX	ION	TC	SSC	ANG	EX	ION
Be^+						E_1							T_1 E_1	T_p E_p	
Be^{2+}	T	T			T_t	T_1 E_1	T_1								T_t
Be^{3+}	T	T				E_1	T_1					T_1			
Be^{4+}	T	T		T_t	T_t	E_1	T_1				T_1			T_t	
B^+	E				E_p	E_1					E_1				
B^{2+}	E				E_p	E_1			E_p		E_1 E_2				
B^{3+}	T E	T				E_1 E_2	T_1				T_1 E_1 E_2	T_1 E_1			E_t
B^{4+}	T E					E_1 E_2					E_1				E_t
B^{5+}	T E	T	T_t	T_t	T_t	T_1 E_1					T_1 E_1 E_2				T_t E_t

TC — total electron capture (summed over final states)
SSC — state selective electron capture
ANG — data on angular distribution of products of electron capture collisions
EX — excitation of projectile (p) or target (t)
ION — ionization of projectile (p) or target (t)
E — experimental data
T — theoretical data
1,2 — single or double electron capture.

Semi-empirical scaling relationships for heavy particle collisions are often applied for higher-Z impurities. For example, a general formula for the charge exchange cross-section, derived in Ref. [1], may be used quite reliably for impurities such as Fe or Ni in ionization stages higher than 5. This general formula is, however, not applicable to low-Z impurities such as Be and B, for which each collision system must be considered individually. One exception is the ionization of H, H_2 or He by Be^{q+} or B^{q+} ions at energies above 20q keV/amu, where scaling formulas based on the Bethe approximation [2, 3] may be used with some reliability.

2. CHARGE EXCHANGE

Charge exchange (electron capture) collisions between impurity ions and neutral H, H_2 and He are by far the most important heavy particle processes occurring in fusion plasmas because of their relatively large cross-sections at lower kinetic energies. This results from the exothermicity of such reactions involving multiply charged ions. At near-thermal energies such as those prevailing in the edge plasma, cross-sections for charge exchange are very sensitive to the degree of exothermicity of a particular channel. The channels which have appreciable cross-sections

generally leave the ion in an excited state and are exothermic by several electron volts, depending on the initial charge of the ion. Photon emissions from excited impurity ions are important for plasma diagnostics involving the use of injected neutral beams of H or He.

The data for total and partial cross-sections for electron transfer collisions of Be^{q+} and B^{q+} ions with H, H_2 and He have been recently compiled by Tawara [4]. Extensive coupled state calculations have been recently carried out by Kimura [5] for Be^{q+} + H, Be^{q+} + H_2 (q = 2, 3, 4) and for B^{q+} + H, B^{q+} + H_2 (q = 3, 5). These calculations are based on a molecular orbital (MO) expansion (with appropriate electron translation factors) at low energies, in conjunction with the extended atomic orbital (AO+) method at higher energies. New calculations for Be^{4} + H and B^{5+} + H based on the 'adiabatic hidden crossings' or 'superpromotion' model have also been performed by Krstic et al. [6]. This method gives reliable partial cross-sections for capture into a particular n shell down to 0.3 keV/amu. An intercomparison of the various theoretical methods that have been applied to the electron capture process shows that the predicted cross-sections for capture into specific states are very sensitive to the method applied, whereas this sensitivity is much less pronounced for the total cross-sections.

2.1. Atomic hydrogen target

Be^{+} + H

Neither experimental nor theoretical cross-section data are available for the charge exchange processes in this collision system. Since these processes are endothermic in all channels, the corresponding cross-sections are expected to be very small for E < 1 keV/amu.

Be^{2+} + H

No experimental data are available. The theoretical perturbed stationary state (PSS) calculations of Wetmore et al. [7] agree within 10% with the new coupled state (AO-MO) calculations of Kimura [5], which include electron translation factors and a larger basis. The latter are recommended for the total cross-sections and for capture to the 2s and 2p states. Data are needed at energies above 10 keV/amu.

Be^{3+} + H

No experimental data are available for the charge exchange processes in this system. Molecular coupled state calculations employing electron translation factors have been performed by Shimakura [8] for capture to the 2s, 2p, 3s, 3p and 3d states, and for the total capture cross-section. The accuracy of the total cross-section is estimated to be 30–50% at energies above 25 keV/amu and 20–30% at lower energies. The n = 2 partial cross-sections (dominant channels) are estimated to be accurate to 20–30% and the n = 3 cross-sections to 30–50%.

Be^{4+} + H

No experimental charge exchange data are available for this collision system. Total and partial cross-section calculations have been performed by Fritsch and Lin [9] (AO) and by Kimura [5] (AO-MO). New low energy calculations are also available from Krstic et al. [6] based on the superpromotion model. In the energy range 0.1–5 keV/amu, all three calculations agree to within 5% for the total cross-section, as well as for state selective capture to the dominant (n = 3) channels. For the non-dominant (n = 4) channels, the agreement is less satisfactory. Unitarized distorted wave (UDWA) calculations of Ryufuku [10] are available at energies above 10 keV/amu. The accuracy of the total and n = 3 partial cross-sections is estimated to be 10% at energies in the range of 0.1–5 keV/amu and 20% at higher energies. The accuracy of the n = 4 and n = 5 cross-sections is estimated to be 20–50%. New low energy total and partial cross-section data for capture from H^{*} (n = 2) are available from the superpromotion model [6]. The accuracy of these data is unknown at the present time.

B^{+} + H

Experimental total cross-section measurements using the ion beam/gas target method have been made by Goffe et al. [11] at energies between 10 and 150 keV/amu. The estimated accuracy is 10–20%. Since all channels are endothermic, the cross-section is expected to decrease at lower energies. No state selective or theoretical data have been reported.

B^{2+} + H

Total cross-section measurements based on the ion beam/gas target method have been reported by Goffe et al. [11], McCullough et al. [12], Crandall [13] and Gardner et al. [14]. These data are consistent and cover the energy range from 2 to 200 keV/amu. The estimated accuracy is 10%, except at the lowest and

highest energies where it is 20%. No state selective or theoretical cross-section data are available for this system.

B^{3+} + H

Experimental total cross-section data have been obtained over the energy range 1–200 keV/amu using the ion beam/gas target method by Goffe et al. [11], McCullough et al. [12], Crandall [13] and Gardner et al. [14]. The molecular orbital coupled state calculations by Olson et al. [15] and Wetmore et al. [16] agree well with the experimental data and extend down in energy to 0.3 keV/amu. The uncertainty of the data is estimated to be 20–30% in the energy range 0.3–2 keV/amu and 10–15% in the range 2–200 keV/amu. Partial cross-sections have been calculated by Kimura [5] for capture to the 2s and 2p states, with the estimated accuracies comparable to those of the total cross-section for the 2p state, and somewhat larger for the 2s state.

B^{4+} + H

Experimental data based on the ion beam/gas target method are available for the total charge exchange cross-section at energies between 2 and 200 keV/amu from Goffe et al. [11], Crandall [13] and Gardner et al. [14]. The calculations by Olson and Salop [17], based on the classical trajectory Monte Carlo (CTMC) method in the energy range 10–150 keV/amu, are in agreement with the experimental data. The estimated accuracy of the total cross-section is 10–20%. No state selective or low energy total cross-section data are available.

B^{5+} + H

Both total and state selective cross-section data are available for the charge exchange reactions in this system. Experimental total cross-section data based on the ion beam/gas target method have been reported by Goffe et al. [11], Crandall [13] and Sherwin [18] in the energy range 0.2–200 keV/amu and are in good agreement with each other. The theoretical total cross-section data of Ryufuku [10] based on the UDWA approximation, those of Fritsch and Lin [9] based on the AO coupled states method and those of Krstic et al. [6] using the superpromotion model agree well with experiment. The accuracy of the total cross-section is estimated to be 10% for energies in the range 0.2–200 keV/amu. Total cross-section data are needed at energies below 200 eV/amu. In the energy ranges where they overlap, the partial cross-section calculations by Fritsch and Lin [9], Ryufuku [10] and Kimura [5] agree within the estimated accuracies of 10% for n = 4, 20% for n = 3 and 30% for n = 5. For the non-dominant channels (n = 2, 6, 7, 8), the cross-sections are small, and only the UDWA calculation of Ryufuku [10] at higher energies and the superpromotion model calculation of Krstic et al. [6] at lower energies are available. Since their energy ranges do not overlap, the uncertainty is difficult to assess for these channels. New total and partial cross-section calculations are also available from Krstic et al. [6] for capture from H^* (n = 2). The accuracy of these data is unknown at the present time.

2.2. Molecular hydrogen target

$Be^+ + H_2$

The only reported data are the single-capture measurements by Sherwin [18] in the energy range 1–3 keV/amu. Their accuracy is difficult to assess.

$Be^{2+} + H_2$, $Be^{3+} + H_2$, $Be^{4+} + H_2$

Experimental single-capture cross-section measurements of Ostgaard Olsen et al. [19], based on the ion beam/gas target method, are available in the energy range 0.1–1 keV/amu from Kimura [5], and partial cross-section calculations are in progress. The accuracy of the total cross-section data is estimated to be 20%. Additional data would be useful at energies above 10 keV/amu.

$B^+ + H_2$

The only available data are single-capture cross-section measurements reported by Goffe et al. [11] at energies between 10 and 150 keV/amu, for which the estimated accuracy is about 10–20%. Additional data are needed at lower energies.

$B^{2+} + H_2$

Experimental data based on the ion beam/gas target method are available for the total single-capture cross-sections at energies between 0.3 and 200 keV/amu from Goffe et al. [11], Crandall [13], McCullough et al. [12] and Gardner et al. [14]. The data of Gardner et al. appear to be too low by 50%. An estimated accuracy of 20–25% is assigned to the data for

this reaction. Since the cross-section is unusually large for a doubly charged ion and increases with decreasing energy, additional experimental and/or theoretical data are needed at lower energies.

$B^{3+} + H_2$

Total single-capture cross-section measurements have been reported by Goffe et al. [11], Crandall [13] and Gardner et al. [14] in the energy range 1–200 keV/amu. New theoretical data have been reported recently by Kimura [5] in the energy range 0.1–10 keV/amu, which agree well with the measurements. The accuracy of the data for this reaction is estimated to be 20%. Double-capture measurements have also been reported by Gardner et al. in the energy range 1–5 keV/amu. The double-capture cross-section is unusually large relative to the single-capture cross-section in this case.

$B^{4+} + H_2$

Total single-capture cross-section measurements have been reported by Goffe et al. [11], Crandall [13] and Gardner et al. [14] in the energy range 2–200 keV/amu. The accuracy of the data for this reaction is estimated to be 20%. Double-capture measurements have also been reported by Gardner et al. in the energy range 2–5 keV/amu. The double-capture cross-section is negligibly small relative to the single-capture cross-section in this case.

$B^{5+} + H_2$

Total single-capture cross-section measurements have been reported by Goffe et al. [11] and Crandall [13] in the energy range 5–200 keV/amu. New theoretical data have been reported recently by Kimura [5] in the energy range 0.1–10 keV/amu, which are consistent with these measurements. The accuracy of the data for this reaction is estimated to be 15–20%.

2.3. Helium target

$Be^{+} + He$

The only data for the charge exchange reactions in this collision system are the angular differential total cross-section measurements by Ostgaard Olsen et al. [19] in the energy range 200–500 keV/amu and by Gay et al. [20] at 56.25 keV/amu.

$Be^{2+} + He$

No experimental or theoretical cross-section data are available for the charge exchange reactions in this collision system.

$Be^{3+} + He$

Theoretical Landau–Zener calculations have been reported by Boyd and Moiseiwitsch [21] for capture into the $2\,^3S$, $2\,^3P$ and $2\,^1P$ states in the energy range 0.1–1000 eV/amu. The accuracy of these data is difficult to assess. No experimental data are available.

$Be^{4+} + He$

Only theoretical data are available for the charge exchange reactions in this collision system. Total single-capture cross-sections have been calculated by Olson [22] using the CTMC method, and by Suzuki et al. [23] using the exponential distorted wave approximation. These calculations are consistent with one another at energies where they overlap and cover the range 1–400 keV/amu. The accuracy is estimated to be 15–20%. Partial cross-sections for single and double capture have also been reported by Martin et al. [24] in the energy range 0.25–20 keV/amu.

$B^{+} + He$

The only data available are the total cross-section measurements by Nikolaev et al. [25] at energies in the range 10–100 keV/amu. Data are needed over a wider energy range.

$B^{2+} + He$

Experimental single-capture data have been reported by Sherwin [18], Gardner et al. [14] and Nikolaev et al. [25], covering the energy range 0.5–400 keV/amu. There is a large (order of magnitude) discrepancy between the data of Sherwin and those of Gardner et al. at energies below 5 keV/amu. Above 40 keV/amu, the uncertainty is estimated to be 20%. There is a gap in the data between 4 and 40 keV/amu. Additional data are required at energies below 40 keV/amu.

$B^{3+} + He$

Experimental total single-capture cross-section data have been reported in the energy range 0.04–400 keV/amu by Crandall [13], Gardner et al.

[14], Nikolaev et al. [25], Zwally and Cable [26] and Iwai et al. [27]. Theoretical coupled-state calculations have also been reported by Shipsey et al. [28] in the energy range 0.03–6 keV/amu. With the exception of the measurements of Gardner et al. [14], these data are very consistent with one another, and an accuracy of 10–20% is estimated. Shipsey et al. also reported partial cross-section calculations for capture into 2s and 2p states, whose ratio was confirmed by Matsumoto et al. [29]. Also for these partial cross-sections, an accuracy of 10–20% is estimated. Double-capture cross-section measurements reported by Crandall [13] show an unusual energy dependence. The cross-section is small relative to that for single capture and is probably unimportant for applications.

B^{4+} + He

Experimental data have been reported for the total single-capture cross-section by Gardner et al. [14], Nikolaev et al. [25] and Iwai et al. [27]. These data span the energy range 0.5–800 keV/amu, but a significant gap exists between 8 and 200 keV/amu, where further data are needed. No theoretical or partial cross-section data are available. An accuracy of 20–30% is estimated in the energy ranges 0.5–8 keV/amu and 200–800 keV/amu.

B^{5+} + He

Experimental data have been reported for the total single-capture cross-section by Iwai et al. [27], Nikolaev et al. [25] and Guffey et al. [30]. The theoretical data based on the CTMC method by Olson [22] tie in well with the measurements. While these data span the energy range 0.5–800 keV/amu, a significant gap exists between 2 and 100 keV/amu, where further experimental and/or theoretical data are needed. The accuracy is estimated to be 20% at energies below 2 keV/amu and above 100 keV/amu.

3. EXCITATION

Data on the excitation of H, H_2 and He (targets) by multicharged (projectile) ion impact are extremely limited. A small number of theoretical calculations have been reported for excitation of ground state hydrogen atoms by bare Be and B ions; these are outlined below. No such data exist for partially stripped Be or B ions, although a charge and energy scaling relation has been developed for multicharged ion impact on He (see below). No data exist for excitation in collisions of Be^{q+} or B^{q+} ions with H_2. Dissociative excitation of H_2 could play an important role in fusion plasmas. Excitation of fine-structure ($\Delta n = 0$) transitions in H^+ + Be^{q+} and H^+ + B^{q+} collisions can have relatively large cross-sections and play an important role for partially stripped Be and B impurities.

Be^{4+} + H(1s)

The two-state dipole close coupling (DCC) approximation has been applied by Janev and Presnyakov [31] to $n=1 \rightarrow n=2,3,4$ excitation of H by Be^{4+} ion impact at energies ranging from 2 to 100 keV/amu. Fritsch [32] has recently performed extended atomic orbital close coupling (AO+) calculations for $n=1 \rightarrow n=2$ excitation of H by Be^{4+} impact at energies ranging from 6 to 50 keV/amu. New theoretical data in the energy range 1–30 keV/amu based on the superpromotion model have been recently reported by Krstic et al. [6]. The latter results are recommended, with an estimated accuracy of a factor of two. These data are consistent within a factor of three or better with the AO+ calculations, and to within an order of magnitude with the DCC calculation. Data are needed for $n=1 \rightarrow n=3,4$ and $n=2 \rightarrow n=3,4$ excitation.

Be^{5+} + H(1s)

The UDWA approximation has been applied by Ryufuku [33] to the total excitation cross-section (summed over excitations to all n). New theoretical data in the energy range 1–30 keV/amu based on the superpromotion model are also available from Krstic et al. [6] for $n=1 \rightarrow n=2$ excitation. The latter data are recommended, with an estimated factor of two accuracy. Again, data are needed for $n=1 \rightarrow n=3,4$ and $n=2 \rightarrow n=3,4$ excitation.

Be^{q+} + He, B^{q+} + He

A charge scaling relation has been derived from the experimental data by Reymann et al. [34] for excitation of a He target by a variety of multicharged ion projectiles, with charges ranging from 6 to 44 and energies ranging from 120 to 1000 keV/amu. This scaling relation is estimated to be reliable in predicting the He excitation cross-sections to within a factor of two at 100 keV/amu, and better at higher energies. Experimental and theoretical cross-section data for projectile 2s–2p excitation of Be^+ in collisions with He have also been reported by Andersen et al. [35] and by

Nielsen and Dahler [36], respectively, in the energy range 0.05–40 keV/amu. Such data may be applicable for diagnostic purposes.

4. IONIZATION

The only experimental data for ionization of H, H_2 or He by Be^{q+} or B^{q+} impact are the measurements by Haugen et al. [37] for single ionization of He by B^{3+}, B^{4+} and B^{5+} at energies ranging from 190 to 2310 keV/amu. These have an estimated accuracy of 20%. Andersen [38] has also reported double ionization cross-sections for these reactants and this energy range and has investigated their scaling with ionic charge.

The CTMC method has been employed by Olson [39] and by Pfeifer and Olson [40] to Be^{4+} + He and B^{5+} + He collisions at energies in the range 100–500 keV/amu. New theoretical calculations have been performed by Krstic et al. [6] on the basis of the superpromotion model for ionization of H(n = 1) and H^*(n = 2) by Be^{4+} and B^{5+} impact at energies in the range 0.4–30 keV/amu. The accuracy of these data is difficult to assess. Nikolaev et al. [41] have also reported projectile ionization or stripping cross-section measurements for B^+ and B^{2+} colliding with H and H_2 at energies in the range 10–200 keV/amu.

In general, for ionization of H, H_2 or He by Be^{q+} or B^{q+} ions at energies above 50 keV/amu, where ionization dominates electron capture, the scaling formulas of Gillespie based on the Bethe approximation [2, 3] may be used to predict the target single-ionization cross-section with an estimated accuracy of 10–30%. At lower energies, where the ionization cross-sections become very small and the capture process dominates, theoretical methods and scaling laws are generally unreliable. Tabata et al. [42] have modified the Gillespie scaling relations to better represent the low energy data presently available, but experimental data are needed for all these collision systems at energies E/q < 50 keV/amu to establish the low energy behaviour of the ionization cross-sections. These and additional data at higher energies are needed to provide important tests of such scaling relations.

5. TWO-ELECTRON PROCESSES

For collisions involving H_2 and He, two-electron collision processes must also be considered. Examples are double electron capture and transfer ionization at lower energies, and double ionization at higher energies. Cross-sections for these processes are generally an order of magnitude smaller than those for single-electron processes. Relatively little attention has been devoted to such processes.

REFERENCES

[1] PHANEUF, R.A., JANEV, R.K., HUNTER, H.T., Nucl. Fusion, Special Supplement on Recommended Data on Atomic Collision Processes Involving Iron and its Ions (1987) 7.

[2] GILLESPIE, G.H., J. Phys., B **15** (1982) L729.

[3] GILLESPIE, G.H., Phys. Lett. A **93** (1982) 327.

[4] TAWARA, H., Total and Partial Cross Sections of Electron Transfer Processes for Be^{q+} and B^{q+} Ions in Collisions with H, H_2 and He Gas Targets — Status in 1991, Res. Rep. NIFS-DATA-12, NIFS-DATA Series ISSN 0915-6364, National Institute for Fusion Science, Nagoya (1991).

[5] KIMURA, M., presentation at the IAEA Consultants Meeting on the Atomic Database for Be and B (Vienna, June 1991).

[6] KRSTIC, P.S., RADMILOVIC, M., JANEV, R.K., this issue, p. 113.

[7] WETMORE, A.E., COLE, H.R., OLSON, R.E., J. Phys., B **19** (1986) 515.

[8] SHIMAKURA, N., J. Phys., B **21** (1988) 2485.

[9] FRITSCH, W., LIN, C.D., Phys. Rev., A **29** (1984) 3039.

[10] RYUFUKU, H., Phys. Rev., A **14** (1979) 1538; JAERI Memo-82-031, Japan Atomic Energy Research Institute, Tokai-mura (1982).

[11] GOFFE, T.V., SHAH, M.B., GILBODY, H.B., J. Phys., B **12** (1979) 3763.

[12] McCULLOUGH, R.W., NUTT, W.L., GILBODY, H.B., J. Phys., B **12** (1979) 3763. 4159.

[13] CRANDALL, D.H., Phys. Rev., A **16** (1977) 958.

[14] GARDNER, L.D., BAYFIELD, J.E., KOCH, P.M., et al., Phys. Rev., A **20** (1979) 766.

[15] OLSON, R.E., SHIPSEY, E.JK., BROWNE, R.C., J. Phys., B **11** (1978) 699.

[16] WETMORE, A.E., COLE, H.R., OLSON, R.E., J. Phys., B **19** (1986) 515.

[17] OLSON, R.E., SALOP, A., Phys. Rev., A **16** (1977) 531.

[18] SHERWIN, C.W., Phys. Rev. **57** (1940) 814.

[19] OSTGAARD OLSEN, J., VEDEL, K., DAHL, P., J. Phys., B **12** (1979) 929.

[20] GAY, T.J., REDD, E., BLANKENSHIP, D.M., PARK, J.T., PEACHER, J.L., SEELY, D.G., J. Phys., B **21** (1988) L467.

[21] BOYD, T.J.M., MOISEIWITSCH, B.L., Proc. Phys. Soc. (Lond.) 70A (1857) 55.

[22] OLSON, R.E., Phys. Rev., A **18** (1978) 2464.

[23] SUZUKI, H., KAJIKAWA, Y., TOSHIMA, N., RYUFUKU, H., WATANABE, T., Phys. Rev., A **29** (1984) 525.

[24] MARTIN, F., RIERA, A., YANEZ, M., Phys. Rev., A **34** (1986) 4675.

[25] NIKOLAEV, V.S., DMITRIEV, I.S., FATEEVA, L.N., TEPLOVA, Ya.M., Sov. Phys. - JETP **13** (1961) 695.

[26] ZWALLY, H.J., CABLE, P.G., Phys. Rev., A **4** (1971) 2301.
[27] IWAI, T., KANEKO, Y., KIMURA, M., et al., Phys. Rev., A **26** (1982) 105.
[28] SHIPSEY, E.J., BROWNE, J.C., OLSON, R.E., Phys. Rev., A **15** (1977) 2166.
[29] MATSUMOTO, A., IWAI, T., KANEKO, Y., et al., J. Phys. Soc. Jpn. **52** (1983) 3291.
[30] GUFFEY, J.A., ELLSWORTH, L.D., MACDONALD, J.R., Phys. Rev., A **15** (1977) 1863.
[31] JANEV, R.K., PRESNYAKOV, L.P., J. Phys., B **13** (1980) 4233.
[32] FRITSCH, W. (Hahn-Meitner-Institut für Kernforschung, Berlin), personal communication, 1991.
[33] RYUFUKU, H., Phys. Rev., A **25** (1982) 720.
[34] REYMANN, K., SCHARTNER, K.-H., SOMMER, B., TRABERT, E., Phys. Rev., A **38** (1988) 2290.
[35] ANDERSEN, N., ANDERSEN, T., JENSEN, K., J. Phys., B **9** (1976) 1373.
[36] NIELSEN, S., DAHLER, J.S., Phys. Rev., A **16** (1977) 563.
[37] HAUGEN, H.K., ANDERSEN, L.H., HVELPLUND, P., KNUDSEN, H., Phys. Rev., A **26** (1982) 1950.
[38] ANDERSEN, L.H., IEEE Trans. Nucl. Sci. **NS-30** (1983) 973.
[39] OLSON, R.E., Phys. Rev., A **18** (1978) 2464.
[40] PFEIFER, S.J., OLSON, R.E., Phys. Lett., A **92** (1982) 175.
[41] NIKOLAEV, V.S., SENASHENKO, V.S., SIDOROVICH, V.A., SHAFER, V.Yu., Sov. Phys. — Tech. Phys. **23** (1978) 789.
[42] TABATA, T., ITO, R., SHIRAI, T., NAKAI, Y., HUNTER, H.T., PHANEUF, R.A., At. Plasma-Mater. Interact. Data Fusion **2** (1992) 91.

CHARGE EXCHANGE, EXCITATION AND IONIZATION IN SLOW Be^{4+} + H AND B^{5+} + H COLLISIONS

P.S. KRSTIC, M. RADMILOVIC
Institute of Physics,
Belgrade, Yugoslavia

R.K. JANEV
International Atomic Energy Agency,
Vienna

ABSTRACT. Using the adiabatic superpromotion model for the dynamics of low energy atomic processes, the cross-sections for electron capture, excitation and ionization in Be^{4+} + H($n \leq 2$) and B^{5+} + H($n \leq 2$) collisions have been calculated in the energy range from 0.2 to 100 keV/u. Similar processes for the $H^+ + Be^{3+}(n)$ and $H^+ + B^{4+}(n)$ collisions have also been considered.

1. INTRODUCTION

Collision processes of Be^{4+} and B^{5+} plasma impurities with hydrogen atoms are of considerable interest in transport studies of these ions in a fusion plasma as well as for plasma spectroscopy [1]. In the plasma edge, where these impurities are not completely ionized, their collision processes with the plasma protons (deuterons, tritons) are also of interest for the studies of edge plasma behaviour.

In the present paper we provide a fairly complete cross-section information for the processes involving Be^{4+}, B^{5+} + H and $H^+ + Be^{3+}$, B^{4+} collisions, in which the collision partner carrying the electron may be in an excited state ($n = 2$ for H, $n \leq 7$ for Be^{3+} and B^{4+}). In the case of $H^+ + Be^{3+}$, B^{4+} collisions, transitions between excited states are also considered.

2. METHOD OF CALCULATIONS

The method applied in the present calculations is an extension of the adiabatic approach to slow atomic collision, and in its most general form [2] it is based on the dynamical molecular states (i.e. it includes the momentum transfer effects in all reaction channels). In practice, however, the method is used in its adiabatic limit, which retains the dynamical effects to $O(v^2)$, where v is the relative collision velocity. The solution of the multistate strongly coupled molecular dynamics problem is thus reduced to solving a large set of independent two-state strongly coupled problems in isolated regions of internuclear distance R since, in the adiabatic limit, no transitions between the adiabatic states take place outside these strong coupling regions.

It has been demonstrated by Solov'ev [3] that in the case of the one-electron two-Coulomb-centre system (Z_1, e, Z_2), where Z_1, Z_2 are the nuclear charges, the true strong coupling regions between adiabatic states of the system do not lie on the real R axis, but rather in the complex R plane, where the adiabatic potential energies are analytically continued (and become potential energy surfaces). The strong coupling regions appear as points in the complex R plane at which two potential energy surfaces, belonging to adiabatic states of the same symmetry, are mutually connected by a square root branching point ('hidden crossing' of the two surfaces). In fact, such potential energy surfaces appear as two branches of the same analytic function. Moreover, the potential energies of all adiabatic states with the same symmetry are mutually pairwise connected with branching points, thus forming a unique multivalued analytic function of the system with a given projection of its angular momentum on the real R axis [3]. The branching points connecting the successive adiabatic states (or surfaces) form infinite series, each beginning with the lowest state of a given symmetry. In the (Z_1, e, Z_2) system there exist two types of series of branching points [3, 4], labelled by S and T. (The series connecting the adiabatic states pairwise and successively are called superseries, to distinguish them from the series of transitions from a given state to all higher states.) If the adiabatic states are characterized by the united atomic quantum numbers (N, ℓ, m), the S

and T superseries consists of branch points connecting the states in the following successions:

$$S_{N\ell m}: (N\ell m) \rightarrow (N+1,\ell m) \rightarrow (N+2,\ell m) \rightarrow \ldots \rightarrow (\infty,\ell m) \quad (1)$$

$$T_{N\ell m}: (N\ell m) \rightarrow (N+1,\ell+1,m) \rightarrow (N+2,\ell+2,m) \rightarrow \ldots \quad (2)$$

Since $S_{N\ell m}$ superseries always begin with $N = \ell + 1$, the label N can be omitted (i.e. $S_{N\ell m} \rightarrow S_{\ell m}$). The structure of the branch points $R^{(S)}_{N\ell m}$ within an $S_{\ell m}$ superseries is such that, generally, $\mathrm{Re}\, R^{(S)}_{N+i,\ell m} > \mathrm{Re}\, R^{(S)}_{N+i+1,\ell m} > \ldots \mathrm{Re}\, R^{(S)}_{\infty\ell m}$, i.e. the system follows this series of transitions from lower states to upper states when the nuclei approach each other in the course of the collision. Exceptions to this rule, however, exist. The branch points of the $S_{\ell m}$ superseries are located at relatively small values of $|R|$, and all lie in a small domain in the complex R plane. The system reaching any of these points is rapidly promoted towards the higher states and into the continuum. The structure of the branch points $R^{(T)}_{N\ell m}$ is such that $\mathrm{Re}\, R^{(T)}_{n+i,\ell+i,m} < \mathrm{Re}\, R^{(T)}_{N+i+1,\ell+i+1,m}$, and the system follows these series of transitions on the receding stage of the colliding particles. The $T_{N\ell m}$ superseries also end in the continuum at very large internuclear distances (practically reaching certain sufficiently high N_c values which can be considered as lying in the continuum). We note that for $(\ell - m - \frac{1}{2}) \geq 2$ there are additional $S^{(\kappa)}_{\ell m}$ superseries in the complex plane [5], all connecting the same succession of states (1), but at smaller values of $|R^{(\kappa)}_{N\ell m}|$, $\kappa = 0, 1, 2 \ldots$ (i.e. $|R^{(\kappa+1)}_{N\ell m}| < |R^{(\kappa)}_{N\ell m}|$). The higher numbers ($\kappa > 0$) of these superseries become important when processes involving higher excited states are considered.

Within the adiabatic picture, the collision dynamics is thus reduced to evolution of the system along an initial adiabatic energy surface of a given symmetry and its transitions from one state to another at the branch points of the S and T superseries. Transitions between states of different symmetry are also possible at very small internuclear distances owing to the rotational coupling. The construction of the evolution matrix for the system reduces to multiplication of elementary transition probabilities at the S and T type branch points, and at very small R (rotational transitions), along all possible reaction paths.

The transition probability $p_{\alpha\beta}$ between two adiabatic states $|\alpha\rangle$ and $|\beta\rangle$ at a given branching point R_c is (asymptotically exactly) given [2] by

$$p_{\alpha\beta} = \exp\left(-\frac{2}{v}\Delta_{\beta\alpha}\right) \quad (3)$$

$$\Delta_{\beta\alpha} = \left|\mathrm{Im}\int_{\mathrm{Re}\,x(R_c)}^{x(R_c)} \Delta E_{\beta\alpha}(R(x))\,dx\right| = \left|\mathrm{Im}\int_C E(R(x))\,dx\right| \quad (4)$$

(atomic units $e = m_e = \hbar = 1$ are used throughout this work unless otherwise explicitly stated), where $\Delta E_{\beta\alpha} = E_\beta(R) - E_\alpha(R)$, $x = vt = (R^2 - b^2)^{1/2}$, and b is the impact parameter. We use a straight line approximation for the classical trajectory. The contour C in Eq. (4) starts at the real axis where $E(R) = E_\alpha(R)$, encompasses the branching point $x_c = x(R_c)$ and returns to the real axis where $E(R) = E_\beta(R)$. A remarkable feature of the adiabatic method using hidden crossings in the complex R plane is that the transition probability (3) is expressed in terms of a contour integral around the branching point R_c (i.e. no state wave functions or matrix elements are required in calculating $p_{\alpha\beta}$). For calculation of the energies $E_\alpha(R)$ of the (Z_1,e,Z_2) system in the complex R plane, for determination of the positions of the branching points R_c and for calculation of the contour integral (4), appropriate numerical codes have been developed [3].

The adiabatic method with hidden crossings in the complex R plane (sometimes also called 'super-promotion' model) has so far been used to study the collision dynamics and inelastic processes in the simplest (Z_1,e,Z_2) systems: $H^+ + H$ and $He^{2+} + H$ [6–9]. In Refs [6] and [7], only a few S and T superseries (the most important ones) have been used. More involved calculations for the $H^+ + H$ [8] and $He^{2+} + H$, $He^+ + H^+$ [9] systems included about 100 and 200 branching points, respectively, in the collision dynamics. In the study of the $(HeH)^{2+}$ collision system, more than 160 coupled molecular states were included.

In applying the adiabatic method with hidden crossings to the $Be^{4+} + H$ (and $Be^{3+} + H^+$) and $B^{5+} + H$ (and $B^{4+} + H^+$) collision systems, we shall also employ a large number of molecular states in order to be able to consider processes involving excited atomic states. We note that the probabilities of rotational transitions $p^{\mathrm{rot}}_{\alpha\beta}$ in the small R region were calculated by numerical integration of the coupled equations for different m states within a given $(N\ell)$ manifold [10].

In the calculation of the transition probability P_{if} between two atomic states, $|i\rangle$ and $|f\rangle$ ($|f\rangle$ may also designate the continuum), we first calculate the transition probabilities between all molecular states which asymptotically correlate with the atomic $|i\rangle$ and $|f\rangle$ manifolds and then perform the necessary projections of molecular states to the atomic basis. The cross-

section σ_{if} is then obtained by integrating P_{if} over the impact parameters.

3. INELASTIC PROCESSES IN Be^{4+} + H and H^+ + Be^{3+} COLLISIONS

3.1. General considerations

In the present study of the $(BeH)^{4+}$ collision system, we have included all processes between the n = 1, 2 states in H and the n = 1–7 states in Be^{3+}. In the case of processes within the discrete spectrum (excitation and charge transfer), the calculation of the corresponding molecular channel probabilities along the possible reaction paths requires in certain cases also branching points which directly couple the molecular states of the n = 7 manifold with those correlated with higher-n (up to n = 11) manifolds. The highest molecular state of this kind was the 11kσ state correlating with one of the Stark states of the n = 11 manifold of Be^{3+}. The T coupling of the states from this discrete molecular basis with states above 11kσ was interpreted as ionization. In the case of the S superseries, all couplings (branching points) up to the continuum edge (N → ∞) have been effectively accounted for. The number of adiabatic molecular states included in the consideration in this way was 258. The number of isolated branching points (of both S and T type) in this manifold of molecular states, which were considered to be important for the collision dynamics, was 319. These branching points formed 45 $S^{(\kappa)}_{\ell m}$ superseries and 32 $T_{N\ell m}$ superseries. We note that the branching points of the $S_{f\delta}$, $S_{g\phi}$ and $S_{h\gamma}$ superseries are 'inverted' ($Re\,R^{(S)}_{N+1,\ell m} < Re\,R^{(S)}_{N+i+1,\ell m}$), so that the promotion to higher states (and to the continuum) along these superseries takes place during the receding stage of nuclear motion. A programme was developed for construction and calculation of the evolution (or transition) matrix in this system of branching points (accounting also for the rotational transitions at R ≈ 0) for each collision energy and impact parameter. The calculation of positions of individual branching points and corresponding contour integrals $\Delta_{\beta\alpha}(b)$ was, however, performed for each point separately.

3.2. Cross-sections for Be^{4+} + H inelastic processes

3.2.1. Electron capture processes

We have considered the following shell-selective electron capture reactions:

$$Be^{4+} + H(1s) \rightarrow Be^{3+}(n) + H^+ \qquad n = 1\text{–}6 \qquad (5)$$

$$Be^{4+} + H(n = 2) \rightarrow Be^{3+}(n) + H^+ \qquad n = 1\text{–}6 \qquad (6)$$

in the energy range from 0.2 to 100 keV/u. The initial atomic state in reaction (5) correlates with the molecular 4fσ state, which is strongly coupled with the molecular 3dσ state at Re R ≈ 7.5 a_0 (a_0 is the Bohr radius). The 3dσ state correlates with one of the Stark states of the Be^{3+} (n = 3) manifold, and this is the dominant electron capture channel in the energy range considered. The T coupling of the 3dσ and 2pσ states at Re R ≈ 2.5 a_0 is relatively weak, and the population of Be^{3+} (n = 2) through the 2pσ molecular channel is efficient only at higher (> 10 keV/u) energies. The direct T coupling of the initial 4fσ state with the 5gσ state, correlating with the Be^{3+} (n = 4) manifold, is also weak, but the above mentioned highly populated 3dσ state, through 3dσ–3dπ rotational coupling at R ≈ 0, populates the 3dπ state which, further, through a strong T transition populates the 4fπ state which asymptotically goes over to the Be^{3+} (n = 4) manifold.

In the case of reaction (6), the initial H (n = 2) manifold contains three molecular states (8iσ, 8jπ and 9kσ), all of which have strong T couplings (direct or stepwise) with the molecular states correlating with the n = 5, 6, 7 manifolds of the Be^{3+} ion. The population of these reaction channels is therefore very high.

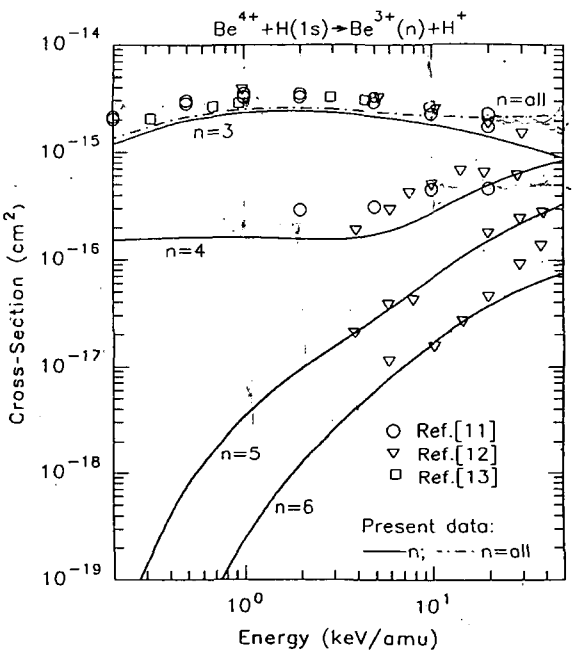

FIG. 1. Cross-sections for electron capture in various final n-shells (n = 3–6) in Be^{4+} + H (1s) collisions. The solid lines are the results of the present calculations; the circles and inverted triangles are the results of AO based coupled channel calculations (Refs [11, 12]), and the squares are the results of MO coupled channel calculations of Ref. [13]. The dot-dashed line represents the total capture cross-section from the present calculations.

TABLE I. CROSS-SECTIONS (in cm^2) FOR THE ELECTRON CAPTURE REACTIONS
$Be^{4+} + H(1s) \rightarrow Be^{3+}(n) + H^+$

E (keV/u)	$\sigma_{ct}(1 \rightarrow 1)$	$\sigma_{ct}(1 \rightarrow 2)$	$\sigma_{ct}(1 \rightarrow 3)$	$\sigma_{ct}(1 \rightarrow 4)$	$\sigma_{ct}(1 \rightarrow 5)$	$\sigma_{ct}(1 \rightarrow 6)$
0.2	0.00	7.28 (-26)	1.20 (-15)	1.54 (-16)	2.96 (-20)	2.95 (-22)
0.4	0.00	4.94 (-23)	1.78 (-15)	1.61 (-16)	3.91 (-19)	9.82 (-21)
0.6	0.00	9.25 (-22)	2.06 (-15)	1.64 (-16)	1.18 (-18)	4.85 (-20)
0.8	9.42 (-43)*	5.40 (-21)	2.21 (-15)	1.63 (-16)	2.23 (-18)	1.26 (-19)
1.0	4.17 (-40)	1.82 (-20)	2.29 (-15)	1.62 (-16)	3.40 (-18)	2.42 (-19)
1.4	1.24 (-36)	9.03 (-20)	2.37 (-15)	1.59 (-16)	5.83 (-18)	5.66 (-19)
2.0	1.54 (-33)	3.83 (-19)	2.38 (-15)	1.56 (-16)	9.39 (-18)	1.21 (-18)
3.0	1.25 (-30)	1.50 (-18)	2.32 (-15)	1.55 (-16)	1.52 (-17)	2.56 (-18)
4.0	6.75 (-29)	3.40 (-18)	2.23 (-15)	1.61 (-16)	2.13 (-17)	4.15 (-18)
6.0	7.56 (-27)	8.89 (-18)	2.06 (-15)	1.88 (-16)	3.50 (-17)	7.91 (-18)
8.0	1.24 (-25)	1.56 (-17)	1.92 (-15)	2.29 (-16)	5.07 (-17)	1.21 (-17)
10.0	8.32 (-25)	2.27 (-17)	1.80 (-15)	2.74 (-16)	6.73 (-17)	1.65 (-17)
12.0	3.36 (-24)	2.97 (-17)	1.70 (-15)	3.21 (-16)	8.45 (-17)	2.09 (-17)
14.0	9.88 (-24)	3.64 (-17)	1.61 (-15)	3.68 (-16)	1.02 (-16)	2.52 (-17)
16.0	2.35 (-23)	4.27 (-17)	1.53 (-15)	4.12 (-16)	1.19 (-16)	2.93 (-17)
18.0	4.79 (-23)	4.85 (-17)	1.46 (-15)	4.55 (-16)	1.36 (-16)	3.33 (-17)
20.0	8.73 (-23)	5.38 (-17)	1.40 (-15)	4.94 (-16)	1.52 (-16)	3.70 (-17)
25.0	2.79 (-22)	6.51 (-17)	1.27 (-15)	5.83 (-16)	1.90 (-16)	4.56 (-17)
30.0	6.52 (-22)	7.40 (-17)	1.17 (-15)	6.56 (-16)	2.24 (-16)	5.32 (-17)
40.0	2.11 (-21)	8.65 (-17)	1.01 (-15)	7.69 (-16)	2.83 (-16)	6.60 (-17)
50.0	4.62 (-21)	9.41 (-17)	8.99 (-16)	8.53 (-16)	3.30 (-16)	7.62 (-17)
60.0	8.16 (-21)	9.88 (-17)	8.14 (-16)	9.13 (-16)	3.69 (-16)	8.46 (-17)
80.0	1.78 (-20)	1.03 (-16)	6.93 (-16)	1.00 (-15)	4.26 (-16)	9.76 (-17)
100.0	2.98 (-20)	1.04 (-16)	6.10 (-16)	1.07 (-15)	4.66 (-16)	1.07 (-16)

* $a(-x) = a \times 10^{-x}$.

The cross-sections of reactions (5) and (6) are given in Table I and Table II, respectively. Figure 1 shows the cross-sections of n = 3, 4, 5, 6 charge exchange reactions, compared with the extensive atomic orbital (AO) [11, 12] and molecular orbital (MO) [13] coupled channel calculations. All three sets of data for n = 3 agree with each other to within 20%. For the n = 5 and n = 6 channels the agreement of the present results with those of the two-centre AO expansion method (below 10 keV/u) is even better (wihin 5–10%), but for the n = 4 channel the agreement becomes worse (30–40%).

3.2.2. *Excitation of the n = 2 level*

In the excitation process

$$Be^{4+} + H(1s) \rightarrow Be^{4+} + H(n = 2) \qquad (7)$$

the initial state $4f\sigma$ is connected with the molecular states $8i\sigma$, $8j\pi$ and $9k\sigma$ through several reaction paths, the most direct ones of which involve the branch points of the $T_{1s\sigma}$, $T_{2p\pi}$ and $T_{3p\sigma}$ superseries. The superseries $T_{1s\sigma}$ is reached by the $T_{4f\sigma,3d\sigma}$ transition, the superseries $T_{2p\pi}$ is attained through the transition sequence $T_{4f\sigma,3d\sigma}$, $T_{3d\sigma,2p\sigma}$, $P^{rot}_{2p\sigma,2p\pi}$, and the superseries $T_{3p\sigma}$ is reached from the $2p\sigma$ state by the $S_{2p\sigma,3p\sigma}$ transition. At each of these transition points the incoming probability flux splits along two different paths, which leads to a rapid increase of the possible reaction paths.

The cross-section of reaction (7) is given in Fig. 2 in the energy interval from 3 keV/u to 60 keV/u. The cross-section is compared with the results of two-centre AO coupled channel calculations [12], which include also a number of pseudo-states in the basis set.

3.2.3. *Ionization of H (1s) and H (n = 2)*

The ionization processes

$$Be^{4+} + H(1s) \rightarrow Be^{4+} + H^+ + e \qquad (8)$$

$$Be^{4+} + H(n = 2) \rightarrow Be^{4+} + H^+ + e \qquad (9)$$

TABLE II. CROSS-SECTIONS (in cm^2) FOR THE ELECTRON CAPTURE REACTIONS
Be^{4+} + H(m = 2) → Be^{3+}(n) + H^+

E (keV/u)	$\sigma_{ct}(2 \to 1)$	$\sigma_{ct}(2 \to 2)$	$\sigma_{ct}(2 \to 3)$	$\sigma_{ct}(2 \to 4)$	$\sigma_{ct}(2 \to 5)$	$\sigma_{ct}(2 \to 6)$
0.6		3.80 (-33)	1.78 (-27)	3.89 (-21)	1.55 (-17)	1.18 (-15)
0.8		5.77 (-31)	5.39 (-26)	2.22 (-20)	3.27 (-17)	1.47 (-15)
1.0		1.77 (-29)	5.48 (-25)	7.25 (-20)	5.41 (-17)	1.74 (-15)
1.4		1.58 (-27)	1.13 (-23)	3.39 (-19)	1.03 (-16)	2.24 (-15)
2.0		8.63 (-26)	1.64 (-22)	1.31 (-18)	1.78 (-16)	2.88 (-15)
3.0		3.64 (-24)	1.96 (-21)	4.53 (-18)	2.85 (-16)	3.72 (-15)
4.0		3.32 (-23)	8.37 (-21)	9.27 (-18)	3.64 (-16)	4.32 (-15)
6.0		4.46 (-22)	4.50 (-20)	2.09 (-17)	4.64 (-16)	5.04 (-15)
8.0		2.05 (-21)	1.19 (-19)	3.27 (-17)	5.18 (-16)	5.38 (-15)
10.0	2.22 (-28)*	5.71 (-21)	2.26 (-19)	4.36 (-17)	5.46 (-16)	5.51 (-15)
12.0	1.43 (-27)	1.20 (-20)	3.58 (-19)	5.31 (-17)	5.60 (-16)	5.54 (-15)
14.0	6.07 (-27)	2.12 (-20)	5.07 (-19)	6.11 (-17)	5.65 (-16)	5.50 (-15)
16.0	1.93 (-26)	3.34 (-20)	6.67 (-19)	6.78 (-17)	5.65 (-16)	5.43 (-15)
18.0	5.01 (-26)	4.82 (-20)	8.32 (-19)	7.34 (-17)	5.61 (-16)	5.35 (-15)
20.0	1.12 (-25)	6.56 (-20)	9.96 (-19)	7.81 (-17)	5.55 (-16)	5.25 (-15)
25.0	5.30 (-25)	1.18 (-19)	1.40 (-18)	8.67 (-17)	5.37 (-16)	4.99 (-15)
30.0	1.65 (-24)	1.79 (-19)	1.78 (-18)	9.22 (-17)	5.17 (-16)	4.73 (-15)
40.0	7.96 (-24)	3.14 (-19)	2.41 (-18)	9.76 (-17)	4.78 (-16)	4.28 (-15)
50.0	2.29 (-23)	4.49 (-19)	2.90 (-18)	9.89 (-17)	4.44 (-16)	3.90 (-15)
60.0	4.93 (-23)	5.76 (-19)	3.28 (-18)	9.81 (-17)	4.15 (-16)	3.59 (-15)
80.0	1.42 (-22)	7.95 (-19)	3.82 (-18)	9.41 (-17)	3.67 (-16)	3.10 (-15)
100.0	2.87 (-22)	9.68 (-19)	4.16 (-18)	8.90 (-17)	3.31 (-16)	2.74 (-15)

* a(-x) = a × 10^{-x}.

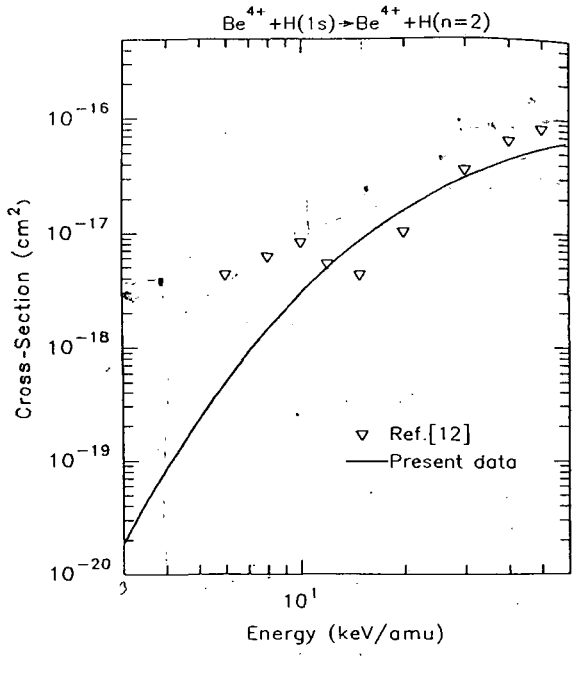

FIG. 2. Excitation of the n = 2 hydrogen level in Be^{4+} + H(1s) collisions. The solid line is the result of the present calculations; inverted triangles are the results of AO coupled channel calculations (Ref. [12]).

proceed in the approaching stage of the collision via all the $S^{(\kappa)}_{\ell m}$ superpromotion channels with $\ell \le \ell_i$, m = m_i, where ℓ_i and m_i are the corresponding quantum numbers of the initial state, and in the receding stage of the collision via all the $T_{N\ell m}$ superpromotion channels, 'opened' by either direct or indirect (sequential) T, S and P^{rot} type transitions from the initial molecular states. In the case of H(1s) ionization, the strongest superpromotion ionization channels are those connected with the $S^{(0)}_{f\sigma}$, $S^{(0)}_{d\sigma}$, $T_{1s\sigma}$, $T_{2p\pi}$ and $T_{3p\sigma}$ superseries. The ionization of H(n = 2) is extremely fast, since the initial molecular states 9kσ, 8jπ and 8iσ are promoted to the continuum already at large internuclear distances: 9kσ is directly promoted to the continuum through the superseries $S^{(0)}_{k\sigma}$ and $S^{(1)}_{k\sigma}$ (with series limits at $Re\,R^{(0)}_{k\sigma} \approx 15.1\,a_0$ and $Re\,R^{(1)}_{k\sigma} \approx 13.0\,a_0$), 8j$\pi$ is promoted to the continuum through the superseries $S^{(0)}_{j\pi}$ and $S^{(1)}_{j\pi}$ (at $Re\,R^{(0)}_{j\pi} \approx 10.7\,a_0$ and $Re\,R^{(1)}_{j\pi} \approx 7.9\,a_0$), while 8i$\sigma$ is directly ionized via $S^{(0)}_{i\sigma}$ (at $Re\,R^{(0)}_{i\sigma} \approx 8.6\,a_0$) and $S^{(1)}_{i\sigma}$ (at $Re\,R^{(1)}_{i\sigma} \approx 6.6\,a_0$). Already these numbers show that the low energy ionization cross-section of H(n = 2) should be of the order of $\pi R^2_{k\sigma} a_0^2 \sim 200\,\pi a_0^2 \sim 10^{14}$ cm^2. Further ionization of the 9kσ, 8jπ and 8iσ states is provided by several strong $T_{N\ell m}$ superseries during the receding of nuclei.

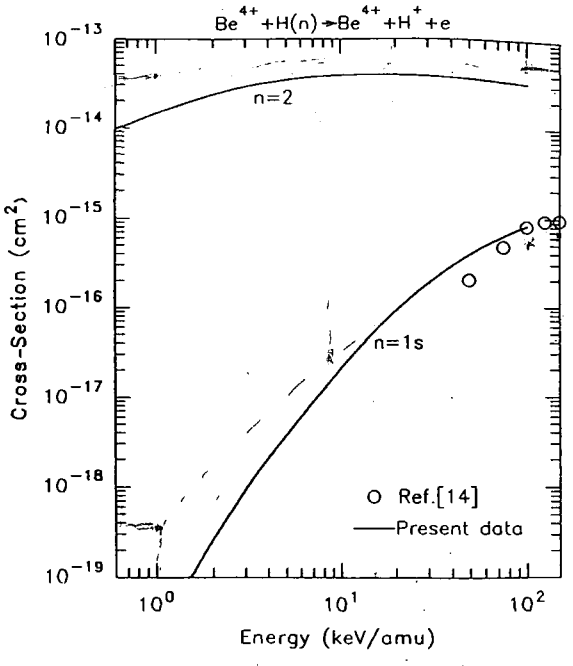

FIG. 3. Cross-section for ionization of H(1s) by Be^{4+} impact (curve n = 1s) and cross-section for transitions from H(n = 2) to the upper states and to the continuum (curve n = 2). The solid lines are the results of the present calculations; the circles are the results for H(1s) ionization from the classical trajectory Monte Carlo calculations (Ref. [14]).

TABLE III. IONIZATION CROSS-SECTION (in cm^2) FOR Be^{4+} + H(1s) COLLISIONS

E (keV/u)	σ_{ion}
0.6	1.39 (-21)*
0.8	6.45 (-21)
1.0	1.84 (-20)
1.4	7.33 (-20)
2.0	2.58 (-19)
3.0	9.03 (-19)
4.0	2.03 (-18)
6.0	5.95 (-18)
8.0	1.22 (-17)
10.0	2.09 (-17)
12.0	3.16 (-17)
14.0	4.44 (-17)
16.0	5.87 (-17)
18.0	7.44 (-17)
20.0	9.13 (-17)
25.0	1.37 (-16)
30.0	1.87 (-16)
40.0	2.89 (-16)
50.0	3.91 (-16)
60.0	4.88 (-16)
80.0	6.64 (-16)
100.0	8.18 (-16)

* $a(-x) = a \times 10^{-x}$.

The calculated ionization cross-sections for H(1s) and H(n = 2) by Be^{4+} impact are shown in Fig. 3 in the energy range 0.6–100 keV/u. At its high energy part, the ionization cross-section for H(1s) is compared with the results of the classical trajectory Monte Carlo calculations [14], which in the energy region of the cross-section maximum ($E \approx 150$ keV/u) should be reliable. The cross-section for n = 2 shown in Fig. 3 is not the true ionization cross-section, since it contains also the excitations from n = 2 to all higher ($n \geq 3$) levels, considered within the present model as being embedded in the continuum. Therefore, the n = 2 curve in Fig. 3 should be considered as the upper limit of the ionization cross-section for H(n = 2). The numerical values of the ionization cross-section for H(1s) are given in Table III.

3.3. Cross-sections for $H^+ + Be^{3+}$ collision processes

The dynamics of inelastic processes in $H^+ + Be^{3+}$ ($n \leq 6$) collisions is very similar to that for the processes in $Be^{4+} + H(n \leq 2)$ and, therefore, will not be discussed in detail. The n-shell selective electron capture processes in these two systems are mutually time reversed, and their cross-sections are related by the detailed balance principle. Therefore, we present here only the results for excitation and ionization processes in $H^+ + Be^{3+}$ collisions.

The cross-sections for the processes

$$H^+ + Be^{3+}(m) \rightarrow H^+ + Be^{3+}(n)$$
$$2 \leq m < n \leq 6 \qquad (10)$$

calculated in the energy range 0.6–100 keV/u are given in Tables IV and V. As expected, the cross-sections for a given energy increase with decreasing difference n–m, because of the decrease of the number of intermediate couplings between the involved initial and final molecular states. The cross-sections for $1 \rightarrow n$ transitions are all very small ($< 10^{-20}$ cm^2 for E < 50 keV/u) because of the extremely weak T coupling of the initial $1s\sigma$ state with the first excited ($2p\sigma$) molecular state at $Re\,R_c \approx 0.4\,a_0$, which is the initial step in the collision dynamics for all these processes.

The cross-sections for the ionization processes:

$$H^+ + Be^{3+}(n) \rightarrow H^+ + Be^{4+} + e$$
$$2 \leq n \leq 7 \qquad (11)$$

are given in Table VI in the energy range 0.6–100 keV/u.

TABLE IV. CROSS-SECTIONS (in cm^2) FOR Be^{3+} (m = 2) → Be^{3+}(n) EXCITATION BY PROTON IMPACT

E (keV/u)	σ_{exc} (2 → 3)	σ_{exc} (2 → 4)	σ_{exc} (2 → 5)	σ_{exc} (2 → 6)	σ_{exc} (2 → 7)
0.6	4.32 (-22)*	7.95 (-25)	7.86 (-26)	2.48 (-26)	1.01 (-26)
0.8	2.08 (-21)	6.24 (-24)	6.83 (-25)	2.38 (-25)	1.13 (-25)
1.0	6.10 (-21)	2.64 (-23)	3.06 (-24)	1.11 (-24)	6.09 (-25)
1.4	2.50 (-20)	1.89 (-22)	2.37 (-23)	8.41 (-24)	6.19 (-24)
2.0	8.76 (-20)	1.20 (-21)	1.67 (-22)	5.29 (-23)	5.69 (-23)
3.0	2.84 (-19)	7.62 (-21)	1.22 (-21)	3.21 (-22)	5.33 (-22)
4.0	5.72 (-19)	2.43 (-20)	4.27 (-21)	1.00 (-21)	2.18 (-21)
6.0	1.31 (-18)	1.01 (-19)	2.02 (-20)	4.16 (-21)	1.24 (-20)
8.0	2.13 (-18)	2.44 (-19)	5.23 (-20)	1.01 (-20)	3.66 (-20)
10.0	2.98 (-18)	4.46 (-19)	1.01 (-19)	1.89 (-20)	7.80 (-20)
12.0	3.82 (-18)	6.98 (-19)	1.66 (-19)	3.01 (-20)	1.38 (-19)
14.0	4.64 (-18)	9.88 (-19)	2.43 (-19)	4.34 (-20)	2.15 (-19)
16.0	5.43 (-18)	1.30 (-18)	3.31 (-19)	5.83 (-20)	3.10 (-19)
18.0	6.19 (-18)	1.64 (-18)	4.27 (-19)	7.45 (-20)	4.19 (-19)
20.0	6.91 (-18)	1.98 (-18)	5.29 (-19)	9.16 (-20)	5.43 (-19)
25.0	8.58 (-18)	2.86 (-18)	8.01 (-19)	1.37 (-19)	9.01 (-19)
30.0	1.01 (-17)	3.73 (-18)	1.08 (-18)	1.83 (-19)	1.31 (-18)
40.0	1.26 (-17)	5.30 (-18)	1.63 (-18)	2.74 (-19)	2.23 (-18)
50.0	1.47 (-17)	6.64 (-18)	2.13 (-18)	3.58 (-19)	3.21 (-18)
60.0	1.64 (-17)	7.76 (-18)	2.58 (-18)	4.33 (-19)	4.20 (-18)
80.0	1.90 (-17)	9.47 (-18)	3.30 (-18)	5.58 (-19)	6.12 (-18)
100.0	2.08 (-17)	1.07 (-17)	3.86 (-18)	6.57 (-19)	7.91 (-18)

* $a(-x) = a \times 10^{-x}$.

TABLE V. CROSS-SECTIONS (in cm^2) FOR Be^{3+} (m) → Be^{3+}(n) EXCITATION BY PROTON IMPACT ($3 \leq m < n \leq 6$)

E (keV/u)	σ_{exc} (3 → 4)	σ_{exc} (3 → 5)	σ_{exc} (3 → 6)	σ_{exc} (4 → 5)	σ_{exc} (4 → 6)	σ_{exc} (5 → 6)
0.6	1.47 (-17)*	1.11 (-19)	5.25 (-21)	6.49 (-17)	1.60 (-18)	2.22 (-16)
0.8	1.79 (-17)	2.54 (-19)	1.59 (-20)	7.43 (-17)	2.63 (-18)	2.77 (-16)
1.0	2.06 (-17)	4.47 (-19)	3.44 (-20)	8.42 (-17)	3.83 (-18)	3.25 (-16)
1.4	2.52 (-17)	9.34 (-19)	9.56 (-20)	1.04 (-16)	6.56 (-18)	4.06 (-16)
2.0	3.07 (-17)	1.79 (-18)	2.39 (-19)	1.34 (-16)	1.11 (-17)	5.02 (-16)
3.0	3.82 (-17)	3.29 (-18)	5.60 (-19)	1.81 (-16)	1.87 (-17)	6.26 (-16)
4.0	4.46 (-17)	4.73 (-18)	9.22 (-19)	2.21 (-16)	2.59 (-17)	7.21 (-16)
6.0	5.64 (-17)	7.33 (-18)	1.64 (-18)	2.86 (-16)	3.87 (-17)	8.63 (-16)
8.0	6.67 (-17)	9.62 (-18)	2.30 (-18)	3.35 (-16)	4.99 (-17)	9.57 (-16)
10.0	7.59 (-17)	1.17 (-17)	2.90 (-18)	3.74 (-16)	5.96 (-17)	1.02 (-15)
12.0	8.42 (-17)	1.35 (-17)	3.44 (-18)	4.04 (-16)	6.82 (-17)	1.06 (-15)
14.0	9.15 (-17)	1.52 (-17)	3.93 (-18)	4.29 (-16)	7.59 (-17)	1.10 (-15)
16.0	9.80 (-17)	1.67 (-17)	4.39 (-18)	4.50 (-16)	8.28 (-17)	1.12 (-15)
18.0	1.04 (-16)	1.81 (-17)	4.83 (-18)	4.67 (-16)	8.90 (-17)	1.14 (-15)
20.0	1.09 (-16)	1.93 (-17)	5.24 (-18)	4.81 (-16)	9.46 (-17)	1.16 (-15)
25.0	1.20 (-16)	2.21 (-17)	6.17 (-18)	5.08 (-16)	1.06 (-16)	1.18 (-15)
30.0	1.29 (-16)	2.43 (-17)	7.00 (-18)	5.26 (-16)	1.16 (-16)	1.20 (-15)
40.0	1.42 (-16)	2.79 (-17)	8.43 (-18)	5.48 (-16)	1.30 (-16)	1.21 (-15)
50.0	1.50 (-16)	3.04 (-17)	9.60 (-18)	5.59 (-16)	1.40 (-16)	1.22 (-15)
60.0	1.57 (-16)	3.23 (-17)	1.06 (-17)	5.66 (-16)	1.47 (-16)	1.21 (-15)
80.0	1.65 (-16)	3.50 (-17)	1.21 (-17)	5.73 (-16)	1.57 (-16)	1.20 (-15)
100.0	1.69 (-16)	3.66 (-17)	1.32 (-17)	5.75 (-16)	1.63 (-16)	1.17 (-15)

* $a(-x) = a \times 10^{-x}$.

TABLE VI. IONIZATION CROSS-SECTIONS (in cm^2) FOR $H^+ + Be^{3+}(n)$ COLLISIONS

E (keV/u)	σ_{ion} (n = 2)	σ_{ion} (n = 3)	σ_{ion} (n = 4)	σ_{ion} (n = 5)	σ_{ion} (n = 6)	σ_{ion} (n = 7)
0.6	8.89 (-27)*	4.02 (-22)	3.14 (-20)	2.18 (-18)	9.26 (-17)	8.80 (-16)
0.8	1.04 (-25)	1.48 (-21)	9.03 (-20)	4.69 (-18)	1.37 (-16)	1.13 (-15)
1.0	5.65 (-25)	3.84 (-21)	1.96 (-19)	8.14 (-18)	1.85 (-16)	1.33 (-15)
1.4	5.34 (-24)	1.52 (-20)	5.79 (-19)	1.74 (-17)	2.88 (-16)	1.66 (-15)
2.0	4.26 (-23)	5.71 (-20)	1.62 (-18)	3.57 (-17)	4.48 (-16)	2.03 (-15)
3.0	3.43 (-22)	2.10 (-19)	4.57 (-18)	7.31 (-17)	7.04 (-16)	2.46 (-15)
4.0	1.31 (-21)	4.66 (-19)	8.79 (-18)	1.14 (-16)	9.39 (-16)	2.78 (-15)
6.0	7.31 (-21)	1.23 (-18)	2.00 (-17)	1.98 (-16)	1.34 (-15)	3.23 (-15)
8.0	2.20 (-20)	2.23 (-18)	3.33 (-17)	2.77 (-16)	1.66 (-15)	3.54 (-15)
10.0	4.87 (-20)	3.37 (-18)	4.79 (-17)	3.49 (-16)	1.93 (-15)	3.77 (-15)
12.0	8.95 (-20)	4.60 (-18)	6.29 (-17)	4.14 (-16)	2.15 (-15)	3.94 (-15)
14.0	1.46 (-19)	5.90 (-18)	7.80 (-17)	4.72 (-16)	2.34 (-15)	4.08 (-15)
16.0	2.18 (-19)	7.23 (-18)	9.29 (-17)	5.25 (-16)	2.50 (-15)	4.20 (-15)
18.0	3.06 (-19)	8.59 (-18)	1.07 (-16)	5.73 (-16)	2.64 (-15)	4.29 (-15)
20.0	4.10 (-19)	9.96 (-18)	1.22 (-16)	6.18 (-16)	2.76 (-15)	4.36 (-15)
25.0	7.32 (-19)	1.34 (-17)	1.55 (-16)	7.14 (-16)	3.00 (-15)	4.50 (-15)
30.0	1.13 (-18)	1.68 (-17)	1.85 (-16)	7.97 (-16)	3.19 (-15)	4.59 (-15)
40.0	2.12 (-18)	2.32 (-17)	2.38 (-16)	9.34 (-16)	3.45 (-15)	4.69 (-15)
50.0	3.26 (-18)	2.96 (-17)	2.82 (-16)	1.04 (-15)	6.63 (-15)	4.72 (-15)
60.0	4.48 (-18)	3.57 (-17)	3.20 (-16)	1.14 (-15)	3.75 (-15)	4.73 (-15)
80.0	7.02 (-18)	4.64 (-17)	3.81 (-16)	1.28 (-15)	3.91 (-15)	4.70 (-15)
100.0	9.53 (-18)	5.59 (-17)	4.30 (-16)	1.38 (-15)	4.01 (-15)	4.66 (-15)

* $a(-x) = a \times 10^{-x}$.

The cross-section for ionization of Be^{3+} (1s) is below 10^{-20} cm^2 in the entire energy range considered, for the same reason as in the case of excitation.

4. INELASTIC PROCESSES IN $B^{5+} + H$ and $H^+ + B^{4+}$ COLLISIONS

4.1. General remarks on the collision dynamics

In considering the collision dynamics of the $(BH)^{5+}$ system, we have included all molecular states which in the separated atom limit are correlated with the n = 1 and n = 2 manifolds of Stark states centred on H^+ and with the $n \leq 8$ atomic manifolds centred on B^{5+}. We have also included those upper molecular states $(N_c \ell_c m_c)$ which are directly coupled with the above mentioned ones (up to the state $11m\pi$). Transitions to states above $(N_c \ell_c m_c)$ have also been included, but have been interpreted as ionization. The number of molecular states of the $(BH)^{5+}$ system included in this way in the consideration amounts to 285. The number of S and T branching points in this set of states, which was found to be important for the collision dynamics and was used in calculations, is 347. These branching points are elements of the 45 $S^{(\kappa)}_{\ell m}$ and the 34 $T_{N\ell m}$ superseries. The series $S^{(0)}_{f\delta}$ and $S^{(0)}_{g\phi}$ were found to be 'reversed' and were used as ionization channels in the second half of the collision. The rotational transitions between the m states of an $(N\ell)$ manifold at $R \approx 0$ were also included by numerical integration of the corresponding coupled equations.

4.2. Inelastic processes in $B^{5+} + H$ ($n \leq 2$) collisions

4.2.1. Electron capture processes

In accordance with the selected molecular basis, we were able to calculate the cross-sections for the following electron capture processes:

$$B^{5+} + H(1s) \rightarrow B^{4+}(n) + H^+ \quad 1 \leq n \leq 8 \tag{12}$$

$$B^{5+} + H(m = 2) \rightarrow B^{4+}(n) + H^+ \quad 1 \leq n \leq 8 \tag{13}$$

The initial molecular state in reaction (12) is $5g\sigma$ and it has an extremely strong T coupling with the next lower $4f\sigma$ molecular state at $Re\,R_c \approx 13\,a_0$. This coupling is responsible for the predominantly populated n = 4 channel in reaction (12) in the entire energy range considered (0.2–30 keV/u). In its turn, the $4f\sigma$ state is strongly coupled with the $3d\sigma$ state at $Re\,R_c \approx 5\,a_0$, and the n = 3 channel in reaction (12) is also considerably populated. The $5g\sigma$ initial state interacts relatively strongly also with the $6h\sigma$ state which populates the n = 5 channel of reaction (12). This reaction channel is also populated by the $5g\sigma$–$5g\pi$ rotational transitions. The cross-sections of the n = 3, 4, 5 channels in reaction (12) are shown in Fig. 4, where they are compared with the results of AO [11] and MO [13] coupled state calculations.

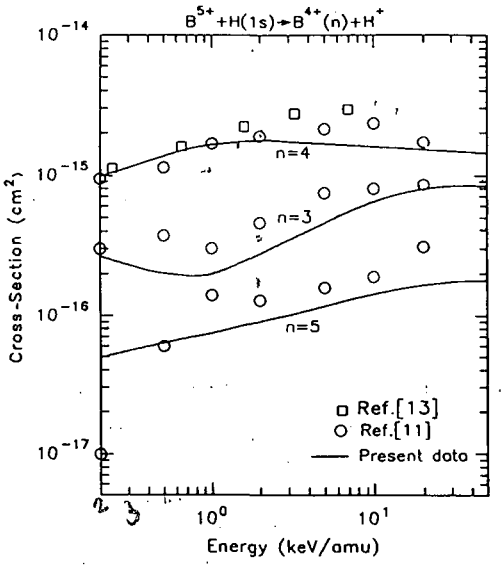

FIG. 4. Cross-section for capture into n = 3, 4, 5 final shells in B^{5+} + H(1s) collisions. The solid lines are the present results; the circles and squares are the results from the AO and MO coupled state calculations of Refs [11] and [13], respectively.

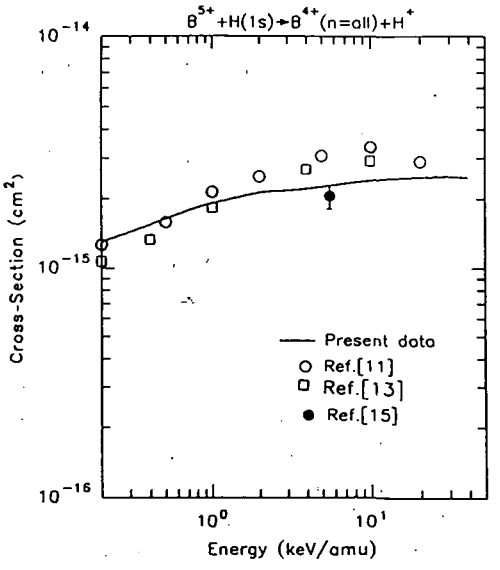

FIG. 5. Total electron capture cross-section for B^{5+} + H(1s) collisions. The solid line is the result of the present calculations; the open circles and open squares are the results from the extensive AO and MO coupled state calculations of Refs [11] and [13], respectively, and the closed circle is the experimental cross-section value from Ref. [15].

TABLE VII. CROSS-SECTIONS (in cm^2) FOR THE ELECTRON CAPTURE REACTIONS
$B^{5+} + H(1s) \rightarrow B^{4+}(n) + H^+$

E (keV/u)	$\sigma_{ct}(1 \rightarrow 1)$	$\sigma_{ct}(1 \rightarrow 2)$	$\sigma_{ct}(1 \rightarrow 3)$	$\sigma_{ct}(1 \rightarrow 4)$	$\sigma_{ct}(1 \rightarrow 5)$	$\sigma_{ct}(1 \rightarrow 6)$	$\sigma_{ct}(1 \rightarrow 7)$	$\sigma_{ct}(1 \rightarrow 8)$
0.2		3.84 (-34)	2.65 (-16)	9.85 (-16)	5.00 (-17)	3.98 (-20)	8.46 (-22)	3.01 (-24)
0.6		9.75 (-27)	1.96 (-16)	1.46 (-15)	6.61 (-17)	1.09 (-18)	9.42 (-20)	3.33 (-21)
1.0		2.01 (-24)	1.99 (-16)	1.65 (-15)	7.44 (-17)	3.17 (-18)	4.31 (-19)	3.08 (-20)
2.0	2.88 (-39)*	4.57 (-22)	2.77 (-16)	1.77 (-15)	9.06 (-17)	1.01 (-17)	2.10 (-18)	3.10 (-19)
3.0	3.47 (-35)	5.23 (-21)	3.46 (-16)	1.73 (-15)	1.01 (-16)	1.75 (-17)	4.29 (-18)	8.93 (-19)
5.0	4.27 (-31)	6.16 (-20)	4.58 (-16)	1.68 (-15)	1.18 (-16)	3.12 (-17)	8.70 (-18)	2.64 (-18)
7.0	6.37 (-29)	2.31 (-19)	5.52 (-16)	1.64 (-15)	1.30 (-16)	4.29 (-17)	1.26 (-17)	4.73 (-18)
10.0	5.48 (-27)	7.51 (-19)	6.49 (-16)	1.60 (-15)	1.44 (-16)	5.69 (-17)	1.73 (-17)	7.94 (-18)
14.0	1.86 (-25)	1.90 (-18)	7.31 (-16)	1.57 (-15)	1.55 (-16)	7.11 (-17)	2.21 (-17)	1.19 (-17)
20.0	4.26 (-24)	4.34 (-18)	7.96 (-16)	1.52 (-15)	1.66 (-16)	8.62 (-17)	2.75 (-17)	1.69 (-17)
30.0	7.96 (-23)	9.37 (-18)	8.35 (-16)	1.49 (-15)	1.75 (-16)	1.02 (-16)	3.39 (-17)	2.30 (-17)

* a(-x) = a × 10^{-x}.

TABLE VIII. CROSS-SECTIONS (in cm^2) FOR THE ELECTRON CAPTURE REACTIONS
$B^{5+} + H(m = 2) \rightarrow B^{4+}(n) + H^+$

E (keV/u)	$\sigma_{ct}(2 \rightarrow 1)$	$\sigma_{ct}(2 \rightarrow 2)$	$\sigma_{ct}(2 \rightarrow 3)$	$\sigma_{ct}(2 \rightarrow 4)$	$\sigma_{ct}(2 \rightarrow 5)$	$\sigma_{ct}(2 \rightarrow 6)$	$\sigma_{ct}(2 \rightarrow 7)$	$\sigma_{ct}(2 \rightarrow 8)$
0.2			8.35 (-39)	9.71 (-32)	2.06 (-25)	2.74 (-19)	6.83 (-17)	6.03 (-17)
0.6		1.74 (-39)	1.08 (-29)	2.16 (-25)	4.08 (-21)	2.44 (-17)	4.06 (-16)	3.79 (-16)
1.0		8.13 (-35)	7.01 (-27)	2.22 (-23)	9.38 (-20)	1.04 (-16)	6.64 (-16)	8.83 (-16)
2.0		5.70 (-30)	4.62 (-24)	3.04 (-21)	2.38 (-18)	4.55 (-16)	1.03 (-15)	2.45 (-15)
3.0	2.64 (-42)*	8.81 (-28)	7.96 (-23)	3.12 (-20)	1.02 (-17)	8.68 (-16)	1.22 (-15)	4.00 (-15)
5.0	3.23 (-37)	1.38 (-25)	1.32 (-21)	3.59 (-19)	4.55 (-17)	1.63 (-15)	1.47 (-15)	6.62 (-15)
7.0	1.58 (-34)	1.98 (-24)	5.76 (-21)	1.38 (-18)	9.74 (-17)	2.24 (-15)	1.65 (-15)	8.62 (-15)
10.0	3.81 (-32)	2.04 (-23)	2.10 (-20)	4.67 (-18)	1.94 (-16)	2.93 (-15)	1.86 (-15)	1.08 (-14)
14.0	2.83 (-30)	1.24 (-22)	5.79 (-20)	1.24 (-17)	3.29 (-16)	3.57 (-15)	2.07 (-15)	1.27 (-14)
20.0	1.26 (-28)	5.84 (-22)	1.42 (-19)	2.96 (-17)	5.17 (-16)	4.20 (-15)	2.29 (-15)	1.45 (-14)
30.0	4.20 (-27)	2.35 (-21)	3.26 (-19)	6.63 (-17)	7.72 (-16)	4.79 (-15)	2.48 (-15)	1.60 (-14)

* $a(-x) = a \times 10^{-x}$.

The cross-sections for all electron capture reaction channels in the energy range 0.2–30 keV/u are given in Table VII. The total electron capture cross-section (summed over all n channels) is given in Fig. 5, where it is compared with the AO and MO coupled state calculations and with the single experimental point at the collision energy E = 5.5 keV/u available from Ref. [15].

In reaction (13) there are three molecular states in the initial channel, having united-atom quantum numbers (10, 8, 0) (10, 9, 1) and (11, 10, 0). All of these initial states have strong T couplings with the lower molecular states, which provides large cross-sections for the population of the n = 9, 8, 7, 6 final channels of reaction (13). The calculated cross-sections are shown in Table VIII for the energy range 0.2–30 keV/u.

4.2.2. Excitation and ionization processes

Within the selected molecular basis, the only excitation process which can be considered in B^{5+} + H collisions is

$$B^{5+} + H(1s) \rightarrow B^{5+} + H(n = 2) \qquad (14)$$

The excitation of the n = 2 molecular manifold [(10, 8, 0), (10, 9, 1), (11, 10, 0)] is provided mainly through the $T_{1s\sigma}$, $T_{2p\pi}$ and $T_{3p\sigma}$ superseries; the first of these superseries is reached from the initial $4f\sigma$ state by the direct $T_{4f\sigma,3d\sigma}$ transition, the second one is reached by the $T_{4f\sigma,3d\sigma} \cdot P^{rot}_{3d\sigma,3d\pi}$ successive transitions and the third one is reached by the $T_{4f\sigma,3d\sigma} \cdot S_{4f\sigma,3d\sigma}$ transitions.

There are, of course, many other reaction paths connecting the initial and final states in reaction (14), which, however, involve a large number of transition points.

The cross-section of excitation process (14) in the energy range 0.2–100 keV/u is shown in Fig. 6. It is compared with the results of AO coupled channel calculations [16], and the agreement is excellent.

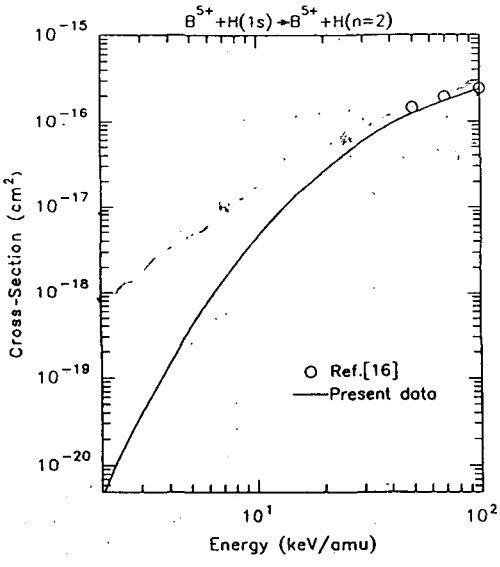

FIG. 6. Cross-section for excitation of the n = 2 hydrogen level in B^{5+} + H(1s) collisions. The solid line is the result of the present calculations; the circles are the results from the AO coupled channel calculations of Ref. [16].

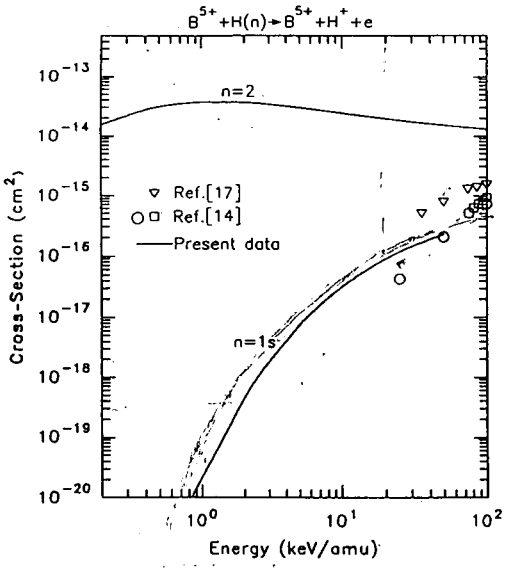

FIG. 7. Cross-sections for ionization of H(1s) in collisions with B^{5+} (curve n = 1s) and for transitions from H(n = 2) to all upper states and to the continuum (curve n = 2). The squares and circles are the results for ionization of H(1s) from the classical trajectory Monte Carlo calculations (Ref. [14]), and the inverted triangles are the ionization results obtained by the Keldysh quasi-classical method (Ref. [17]).

The ionization process

$$B^{5+} + H(1s) \rightarrow B^{5+} + H^{+} + e \qquad (15)$$

proceeds mainly through the $S_{f\sigma}^{(\kappa)}$ ($\kappa = 0, 1$), $S_{d\sigma}$, $T_{1s\sigma}$, $T_{2p\pi}$ and $T_{3p\pi}$ superpromotion channels. Its cross-section is shown in Fig. 7, together with the results of the classical trajectory Monte Carlo calculations [14] and of the Keldysh quasi-classical method [17]. Also shown is the cross-section (curve n = 2) for all transitions from the H(n = 2) manifold to higher [(Nℓm) $\geq$ ($N_c\ell_c m_c$)] states and to the continuum.

The accurate calculation of the ionization cross-section from the H(n = 2) level would require a considerable extension of the molecular basis.

4.3. Inelastic processes in $H^{+} + B^{4+}$ ($N \leq 8$) collisions

The cross-sections for electron capture to the H($n \leq 2$) levels in $H^{+} + B^{4+}$ ($n \leq 8$) collisions can be obtained from those for the inverse reactions (12) and (13) (see Tables VII and VIII) by using the detailed balance principle. We therefore consider only the excitation and ionization processes

$$H^{+} + B^{4+}(m) \rightarrow H^{+} + B^{4+}(n)$$
$$1 \leq m < n \leq 8 \qquad (16)$$

$$H^{+} + B^{4+}(n) \rightarrow H^{+} + B^{5+} + e$$
$$1 \leq n \leq 8 \qquad (17)$$

The cross-sections for these processes have been calculated in the energy range 0.2–50 keV/u. The excitation cross-sections are shown in Figs 8a–e, while the ionization cross-sections are given in Table IX. No data for these processes are available from other sources to compare with.

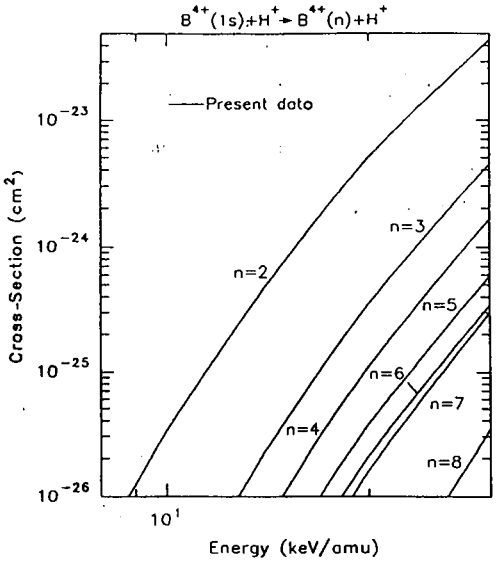

FIG. 8a. Cross-sections for B^{4+} (1s) → B^{4+} (n = 2–8) excitation by proton impact.

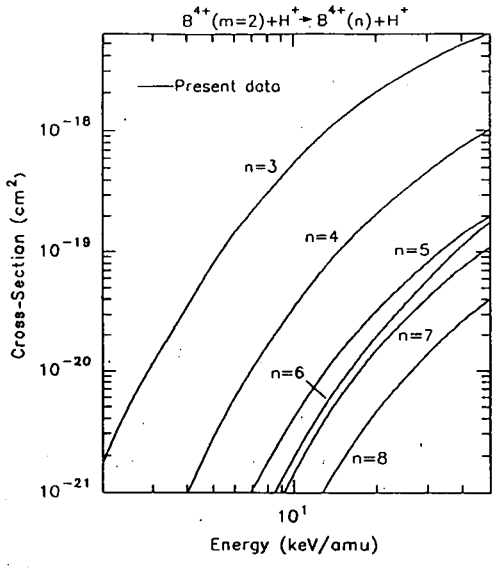

FIG. 8b. Cross-sections for B^{4+} (m = 2) → B^{4+} (n = 3–8) excitation by proton impact.

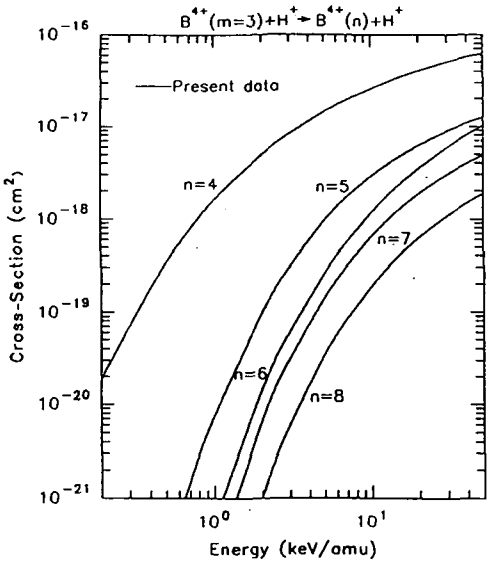

FIG. 8c. Cross-sections for B^{4+} ($m = 3$) → B^{4+} ($n = 4$–8) excitation by proton impact.

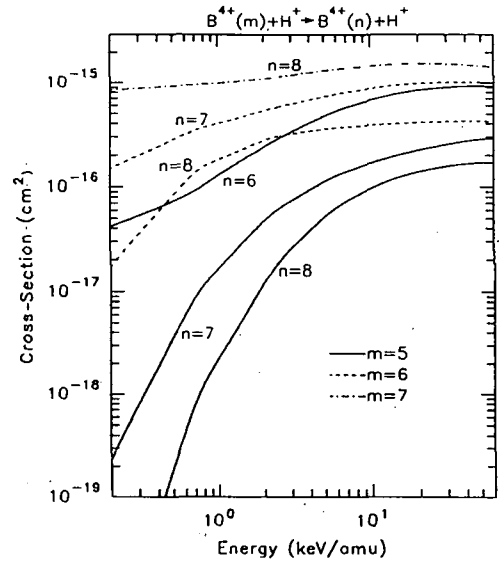

FIG. 8e. Cross-sections for B^{4+} ($m = 5, 6, 7$) → B^{4+} ($m < n \leq 8$) excitation by proton impact.

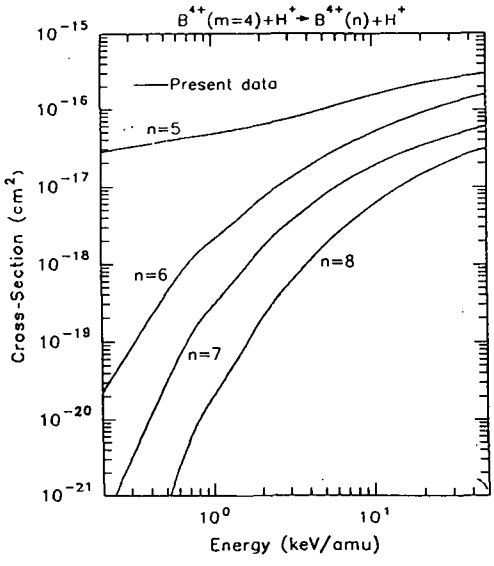

FIG. 8d. Cross-sections for B^{4+} ($m = 4$) → B^{4+} ($n = 5$–8) excitation by proton impact.

5. CONCLUDING REMARKS

We have calculated the cross-sections for charge exchange, excitation and ionization processes in slow collisions of Be^{4+} and B^{5+} ions with hydrogen atoms in the ground state and the first excited level. We have also considered the analogous processes in collisions of protons with incompletely stripped Be^{3+} and B^{4+} ions in the ground state and in excited states. The collision dynamics of these processes is described by the adiabatic hidden crossing approach and includes a large number of coupled molecular states. The validity of this theoretical approach is restricted to the energy region well below the energy at which the cross-section maximum for a particular process appears. The low energy limit of validity of the method, in the form applied in the present study, is defined by the validity of the classical description of the motion of colliding nuclei (~0.1 keV/u). The accuracy of the results obtained is expected to increase with decreasing collision energy, when the assumptions incorporated in the dynamical model become increasingly better satisfied. In principle, provided an adequately large molecular basis is used in the calculations, the method should provide exact results in the low energy limit (still consistent with the classical description of the nuclear motion). Previous experience with the application of this method to the $H^+ + H$ and $He^{2+} + H$ systems [6–9], as well as the few examples shown in Figs 1–6, where it is compared with very elaborate coupled channel calculations, show that the accuracy of the cross-sections for electron capture and ionization processes calculated by this method is well within 30–50% in the energy region below the cross-section maximum. In some cases, this degree of accuracy extends up to the energy of the cross-section maximum. For the excitation processes with a large energy difference between the states (e.g. excitation from the ground state), the present method provides less accurate results (within a factor of two),

TABLE IX. IONIZATION CROSS-SECTIONS (in cm^2) FOR $H^+ + B^{4+}(n)$ COLLISIONS

E (keV/u)	σ_{ion} (n = 1)	σ_{ion} (n = 2)	σ_{ion} (n = 3)	σ_{ion} (n = 4)	σ_{ion} (n = 5)	σ_{ion} (n = 6)	σ_{ion} (n = 7)	σ_{ion} (n = 8)
0.2		6.46 (-38)	2.36 (-28)	1.09 (-24)	8.42 (-22)	6.01 (-20)	1.39 (-18)	3.67 (-15)
0.6		5.72 (-30)	1.52 (-24)	7.74 (-22)	5.38 (-20)	1.59 (-18)	1.63 (-17)	3.82 (-15)
1.0		1.34 (-27)	2.94 (-23)	7.97 (-21)	2.83 (-19)	5.37 (-18)	3.62 (-17)	3.91 (-15)
2.0	1.70 (-41)	3.36 (-25)	1.29 (-21)	1.06 (-19)	1.90 (-18)	1.94 (-17)	8.24 (-17)	4.10 (-15)
3.0	2.38 (-37)	4.33 (-24)	8.56 (-21)	3.65 (-19)	4.78 (-18)	3.47 (-17)	1.23 (-16)	4.28 (-15)
5.0	2.76 (-33)	6.78 (-23)	6.20 (-20)	1.35 (-18)	1.28 (-17)	6.29 (-17)	1.95 (-16)	4.62 (-15)
7.0	5.56 (-31)	4.26 (-22)	1.79 (-19)	2.82 (-18)	2.20 (-17)	8.74 (-17)	2.59 (-16)	4.90 (-15)
10.0	5.18 (-29)	2.25 (-21)	4.69 (-19)	5.59 (-18)	3.64 (-17)	1.19 (-16)	3.46 (-16)	5.25 (-15)
14.0	1.89 (-27)	9.03 (-21)	1.01 (-18)	9.82 (-18)	5.49 (-17)	1.55 (-16)	4.46 (-16)	5.61 (-15)
20.0	4.66 (-26)	3.23 (-20)	2.02 (-18)	1.66 (-17)	8.03 (-17)	2.01 (-16)	5.70 (-16)	6.00 (-15)
30.0	9.48 (-25)	1.09 (-19)	3.91 (-18)	2.78 (-17)	1.16 (-16)	2.65 (-16)	7.33 (-16)	6.43 (-15)
50.0	1.79 (-23)	3.80 (-19)	7.72 (-18)	4.83 (-17)	1.74 (-16)	3.66 (-16)	9.55 (-16)	6.91 (-15)

possibly owing to the role of interference effects between adiabatic phases. However, for transitions between the excited states, characterized by strong localized couplings, the method should provide cross-sections accurate to within 20–30%. Because of the many transitions involved in the low energy dynamics of inelastic processes, no simple scaling relationships can be expected for their cross-sections with respect to the collision parameters (energy, ionic charge and initial (or final) quantum state).

REFERENCES

[1] SUMMERS, H.P., HELLERMANN, M. von, de HEER, F.J., HOEKSTRA, R., this issue, p. 7.

[2] SOLOV'EV, E.A., Usp. Fiz. Nauk **157** (1989) 437; Engl. transl.: Sov. Phys. Uspekhi **32** (1989) 228.

[3] SOLOV'EV, E.A., Zh. Ehksp. Teor. Fiz. **81** (1981) 1681; Engl. transl.: Sov. Phys.-JETP **54** (1981) 893.

[4] OVCHINNIKOV, S.Yu., SOLOV'EV, E.A., Zh. Ehksp. Teor. Fiz. **90** (1986) 921; Engl. transl.: Sov. Phys.-JETP **63** (1986) 538.

[5] JANEV, R.K., KRSTIC, P.S., Phys. Rev., A **44** (1991) R1436.

[6] GROZDANOV, T.P., SOLOV'EV, E.A., Phys. Rev., A **42** (1990) 2703.

[7] OVCHINNIKOV, S.Yu., Phys. Rev., A **42** (1990) 3865.

[8] JANEV, R.K., KRSTIC, P.S., Excitation and ionization processes in slow collisions of ground state and excited hydrogen atoms with protons, to be published in Phys. Rev., A.

[9] KRSTIC, P.S., JANEV, R.K., Excitation, ionization and electron capture processes in slow He^{2+} + H collisions, submitted to Phys. Rev., A.

[10] GROZDANOV, T.P., SOLOV'EV, E.A., J. Phys. B: At. Mol. Phys. **15** (1982) 3871.

[11] FRITSCH, W., LIN, C.D., Phys. Rev., A **29** (1984) 3039.

[12] FRITSCH, W. (Hahn-Meitner Institut für Kernforschung, Berlin), personal communication, 1991.

[13] KIMURA, M. (ANL), personal communication, 1991.

[14] OLSON, R.E., SALOP, A., Phys. Rev., A **16** (1977) 531.

[15] CRANDALL, D.H., PHANEUF, R.A., MEYER, F.W., Phys. Rev., A **19** (1979) 504.

[16] REINHOLD, C.O., OLSON, R.E., FRITSCH, W., Phys. Rev., A **19** (1979) 504.

[17] USKOV, D.B. (Lebedev Phys. Inst., Moscow), personal communication, 1992.

Contents of previous volumes of Atomic and Plasma-Material Interaction Data for Fusion

Volume 1

Volume 2

HOW TO ORDER IAEA PUBLICATIONS

An exclusive sales agent for IAEA publications, to whom all orders and inquiries should be addressed, has been appointed for the following countries:

CANADA UNITED STATES OF AMERICA	UNIPUB, 4611-F Assembly Drive, Lanham, MD 20706-4391, USA

In the following countries IAEA publications may be purchased from the sales agents or booksellers listed or through major local booksellers. Payment can be made in local currency or with UNESCO coupons.

ARGENTINA	Comisión Nacional de Energía Atómica, Avenida del Libertador 8250, RA-1429 Buenos Aires
AUSTRALIA	Hunter Publications, 58 A Gipps Street, Collingwood, Victoria 3066
BELGIUM	Service Courrier UNESCO, 202, Avenue du Roi, B-1060 Brussels
CHILE	Comisión Chilena de Energía Nuclear, Venta de Publicaciones, Amunategui 95, Casilla 188-D, Santiago
CHINA	IAEA Publications in Chinese: China Nuclear Energy Industry Corporation, Translation Section, P.O. Box 2103, Beijing IAEA Publications other than in Chinese: China National Publications Import & Export Corporation, Deutsche Abteilung, P.O. Box 88, Beijing
CZECHOSLOVAKIA	S N T L, Spálená 51, CS-113 02 Prague 1 Alfa, Publishers, Hurbanovo námestie 3, CS-815 89 Bratislava
FRANCE	Office International de Documentation et Librairie, 48, rue Gay-Lussac, F-75240 Paris Cedex 05
HUNGARY	Kultura, Hungarian Foreign Trading Company, P.O. Box 149, H-1389 Budapest 62
INDIA	Oxford Book and Stationery Co., 17, Park Street, Calcutta-700 016 Oxford Book and Stationery Co., Scindia House, New Delhi-110 001
ISRAEL	YOZMOT Literature Ltd., P.O. Box 56055, IL-61560 Tel Aviv
ITALY	Libreria Scientifica Dott. Lucio di Biasio "AEIOU", Via Coronelli 6, I-20146 Milan
JAPAN	Maruzen Company, Ltd, P.O. Box 5050, 100-31 Tokyo International
PAKISTAN	Mirza Book Agency, 65, Shahrah Quaid-e-Azam, P.O. Box 729, Lahore 3
POLAND	Ars Polona, Foreign Trade Enterprise, Krakowskie Przedmieście 7, PL-00-068 Warsaw
ROMANIA	Ilexim, P.O. Box 136-137, Bucharest
RUSSIAN FEDERATION	Mezhdunarodnaya Kniga, Sovinkniga-EA, Dimitrova 39, SU-113 095 Moscow
SOUTH AFRICA	Van Schaik Bookstore (Pty) Ltd, P.O. Box 724, Pretoria 0001
SPAIN	Díaz de Santos, Lagasca 95, E-28006 Madrid Díaz de Santos, Balmes 417, E-08022 Barcelona
SWEDEN	AB Fritzes Kungl. Hovbokhandel, Fredsgatan 2, P.O. Box 16356, S-103 27 Stockholm
UNITED KINGDOM	HMSO, Publications Centre, Agency Section, 51 Nine Elms Lane, London SW8 5DR
YUGOSLAVIA	Jugoslovenska Knjiga, Terazije 27, P.O. Box 36, YU-11001 Belgrade

---

Orders from countries where sales agents have not yet been appointed and requests for information should be addressed directly to:

Division of Publications
International Atomic Energy Agency
Wagramerstrasse 5, P.O. Box 100, A-1400 Vienna, Austria

92-02407

INFORMATION FOR AUTHORS

General

Atomic and Plasma–Material Interaction Data for Fusion (APMIDF) publishes papers, letters and reviews which deal with elementary atomic collision processes in fusion plasmas, collision processes of plasma particles with surfaces and plasma–material interaction phenomena, including the thermophysical and thermomechanical response of candidate fusion reactor plasma facing materials. Each contribution submitted to APMIDF should be highly fusion relevant and should contain a significant amount of quantitative data information in one of the above fields. Review articles are normally prepared on invitation of the Scientific Editor or with his prior consent. APMIDF is a regular Supplement to the journal NUCLEAR FUSION (NF) and its abbreviation for the purpose of referencing is: At. Plasma–Mater. Interact. Data Fusion.

Manuscripts, which may be submitted in Chinese, English, French, Russian or Spanish, will be published in English. For a manuscript submitted in a language other than English, a translation into English of technical terms should be provided. Manuscripts must be submitted in triplicate and typewritten double spaced on good quality standard size paper. All copies should include the main text, an abstract, tables, references, figures, captions and appendices, as appropriate. One set of glossy prints or reproducible transparencies of the figures should also be provided. *Final manuscript versions may be submitted in camera ready form or on diskettes (see NF's Note for Authors, available on request from the NF Office).*

Every manuscript submitted must be accompanied by a disclaimer stating that the paper has not been published and is not being considered for publication elsewhere. If no copyright is claimed by the authors, the IAEA automatically owns the copyright of the paper.

Authors will receive proofs of the text of accepted manuscripts. Proofs of figures are sent only if requested. Rejected manuscripts will not be returned unless this is expressly requested within six weeks of rejection.

Fifty reprints are provided free of charge; additional reprints may be ordered at the time the author returns the proofs. Manuscripts and correspondence should be addressed to: The Editor, NUCLEAR FUSION (A+M Supplement), International Atomic Energy Agency, Wagramerstrasse 5, P.O. Box 100, A-1400 Vienna, Austria.

Manuscript preparation

Authors are referred to any recent issues of APMIDF or NF for examples of *format* and *style*.

All submitted articles should be *concise* and written in a *clear style*. The description of the methods used for obtaining the presented original data information should be kept to a reasonable minimum. The review papers should provide a critical analysis of a broader class (or classes) of data or processes together with a set of recommended data of specified accuracy.

Titles should be as concise as possible but sufficiently informative to describe the subject of the paper.

Abstracts must briefly summarize the contents of the article. They should state the principal objectives, mention the methodology employed, summarize the results (emphasizing the new findings) and present the main conclusions. They should be concise and self-contained so that they can be used by the International Nuclear Information System (INIS) and other abstracting systems without changes. General, well known information should be avoided in the abstract and accommodated in the introduction.

Letters to APMIDF are short communications of net sets of data obtained with a standard, highly accurate method. As a rule, they should be not longer than ten typewritten double spaced standard pages, including references and figures.

Guidelines for *bibliographical citations* can be found in issues 2, 3 and 4 of NF **28** (1988). In short, references should be accurately described in sufficient detail for easy identification. In the text, they should be indicated consecutively by Arabic numerals in square brackets. All references should be listed on a separate page at the end of the text. In this list, the names of all authors (or, if there are more than six, of the first three authors plus 'et al.') should be given. All unpublished material, e.g. laboratory reports, doctoral theses or papers in proceedings that have not yet been published, should be cited with full titles, place and year; citations of reports should also contain the laboratory prefix and number, date of issue, etc. References to periodicals should contain the name of the journal, volume number, page number and year of publication; the title of the article is not needed. References to books should contain the full title of the book, names of editors (if any), name and location of the publisher, year of publication and page number (if appropriate). References to personal communications should be avoided if possible. For journal citations use the list of abbreviations given in "IAEA-INIS-11, INIS: Authority List for Journal Titles". Russian names should be transliterated according to "IAEA-INIS-10, INIS: Transliteration Rules for Selected Non-Roman Characters". Examples of the style followed by NF for references are:

REFERENCES

[1] SHAH, M.B., GILBODY, H.B., J. Phys., B (Lond.). At. Mol. Phys. **14** (1981) 2361.

[2] WILSON, K.L., BASTASZ, R.A., CAUSEY, R.A., et al., At. Plasma–Mater. Interact. Data Fusion **1** (1991) 31.

[3] BRANSDEN, B.H., Atomic Collision Theory, 2nd edn., Benjamin, New York (1982).

[4] MÄRK, T.D., DUNN, G.H. (Eds), Electron Impact Ionization, Springer-Verlag, Berlin, Heidelberg, New York, London (1985).

[5] MÖLLER, W., ROTH, J., in Physics of Plasma–Wall Interactions in Controlled Fusion (POST, D.E., BEHRISCH, R., Eds), Plenum Press, New York (1986) 45.

[6] McGRATH, R.T., Thermal Loads on Tokamak Plasma-Facing Components During Normal Operation and Disruptions, Rep. SAND89-2064, Sandia National Laboratories, Albuquerque, NM (1990).

[7] TRUBNIKOV, B.A., in Problems of Plasma Theory, Vol. 1 (LEONTOVICH, M.A., Ed.), Gosatomizdat, Moscow (1963) 98 (in Russian). (English translation: Reviews of Plasma Physics, Vol. 1, Consultants Bureau, New York (1965) 105.)

[8] HUBER, B.A., Zum Elektronentransfer zwischen mehrfach geladenen Ionen und Atomen oder Molekülen, PhD Thesis, Ruhr-Universität, Bochum (1981).

[9] de HEER, F.J., HOEKSTRA, R., KINGSTON, A.E., SUMMERS, H.P., Excitation of neutral helium by electron impact, to be published in At. Plasma–Mater. Interact. Data Fusion.

[10] MOORES, D.L., Electron impact ionisation of Be and B atoms and ions, submitted to At. Plasma–Mater. Interact. Data Fusion.

All figures should be on separate sheets and numbered consecutively with Arabic numerals, e.g. Fig. 1. A separate list of captions must be provided (see also *General* above).

Tables must carry a heading and be numbered consecutively with Roman numerals in the order in which they are mentioned in the text, e.g. Table II. Footnotes to tables should be indicated by raised letters (not numbers or asterisks) and set immediately below the table itself. Tables should be typed clearly for possible direct reproduction.

Footnotes to the text should be numbered consecutively with raised Arabic numerals; excessive use of footnotes should be avoided.

All *equations* should be typed as carefully as possible, with unavailable Greek letters and other symbols clearly inserted by hand. Specifically:

(1) To eliminate confusion between symbols with similar appearance (e.g. between ones, ells and primes), make them as distinct as possible, if necessary marking them clearly by hand. In manuscripts with handwritten formulas, all further sources of confusion (such as n's and u's, u's and v's, e's and l's, J's and I's) should also be marked.

(2) Indicate a vector by an arrow on top rather than by bold face lettering.

(3) Tensors of second rank should bear two arrows on top; if higher rank tensors are required, choose an appropriate symbol and explain it.

(4) Indicate the normal algebraic product by simple juxtaposition of symbols, i.e. without multiplication sign.

(5) Write scalar products of vectors with a raised point, e.g. $\vec{A} \cdot \vec{B}$.

(6) Use the multiplication sign ($\times$) solely to designate: (i) a vector product, (ii) an algebraic (but not a scalar) product in the case where an equation has to be split over two lines, and (iii) in expressions like 3 cm $\times$ 3 cm or 2 $\times$ 10^6 cm.

(7) The nabla operator (∇) does not carry an arrow.

(8) When equations are split over two or more lines, place operational signs only at the beginning of each new line, not at the end of the preceding line. For direct reproduction of an equation, the length of the lines should not exceed 9 cm.

(9) Where it is impossible to split long fractions over two lines, use negative exponents: similarly, replace root signs by fractional exponents where appropriate.

(10) Do not use symbols, abbreviations and formulations that are recognizable only in a particular language.

Use *SI units* as far as possible; where this is not possible, please give the appropriate conversion factor.